Università degli studi di Genova
Dipartimento di Ingegneria navale, elettrica, elettronica e delle telecomunicazioni (DITEN)
Scuola Politecnica

Study of innovative autonomous marine vehicles for monitoring in remote areas and shallow waters

The Shallow Water Autonomous Multipurpose Platform (SWAMP)

A thesis submitted for the degree of
Dottorato di Ricerca in
Scienze e tecnologie per l'Ingegneria Elettrica, l'Ingegneria Navale, i Sistemi complessi per la mobilità
XXXII Ciclo

ING. ANGELO ODETTI

Advisor: Prof. Marco Altosole
Co-advisor: Prof. Michele Viviani
Co-advisor: Ing. Gabriele Bruzzone
Co-advisor: Ing. Massimo Caccia

Genova, 2019

Università degli studi di Genova
Dipartimento di Ingegneria navale, elettrica, elettronica e delle telecomunicazioni (DITEN)
Scuola Politecnica

Study of innovative autonomous marine vehicles for monitoring in remote areas and shallow waters

The Shallow Water Autonomous Multipurpose Platform (SWAMP)

A thesis submitted for the degree of
Dottorato di Ricerca in
Scienze e tecnologie per l'Ingegneria Elettrica,
l'Ingegneria Navale, i Sistemi complessi per la mobilità
XXXII Ciclo

ING. ANGELO ODETTI

Advisor: Prof. Marco Altosole
Co-advisor: Prof. Michele Viviani
Co-advisor: Ing. Gabriele Bruzzone
Co-advisor: Ing. Massimo Caccia

Genova, 2019

Contents

Abstract

The main objective of the research activity covered by the present thesis is the design of an Autonomous Surface Vehicle for the monitoring of environmental areas characterised by shallow water, difficult access and harsh environment, namely the Wetlands.
Wetlands are those geographic areas where water meets the earth that cover between 5 and 8% of the Earth's surface. Wetlands include mangrove zones, swamps, bogs and marshes, rivers and lakes, alluvial plains and flooded forests, shallow coasts and coral reefs. In recent years, their importance is becoming more and more recognized and various international conventions, directives and projects work on their protection. Their importance is related to the fact that these areas are essential ecosystems considered among the world's most productive environment. Classified as natural purification systems and carbon resources for fauna, Wetlands provide the water and productivity upon which biological diversity relies for the growth of an enormous amount of species of plants and animals. Their importance is also related to human activities since Wetlands can be exploited commercially for fishing but especially become important when thinking that the protection of these areas can also help fighting the disasters resulting from human impact on the environment and its role in the climate change.
The lack of a hydro-graphic vessels capable of performing shallow water measurements at depths of less than $1\,m$ has led to unreliable maps and data, thus motivating research on innovative technical approaches for executing the tasks of water sampling, limnological surveys, bathymetric analyses and monitoring of water quality. In recent years a variety of robotic approaches to improve the quality, speed, and accessibility of surveys have been explored by research groups using both commercial and ad-hoc solutions.
In this thesis a prototype of Autonomous Surface Vehicle (ASV) named SWAMP (Shallow Water Autonomous Multipurpose Platform) is proposed as the base for an innovative class of reliable modular re-configurable lightweight ASVs for extremely shallow water applications. The vehicle was studied to solve the problem of monitoring the water status in the Wetlands but the SWAMP class ASV will also be able to support, as test-bed, the research on many aspects of marine engineering and robotics like propulsion issues, structure issues, artificial intelligence, cooperative distributed control, Guidance, Navigation and Control (GNC) systems as well as innovative technological solutions in terms of communication, materials, sensors and actuators.
The heterogeneity of the themes treated by this thesis relies on the fact that the whole aspects of design were taken into consideration.
In this thesis the description of the design, modeling, construction and testing of the new concept of Autonomous Surface Vehicles (ASV) is illustrated. The motivations behind the necessity of a new system are described in Chapter 1 and 2 while in Chapter 3 the general considerations on the requirements that led to the definition of the specifications of a special layout are reported.
In Chapter 4 the design of the vehicle layout is illustrated together with the description of an innovative soft-material hull structure on which extensive analyses in towing tank were performed. The tests were carried out both in deep and shallow water to completely identify the surge motion of the ASV.
The hardware, software and mechanical modularity represent some main ideas behind the conception of SWAMP. The two hulls of SWAMP are two separate modules. Each hull can be composed

of more or less structural elements, actuation modules, powering elements, control units, sensors. This can be done without constraints thanks to the novel communication architecture all based on Wi-Fi modules.
In Chapter 5 the thrusters expressly studied for environmental monitoring in the extremely shallow waters of the Wetlands (rivers, lakes swamps, marshes, mangroves..) are illustrated. These systems were modeled, designed and constructed on the Pump-Jet concept. Four Pump-Jet Module s for a class of small/medium size ASV were built and the description of the design and tests are reported in the thesis. The extremely modular hardware control system of SWAMP is described in Chapter 6 where also the modules composing the vehicle are described. Once assembled, the vehicle was tested at sea in various environments. A series of pioneering tests with the application of Machine Learning and the citizen's engagement in teaching to a robot to self-control are described in the Chapter 7, together with more standard results. The algorithm for the training of a neural network for the control of SWAMP was tested also by using the simulator described in Chapter 8.
The conclusions of this work, reported in Chapter 9, are correlated with a visionary analysis of the possible applications of SWAMP in a series of futuristic research trends of marine robotics.

Chapter 1

Introduction

1.1 Motivation

Looking at Robotics with an holistic approach, it is an interdisciplinary science whose scope is the design and development of robots by involving many aspects of engineering and science like mechanics, electrical engineering, electronics, computer science, biology, physiology, psychology, physics, mathematics and linguistics. Robotics deals with the design, construction, operation and use of highly automated machines, as well as IT systems for their control, sensory feedback and information processing. As a consequence of this multidisciplinary nature happens that an acceleration in the development of these disciplines brings to the accelerated development of robotics.
In the recent years the continuously increasing technological innovation related to electronics, artificial intelligence, additive manufacturing, nanotechnology, virtual reality and sensors is influencing the acceleration of the widespread of robots. This type of acceleration means that not only technologies grow in capacity but also that prices fall very quickly.
Some years ago we usually identified a robot as something far from our daily life. The robot was a science-fictional entity or, on the other-hand, an expensive mechatronics tool widely used in industries and factories, replacing humans in dangerous and/or strenuous jobs. Nowadays, thanks to an extraordinary advancement of this technology [1], robots are increasingly present in many different moments and places in our lives.
The next generation of everyday life robots will have to look, feel and act in a more humane way, to make it easier for us to have an emotional connection with a machine. Also intelligent vehicles are rapidly taking place in commercial and societal scenarios, such as autonomous cars and flying drones and nowadays it is a common perspective to foresee the use of autonomous ships [2] also thanks to projects like MV Yara Birkeland.
On the other hand there's a part of robotics called *Applied Robotics*, which is less emotional but is affecting and will affect our vision of the world helping us to increase our knowledge of the surrounding. This part of robotics is helping us to understand how our world behaves and how our world is changing even as a result of the effects related to the anthropic impact.
With the rise of robotic technologies the number of robotic solutions is pushing environmental scientists and engineers to explore research and monitoring applications of robotics, as well as exploring ways of integrating robotics into ecosystems to aid in responses to accelerating environmental, climatic, and biodiversity changes.
As shown in [3] robotic systems are increasingly being utilized as fundamental data-gathering tools by scientists, allowing new perspectives and a greater understanding of the planet and its environmental processes. Robotic systems make it possible to measure efficiently and precisely and have the potential to reduce environmental events is way that were not previously thought to be possible. With the increasing public awareness of the fact that robots are able to collect scientifically relevant information and interact with the environment, new opportunities are emerging for large-scale environmental monitoring that should push the boundaries of robotic and natural sciences. An obvious

advantage of using robotics in environmental sciences is that they allow the monitoring and sampling of events that are too dangerous or impossible to measure for humans such as the fall of large pieces of ice in the Arctic fjords [4]. This ability allows to collect scientifically relevant measurements on unprecedented spatial and temporal scales of previously immeasurable events.
The Autonomous, Semi-Autonomous or Remotely Operated vehicles, thanks to their intrinsic motion precision and capability of operating multiple sensors at the same time, allow the collecting high-dimension geo-referenced multi-spectral data. Autonomous marine systems can also be employed in intervention scenarios where the exploitation of remote robotic systems enhances the overall safety, keeping the human personnel far from the dangerous scenarios.
Advanced autonomous capabilities are achieved thanks to the continuous research, design and development of suitable techniques for automatic navigation, guidance and control operations, as well as the exploitation of cutting-edge technological results such as new materials, high-performance actuators and accurate sensors.
Autonomous operations in hardly accessible areas such as wetlands and Polar Regions or remote areas as open or protected waters require specific designs and ad-hoc studied solutions. Usually different requirements have to be met. Particular care is brought on the most suitable platform for the required operation, if on one side the problem is designing small, portable and highly controllable targeted solutions (e.g. [5]) on the other the aim is the seeking of long range and extended duration of autonomous operations with the problem of motion efficiency, low energy consumption and sea keeping ability.
An holistic approach involving a continuous trade-off between conflicting requirements brings to a circle including Research Innovation and Application. As presented in [5] the *Ecorobotics* paradigm is the integration of ecological approaches and robotics to develop technological tools for environmental monitoring. The Robotics applied to environmental sciences is intended to help the human to improve the precision and the quality of the surveys and to perform tasks in those areas where the access is dangerous or difficult. For this reason the main concept behind the design and development of a robots expressly addressed for a peculiar ambient should be its adaptability to the specific environment in order to extend the operations to the largest possible areas.
The research presented in this thesis is inspired by the practical needs of monitoring wetlands (*Application*) for a better acquisition of environmental parameters. The *Innovation* brought is constituted by the use of both solutions that match with the necessity of solving the difficult problem of accessing, monitoring and sampling in the wetlands both with the final idea of including new solutions in the Robotics *Research* area.

1.2 Wetlands

Generally known as *Wetlands*, ponds [6], peat bogs and swamps, rivers and lakes, rivers mouths and deltas, floodplains and flooded forests, rice paddies, shallow coasts, flooded forests, coral reefs and mangroves [7] and tidal fresh waters [8] are considered an important natural resource that requires continuous protection and monitoring. Wetlands are of global interest. Present in every country and in every climatic zone, from the polar regions to the tropics, from high altitudes to arid regions they cover between 5% and 8% of the land area [9], and are essential ecosystems for life. In fact these areas are rich of activity, are a very important sources of water, but also act as natural purification systems.
These ecosystems are of critical importance [10] since the biological activity present in these areas is fundamental in the global scheme of things because they provide shelter to plants and animals, food and continuous renewal of nutrients. Moreover, despite the human activities resulting in

Figure 1.1: *Wetlands are marshes, peat bogs, natural or artificial permanent or temporary basins, with stagnant, running, fresh, brackish, or salty water, including stretches of sea water whose depth, at low tide, does not exceed six meters*

anthropogenic climatic change are influencing the life of such vulnerable areas, these result to be some of the most economically important ecosystems on Earth thus becoming essential ecosystems also for human life [11]. The natural purification of waters operated by Wetlands brings particular interest on the discussion on the degradation and remediation of these areas since the richness of life here present makes Wetlands of great importance also for carbon resilience to climate change [12]. But the preservation of these areas is especially essential to preserve sharing and distribution of water. For this reason FAO itself is directly involved in the protection: a better widely distributed supply of water can also enhance the agriculture and the protection of coastal and internal waters may increase fishing reserves and push the aquaculture resource for the future.

Figure 1.2: *Various examples of Wetlands*

Furthermore, proper monitoring of wetlands is a key element to plan a protection from disasters caused by the above mentioned Anthropocene climate changes especially related to environmental degradation. In addition recent authoritative analysis on climate changes are forecasting an impor-

tant reduction of Sea Ice [13] with unpredictable consequences on the climate. Besides to the effects caused on wetlands by the release of huge amounts of freshwater from the ice calving, the polar regions themselves represent a substantial part of the world's wetlands that need to be monitored and preserved.
In this scenario the importance of wetlands becomes clear: these are not only important for an ecological reason but are also closely related to human activities.

In general, five main types of wetlands are recognized:

- Marine: coastal wetlands, including coastal lagoons, rocky coasts and coral reefs;
- Estuarines: including deltas, tidal marshes and mangroves;
- Lakes: wetlands associated with lakes;
- Riverside: wetlands adjacent to rivers and streams, riversides and shores;
- Palustres: swamps and marshes.

In addition, there are artificial wetlands, such as fish breeding ponds and shrimp, farm ponds, irrigated farmland, depressions flooded salt flats, reservoirs, gravel ponds, sewage pools and channels.
In sum, Wetlands can be grouped into three categories: marine and coastal wetlands, inland wetlands and artificial wetlands. Marine wetlands are considered to be those that reach a depth of up to six meters at low tide; this corresponds to the maximum depth to which marine ducks can dive in search of food. It should also be noted that it is understood that lakes and rivers as a whole are included in the definition of wetlands, whatever their depth.
Even tough the degradation and loss of wetlands is more rapid than that of other ecosystems, wet areas are of considerable importance for different aspects [14]:

- Biological. Because it represents, globally, one of the most important habitat types for biodiversity conservation. An immense variety of species of microbes, plants, insects, amphibians, reptiles, birds, fish and mammals can be part of a wetland ecosystem. Wetlands suffer for a huge number of threatened species. As an example among the birds threatened with extinction more than hundred species depend on wetland;
- Carbon sequestration. Wetlands store carbon within their plant communities and soil instead of releasing it to the atmosphere as carbon dioxide. Wetland ecosystems provide an optimum natural environment for the sequestration and long-term storage of carbon dioxide. Thus wetlands help to moderate global climate change [15]. This means that restoring and safeguarding the wetlands is important for the preservation of carbon reserves and biodiversity [16];
- Chemical and physical. In fact, wetlands are nutritional traps. The rich and diverse vegetation of wetlands offers these environments the ability to assimilate nutrients like potassium and nitrogen compounds. The presence of this vegetation offers the possibility of creating favorable conditions for microbial decomposition of organic matter. This enriched material feeds many small aquatic insects, shellfish and small fish that are food for larger predatory fish, reptiles, amphibians, birds and mammals.;
- Hydro-geological, because they fulfill the function of attenuation and regulation of phenomena such as river floods. The marshes adjacent to the watercourses, for example, create a sponge effect, that is, they collect water during the floods (slowing the flow of water and reducing the risk of flooding) then returning them during the weak periods. They are also important reservoirs for aquifers. The holding capacity of wetlands helps control floods and prevents water logging of crops;

- Human activities. Wetlands [17] have provided ecosystem services to population for more than 6000 years (Nile, Mesopotamian civilizations). Initially these wetlands provided drinking water, fishing and hunting grounds, as well as protection against flooding from rivers and seas. Later, these services extended to the supply of water for agriculture, households, energy and industries, and the supply of material for construction resulting strictly connected to the progress of the society.

- Productive, due to their importance in the fields of small culture or mollusc culture and for salt production. Many of the nation's fishing and shell-fishing industries harvest wetland-dependent species. As mentioned, the combination of shallow water, high levels of nutrients and primary productivity is ideal for the development of organisms that form the base of the food web that is at the base of fisheries.

- Scientific: from the study of pollen profiles from peat bogs, for example, it is possible to reconstruct the ecological, climatic and evolutionary events of the territory in which these environments are located.

Several national (Italian) and international projects, conventions and directives exist aimed at stimulating the monitoring, prevention and protection of wetlands.
The *Ramsar Convention* [18], namely the Intergovernmental Convention on Wetlands (1971), is the first treaty with a global aim concerning the conservation and management of natural ecosystems. It provides the framework for international cooperation aimed at the conservation and rational use of wetlands and their resources [19].
The European Environment Agency is in the forefront in the protection of *Wetlands and Water-bodies* and the EU Water Framework Directive (WFD) (2000/60/EC) [20] establishes the necessity of protecting and improving the conditions of aquatic ecosystems. This directive is implemented in Italy with *Environmental Consolidation Act (Testo Unico Ambientale (T.U.A.))* [21] that has, for the first time, introduced the obligation for the regions to systematically monitor the coastal ecosystem and to implement monitoring programs to assess if a good environmental status has been achieved. Local administrations should provide for the arrangement, conservation and recovery of soil in river basins, and for the defense, arrangement and regulation of waterways, rivers and their estuaries, as well as wetlands. The T.U.A. provides space for a *'Community action in the field of qualitative and quantitative water protection for the implementation of a sustainable long-term use and protection policy for all inland waters (surface and underground), for transitional waters and for coastal marine waters'*. The priority objective is to maintain good water status, protect and improve the conditions of aquatic ecosystems, wetlands and terrestrial ecosystems, in consideration of their need for water.
But the effective actions related to the directives, laws and trends are often ineffective as shown in various recent reviews as [22], [23] and [24] that suggest for more efficient assessment.
In this context it is clear that there are still many problems of a different nature to be solved. Especially from an operative and strictly technical point of view some problems arise from the lack of adequate resources as shown in fig. 1.3. As an example [25] show how no holistic solution exists to cover all steps of water quality monitoring programs and it is necessary to enhance approaches and solutions.
Innovative solutions are necessary and while the overall assessment of the status can be achieved by the adoption of various remote sensing techniques ([26] and [27]) , the local monitoring of physical, geological and biochemical parameters cannot be performed in many of the most inaccessible or dangerous areas. Some works can be performed with aerial solutions as shown by [28] but existing technical solutions cannot cover widespread and long-time analyses and surveys that can be performed by the adoption of water-going robotic solutions. In particular on shallow or mixed water

(where water and soil occupy the same area), the monitoring consists in the execution of surveys of different nature with data to be provided to the various sciences like physical geography, geology, biology, hydrology, meteorology, chemistry, physics, botany, zoology. The sum of all these data, in the end, allows to obtain an integrated knowledge of the physical, chemical and biological dynamics of a body of water. Morpho-bathymetric and stratigraphic surveys are used to study the evolution

Figure 1.3: *Wetlands traditional surveys*

of watercourses and water reservoirs and monitor their progress even during catastrophic events like flooding. These are made using sensors of different nature: bathymetry made with single or multi-beam echo-sounders, geomorphological analysis using Side Scan Sonar, seismic-stratigraphic analysis using Sub-Bottom Profiler and magnetometer analysis. The assessment of physical, ecological and chemical status of water is achieved through the collection and analysis of samples in different areas such as rivers, lakes, reservoirs, coastal areas and transitional waters. The parameters monitored are physical (Conductivity, Temperature, Pressure) and are related to the conditions of nutrients, oxygenation, salinity, turbidity, bacteria concentration, ammonium concentration, the presence of Posidonia and other factors indicating the water quality status. In addition it is sometimes important to monitor these parameters at different depths down to a maximum of 50 m.
All these actions are often carried out in areas that are difficult to access, with unsuitable tools and without a planned "strategy". Usually the strategies depend on the operational limits of the vehicle or operator. At the moment there is a certain difficulty in finding a single technological solution that allows to monitor the different wet areas, which is efficient, effective and low-cost. The solution could be to create a series of vehicles that are compatible as much as possible with the different specific activities to allow an effective protection of these sensitive areas that may integrate the surveys carried on with remote sensing systems and autonomous fixed and distributed sensors.
However the surveys of these areas are quite difficult due to the use of solutions not always suitable for the peculiar environment. Water sampling, limnological surveys, bathymetric analysis and water quality monitoring are complicated due to the difficulties in accessing the uneven underwater terrains and the extremely shallow waters that characterise ponds, rivers, lakes and coastal areas that make it hard to access with traditional means as shown in fig. 1.3 resulting in approximate and inefficient surveys. The commonly used exploratory methodologies (see Figure fig. 1.4) are often of an obsolete technological level. In some cases, surveys, analyses and sampling are carried out by walking operators and this means that the use of boats of any shape is already a good advantage. Almost all the analyses use classic boats: crafts equipped with an outboard motor or, in case of very shallow waters, boats are propelled by oars or even pushed by the operators. In some cases

semi-automatic wire-propelled systems are used as shown in [29]. Some companies use innovative Air Cushion Vehicles like [30] but the presence of the man is still a constant and in many situations the risk that the operator gets is not easily acceptable; moreover, in any case the precision of surveys is less than the one that can be obtained by a robotic system.

For these reasons most of the research groups are developing solutions finding out that the lack of

Figure 1.4: *Some examples of the commonly used systems*

hydrographic vessels, capable of carrying out measurements for shallow waters at depths below $1\,m$ gave birth to the existence unreliable maps and data. To improve the quality, speed and accessibility of the surveys in the recent years a great number of robotic-aided solutions have been studied from research groups, adopting both commercial and ad-hoc studied solutions.

The use of Autonomous Surface Vehicles (ASV) is the mostly reliable tool to provide extended and more quality surveys even-if the rush of scientists to find new tools for surveys in shallow environment has brought the attention to aerial drones that nowadays represent an alternative option [31] for operations with small endurance and low payload. Also for the increasing interest in unmanned solutions, some studies like [32] made a comparison between the bathymetric maps obtained with ASVs and with standard surveys showing the good ability of robots to carry on surveys in large and extremely shallow environments.

The principle adopted in the choice of ASV for shallow water surveys is often the adaptation of existing vehicles that were studied for other environments or the design of new solutions defined *"for shallow waters"* that, on the other hand, are based on existing solutions often not suitable for

this peculiar environment.
In this framework fits this work, which is based on the design of robotic solutions relying on the operational requests arising from operators of Italian private and public bodies that usually monitor shallow waters and wetlands. The design was guided by the constraints due to the experience of surveys carried out in harsh environment by CNR-INM and by the naval architecture and marine engineering competences of DITEN Unige.

Moreover, to support the need of ad-hoc robotic solutions, it is important to report that various studies like [33] and [34] identify the criteria used to evaluate the assessment methods for wetlands integrity. In the criteria the following four considerations result to be important:

1. The method can be used to measure condition. A principal goal is to maintain and restore the physical, chemical and biological integrity of the waters. Condition can be defined as the relative ability of a wetland to support and maintain its complexity and capacity for self-organization with respect to species composition, physic-chemical characteristics and functional processes as compared to wetlands of a similar class without human alterations. Ultimately, condition results from the integration of the chemical, physical and biological processes that maintain the system over time.
   This means that the capacity of multi-parameter analysis is required.

2. The method should be rapid. It should provide an accurate assessment of condition in a relatively short time period. No more than two people a half day in the field and requiring no more than a half day of office preparation and data analysis to come to an answer. The relative ease of collecting field data is also considered.
   This means that rapidity, easiness, precision and intelligent data collection are required.

3. The method must be an on-site assessment. An accurate evaluation using a rapid method requires a site visit to ensure that the method captures the current condition of the wetland and does not infer condition based solely on surrounding landscape characteristics or the potential of a wetland to perform certain wetland functions.
   This means that rapidity, repeat ability, high positioning precision are required

4. The method can be verified. *This means that a high degree in the control of the system is required.*

All these criteria, even if referred to a wider assessment of the methods, show that the requirements match in a perfect way with the adoption of unmanned solutions that would increase all the points taken into consideration.

Chapter 2

Related works

2.1 Preface

As shown in Chapter 1 the concept of Wetlands embraces a wide variety of mixed terrain areas: swamps, marsh, bog, floodplains, coastal areas, rivers, lake, polar regions and many others. It is easy to understand that, if there is a profound difference between these areas, on the other hand there are several peculiarities that are common to most of these zones that represent operational (and design) constraints. Wetlands are, for definitions, areas where the earth is covered by shallow water so, in the wetlands surveys are carried on in narrow and shallow waters that are often difficult to access with classic vehicles such as boats or wheeled vehicles, sometimes inaccessible or dangerous for human beings like in *critical or extreme environments*. This makes the analyses described in the previous chapter of difficult implementation.
The practical peculiarities of the surveys in wetlands and shallow waters are:

- the presence of a heterogeneous terrain that changes from water to mixed terrain and where the depth can be in the order of a few centimetres and where it is hard to access both with boats both with cars;
- the missions have to be carried out safely in critical and dangerous environments in the presence of: stream currents up to 1.5 m/s (as shown in [35]);
- often the terrains are difficult to be accessed with an important logistics. Rivers and lakes present steep terrains where landslides can occur, marshes and bog are swampy areas where people can hardly walk while polar regions present a huge danger of falling elements (for example ice sheets [36]) or extremely cold waters;
- environments often subject to restrictions where noise and pollution have to be contained thus implying that monitoring must be as non-invasive as possible;
- due to the difficult access there is a need of reducing logistics and the transport of equipment must be as simple as possible
- the time for making an analysis is often important

From these assumptions it is easy to understand that monitoring in these areas requires the use of ad-hoc solutions that should also match the possibility of:

- making repetitive tasks with a high precision
- having a good ability to scan efficiently
- having a good ability to perform sampling in specific areas also in presence of external disturbances

- having a good ability to perform pre-planned trajectories
- having a good flexibility and modularity giving the possibility of adding and removing tools and instruments

All these operations are difficult to achieve without adequate control of the instrumentation.
From these considerations it is clear how the use of autonomous (i.e. *unmanned*) vehicles can be a solution for almost all the problems.
The use of autonomous surface vehicles allows the human operator to be protected and to acquire more efficient data (less perturbed by the system to be measured). Furthermore, unmanned technologies are less expensive, faster and more precise than traditional ones. It is possible to act continuously for extended periods of time and less staffing is required thanks to the high degree of autonomy of the robots and to the reduced dimensions of the crafts.

2.2 State of the Art

Unmanned surface vehicles (USV) are vessels that operate on the surface of the water without the need of human onboard. The advances in USV control systems and navigation technologies led to the development of vessels that can be operated remotely by an operator on land or on a nearby manned vessel. USVs that operate with partially or fully autonomous control are defined Autonomous Surface Vehicle (ASV) and are the subject of the present study.
As shown in recent [37,38] and more recent [39–41] surveys, a great number of Autonomous Surface Vessels (ASV) with more or less enhanced capabilities was developed in the last years arising from academic and research institutions. The growing maturity of autonomous technologies with the possibility of long-duration of the measurements and observations desired, the possibility of removing personnel from the risk [42], the quality of surveys with respect to traditional methods and the possibility of extending the operations to otherwise inaccessible zones make ASV the most reliable solutions for the environmental surveys. ASV and in general USV have long been used to develop technology and control systems, but are now available as COTS products with main players like Liquid Robotics [43] (Wave Gliders), Teledynemarine [44], SeaRobotics [45], Maribotics [46] (Scout) and research and academic institutions that play an important role in the widespread. Thanks to these and other players starting from *2010*, the number of commercial vessels has risen from almost zero up to a good number of vessels, all responding to the needs of environmental monitoring and protection that means that the ASV has become a reliable and affordable system.
Expressly focusing on the wetlands monitoring, as above mentioned, these often are remote areas that require robotic solutions characterised by low logistics, low weight, small dimensions and modularity.
Under the assumption that Wetlands occur where water meets land it is natural to classify Wetlands within the extremely shallow waters. We define **extremely shallow water** those water bodies where water depth can reach up to $0.2\,m$. This peculiarity is important to define the operative limits for ASVs that should operate in these areas. Not to reduce the operative area, the structure, the propeller and the steering system require not to be susceptible to possible damages from the very probable grounding that may occur in shallow waters. The operative profiles require vehicles with good controllability, good stability for sensors management and open hardware and software architecture for an easy reconfigurability. Most of the existing vehicles do not match all these requirements. In particular the system of propulsion and the propulsion layout are usually not suitable to work in extremely shallow waters. This issue will be better explained in Chapter 5.
One of the first low-cost ASVs addressed to work in shallow waters was designed in 2005 by the Massachusetts Institute of Technology (MIT): it was the SCOUT sit-in kayak [47] originally designed

to test ASV control software and lately used in many projects. There are many recent projects that include vehicles defined *"suitable for shallow waters"* such as the ASV [48], USV-2600 [49], ROAZ II [50] and Hydronet [51]. In particular the ASV [48] expressly addresses the vessel to "survey on water surface of river, lake and ocean, especially suitable for exploration of shallow areas". In [49] it is reported the application of unmanned surface vehicles for autonomous shallow water bathymetric measurements, for naval mine counter-measures and hydrographic charting. Both catamarans have with big dimensions and low logistics.
The Hydronet vehicle, reported in [51], is a highly automated aluminum made catamaran with high power, size and with a not small draft which is not suitable for extremely shallow environment. These kinds of vehicles, even if expressly mention the shallow water, have a structure, a propulsion and a steering system prone to possible breaking due to grounding in very shallow waters making these solutions not really flexible enough to work in every water depth.

Other inland water vehicles like [52] are capable of navigating throughout complex inland water

Figure 2.1: *Hydronet and USV-2600 Catamaran ASV for research purpose*

storages and measuring a range of water quality properties and are characterised the presence of precise control strategies implemented to avoid "regions of non-traversable shallow water". This solution has a high degree of automation but intrinsecly shows how the adoption of inadequate technical solutions reflects on the need of highly automated and highly sensorised systems (in this case to avoid a passage in shallow waters).
ASV solutions like [53] and [54] (propelled by a Waterjet) on the other hand have a propulsion enclosed in a protected part of the hull but present big dimensions and weights that are not suitable when the logistics is reduced.
The ASVs used in academic research in shallow, shoreline environments are typically small, often catamarans, and operate at relatively modest speeds. But there are small dimensions and high performances monohull vehicles like LORCA [55]. It was designed to have a compact size while providing high performance and a robust design capable of operations in "both shallow water and in the ocean" under a range of sea states. The vehicle is made with carbon-fiber shells (thus resulting in constrained design) and is propelled with classical propeller with rudder resulting lowly controllable and fragile in the most important element.
The issue of propulsion in addition to a lower stability is tipical of these monohulls boats, other examples are [56], [57] and [58], small ASVs studied for shallow water taking inspiration from commercial vehicles. The mostly used commercial ASVs are Geomar's [59], Tecdron's [60], Dotocean's [61] and Teledyne's [62], a series of modular monohull boats made in plastics. Monohulls and kayak ([63]) present an intrisic low roll stability. Catamarans are more stable and allow to have higher payload with lower immersion. A way of solving the issue of stability is the use of Small Water Plane Twin Hull (SWATH), like in the SeaWASP ASV [64] also used in shallow water [65]. As demonstrated in literature by [66], [67] and [68], the SWATH model has acknowledged advantages, such as a natural platform stability also at a relatively high speed, combined to an effective wave disturbance rejection

Figure 2.2: *Geomar and Teledyne commercial mononhull ASV*

with a remarkable seakeeping ability. The SWATH boat stability is attributed to its submerged hull design, small water-plane area, and high mass to damping ratio.
Catarmaran is anyway a good compromise between stability and small immersion. Also for this reason in the recent years the number of Commercial off-the-shelf ASV catamarans is increasing with products like [69], addressed for professional surveyors and [70], especially used for sampling. Hycat is a fully integrated, and rapidly deployable vessel. It is studied for professional surveyors requiring high-quality data, reliability, and rapid deployment. Hycat is also designed to easily navigate shallow areas with propulsion units streamlined with the vessel but not suitable for working properly in shallow environment. In particular M300 Heron [71] is a Catamaran ASV with a wa-

Figure 2.3: *Hycat and Heron commercial ASV catamarans*

terjet propulsion and a modular and expandable system architecture that responds well to some of the above and below mentioned requirements. The enclosed waterjet thrusters protect impellers from weeds and ground contact. Unlike other above mentioned ASVs, Heron can be transported, deployed and retrieved by one person. Heron is a good commercial solution and some research institutions are developing tailored ASVs driven by almost the same logistics requirements. An example is ARCAB [72] which is an open-source vehicle expressly targeted for harsh polar environment responding to lightness, cheapness and reliability. ARCAB operated autonomously in winter-time conditions in Greenland and measured bathymetry and ocean currents in shallow and rocky areas that would make the use of manned vessels too risky. It contributes to demonstrate the potential for a small, portable, low-cost, and open-source ASV to enhance the understanding of shallow, near-shore coastal environments also in harsh environment as Greenland coast.
MARV [73] is another low-cost portable solution to be dismounted and transported. This was specifically developed to be transported by helicopter and backpacked in the Arctic. The resulting system has a modular aluminum chassis, marine grade thrusters, and an open source autopilot system. Both the vehicles are characterised by the use of improper protruding propulsion systems but support the need of solutions based on easiness and flexibility. These criteria are used, as an example, by the Duckling project [74]. Among the interesting projects of portable solutions, the conceptual design

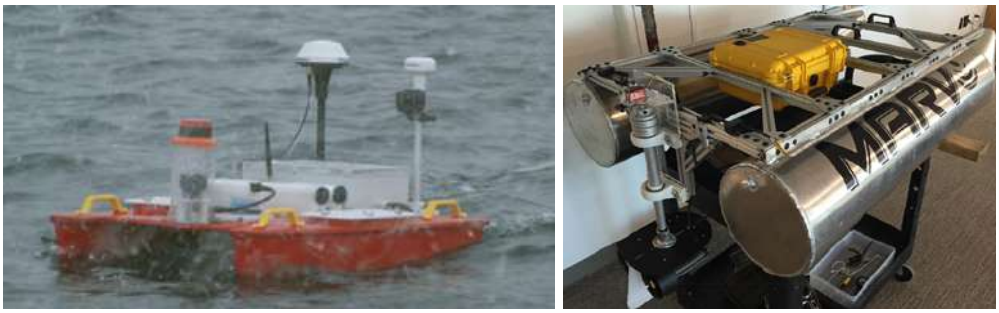

Figure 2.4: *ARCAB and MARV portable vehicles*

of [75] takes into consideration low weight simple concepts and an aerial propulsion which is suitable for shallow water. Aerial propulsion was used by aerRobotix [76] which is a high quality Italian commercial vehicle. This kind of propulsion is used also in an open-source low cost ASV [77] for water quality monitoring in developing countries with low logistics.
Small ASV based on a traditional airboat design with flat bottom have been shown to work robustly in shallow waters [78] but the small size of these vehicles limits their capability in water monitoring and, in case, sampling.
By the way most of the solutions have a simple actuation system that makes difficult to provide high controllability. Solutions with enhanced manoeuvrability where developed like [79], which is a small solution with four thrusters to produce efficient holonomic motions for shallow water archaeology surveys that require highly manoeuvrable robots. A similar configuration is reported by [80] which is a robot designed for future applications of bigger vehicles. The robot is easy to manufacture and highly maneuverable and will be used in cooperative robotics more than in environmental monitoring. An interesting solution is represented by the Catamaran [81] which is characterised by classical main propulsion modules but is equipped with four transverse thrusters to increase the manoeuvrability.

2.3 Monitoring techniques

As shown in Chapter 1 the application of the (WFD) (2000/60/EC) EU Water Framework Directive is pushing the local administrations to increase the number and quality of the water bodies monitoring surveys. In this direction the necessity of unmanned vehicles is becoming more common thanks to the increase in speed, spacial resolution and quality of surveys. If companies are focusing on the development of reliable solutions that can respond to this need, nowadays the attention of researchers is held on the development of new robotic solutions and on the improvement of the searching techniques, that are at the core of environmental monitoring strategies using autonomous vehicles [82]
In Italy, which is a member of the Mediterranean Wetlands Committee (MedWet) [83] the effective impact on Italian robotics is the increasing interest in the construction of ad-hoc solutions to improve the efficiency and effectiveness of wetlands monitoring. In Italy this kind of surveys have started with the ASV Charlie [84], developed by CNR-ISSIA [85], and is continuing with newer and lighter vehicles.
In [86] some case studies of geophysical surveys carried out in different shallow-water environments using an ASVs are reported. The vehicle SWAP based on open technologies and software packages was used in the execution of repeated surveys even in those area not accessible through conventional systems earth scientist that study geological processes.

[87] describes the adoption of the MicroVeGA ASV [88]) optimized for very shallow water in two operational scenarios in the Gulf of Naples, where bathymetric survey with traditional boat is impossible. The adoption of ad-hoc solutions enabled bathymetric surveys to be performed in presence of submerged archaeological remains that produce rapid changes in depth values.
Many of the above mentioned vehicles have been used in various projects all over the world showing satisfactory use of ASV and identifying some of the limits of this technology that anyway is much more reliable than classical methods.
A mono-hull [56] mentioned before was used in a Polish real environment and the article describes how, in the 2017, none of the institutions (maritime offices, Hydrographic Office of the Navy) in Poland had a hydrographic vessel capable of carrying out bathymetric measurements for shallow waters (at depths below 1 m). Here for many years, [89], geodetic basic maps for the protection of many habitats of plant and animal species has been of low quality and it is necessary to update them and improve their accuracy with the use of modern measurement instruments and geoinformatic tools. With new ASV tools some inaccessible areas could be mapped in the 2018.
The use of ASV with a combined survey campaign integrating a side scan sonar and two magnetometers in a gradiometer set-up in very shallow water of the coastal transition zone (land to water) is described in [90], where it is shown that the presence of underwater tools makes it difficult to access extremely shallow environment. This can especially happen if the vessel is not expressly addressed to work in extremely shallow water.
AS state before, shallow waters are present not only in inland waters but also in coastal areas. This is the case of Coral Reefs where monitoring is of critical importance. The use of ASV with simultaneous measurements of bathymetry and reflectance from acoustical sensors in combination with remote sensing was tested for the rapid survey of physical and optical properties of the coconut patch reef [91].
Not only in coral reef but the impacts of human activity on coastal ecosystems are becoming increasingly evident across the world, especially in Italy with recent stormy events [92]. As a consequence, there is a growing need to map, monitor, and manage these regions in a sustainable way. In [93] it is present a novel mapping technique for shallow-water seafloor habitats in Norway coasts: Underwater hyperspectral imaging (UHI) obtained using the Heron [71] commercial vehicle.
Another use of commercial vehicles is reported in [32] where several experiments were performed in Mexico with Qboat [62] with the aim of autonomously performing accurate bathymetric mapping in very shallow waters.
Various papers concerning the development and fieldwork trial of ASV in shallow water were presented in the recent past using multiple marine vehicles like [94] or trying to integrate Aerial and Surface combined robot systems as reported in [95]. An example is reported in [96] that introduces a system named Aerial and Surface Combined Robot System, which consists of a USV, a UAV and a take-off and landing assist during flooding. This kind of multi vehicle in littoral inspections was performed by [97] and [98].
In table 2.1 is reported a list of the ASV defined "for shallow water" that most fit in the requirements for surveys in very shallow water. All these vehicles have its own peculiarities but none of the above mentioned vehicles responds to the whole requirements that were identified. Also for this reason the vehicle SWAMP, subject of this thesis, was conceived based on a list of specific technical exigencies that will be described in Chapter 3. The main requirements are high manoeuvrability, a structure and a system of propulsion suitable for extremely shallow water, portable dimensions, a high modularity and reconfigurability.

Table 2.1: *Characteristics*

	Year	Type	Material	L	B	T	H	W	Payload	Propulsion	Steering	P	V	Endurance	Power	Research
				[mm]	[mm]	[mm]	[mm]	[kg]	[kg]			[W]	[m/s]	[h]		
ARCAB [72]	2019	Catamaran	Fiberglass	900	700	120		25	5	Propeller	Differential	100	0,25	2	Battery	Polar
Heron [71]	2019	Catamaran	Plastics	1300	980	150	320	30	15	Waterjet	Differential			1,7	2,5	Battery	Multipurpose
HYCAT [69]	2019	Catamaran	Plastics	1800	860	150		53	15	Podded Duct	Differential	1500	0,1	1,6	3	Battery	Multipurpose
Z-Boat [62]	2019	Trimaran	ABS Plastics	1270	940	250	320	22	4,5	Podded Duct	Differential			1	4	Battery	
DEVSS [99]	2019	Catamaran	Neoprene inflatables	1500	1450	150	750	45	15	Aerial	Differential	500				Battery	Multipurpose
Duckling [74]	2018	Catamaran	Polystirol	1115	720	80		7,6	10	Ducted Propellers	Differential		0,5	1	6	Battery	Mapping
Lizbeth [53]	2017	Catamaran	Fiberglass	2500	1800	150		120	150	Protected Propeller	Differential		1	1,5		Battery	Limnology
Microvega [88]	2016	Catamaran	Inflatables	1350	850	150	500	20	15	Podded Propeller	Differential	400	2		3	Battery	Bathimetry
Si-USV [54]	2015	Trimaran	Fiberglass	2100	1600	170		140	80	Waterjet	Waterjet				8	Battery	Shallow
MARV [73]	2015	SWATH	Aluminum	1210	900	150	300	60	60	Podded Duct	Steering Module			1	6	Battery	Arctic Remote
CATONE [100]	2015	Catamaran	Plastics	1600	1200	150		20	12	Aerial	Differential			1,3	8	Battery	Limnology
Aquadrone	2015	Catamaran	Plastics	1170	360	150				Propeller	Differential					Battery	
The HydroNet ASV [51]	2014	Catamaran	Fiberglass	1991	1164	180		85	20	Protected Propeller	Rudder	250	0,25	1,25	6	Battery	Coastal
ASC [101]	2013	Catamaran	Plywood	1500	1000	370	500	146		Podded Propeller	Steering Module			1		Battery	
ASV [48]	2008	Catamaran	Aluminum	2700	1480	130	360	60	60	Podded Duct	Differential	1500	0,25	2,2	2	Battery	Coastal
NIMS-AQ [29]	2008	Catamaran	Plastics	2200	1250	200		100		Tethered	Differential pull		0,1	3	12	Battery	Sensing
The WASP [64]	2005	SWATH	Fiberglass	2400	1700	300		60	100	Propeller	Differential				8	Battery	

Chapter 3

Project Requirements and the SWAMP concept

As stated in in Section 2.1 there are several peculiarities that are common to most of the Wetlands that represent design constraints to study an autonomous *survey* system. Wetlands are characterised by shallow water, low logistics, difficult access with steep and slippery terrains, swampy muds and flowing water.

3.1 Vehicle Design Parameters

A series of project requirements have been identified to drive the design of an ASV for the monitoring the Wetlands. These Project requirements derive both from the experience of CNR-INM (former group of Marine Robotics of CNR-ISSIA) and MACP Hovercraft [102] operators and the analysis made with DITEN department of *University of Genoa*.
CNR-INM has a long experience with UMV design and exploitation. *ALANIS* boat has been developed for coastal monitoring [103], Charlie is a catamaran used for bathymetric surveys [104] and sampling also in Antarctica [84], while the semi-submersible vehicles *Shark* and *Proteus* have been used for sampling in dangerous areas in front of Arctic Tidewater Glaciers [36], [105] [4]. Recently *e-URoPe* ROV [106] has been used in coastal waters for environmental monitoring purposes related to the mapping of Posidonia meadows [107].

Technical specifications

The earlier mentioned requirements identified for the ASV can be listed in:

- General arrangement:
  The number and variety of surveys that can be performed goes from morpho-bathymetric and stratigraphic surveys up to biological, chemical and physical samplings. To perform different analyses, the vehicle should be modular and flexible. Modularity and reconfigurability are fundamental parameters. The vehicle should be a multi-purpose craft allowing different payloads. Ideally it should be a floating platform with enhanced manoeuvring ability and a high capacity of adapting to the various types of missions such as repetitive tasks, efficient scan, sampling in specific spots, pre-programmed trajectories.
  Moreover, dealing with a novel robot, the vehicle should be modular also to allow for robotic improvements and research.

- Overall dimensions:
  Dimensions are fundamental to give constrains to the design. The access to some of Wetlands and critical zones can be done only with small cars, boats or helicopters. For this reason the vehicle has to be easily transportable in standard trunk. Standard dimensions of the cargo space are 1350 mm x 1400 mm and so for a good logistics the optimal dimensions for the ASV

are considered as:
length $\leq$ 1400 mm, width $\leq$ 1200 mm, height $\leq$ 700 mm.
Regarding the weight, transportability is one of the main parameters in harsh environments. Usually two or more operators have to carry the vehicle to the zone where it will be deployed. Therefore the maximum weight has to be contained within a maximum portability parameter taking into account the *UNI-EN 1005-2 Safety of machinery-Human physical performance* standards.
Total lightweight including batteries should not exceed a maximum of 50 kg when transported by two people.
A reasonable payload can be mounted in-situ and it should be around a maximum of 20 kg.
The driving requirement leads to the idea of designing a robot that can be dismounted and transported by one just person, with a maximum transportable weight of 25 kg, as shown in [108].

- Operative speed, weather conditions and autonomy:
  standard surveys require a battery life of at least 4 hours for full operations including sampling. Since standard operations do not require very high speeds, the maximum speed is only considered during transition paths or to counteract strong streams.
  Maximum adverse current is considered to be 1.5 m/s, and wind up to 20 $knots$. For this reason the maximum speed for the vehicle is $1.5 - 2$ m/s. This value is a compromise between autonomy, battery weight and cost and takes into consideration the maximum speed normally used during underwater surveys, which do not exceed 0.75 m/s.

- Controllability: the vehicle should be able to access restricted spaces and have the possibility of sampling in specific areas even in the presence of external disturbances (current and wind). For these reasons the vehicle should be controllable both during the path and during the maintenance of a station. An adequate propulsion layout is essential.

- Draft and propulsion:
  since we are dealing with shallow waters, the maximum draft is a fundamental parameter to be considered and it is identified in 200 mm. The propulsion unit choice, better shown in Chapter 5, should be adequate to access in very shallow waters without the risk of damages that can be caused e.g. by grounding, vegetation, ice.
  In shallow waters, propulsion units with free propellers or ducted propellers are efficient but subject to damages, caused by obstacles at low depths or to breakages due to the suction of extraneous objects and therefore not recommended. Hull-contained propellers (e.g. Charlie [84]) have very low efficiencies and should be avoided. On the other hand, the use of a waterjet unit could be a good choice, especially because of the lack of protruding appendices solves the problems of drafting and navigation in shallow waters (e.g. Sonobot [109]). However, this system is penalized by low efficiency at low speeds [110] and by suction issues.
  The adoption of paddle wheels could be a good solution for shallow water problems (also in mixed terrain) and its adoption has recently been investigated by [111] and [112]. A paddle wheel system that includes a wheel for both sides of the vehicle has already been used in manned applications and proved to be exceptionally manoeuvrable and with good directional control [113]. One of its variations could be the systems that are already widely used in amphibious vehicles that use wheels, tracks or screw-propelled [114]. Another solution is the aerial propulsion used by AerRobotix [76]. This is a good solution but has the disadvantage of noisiness and low thrust efficiency, resulting in higher power consumption especially in case

of adverse currents.

- Impact ability:
  Since the vehicle will be deployed in harsh environment, it is required that the hull structure, the system of propulsion and the sensors supports are designed and built taking into account the possible impact of the vehicle with stones, shores, roots or similar that can damage a fragile structure with consequent loss of the vehicle or have a bed effect on the sensors. For this reason also the sensors should be Protected from external impacts.
  Soft structures and innovative materials are of great help.

- Use of inert materials:
  Since wetlands are often protected areas with a peculiar biodiversity, it is important to adopt inert materials as in ([115]) for the construction of the solutions. The use of inert materials is requested for the reduction of chemically invasive agents.

- Power supply:
  Electric systems and batteries have to be chosen for power supply.
  The use of materials and power sources that do not have an impact on the monitored areas is a design constraint because the monitoring should be minimally invasive. Missions have to be carried-out in zones with environmental restrictions in which acoustic noise and pollution have to be kept at a minimum.

- Protection:
  The totality of vehicle components must have a degree of resistance to atmospheric agents at least *ip68* (protection from continuous immersion at least 1 m).
  Temperature may be many degrees under 0°C in harsh environment. The use of material and protection for elements adequate to low and high temperatures is important.

- Navigation mode:
  The vehicle should be remotely controllable within a range up to 500 m. Autonomous use with pre-set route and remote control should be implemented. Wi-Fi or radio-modem communication systems have to be provided. Telemetry has to be recorded in a data logger. Communication system should be installed on-board.

- Basic Payload:
  A basic payload will should be mounted on the vehicle. It has to be composed of one or two cameras (one can be infrared (IR), allowing night view) and live viewing during operations from the control station on the shore, either an Inertial Motion Unit (IMU) or an Attitude and Heading Reference System (AHRS) and a GPS system for precise data acquisition. RTK-GPS will increase the precision of the positioning.
  Other basic payload may be constituted by an altimeter and data logging of basic parameters such as air temperature, surface water temperature and sensor of wind direction and intensity.

- Survey Payload:
  The vehicle can be equipped with different payloads depending on the type of mission:

  – Multi-parameter monitoring mission:
    In this mission the vehicle has to perform data recording by precisely keeping a position. The payload is composed of a deployable underwater multi-parameter probe (with sensors for conductivity, temperature, fluorescence, depth, turbidity, pH and dissolved oxygen etc.) and air parameters probes.
    A winch for the deployment has to be studied.

  - Sampling mission:
    In this mission the vehicle has to be equipped with a water sampling system. This kind of system can be deployed underwater or on the surface. This may be implemented by a sampling system for liquid/film present on the surface (algal blooms, hydrocarbons, foams).
    Water sampling significantly contributes to the final total weight of the vehicle.
    The vehicle should be able to sample big quantities of water, thus having the possibility of modifying its draft and with a buoyancy reserve sufficient to carry all the samples and the equipment without a big increase in the initial draft, that can reduce the operative profile of the vehicle.
  - Morpho-bathymetric and stratigraphic surveys:
    In this type of mission a platform is required with different kind of sensors to be mounted in the hull, under free water surface or in direct contact with water which are used for bed mapping and monitoring: multi-beam sonar, single-beam sonar, side-scan sonar, Sub-Bottom Profile, Magnetometer, Ground penetrating radar.
    The use of underwater scanning system requires to have a stable platform.
    Also this kind of sensors has a significantly high contributing to the final total weight of the vehicle.
  - Cooperative mission, Aerial drone landing and take-off survey:
    In this kind of mission the presence of enough space for the take off and landing of an aerial multi-copter drone, whose dimensions are contained in a diameter of 550 mm, is required.
    Video cameras and other sensors can be installed on board for monitoring the mutual interactions of the two autonomous vehicles.

- Open Hardware and Software architecture:
  The vehicle should have an open hardware and software architecture and it will thus have the ability to easily mount different payloads and in manifold working configurations.

- A highly stable hull configuration:
  As shown in Chapter 2 the number of vehicles used today for unmanned surveys is high [37] but the geometric typologies are essentially the monohull and the catamaran (or multi-hull). While the monohull vehicles are studied to travel wide sections at high speed (not suitable for the restricted and difficult-to-access areas of wetlands), the reduced stability does not allow the precise use of sensors for monitoring and scanning of the seabed. Moreover, as stated in the previous point, the payload capability has to be maximised and therefore a good trade-off is the adoption of multi-hulls such as Catamaran and the SWATH (Small Water-plane Area Twin Hull). By adopting a double hull, it is possible to create platforms characterized by a capacious payload space, constituted by a wide main deck above the surface, and submerged or semi-submerged structures that contain control units, propulsion units, batteries and payload, and that provide buoyancy.
  The catamaran type is most suited for this type of survey: it is stable enough to support analysis with sensors of any kind, has a good load capacity and allows the use of double propulsion systems that can be used in a differential configuration, increasing the manoeuvring capacity. Catamarans also allow the possibility of innovative constructive solutions which are always possible thanks to the multi-hull flexibility, as demonstrated by the Wam-V [116] with its articulated catamarans.
  The Small-Waterplane-Area Twin Hull (SWATH) solution has the peculiarity of being very stable and less subject to interface effects, but due to its submerged nature, it is not so suitable

for operating in shallow waters and for this reason also the other submerged geometries are not suitable too.
A very interesting solution could be the air cushion design, that would certainly be a novelty but the unmanned technology is at very preliminary stages in this field.

- Wide deck:
  Furthermore, most of the above mentioned requirements suggest the presence of a wide main deck on the top of the vehicle.

3.2 The operative requirements

From the above described points it is possible to understand that the requirements are often hardly compatible with each other and the choices to be made are constrained. For this reason it is necessary to use ad-hoc solutions that are suitable for the environment in which the vehicle will operate and are, at the same time, well balanced with the other requirements.
A resume of the main geometrical characteristic required for the design of the ASV is reported in table 3.1.

Table 3.1: *Characteristics*

Type:	Catamaran / Twin Hull / ACV	
Main Requirements:	Modularity & Flexibility	
Propulsion:	Suitable for shallow waters	
Maximum Length	$[mm]$	≤ 1400
Maximum Width	$[mm]$	≤ 1200
Maximum Height	$[mm]$	700
Maximum Draft	$[mm]$	≤ 200
Design Draft	$[mm]$	≤ 150
Maximum Lightweight	$[kg]$	45
Expected Payload	$[kg]$	20
Total Weight	$[kg]$	65
Payload Area	[mm x mm]	$\leq$ 950 x 950
Autonomy	$[h]$	4
Operating speed	$[m/s]$	1
Water Current	$[m/s]$	1.5
Wind Speed	$[kn]$	20
Maximum wave height	[mm]	~300
Expected Consumption	$[W]$	$300 \div 800$
Battery voltage	$[V]$	36 *or* 48

Chapter 4

Vehicle Design

Figure 4.1: *SWAMP (Shallow Water Autonomous Multipurpose Platform)*

4.1 Design methodology

In the common sense the *Applied research* is the effort aimed at using basic research for solving problems or developing new processes, products, or techniques. This concept usually brings to *Innovation* [117] which is the process of translating an idea or invention into a good or service that creates value or for which customers will pay. Innovation often results when new ideas are generated and converted into useful products, the application. *Application* is the practical impact of a scientific discovery in the form of a product or service that is innovative.
These concepts are applied in order to further satisfy the needs of a customers.

The design of SWAMP was driven by the application (a specific need) that led to research (new concepts to be applied) and can bring to innovation (an appealing system).

This means that a novel design technique was applied. And, as a consequence, the classical ship

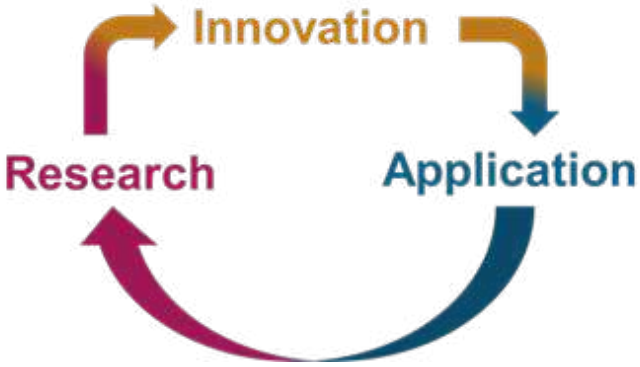

Figure 4.2: *The relation between research, innovation and application applied to SWAMP design*

design spiral [118], which is a traditional way of describing the design project, resulted inapplicable and unreliable.

The design spiral, describing the vessel design at every iterative level, is useful to describe an acknowledged complex process. Particularly, it recognizes the vessel design as an interactive and converging process. But in case of a novel design, the smoothness of the process is not the same, in the case of SWAMP a balanced solution had to be found to search for a compromise between conflicting requirements. The design output, namely the perfect balance between these requirements, does not lead to the optimised solution but to optimum reachable.

This means that every step has to take simultaneously into consideration a variety of parameters that have to be continuously balance at the same time. This brings to a final design without need of iterative processes.

In the SWAMP design the conflicting requirements have led to solutions that seemed to be inconvenient if watched from their perspective (e.g. higher wave resistance) but that resulted to be the correct if watched from the global project perspective.

4.2 The SWAMP Vehicle

4.2.1 The general layout

On the basis of the requirements described in Chapter 3 an Autonomous Surface Vehicle which characteristics can be modified by specifications of the different missions and task was designed. The vehicle, whose acronym is SWAMP, is called *(Shallow Water Autonomous Multipurpose Platform* is shown in fig. 4.1, is an unmanned surface vehicle expressly conceived and designed to work in shallow and confined waters.

The vehicle is a sum of innovative concepts that are summarised in fig. 4.4 SWAMP is a full-electric Catamaran 1.23 m long with a design breadth of 1.1 m; by adopting a sliding structure the breadth is variable between 0.7 m and 1.25 m. The hull height is 0.4 m and the vehicle with the structure and the antennas is 1.1 m high. SWAMP lightweight is 38 kg with a draft of 0.1 m, the standard maximum payload is 20 kg with a consequent maximum design draft of 0.14 m but the reserve of buoyancy of SWAMP allows to embark up to 60 kg with a draft of 0.22 m. The small dimensions of the vehicle comply with the idea of a reduced logistics.

The hull shape is inspired by the double-ended Wigley series but with a flat bottom as shown in

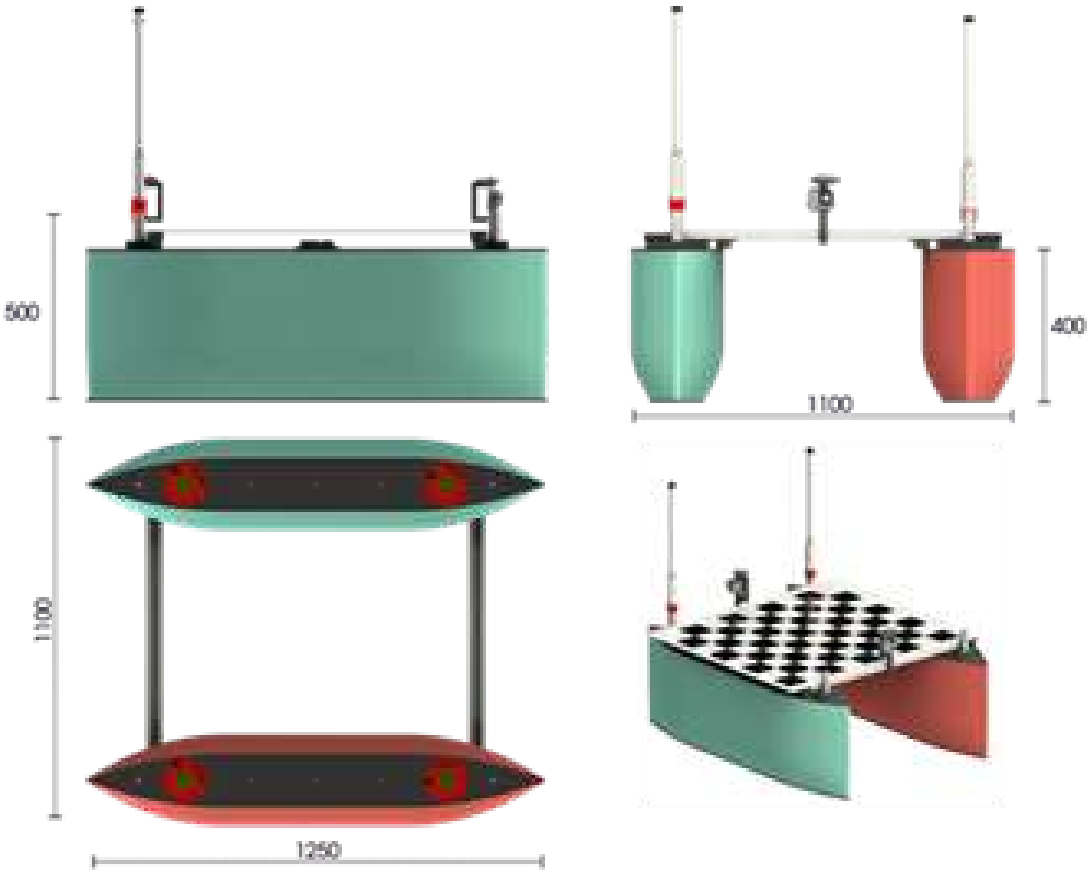

Figure 4.3: *Vehicle general layout with measures*

fig. 4.3. The double-ended hull form and propulsion system is characterised by equally efficient sailing ahead and astern with the possibility of manoeuvring in narrow spaces. This hull shape is characterised by longitudinal centre of buoyancy LCB centered mid-hull and, usually, large B/T ratios. The hull configuration shape was chosen both for hosting four Pump-Jet type 360° azimuth thrusters expressly designed and studied for this project and to create an innovative structure that also avoids the presence of sharp edges on the hull bottom. Indeed one of the main peculiar aspects of SWAMP is the use of light, soft and impact-survival flexible structure made with a sandwich of soft closed-cell HDPE foam, HDPE plates and pultruded bars. With this design SWAMP is a completely modular vehicle that can be dismounted and transported to be remounted in various possible configurations. This flexible design allows to host various types of tools, thrusters, control systems, samplers and sensors. Also for this reason for the propulsion the choice has fallen on the design of a modular propulsion unit based on Pump-Jet that can be easily installed on the vehicle. Such a solution allows also to remove, if necessary, some of the thrusters and/or substitute them with sensors, tools or even other thrust units. Using four azimuth thrusters gives SWAMP the controllability that is required for high quality surveys.

One of the main peculiarities of SWAMP consists in the fact that each hull is conceived to be a single vehicle with its propulsion, navigation, guidance and control (NGC) and power system from the battery. Each monohull results to be an ASV and, thanks to the azimuth thrusters, is highly controllable. Moreover the intelligent core of each vehicle controls the monohull but is able to take over the control of the entire vehicle in the event of failure of the other core. This possibility is guaranteed by the existence of a Wi-Fi-based communication architecture.

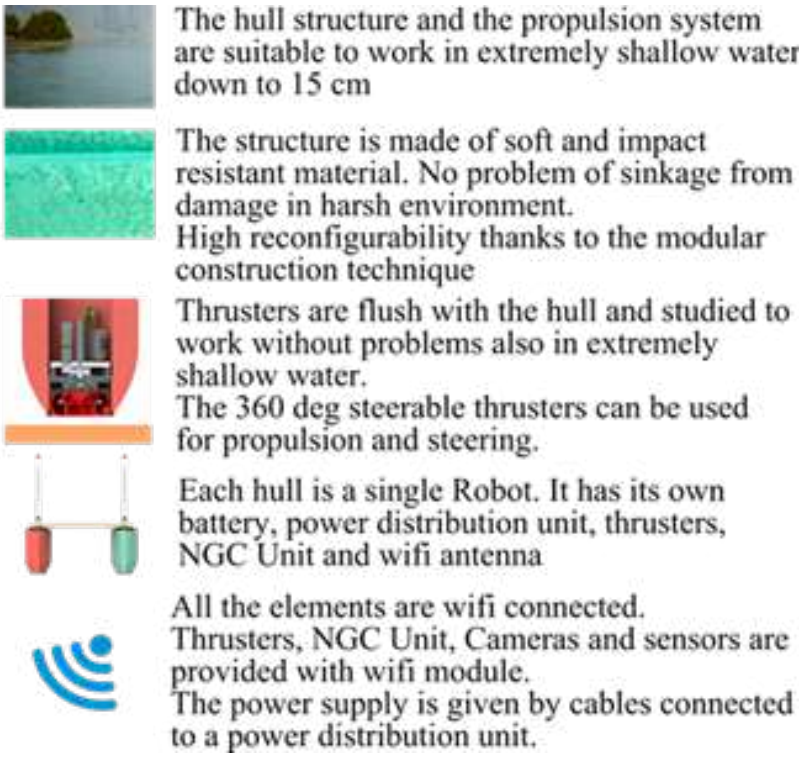

Figure 4.4: *The main novel concepts of SWAMP*

Maximum speed of SWAMP in infinite depth waters is $1.6\,m/s$, while the speed in extremely shallow waters down to $200\,mm$ is reduced to $1\,m/s$ due to the peculiar hydrodynamic effects occurring in shallow waters and better illustrated in the following sections.
The software architecture of SWAMP is based on Commercial off-the shelf components. As mentioned before one of the main hardware innovations introduced in SWAMP is the elimination of most of the possible wiring reducing the number of wires to just the power connections.
The basic NGC package of each hull is composed by an IMU and a GPS. The communication is created by one communication module each hull that provides a communication framework for both its same hull and for the other hull's modules when its work is required. A resume of the main characteristic of SWAMP is reported in Table 4.1.

Table 4.1: *Characteristics and native payload*

Type:	Double Ended Catamaran
Overall Length	[mm] 1230
Minimum Breadth	[mm] 700
Maximum Breadth	[mm] 1250
Distance Between Hulls	[mm] 800
Construction Height	[mm] 500
Maximum Draft	[mm] 150
Light Weight	[kg] 35
Maximum Weight	[kg] 60
Buoyancy Reserve	[kg] 70
Propulsion Unit Thrust	[N] 12.5
Propulsion Units	nr 4
Autonomy at maximum power	[h] 2
Operating Speed	[m/s] 1
Maximum Speed	[m/s] 1.6
Mean Energy Consumption	[Wh] 400
Voltage	[V] 44,4
Single Battery	[Ah] 13
Number of batteries	nr 2
Communication	Wifi - Radio
Steering Ability	DP
NGC Sensors	2 x (GPS, AHRS, Camera)

4.3 Hull and Structure

4.3.1 The concept and Vehicle Layout

As mentioned before and as shown in fig. 4.3, SWAMP is a Catamaran ASV with double-ended hulls. Catamarans allow to have much more payload space than on monohulls, they are more stable, have smaller draft with higher payload and the presence of thrusters on each hull gives the possibility to manoeuvring in narrow space with agility. Achieving a good stability was the main driver in the choice of the Catamaran shape since payload elements like (single or multibeam) sonars used for mapping the bottom request for stable platform with less roll and pitch motions. Another point in this direction was the possibility of having a wide payload area suitable for modularity and reconfigurability. Such a solution make it possible to host the docking and take off of an aerial vehicle as described in [95].
The main idea behind the choice of double-ended hull was the possibility of coupling this solution with the adoption of four azimuth thrusters to be adequately manoeuvrable also in restricted waters and in presence of external disturbances.

4.3.2 The soft sandwich structure

This section outlines the structural solution for the hulls of the vehicle. As above mentioned, each hull consists in an unsinkable element principally made of a very low density non-hygroscopic Polyethylene (PE) foam based on the concept of Softhull [119] already adopted for bigger vehicles. This material is globally rigid but locally very elastic and capable of absorbing shocks and matching the deformations due to impacts with external bodies. In harsh and extremely shallow environment the impact with external bodies is probable since rocks in rivers, icebergs in polar environment, boats, shores, transportation may affect the structural integrity of the vehicle.
Vehicles made with thin layers of fibreglass, aluminium or plastics with the time become subject to wear that limits the operative profile of the vehicles. In-fact it is hard to see one of the existing

vehicles that makes surveys near the shore or on a mountain stream (not without the worry of the operator).
Each single hull structure is constituted by a Soft Sandwich Structure solution consisting in an unsinkable hull made of foam. Such a material is very elastic and capable of absorbing shocks and

Figure 4.5: *The single hull. The holes for the fast on-board systems installation can be seen.*

matching the impacting deformations. Due to its lack of rigidity the foam has to be stiffened by the creation of a stiff structure. This is made by creating a new sandwich structure composed by a skin of $8\,mm$ HDPE plate at the bottom, various horizontal sections of $45kg/m^3$ PE-foam and another plate skin of $8\,mm$ HDPE. Vertical elements made with pultruded bars and threaded plastic bars are used to compress the sandwich and create a globally rigid structure. The resulting structure is illustrated in fig. 4.6. The presence of the skin that covers the entire bottom surface of the hull and donates a global stiffening to the entire structure also acts as a protection element for both the foam and the sensors and actuators present in the hull. The propulsion units, the sensors, the batteries and the intelligent core of each hull are hosted into $125\,mm$ diameter holes drilled in the foam. When no element is present in the holes these are filled with a cylinder of the same PE foam.
The hull made with bulky volume of foam is advantageous: the non-hygroscopic PE foam prevents the water from entering the hull giving an intrinsic reserve of buoyancy, the events of laceration/-hole/tearing do not affect buoyancy, the soft structure protects sensors and actuators from external loads and impact (e.g. ice falling, impact with shore in coastal areas or rocks in rivers) also reducing the disturbances and vibrations due to transport: the foam permits the shock adsorption.
Some vehicles made of foam where recently studied and constructed in styrofoam [120], foam-cored with a composite skin [121] or with a PVC rib [122] thus resulting unsinkable but without the advantage of the elasticity given by the PE-foam that allows the vehicle to absorb impacts and to dampen the vibrations. Vehicles with side bumpers may take advantage of a similar characteristic but an impact with the bottom may be dangerous for the intactness of the vehicle.
The catamaran is composed by two hulls made with the above described sandwich structure and weighing $7\,kg$ each. The hulls are connected with two pultruded C-shaped bars that are studied to slide on their supports. The supports, made in HDPE are structurally connected to the upper HDPE plate. The sliding elements make it possible for the catamaran breadth to be modified in function of the operational requirements. This solution also allows the hull to be dismounted and easily transported and allows the vehicle to be splittable into two different monohull vehicles. The catamaran deck is constructed either with a thin panel or with a series of plates that are installed on the two transversal bars.
Modularity was one of the main ideas behind the conception of this kind of structure. Every hull

Figure 4.6: *Expanded view of the Hull sandwich*

can be composed of more or less sections of lightweight foam. Operational needs may lead to a reduction of the number of sections, to the increase or modification of the geometry of the sections. As examples the hull geometry may be modified to increase the volume and reduce the immersion or to augment stability or to reduce the drag. The height of the catamaran can be modified as an example to reduce the effect of strong adverse winds or to increase the seaworthiness. Modularity concept is supported by the solution of holes drilled in the foam. This allows to think the hull as a modular structure where propulsion units, batteries in a various number, sensors and payloads may

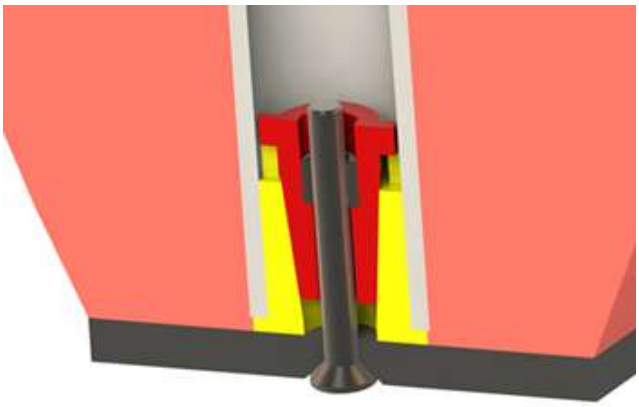

Figure 4.7: *Particular of the conic joint that connects the lower panel and the pultruded bar*

Figure 4.8: *The rigid frame of SWAMP structure*

be positioned or removed from the hull by just pushing into or pulling from the holes.
The vehicle is constituted by the two hull and the two connection bars while most of the payload like winches, samplers, sensors, landing pads etc.. can be installed on the payload deck.
The final weight of the entire catamaran structure is $15\,kg$.

As far as the materials are concerned the characteristics of the used elements are reported below.
PE is a strong and resilient closed-cell foam. It is rot-proof, resistant to fungus and bacteria and non-toxic. For all these properties it is widely used in the production accessories for sea, gyms and swimming pools and its shock-absorbing characteristic makes it a fundamental part of running shoes. Ideally suited as a shock absorbing product, this closed-cell foam is a great way to dampen the effects of vibrations.
As shown in [123] PE foam behaves according to elastomeric foam materials laws and it is characterised by a high elasto-plastic phase where recovery happens up to big deformations.
PE foam produced for physical expansion, offer high performance at low cost. Being made up of

closed micro-cells is waterproof, resilient and has good resistance to compression at less than 10% of strain, as shown in the graphic of fig. 4.9). In particular, the closed cells are filled by gas which augments the resistance to permanent deformation: when it is stressed the pressure of the gas opposes the compression aided by the tensile strain of the faces constituting the polymer [124]. The characteristics of the material used in SWAMP manufacturing are reported in table 4.2. The low

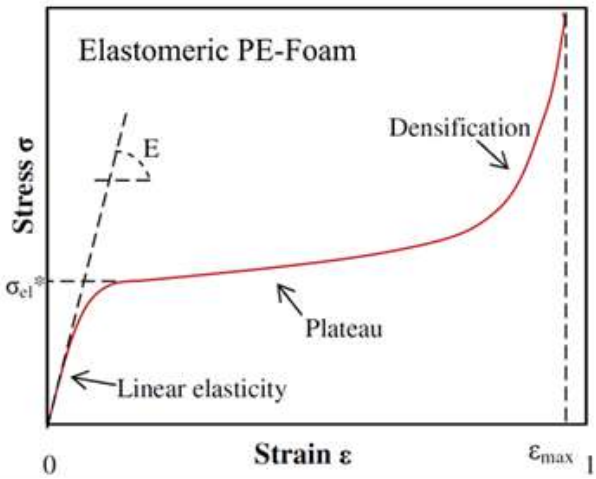

Figure 4.9: *Non Hygroscopic Closed Cell Foam Compression Curve [125]*

thermal conductivity of PE foma gives it excellent heat resistance suitable to work both in hot and extremely cold (polar regions) areas.

Besides having effect of protecting the foam from the attrition, the bottom HDPE plate also has

Table 4.2: *Characteristics of the materials. Compressive Strength, is the force necessary to produce a 25% compression over the entire top area of the foam specimen.expresssed as kPa*

Charcateristic	Unit	Value
Density	$[Kg/m^3]$	42-48
Hardness	$[(JisC)]$	27-32
Tensile strength	$[KPa]$	500
Tear strength	$[Kn/m]$	4.00
Elongation @ break	[%]	150-200
Compressive strength (25%)	$[KPa]$	60
Water absorption	$[g/cm^3]$	0.002
Thermal conductivity	$[W/m.C]$	0.040
Service temperature	$[°C]$	-70 / +70

the effect of distributing the punctual tensions produced by sharp surfaces to a wide portion of the foam. In this way it is eliminated the passage of the foam from the elastic phase to the the plateau phase when resting on the shore or on during transport. In fact the passage to hysteresis loops in the plateau zone, which produces a plastic stretching of the cell's walls [124], leading to a loss of volume and thus of buoyancy, is avoided.

The functional logic of this soft structure is absorbing most of the stresses and only a small amount of these is transferred to the on-board systems that are contained in the structure With this solution the hull assumes the required characteristic of being locally soft but globally rigid.

HDPE has a high impact resistance, outperforming some commonly used aluminium alloys. It behaves according to visco-elastic materials laws, further it is highly deformable: after the elastic phase there is a long plastic phase as shown in fig. 4.10. which gives the possibility of deforming under external loads up to high values without breaking. If an applied load is released (without creep rupture), it is possible to observe an immediate elastic recovery equal to the elastic deformation,

followed by a period of slow recovery. HDPE in most cases does not recovery to the original shape and a permanent deformation remains, the magnitude of the permanent deformation depends on the time of strain and on the temperature.

One of the main characteristics of HDPE is the not negligible property of slickness. For transport

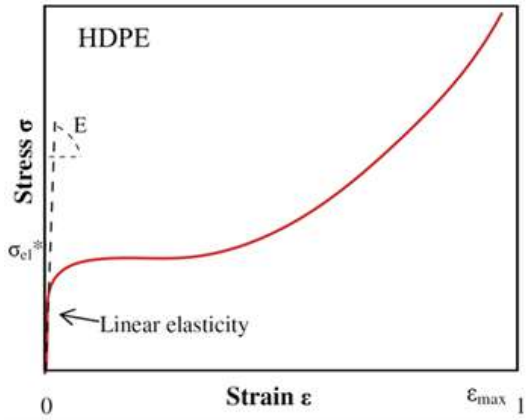

Figure 4.10: *HDPE Behaviour [126]*

and deployment and When moving in shallow water the slickness allows to slide minimising the stranding.

The characteristics of the HDPE used in SWAMP manufacturing are reported in table 4.3. Both

Table 4.3: *Characteristics of HDPE*

Characteristic	Unit	Value
Density	$[g/cm3]$	0.95
Yield strength	$[MPa]$	28
Elongation at break	[%]	300
Tensile elastic module	$[MPa]$	850
Elastic flexural modulus	$[MPa]$	850
Flexural strength	$[MPa]$	40
Hardness with ball penetration H358 / 30	$[MPa]$	45
Creep traction test: 1% elongation	$[MPa]$	3
Dry dynamic friction coefficient on polished steel	$[-]$	0.29
Dry wear value on steel	$[\mu m/km]$	1.0
Thermal conductivity	$[W/(K*m)]$	0.38
Linear expansion coefficient	$[10^{-5}\,K^{-1}]$	18
Range of temperatures	$[°C]$	-100 / +50
Water absorption at saturation	[%]	$\leq$ 0.01

PE foam and HDPE have the peculiarity of good resistance in salty environment moreover both are inert materials. The adoption of inert materials for the whole structure (exception made from bolts) allows to work well in protected environment without influencing the biological analysis and to perform different kind of sampling (e.g. heavy metals).

The main structure is composed by Pultruded Bars. Pultrusion is a continuous process in which fibers reinforced with a duroplastic resin are impregnated. The resin-impregnated glass fibers are pulled into a hot matrix, where hardening takes place and the shape is taken.

The results of this process are therefore fiberglass reinforced composite elements that have a high resistance to corrosion and atmospheric agents and UV beams with a tensile module that can be compared to Steel and is higher than aluminum as shown in fig. 4.11.

Moreover these elements are light, with a density of 2000 kg/m^3 The characteristics of the PRVF bars used in SWAMP manufacturing are reported in table 4.4. These elements, thanks to their

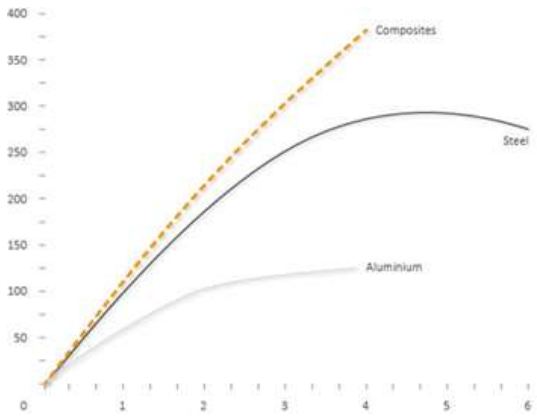

Figure 4.11: *Pultruded bars behaviour [127] in comparison with Steel and Aluminum*

Table 4.4: *Characteristics of the pultruded Bars*

Charcateristic	Unit	Value	
		Z	X
Density	$[kg/m^3]$	2000	
Tensile strength	$[Mpa]$	250 - 450	20 - 60
Flexural strength	$[Mpa]$	250 - 450	20 - 60
Modulus of elasticity and flexion	$[Mpa]$	25000	9000
Torsion resistance	$[Mpa]$	25000	9000
Breaking strength Resistance to compression	[%]	1,0 - 1,8	1,0 - 1,8
Resistance to compression	$[Mpa]$	150 - 300	30 - 60
Compression module	$[Mpa]$	10000	4000
IZOD strength	$[kJ/m^2]$	90 - 120	
Barcol hardness	$[-]$	> 40	
Temperature	$[°C]$	-100 $+155$	

stiffness, where used to make a stiff global structure as the one shown in fig. 4.8.

4.3.3 The soft structure manufacturing

The hull was built by adopting an ad-hoc system of construction expressly studied for this brand new structure. The hull shape choice is better explained in Section 4.3.4.
The hull foam horizontal sections were machined by fastening foam plates to the CNC machine and milling the flexible and soft foam with a $10\,mm$ milling cutter ($7000\,rpm$ and $2000\,mm/s$). In fig. 4.12 is depicted the machining of the hull. The foam is fixed to the table using the holes drilled to host the pultruded elements constituting the structure.

Figure 4.12: *Pictures of the hull machining process*

The same machine used to mill the foam was used to cut the HDPE plates with a $3\,mm$ milling cutter ($7000\,rpm$ and $2000\,mm/s$). The conical connecting elements where built in PLA with a 3D printing machine.
This kind of structure and construction technique can be used also for bigger vessels that present the same issues as SWAMP.
The vertical and transverse elements made bars are commercially available elements obtained from pultrusion. A continuous process for extruded manufacturing of composite materials with constant cross-section.
The elements resulting from these processes are reported in fig. 4.13. In the second and third from left pictures at the top show the HDPE elements that slide inside the C-pultruded bars.
In fig. 4.14 it shown the construction of the sandwich using the tirants. The tirants are Nylon threaded bars hooked to the bottom HDPE plate and pulled by using screw nuts.
In fig. 4.15 the whole process of creation of the structure is shown with the final resulting hull sandwich structures. The two hulls are connected with the two transversal bars. These allow the vehicle breadth to be modified in function of the need.

Figure 4.13: *Some pictures of the construction process of the conical elements and of the structure*

Figure 4.14: *Pictured showing the tirants*

4.3.4 Naval Architecture of SWAMP

This section describes the Naval Architecture design of SWAMP with the tests performed in shallow waters characterised by peculiar effects on the vessel's hydrodynamics. For the seeking of maximum usability in harsh environment it was logically inevitable to mediate to find a good matching between controllability, integrity, transportability, payload requirements and hydrodynamic performances. The main driving parameters were:

- the length contained within $1250\,mm$
- a vehicle weight of $35/40\,kg$

Figure 4.15: *Some pictures of the construction process*

- a payload of $25/20\,kg$
- a maximum draft of $150\,mm$
- the Pump-Jets fitting with a flat bottom and the double-ended shape
- the operative speed of $1, m/s$
- the maximum speed of $1.75, m/s$
- the pursuit of simple hull shapes for the easy manufacturing of the PE-foam
- bow-stern symmetry

Bow-stern symmetry was decided to increase the controllability of the vehicle. This kind of symmetry is applied for its versatility in double-ended ferries (DEF) [128]. These boats are used in congested waters, confined ferry terminals and in shallow water conditions for their manoeuvring ability leading to a substantial reduction in cruise time [129]. As in SWAMP the DEF operative profile in shallow water in many cases leads to larger boats with a shallow draft.
The symmetry with respect to mid-ships constrains the hydrodynamic characteristics of the vehicle resulting in a LCB centered mid-ships irrespective of the vessel design speed and a symmetrical (fwd/aft) propulsion arrangement.
Even if various DEF hull exist [128] the SWAMP hull shape was designed on the basis of the equations of a mathematically defined hull shape: the Wigley hull. Wigley hull is a series of double-ended hulls widely studied in literature [130] especially for canoes and, for their geometric shape, for the comparison with other hull shapes. As an example some slender body wigley hull analysis were performed also in shallow water with numerical simulations [131].
The SWAMP wigley hull was designed with a central cylindrical element to increase the buoyancy and reduce the draft. The bottom was cut at a certain height to host the Pump-Jet Module

propulsion units that should be flush with the hull and whose diameter was chosen to $120/, mm$.
The Wigley Hull equations used for SWAMP are the following: For $x > a$ and $x \leq l + a$.

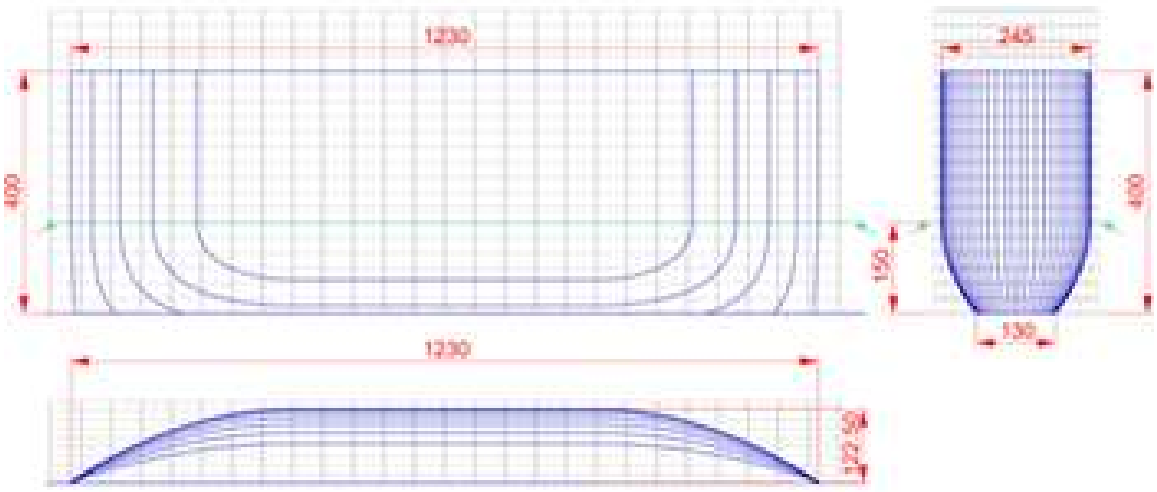

Figure 4.16: *SWAMP lines plan*

Upper-works:

$$y(i,j) = (B/2) * \left(1 - (\frac{x(i) - a}{l}\right)^2\right) \tag{4.1}$$

Below free-board:

$$y(i,j) = (B/2) * \left(1 - \frac{z(j)}{T_{prog}}\right)^2\right) * \left(1 - \left(\frac{x(i) - a}{l}\right)^2\right) \tag{4.2}$$

For $x \leq a$ and $x > -a$
Upper-works:

$$y(i,j) = (B/2) \tag{4.3}$$

Below free-board:

$$y(i,j) = (B/2) * \left(1 - \left(\frac{z(j)}{T_{prog}}\right)^2\right) \tag{4.4}$$

For $x \leq -a$ and $x \geq -l - a$
Upper-works:

$$y(i,j) = (B/2) * \left(1 - \left(\frac{x(i) + a}{l}\right)^2\right) \tag{4.5}$$

Below free-board:

$$y(i,j) = (B/2) * \left(1 - \left(\frac{z(j)}{T_{prog}}\right)^2\right) * \left(1 - \left(\frac{x(i) + a}{l}\right)^2\right) \tag{4.6}$$

As reported in fig. 4.17 various solutions have been investigated to fine a solution to host the Pump-Jet Module in the wigley hull. The one resulted mostly reliable was the second from left because not only creates a smoother surface but also allows the vehicle to be more modular and in

the end led to the easiest way of constructing a solution with the soft sandwich structure.

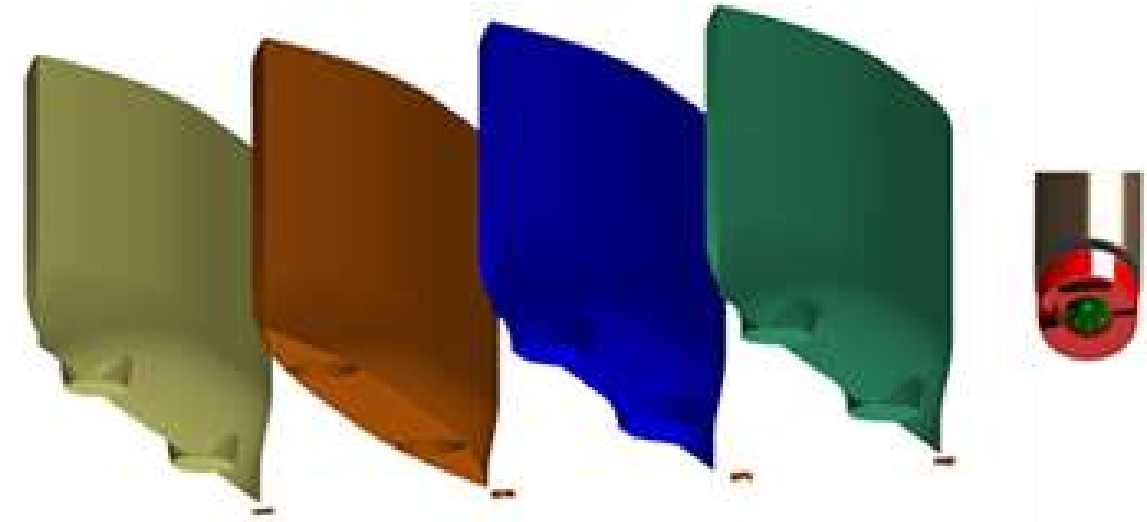

Figure 4.17: *Various modified Wigley hull solutions to host the Pump-Jet Module*

Where the constants are: $T_{prog} = 220/, mm$, the height of the immersible part of the hull without the horizontal cut of the bottom, $Cut_{prog} = 70/, mm$ is the vertical height of the cutting plane that results in a design maximum draft of $T = 150/, mm$, $B = 240/, mm$, the design breadth of the single hull, $a = 250/, mm$, the semi-length of the cylindrical body, $l = 370/, mm$, the semi-length of the non-cylindrical body. The variables are: $x(i)$,the actual longitudinal position, $y(i, j)$, the actual transversal position, $z(j)$,the actual vertical position. The lines-plan of the resulting hull is reported in fig. 4.16 The hull was drawn with a Matlab® code that allowed to try different configurations. The use of a Wigley hull shape and the code also allows to calculate all the geometric parameters of the hull giving the possibility to easy evaluate the stability characteristics of the vessel. With this code it was easy to modify the project in the initial phase. The graphic result of the Matlab® code output is reported in fig. 4.18, where the main characteristics of the hull are reported. The hull lenght is $L = 1.24\,m$ with a breadth of $0.24\,m$ and a maximum draft of $0.15\,m$ and a design draft of $0.14\,m$ at the design weight of $\Delta = 58\,kg$.
The single hull has a block coefficient $C_B = 0.67$ and the peculiar ratios are $L/B = 5$, $L/\nabla^{1/3} = 4.1$ and B/T=1.7.

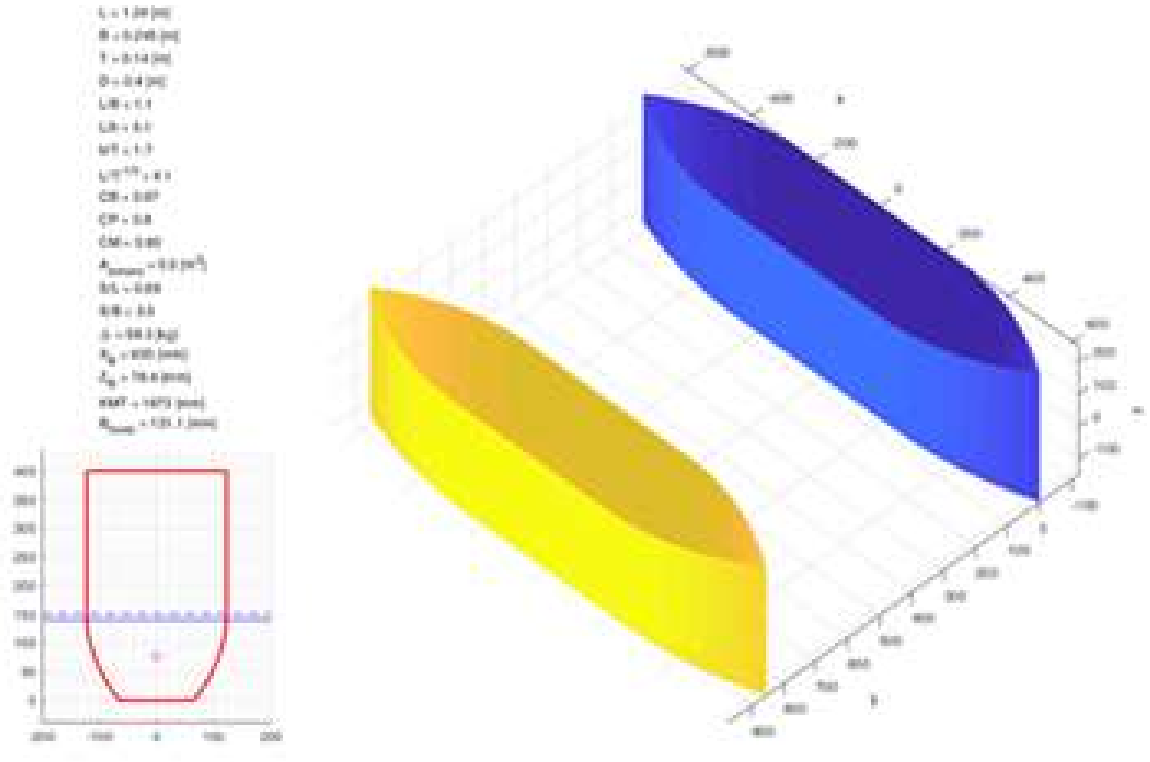

Figure 4.18: *SWAMP lines plan*

4.4 Catamaran Resistance

The resistance of multihull vessels is derived from the experience on the monohulls. The difference between monohulls and multihulls is the interference between the hulls [132]. The resistance breakdown usually applied includes residual and frictional resistance components. Frictional resistance R_f is due to the effect of hull motion in viscous fluid, while residual R_r resistance can be divided into wave-making resistance (affected by the energy density of the propagated wave) and viscous pressure resistance [133]. Frictional resistance is influenced by the hull wetted surface area A_w (wetted area of both demihulls in the case of the catamarans) and partly from surface roughness and water viscosity. The residual resistance is influenced by hull shapes and the wave pattern is modified according to the vessel speed U. The interference resistance coefficient of a multihull also affects the resistance components. While some interference increase the total resistance, others reduce it.
The total resistance R_t of multi-hull vessels is defined as:

$$R_t = 1/2 * \rho_w * A_w * C_t * U^2 \; ; [N] \tag{4.7}$$

And, according to [133], the resistance coefficient for a catamaran C_t is defined as:

$$C_t = (1 + \beta k)\, C_f + \tau\, C_w \tag{4.8}$$

where C_f is the frictional resistance coefficient, C_W is the wave-making resistance coefficient, β is the viscous interference factor, k is the hull form factor, and τ is the wave-resistance interference factor.
C_r is obtained from Ct using $C_r = C_t - C_f$, while C_f is derived from the ITTC'57 correlation:

$$C_f = \frac{0.075}{\log_{10}(Fn_L * 5.56 * 10^6) - 2)^2} \tag{4.9}$$

With the Kinematic viscosity $\ni = 1.14 * 10^{-6}\, m^2/s$ and the Froude number depending on length defined as:

$$Fn_L = U/\sqrt{g * L_{wl}} \tag{4.10}$$

The operative profile of SWAMP, for its nature, comprises the presence of shallow waters. In this kind of water changes in trim and sinkage occur that modify the pressure distribution around the hull. This modification influences the frictional resistance (wetted surface dependence) and more strongly influences wave pattern formation around the hull [134]. This influence depends on water depth h, and in particular on the ratio between water depth and vessel draft: h/T ratio.
According to [135] shallow water can be distinct in:

- deep water if $h/T \geq 3$
- medium shallow water if $1.5 \leq h/T \leq 3\,3$
- shallow deep water if $1.2 \leq h/T \leq 1.5\,3$
- very shallow water if $h/T \leq 1.2$

Below deep water the hydrodynamics of a vessel changes and usually a substantial reduction in the performances of the vessel in terms of manoeuvrability and resistance is faced. When a vessel moves through shallow water, the water flowing below the vessel is accelerated and, according to Bernoulli's law, a pressure reduction is created (Venturi effect) between the bottom of the vessel and the waterway bottom. The pressure drop causes a consequent sinking of the vessel in the water. In addition to this sinking the vessel usually trims aft or bow in a manner usually different from the one happening in deep waters, this effect is called *Squat*. If the h/T ratio is low, then grounding due to excessive squat could occur at the bow or at the stern.
In literature various, more or less sophisticated, tools and diagrams can be found to estimate the squatting effect by analysing the results obtained from different ships and models. As an example in [136] several empirical formulas for squat for various ship and channel are published. For strong shallow waters influence, a simple correction is impossible to estimate since wave breaking, squat and deformation of the free surface introduce complex physical interactions and non-linearity. In this case, only model tests or CFD may help [137].
As mentioned, not only the danger of grounding is important but the wave resistance effect is also critical. In shallow water the wave resistance enlarges [138] and is more significant in longer generated waves [139]. The limited depth in shallow water makes the phenomena become critical with the influence of generated wave characteristic and dynamic behavior of the vessel.
It is known that the generated wave pattern of vessels depends on another non-dimensional number, the Froude Depth number, Fn_H, which is defined as the ratio of ship speed to the maximum velocity a wave can travel in a given water depth. It is calculated as:

$$Fn_H = U/\sqrt{g * h} \tag{4.11}$$

When a vessel is moving into water the Froude Depth Number is defined:

- sub-critical when $Fn_H \leq 1$
  the wave system is with a transverse wave system at the kelvin angle of 19.5° and a divergent wave system propagating away from the ship at an angle of about 35°

- critical when $Fn_H = 1$
  the wave angle approaches 0°, perpendicular to the track of ship
- super-critical when $Fn_H > 1$
  the diverging wave system returns to a smaller wave propagation angle and transverse waves do not exist

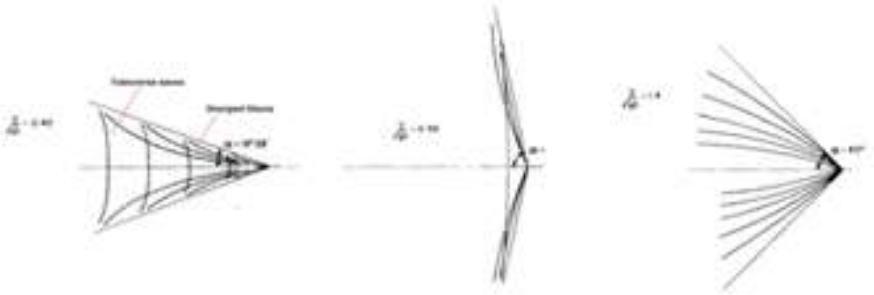

Figure 4.19: *The wave formation in shallow water depending on Fn_H [140]*

The wave pattern is strongly influenced by Fn_H as shown in fig. 4.19. In shallow water, as the speed approaches critical Fn_H, the vessel firstly rises then sinks significantly through the critical region before rising again at higher speeds. The significant running sinkage might be an important operational consideration if keel to ground clearances become small.
In the case of SWAMP with a maximum speed $U_{max} = 1.75\,m/s$ and a water depth $h = 0.2\,m$ it is expected that the vessel always remains in sub-critical zone.

Heading back to the above mentioned requirements the B/T, L/B and $L/\nabla^{1/3}$ values of SWAMP result to be small and the bow (and stern) results to be bluff if compared to commonly adopted catamarans like those reported in [141], [132], [142] [143] and [144] that are characterised by $L/B \geq 7$ and $L/\nabla^{1/3} \geq 6$ as shown in the fig. 4.20 and fig. 4.21. Usually when C_B is high the L/B ratio is high too. In [145] it is suggested that the "thick boundary layer and possible separation makes the effective hull longer".

This difference resulted in a difficult preliminary assessment of the resistance coefficients of the

Parameters	Molland et al. (1994)	Zips (1995)	Pham et al. (2001)	Schwetz and Sahoo (2002)	Sahoo et al. (2004)
L/B	7.0–15.1	7.55–13.55	10.40–20.80	8.80–15.0	10.0–15.0
$L/\nabla^{1/3}$	6.27–9.5		6.30–12.60	6.39–9.56	8.04–11.2
B/T	1.5–2.5		1.5–2.5	1.47–2.31	1.5–2.5
C_B	0.397		0.50–0.60	0.46–0.68	0.40–0.50
LCB/L (%)	43.6			46–49	
Deadrise angle at amidships β_{ai}		16–38°	16–27°		23–44°
Half angle of entrance in degrees	i_E			2.1–38	5.4–10.71

Figure 4.20: *Various characteristics of widely studied catamarans as reported in [144]*

vehicle. A preliminary analysis based on existing series resulted to be unreal due to these substantial differences in the geometric aspects. The only similar data regarded the existence of some double ended and flat bottom catamarans like [146] that showed that the requirement of shallow draft and high payload results in a higher power requirements than with classic catamarans. This meant that since the B/T, L/B and $L/\nabla^{1/3}$ values of SWAMP are small and the bow (and stern) of SWAMP is bluff the resistance coefficients of SWAMP should have been higher too and this can be related to the wave resistance. Especially in [132] the resistance of model 3*b* is widely more than the resistance

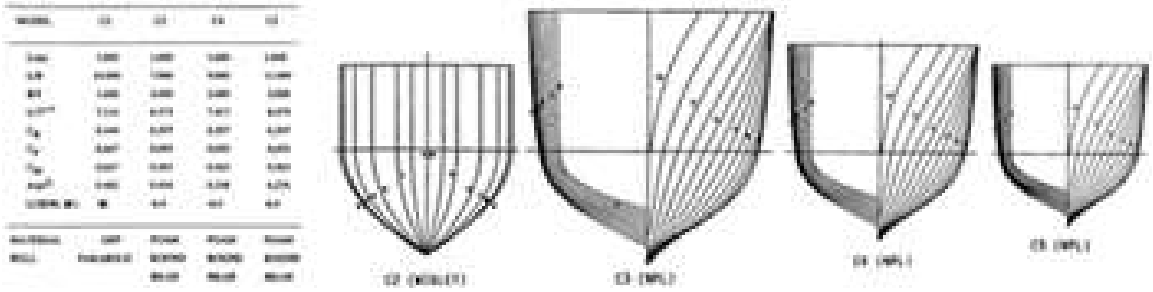

Figure 4.21: *Various characteristics of catamarans studied in [132]*

of the other models, showing the effective influence of $L/\nabla^{1/3}$.
To assess the resistance of SWAMP, towing tank tests were conducted both in deep, and in shallow water.
As mentioned before different studies have been conducted on catamaran with towing tank tests in deep water also with the variation of length-displacement ratio and breadth-draught ratio [147].
But, in the last decades, also shallow water tests on different monohull have become more common, especially in the advanced model testing techniques for ship behaviour in shallow and confined water as shown by [148] with a facility able to conduct manoeuvring tests [149]. In [150] and especially in [151] it is reported a series of tests on various shapes of catamaran in shallow water [152]. From this experience other tests have been done in shallow water on multi-hulls analyzing semi-SWATH resistance in [153] shallow water and its relation to flow around hull.
In all the above mentioned cases the tests were conducted on scaled model with results that have to be reported to the real dimensions. In the case of SWAMP tests could be conducted in the real scale. In marine robotics, only few experiments exist on towing tank on real scale vehicles. As an example in [101] a robust ASV capable of operating in harsh ocean environments is presented with the full-scale resistance and self-propulsion tests performed at the tow tank of Memorial University to obtain drag coefficient and a bi-linear thruster model before sea trials. More recently tests were conducted by [154] for a shallow water catamaran provided with Waterjet propulsion on a scaled model.

4.4.1 Towing Tank Tests in deep and shallow waters

The Facility, the vehicle and testing procedures

Tests were performed in DITEN Hydrodynamic Laboratories towing tank at the University of Genova fig. 4.23 to measure the resistance of SWAMP both in deep and in shallow water. The Towing Tank dimensions are about $60\,x\,2.5\,x3\,m$ with a real running distance of about $45\,m$. It is provided with dynamometric carriage with maximum speed of $3\,m/s$ with capability of measurement of trim and resistance.
The Load cell is a HBM Z6FC3 strain gauge with flexing plate. It works in a range of -10 to $10\,kg$. It is EMC tested according to EN 45501:2015.
The trim and the sinkage are measured by means of two laser range-meter pointing on plates mounted on the model, one bow and one stern, the precision in the measure is $\pm 0.1\,mm$.
The speed is recorded with two methods, a tachometer wheel and an optical reader.
The recorded data are transferred to a PC via Wi-Fi.
The resulting resistance, trim and effective speed is obtained from the average value of the recorded signal in the stable course transient. As a standard procedure each test is performed at least three times.
Due to the small dimension of the tank, and to increase the "useful run" length, the carriage is provided with an electromagnet that is used to tow the model in the first phase of acceleration. In this way the carriage reaches the maximum speed in shorter time and the resulting run has is longer than with a smooth acceleration.
Guiding wheels are used to guide the straight course of the model.

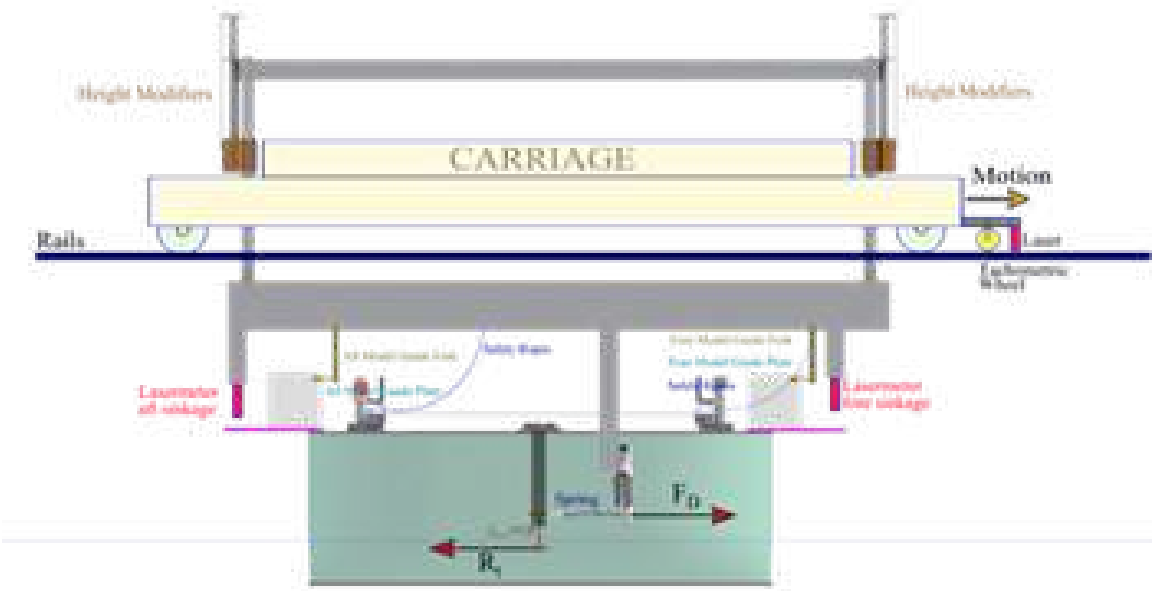

Figure 4.22: *Description of the tests*

Due to the big dimensions of SWAMP hull, to perform the tests some modifications had to be done to the testing facility. The carriage starting and finishing point, made with an electric switch, was shifted forward to allow the introduction of the hull in the tank and to avoid crashes. Also additional batteries were added to the carriage.
To test the hull of SWAMP in the design payload condition a series of lead weights were mounted inside the foam holes to reproduce the future loading condition. The hull and structure of SWAMP weigh $15\,kg$ and the payload condition is $58\,kg$ so $43\,kg$ had to be distributed in the two side hulls.

Figure 4.23: *The towing tank facility of DITEN Hydrodynamic Laboratories UNIGE*

To reproduce the same stability characteristics of the SWAMP vehicle, i.e the same Vertical Centre of Gravity VCG and Δ, the weights were positioned at specific heights in specific positions by using the stability tool shown in stability section.
The vehicle was provided with an aluminum and pultruded bars structure that allowed the installation of the hook connecting a spring to the load cell, as shown in fig. 4.24. Since the model weight is

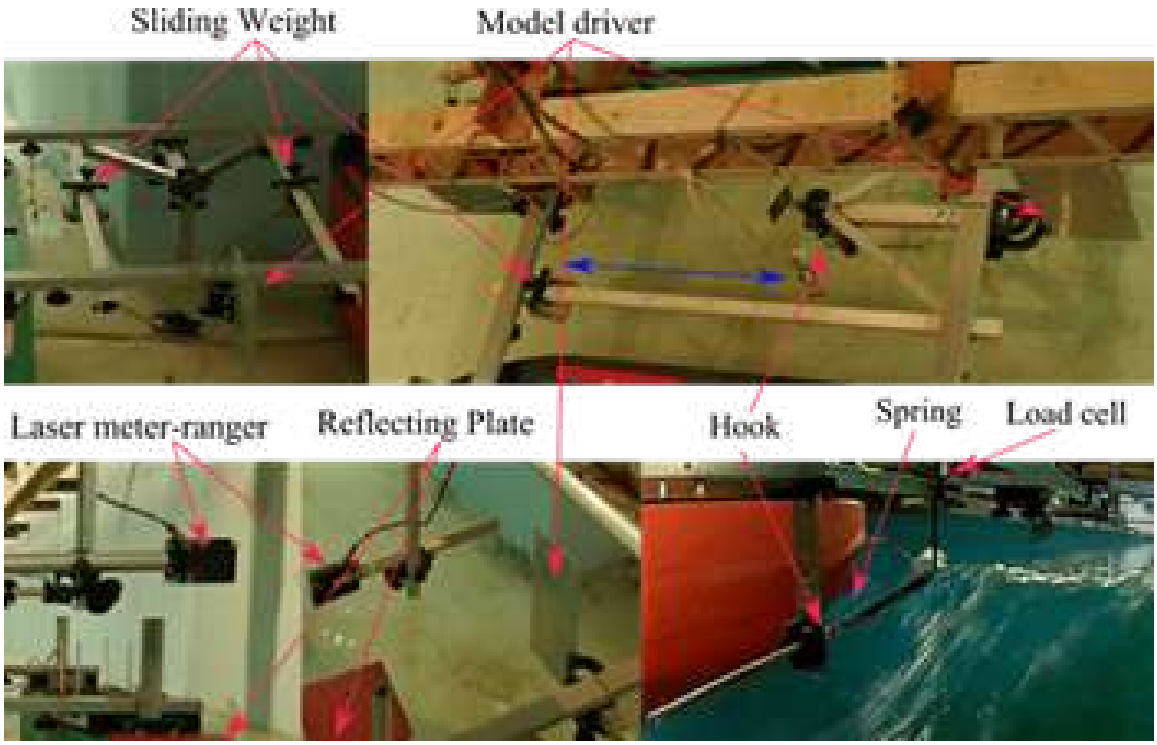

Figure 4.24: *Description of the testing rig*

much higher than the one of the models usually tested in the DITEN facility, then the electromagnet did not tow the vehicle in the first acceleration phases and some precautions had to be taken:

- The tow fitting has to allow free movement in sinkage and trim whilst movements in sway and yaw have to be restrained. The use of at least 1 bow and 2 aft safety lanyards were helpful to contain the rotation of the model and to avoid: the model leaving the guiding wheels (or reach the end of the run), the load cell to reach its operating limit, the spring to reach its elastic-phase end
- Use the proper spring for every test
- Calibrate the model guides so that the model does not leave its test path during the first towing phase and calibrate the lanyards not to prevent surge or trimming motions
- When towing catamarans, as in the case of SWAMP, the towing point is placed above the waterline and above the Vertical Centre of Buoyancy VCB. In this case an induced trimming

moment is generated and a correction has to be applied. This was done by using a mobile mass for the correction of the vehicle's initial trim so that the dynamic attitude could be the exact one. This was done by using the two *sliding weights* shown in fig. 4.24 with the following procedure:

1. Test in the project setup and measure the vehicle resistance
2. $M_{tow} = R_t * (z_{tow} - VCB)$ is the bow lowering trimming moment. where R_t is the total resistance, z_{tow} is the vertical position of the towing centre.
3. From the stability characteristics of the boat correct the trim.
4. Move the sliding weight and move it by X_{weight}.
   Being p the weight to be shifted, KM_L the distance between keel to longitudinal metacentric height and θ_L the trimming angle:
   $\theta_L = atan(R_t * (z_{tow} - VCB)/(\Delta * (KM_L - VCB))$
   $X_{weight} = tan(\theta_L) * \Delta/p * (KM_L - VCB)$
5. In case re-do the procedure if the resistance results much higher or lower than the one recorded in the previous test.

For the tests in shallow water the towing tank was modified fig. 4.25. The water in the tank was removed down to the wanted value and the carriage was additioned with a structure that allowed the lowering of the measuring device. The vertical mechanism that lowers the measuring device allows to test from 150 mm up to 600 mm of water depth.

Figure 4.25: *The project and the construction of the towing tank modification for the shallow water tests*

Since real-scale tests were conducted no turbulence creators were added to the model.

Tests

Various tests were performed on SWAMP to characterise the vehicle in its different operational situations.
Tests were performed in fresh water with a density of 1001 kg/m^3 at an average temperature $T_{=}15°\,C$ in deep water at three different catamaran breadth B and at two different loading conditions. The

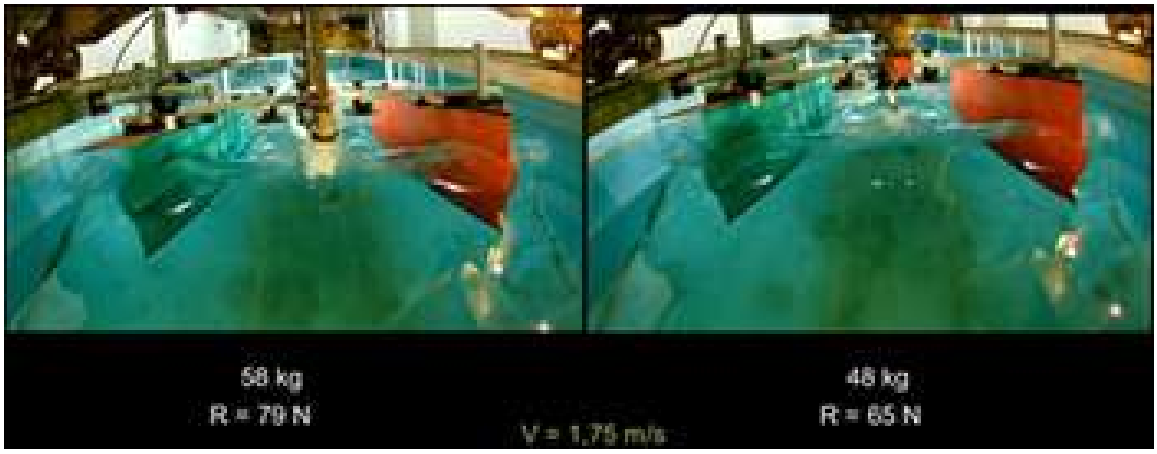

Figure 4.26: *SWAMP in the towing tank facility during high speed tests*

results of this kind of analysis allow to find a way of estimating the resistance of SWAMP during a survey by knowing the initial loading condition and actual step-by-step loading condition (as an example by estimating the amount of sampled water) thus completely identifying the surge motion of SWAMP. Since SWAMP was designed for extremely shallow waters it was important to take into consideration also the peculiar effects affecting a vessel moving into low depth. As described above, tests could be possible in extremely shallow waters by modifying the DITEN facility and emptying the tank. Tests were performed at different water height resulting in different ratios: $h/T = [1.5\,, 2.0\,, 2.5\,, 4.0\,, 9.0]$. The experimental tests performed in the towing tank are listed in table 4.5 with the characteristics of the configurations of the tests. At maximum depth the

Table 4.5: *Tests performed on SWAMP in towing tank*

Test ref	*H/T ratio*	*H* $[mm]$	*T* $[mm]$	∇ $[m^3]$	A_w $[m^2]$	*B* $[mm]$	*S/L*	*U* $[m/s]$
a	1.5	210	140	0.58	0.99	1100	0.68	0.5 0.63 0.75 0.88 1.0
b	2	280	140	0.58	0.99	1100	0.68	0.5 0.75 0.88 1.0 1.25
c	2.5	350	140	0.58	0.99	1100	0.68	0.5 0.75 0.88 1.0 1.25 1.4
d	4	560	140	0.58	0.99	1100	0.68	0.5 0.75 1.0 1.25 1.5 1.6
e	9	1260	140	0.58	0.99	820	0.46	0.5 0.75 1.0 1.25 1.5 1.75
f	9	1260	140	0.58	0.99	1100	0.68	0.5 0.75 1.0 1.25 1.5 1.75
g	9	1260	140	0.58	0.99	1250	0.80	0.5 0.75 1.0 1.25 1.5 1.75
h	9	1260	115	0.48	0.89	1100	0.68	0.5 0.75 1.0 1.25 1.5 1.75

tests were done at 3 different widths: $B = [820, 1100, 1250]\,mm$ resulting in 3 different ratios: $S/L = [0.46, 0.68, 0.8]$, see fig. 4.28.
Test were done at the standard load condition of $58\,kg$, so with $23 \div 25\,kg$ of payload and immersion $T = 140\,mm$. A test was done at the design width of $1100\,mm$ with load condition of $48\,kg$, so with $13 \div 15\,kg$ of payload and immersion $T = 115\,mm$.

Towing tank experimental results in deep water

The results of the deep-water tests are reported in (every curve is the mean value of, at least, three run's value) fig. 4.27 and fig. 4.30. From this it is possible to extract the resistance $R = 49\,N$ at

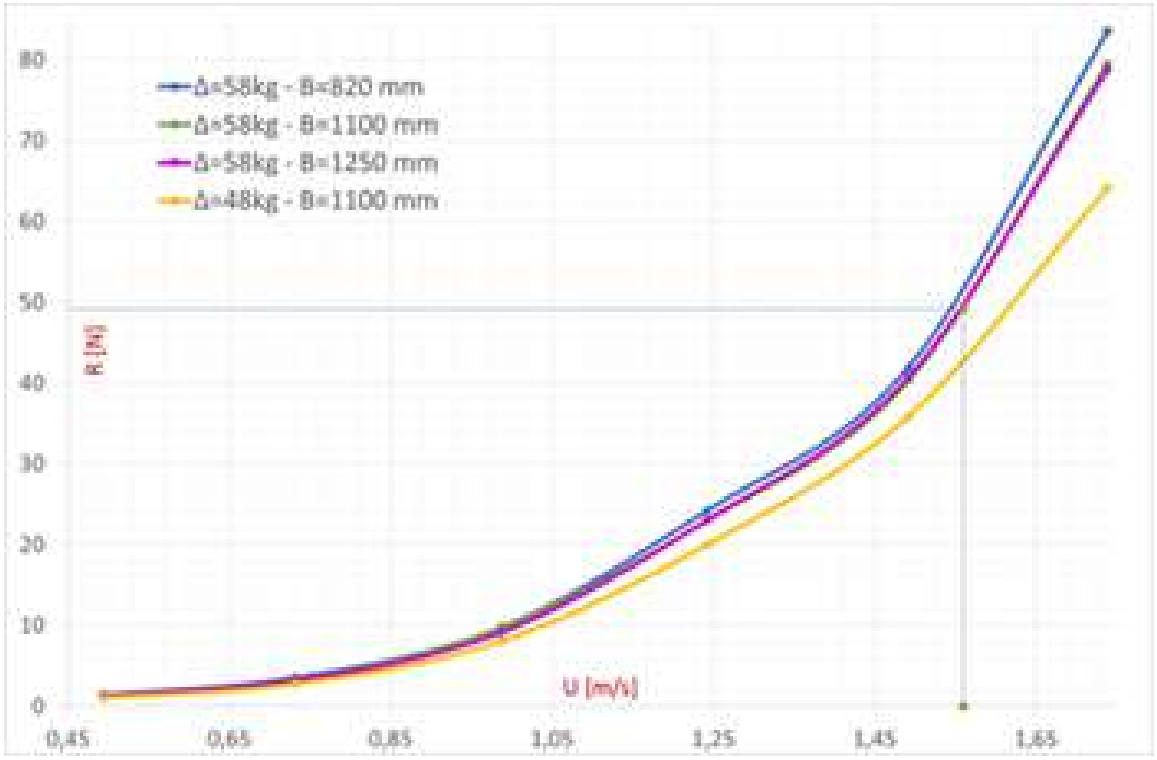

Figure 4.27: *SWAMP Resistance vs Velocity*

a maximum design speed of $1.5\,m/s$ at the maximum loading of the vehicle. The value of $1.5\,m/s$ was considered the reference value to match between maximum payload, autonomy, battery weight and cost and taking into consideration the maximum speed normally used during autonomous surveys that does not exceed $1\ m/s$. From the results reported in fig. 4.27 a low variability on the resistance

Figure 4.28: *Three different configuration* $S/L = [0.46, 0.68, 0.8]$

depending on the width can be seen with a small interference between the two hulls at $B = 820\,mm$ and roughly the same resistance at the intermediate and larger breadth. The difference between the resistance at $B = 1100\,mm$ and the other two is in the order of $-2\% \div +8\%$ at low speeds and is contained between $-1\% \div +5.5\%$ at higher speeds.
Regarding the $\Delta = 48\,kg$ test and the $\Delta = 58\,kg$ test it is possible to see that there is a good relationship between the resistance difference and the wetted surface A_w [1] difference within the operating speed range. In fig. 4.29 the curves of resistance at $B = 1100\,mm$ are reported together with the curves obtained from the values of resistance at reference weight of $\Delta = 48\,kg$ and at

[1] The conclusions in [147] show that the running wetted surface area is difficult to measure experimentally therefore static wetted surface area was applied in this work

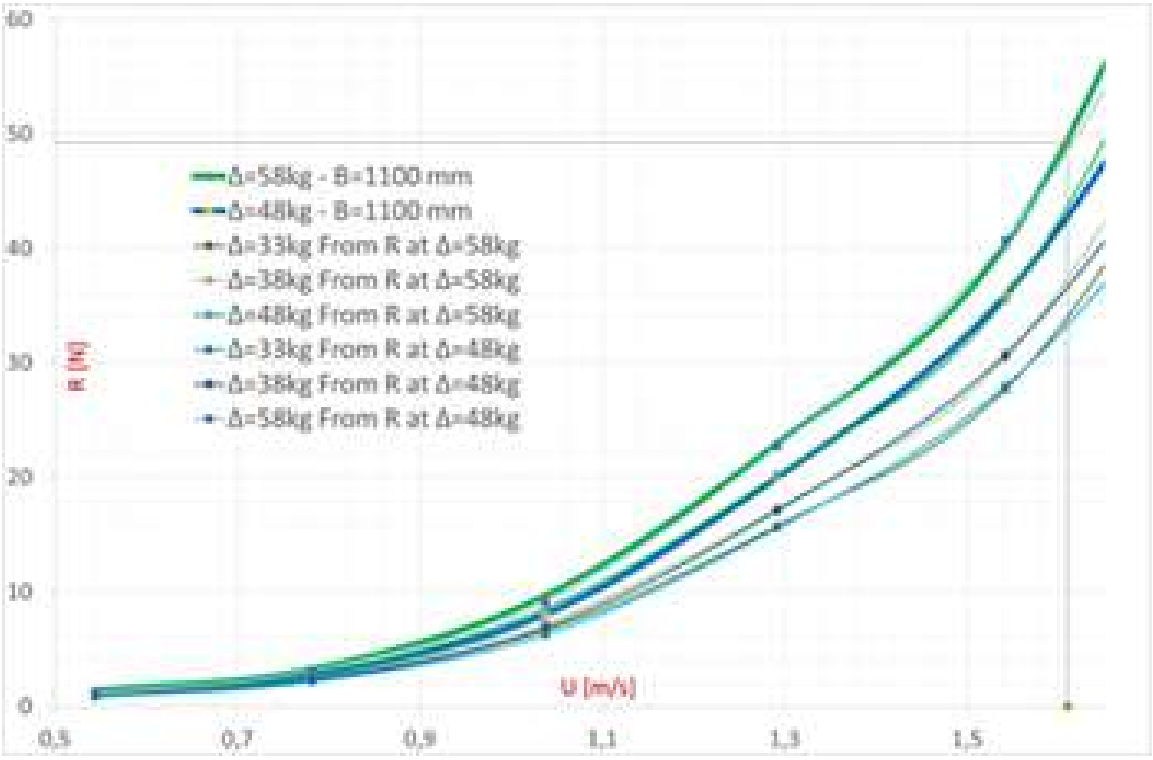

Figure 4.29: *SWAMP Resistance vs Velocity with previsions related to* $\nabla^2/3$ *ratios*

$\Delta = 58\,kg$ multiplied for the actual ratio between the wanted weight and the reference weight's $\nabla^2/3$. From this graphic it is possible to see that the values of resistance for $\Delta = 48\,kg$ obtained from $\Delta = 58\,kg$ and vice-versa can be well superimposed indicating the possibility of foreseeing the actual resistance of the vessel also in the other loading conditions by adopting a total resistance coefficient C_t obtained as:

$$C_t = \frac{2 * R_t}{\rho_w * A_w * U^2} \tag{4.12}$$

As far as the attitude is considered, the catamaran appears to be trimmed by bow up to a speed of around $U = 1.3\,m/s$ i.e a $Fn = 0.46$ after which it passes to an increasingly accentuated trimming by stern fig. 4.31.

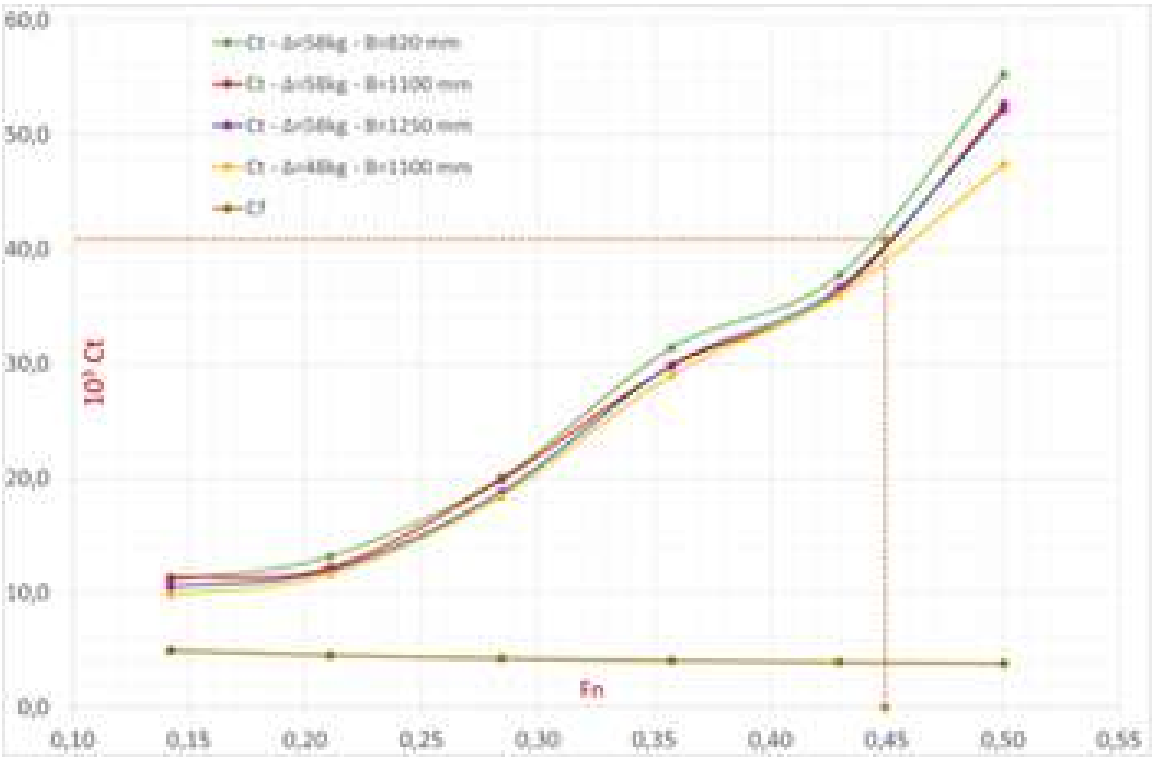

Figure 4.30: *Resistance Coefficient C_t in function of Froude Number*

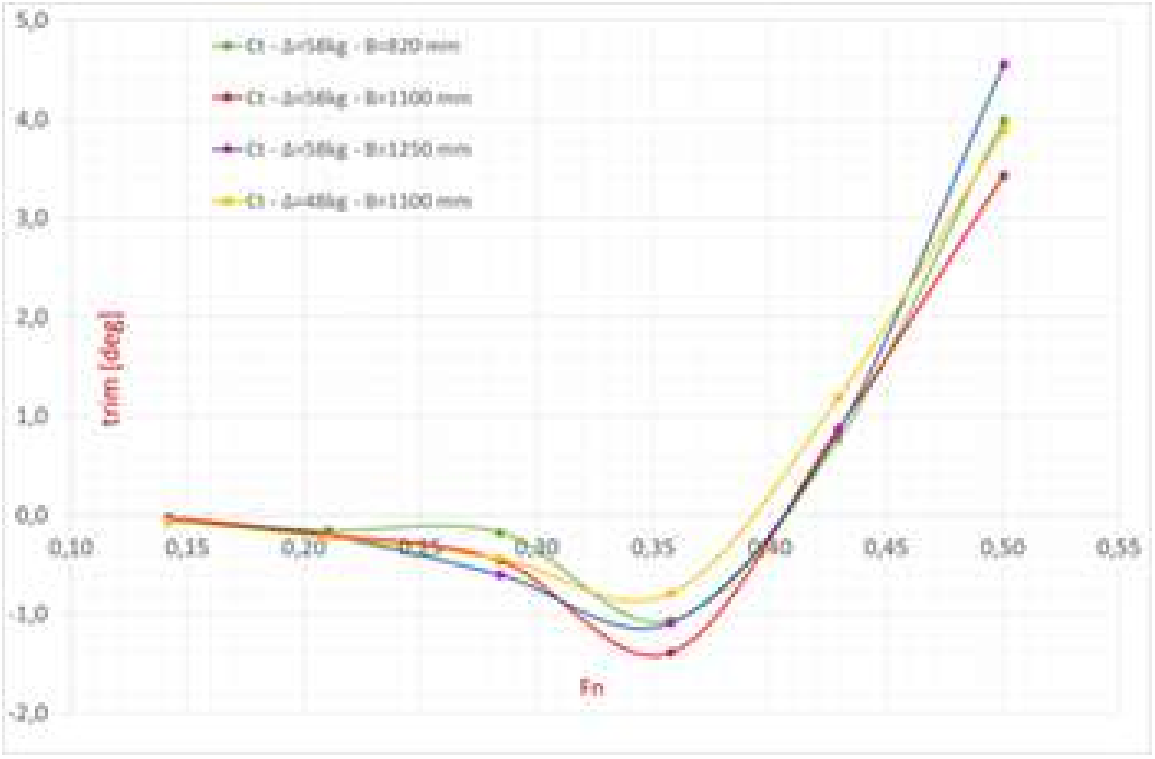

Figure 4.31: *The trim in deg in function of Froude Number*

In fig. 4.32 it is reported, as an example, the difference in the final resistance and the final trim due to initial correction of the static trim to compensate the dynamic trim given by the tow. A slight increase in the resistance is recorded but a substantial difference in the trimming angle exists.

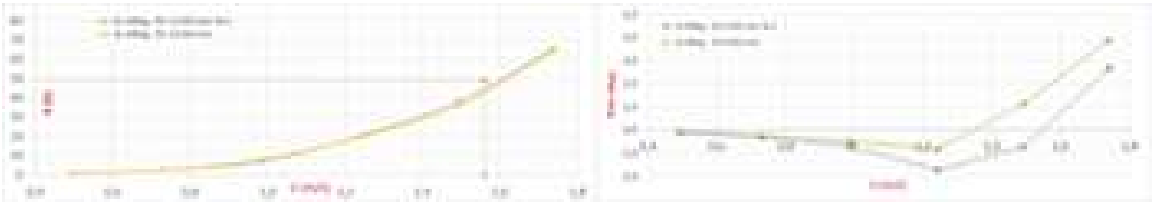

Figure 4.32: *The difference in resistance and trim to static trim correction*

From these deep water tests a resistance higher than expected was recorded. This is due to the substantial geometric difference from the hulls studied in literature [141, 147, 151, 155, 156] and the SWAMP hull. The difference stands in the main geometric parameters of the SWAMP hull. In table 4.6 this difference is shown. The value of L/B and $L/\nabla^{1/3}$ are smaller than usual one while the C_B value is higher. This values are related to the bluff shape of SWAMP hull. On the other hand the value of B/T is within the range of usual catamarans.

Table 4.6: *The characteristics of SWAMP compared to literature catamarans*

DATA	**SWAMP**	**Literature Catamarans**
L/B	5.167	7 - 20
$L/\nabla^{1/3}$	4.06	6.2 - 12
B/T	1.714	1.5 - 2.3
C_B	0.67	0.4 - 0.65

Towing tank experimental results in shallow water

As mentioned before tests were performed at four different water depth at the maximum loading condition. The minimum water depth $H = 210\,mm$ with a clearance of $60\,mm$. To perform the tests the DITEN facility was modified by extending the vertical elements and lowering the level of the water in the tank as shown in fig. 4.33. Test results are reported in fig. 4.35 where it is possible

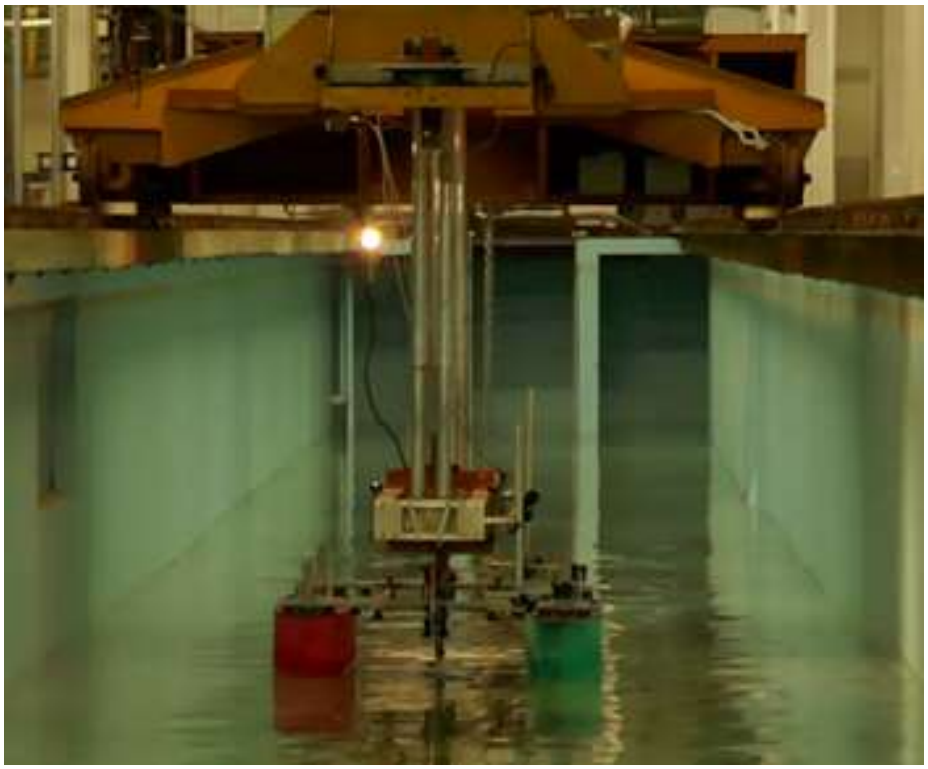

Figure 4.33: *SWAMP in the towing tank facility during shallow water tests*

to see that the resistance substantially increases with the decreasing of water depth.

In particular it is interesting to see that at $H/T = 1.5$ the resistance is about $R = 49\,N$ at

Figure 4.34: *SWAMP hull during a test in shallow water*

$U = 1\,m/s$. The speed loss is of $U = 0.5\,m/s$ if compared to the deep water ($H/T = 9.0$) where the same resistance is obtained at $U = 0.5\,m/s$.

In fig. 4.35 it is also possible to see how the resistance gradually increases with the decreasing of water depth and of the H/T ratio.

This can be seen also in the C_t curves in fig. 4.36.

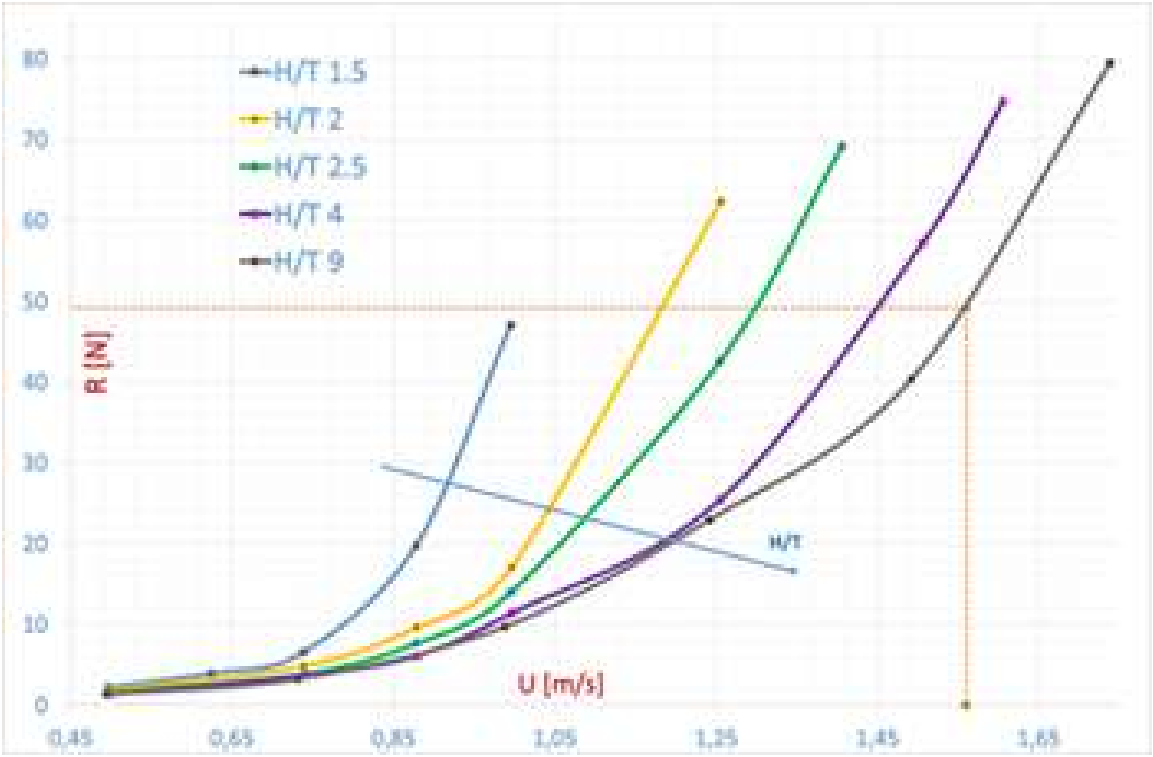

Figure 4.35: *Resistance curves at different H/T*

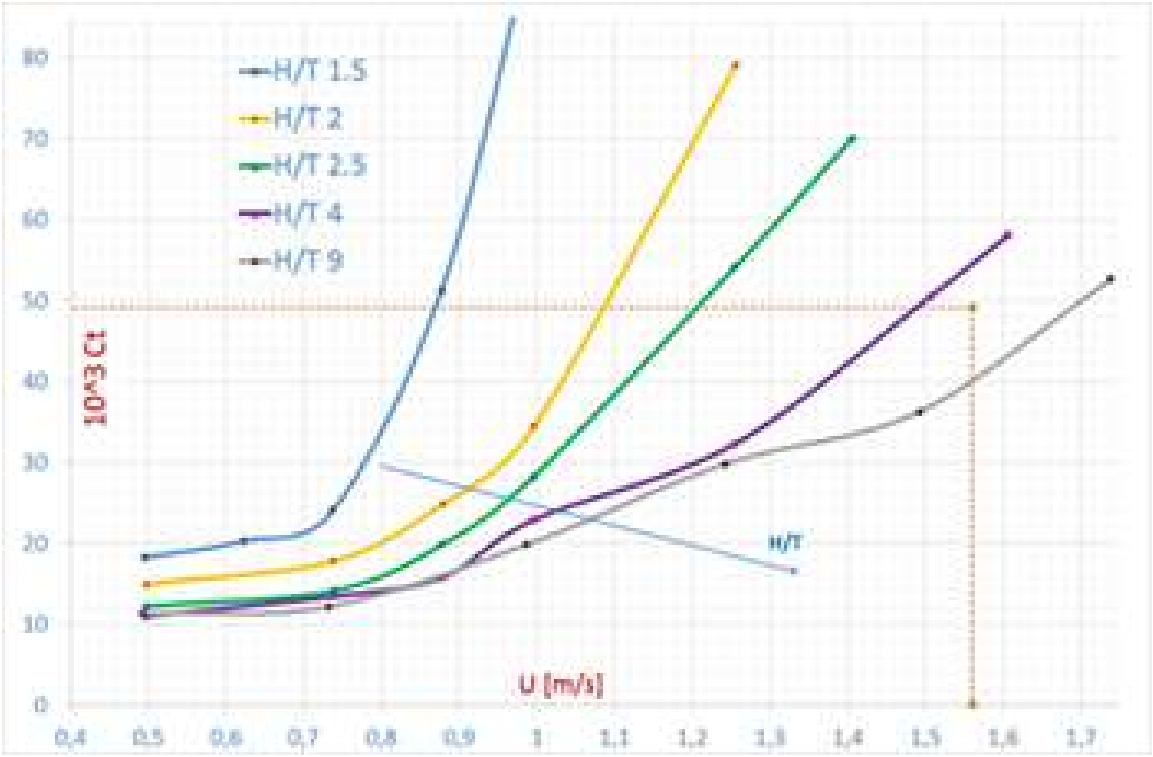

Figure 4.36: *Resistance coefficients curves at different H/T*

From fig. 4.37, fig. 4.38 and fig. 4.39 it is possible to see that the increase in resistance is strictly related to an increase in the sinking of the vehicle due to the Venturi effect with the tank bottom. The consequence is the presence of an evident squat effect. This effect is important even at lower speed where the maximum value was recorded at $U = 1\,m/s$ for $H/T = 1.5$.
In fig. 4.37 the mid-ship sinking, calculated as the mean sinkage between the bow and stern values recorded with the laser meter, is reported. The mean sinkage in deep water is lower also at the small

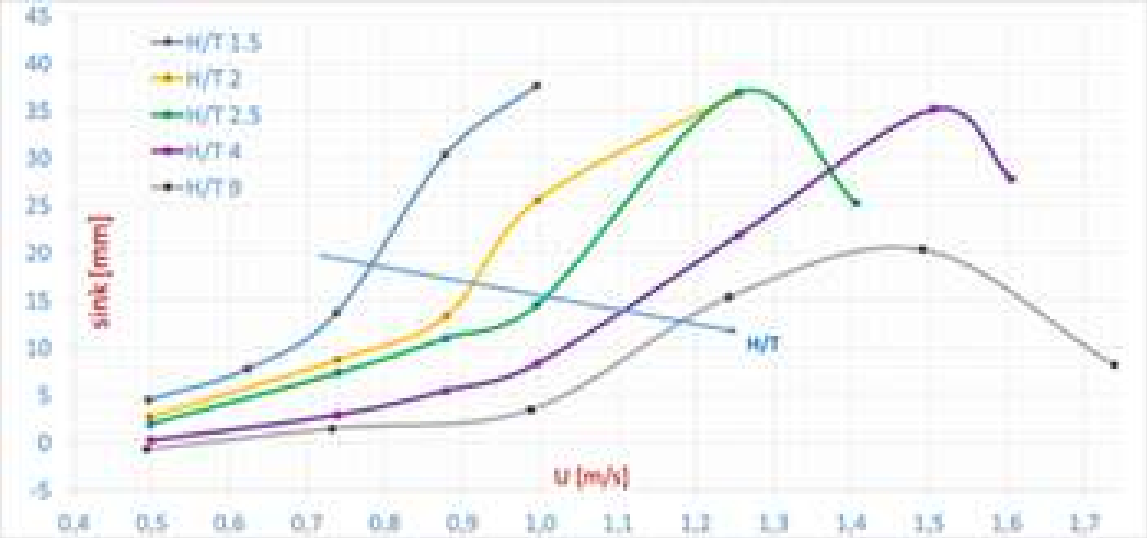

Figure 4.37: *The midship sinkage curves at different H/T*

speed of $U = 0.5\,m/s$ and this difference increases as the water depth decreases. At $U = 1\,m/s$ the difference from the sinkage at $H/T = 1.5$ and $H/T = 9$ is almost $40\,mm$. This value has a high influence on the resistance since the wetted surface substantially augments.
The squat is the maximum reduction in underkeel clearance (bow or stern) between the vessel at-rest and water bottom. In fig. 4.38 the sinkage at bow is reported while in fig. 4.39 the sinkage at stern is shown. The squat value can be defined as the maximum between these values. From the tests on SWAMP hull, the sinkage at stern is higher than the sinkage at bow when $U > 1\,m/s$. Above this value the sinkage substantially increases up to a value of $80mm$ for $H/T = 2$ and $U = 1.25\,m/s$
The squat effect shows the possibility of grounding when going at speed in shallow water supporting the need of an impact resistance hull and propulsion.

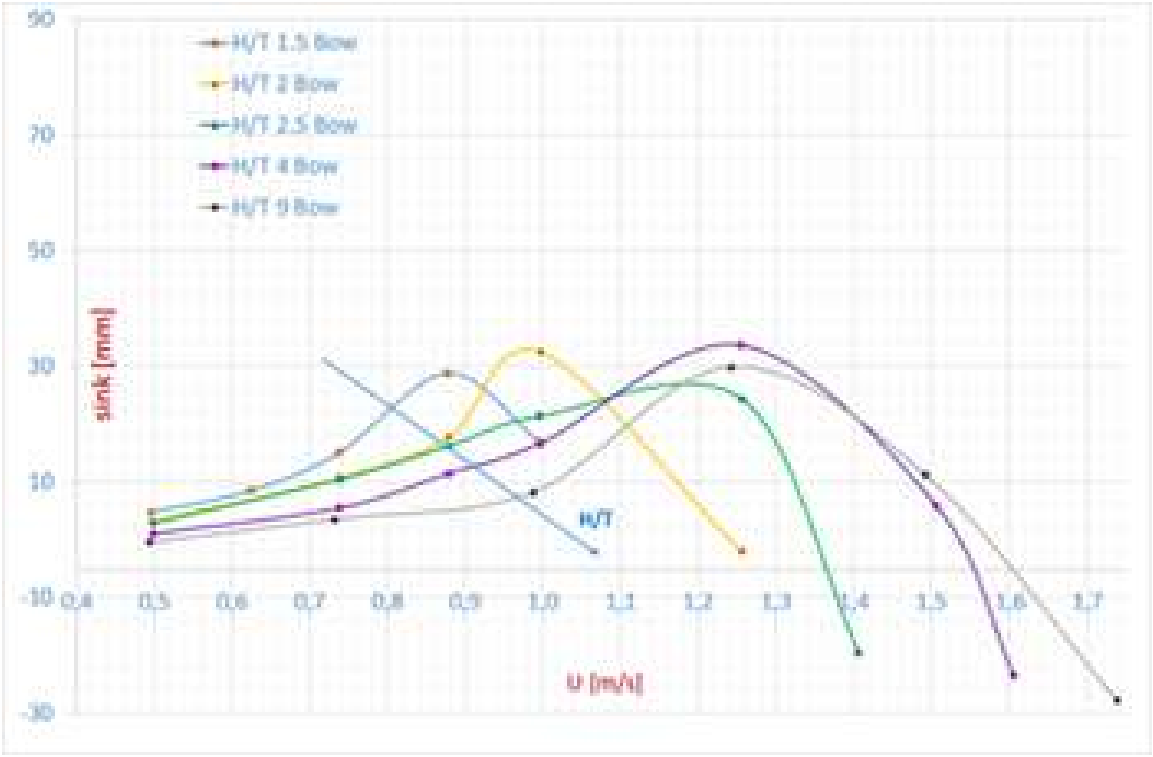

Figure 4.38: *The sink (squat) curves at different H/T for the bow of the vehicle*

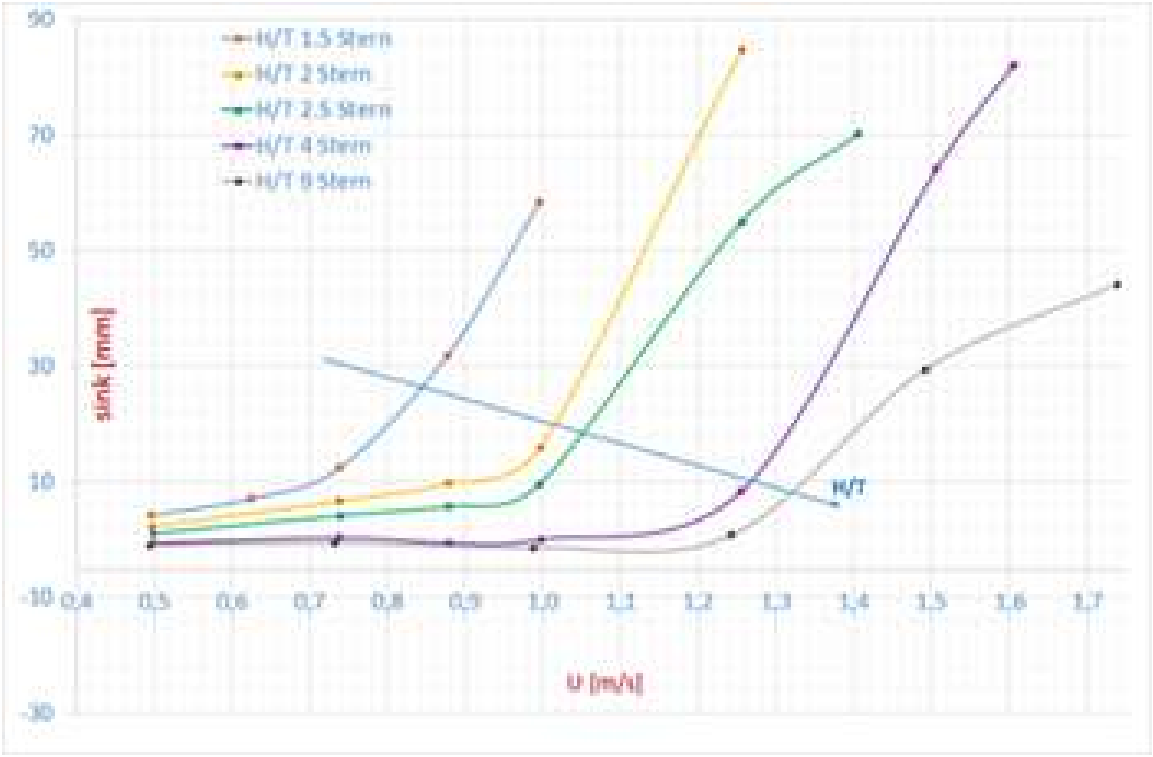

Figure 4.39: *The sink (squat) curves at different H/T for the stern of the vehicle*

In fig. 4.40 the trim modification is shown and reported. From this figure it is possible to see that the trimming of the vessel occurs at lower speed as the water depth decreases. In the case of $h/T \leq 1.5$ the trim is never negative, while in the other cases the vehicle passes from a minimum of negative trim to a maximum of positive trim.

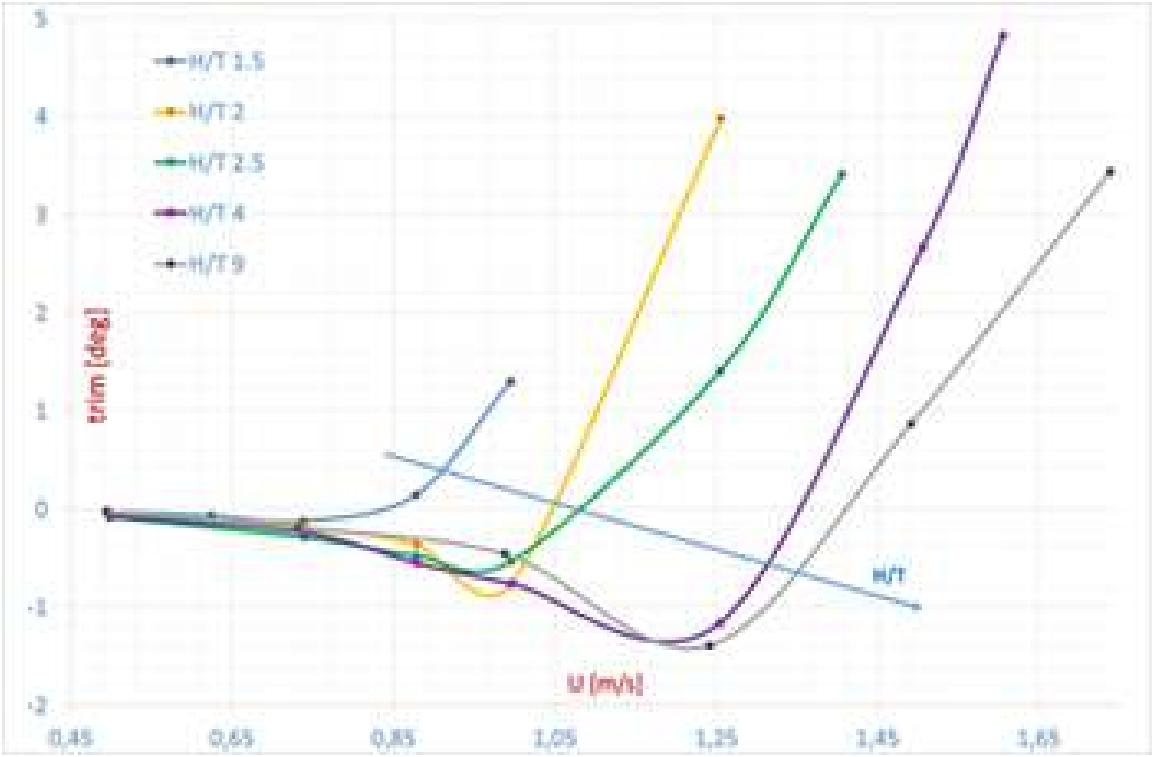

Figure 4.40: *The trim curves at different H/T*

By taking these results into consideration is possible to foresee the effective hydrodynamic resistance of the vessel in presence of shallow water thus knowing the thrust that the thrusters have to impress and which is the maximum reachable speed with the thrusters.
The results of the investigation provide a better understanding of the resistance and distribution of wave resistance of SWAMP in shallow water. As depicted in fig. 4.41 the resistance showed a distinct increase near the critical depth Froude Number (FnH=1.0) that, anyway, was never reached in the tests.
It is interesting to note that the resistance curves (and the contextual curves of C_t versus Fn_H) from $h/T \leq 4$ are quite superimposable showing the effective relation between resistance increase and the value of Fn_H. This increase is larger for the smaller water depth and is strictly related to

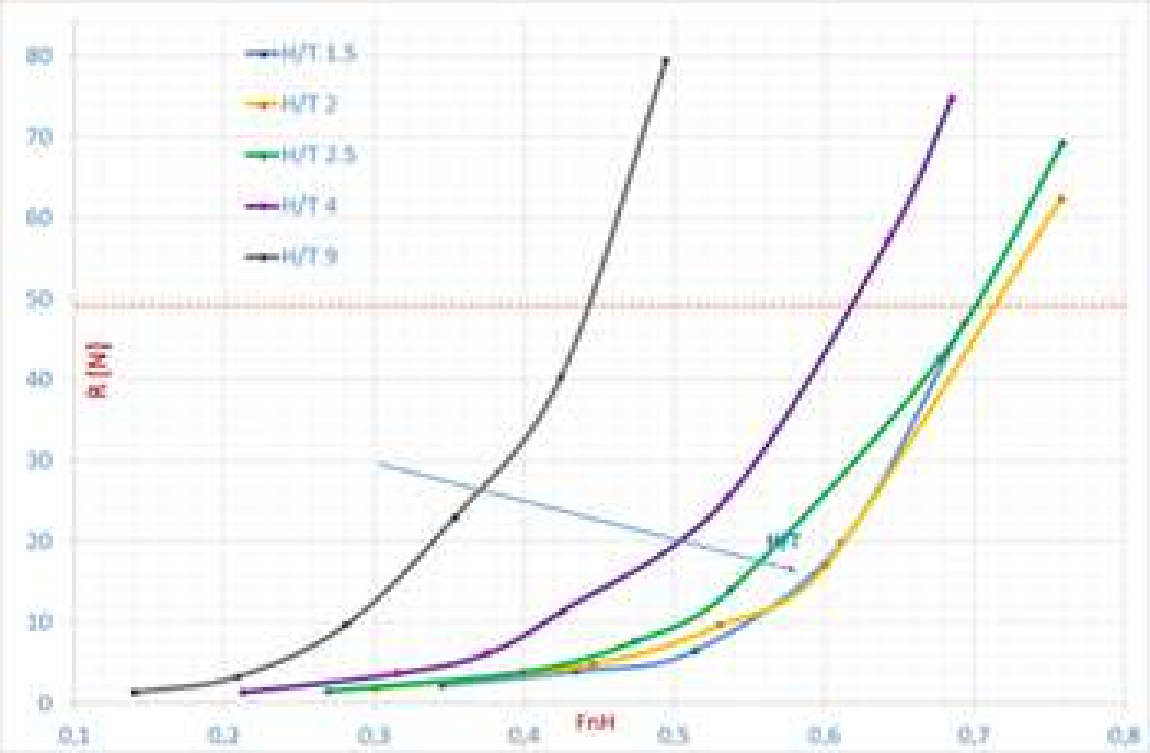

Figure 4.41: *Resistance curves at different H/T in function of Depth Froude Number Fn_H*

the the smaller under keel clearance.
The wave profile was recorded with cameras mounted on-board the carriage and showed the increase in the divergent waves angle as shown in In shallow water as the depth is decreased, the vessel trim passes to be trimmed by bow to be trimmed by stern at a smaller speed with almost no negative trim in case of $H/T = 1.5$.
The vessel sinks significantly through as the critical region is approached. In this direction significant running sinkage might be an important operational consideration if keel to ground clearances become really small.
The data derived from these tests are interesting also to increase the number of available catamaran geometries, also in shallow water.

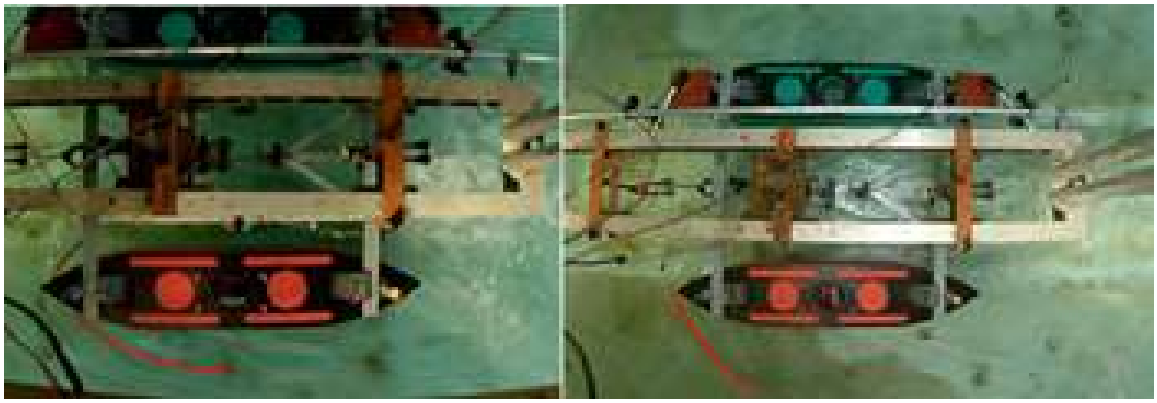

Figure 4.42: *On the left the Wave shape of the catamaran in deep water and on the right the diverging wave shape in shallow water*

Table 4.7: *The towing tank results*

$Depth = 200\,mm$, $h/T = 1.5$								
Fn_H		0,35	0,43	0,51	0,61	0,69		
Fn		0,14	0,18	0,21	0,25	0,29		
V	[m/s]	0,50	0,62	0,74	0,88	1,00		
R	[N]	2,24	3,94	6,53	19,71	47,08		
10^3C_t		18,28	20,30	24,04	51,27	95,16		
trim	[deg]	-0,03	-0,07	-0,12	0,14	1,30		
sink	[mm]	4,49	7,78	13,71	30,35	37,64		
squat	[mm]	4,80	8,50	15,05	32,10	58,32		
$Depth = 280\,mm$, $h/T = 2$								
Fn_H		0,30	0,45	0,53	0,60	0,76		
Fn		0,14	0,21	0,25	0,29	0,36		
V	[m/s]	0,50	0,74	0,88	1,00	1,26		
R	[N]	1,84	4,85	9,60	17,07	62,32		
10^3C_t		14,95	17,81	24,87	34,43	79,09		
trim	[deg]	-0,04	-0,18	-0,36	-0,76	3,98		
sink	[mm]	2,70	8,71	13,35	25,59	36,86		
squat	[mm]	3,48	10,72	17,70	32,52	84,82		
$Depth = 350\,mm$, $h/T = 2.5$								
Fn_H		0,27	0,40	0,47	0,54	0,68	0,76	
Fn		0,14	0,21	0,25	0,29	0,36	0,40	
V	[m/s]	0,50	0,74	0,88	1,00	1,26	1,41	
R	[N]	1,51	3,87	7,64	13,98	42,60	69,20	
10^3C_t		12,22	14,16	19,83	28,24	54,15	70,08	
trim	[deg]	-0,08	-0,29	-0,48	-0,54	1,40	4,11	
sink	[mm]	1,96	7,34	11,00	14,54	36,93	25,23	
squat	[mm]	2,86	10,51	16,19	21,34	55,01	70,22	
$Depth = 560\,mm$, $h/T = 4$								
Fn_H		0,21	0,32	0,37	0,42	0,54	0,64	0,68
Fn		0,14	0,21	0,25	0,29	0,36	0,43	0,46
V	[m/s]	0,50	0,74	0,88	1,00	1,25	1,51	1,61
R	[N]	1,37	3,66	6,10	11,35	25,37	57,19	74,71
10^3C_t		11,04	13,43	15,83	22,90	32,27	50,48	58,02
trim	[deg]	-0,07	-0,24	-0,55	-0,76	-1,16	2,67	4,83
sink	[mm]	0,23	2,92	5,48	8,34	21,86	35,13	27,86
squat	[mm]	1,02	5,51	11,49	16,63	33,67	64,05	82,14
$Depth = 1260\,mm$, $h/T = 9$								
Fn_H		0,14	0,21	0,28	0,35	0,42	0,49	
Fn		0,14	0,21	0,28	0,36	0,43	0,50	
V	[m/s]	0,49	0,73	0,99	1,24	1,49	1,74	
R	[N]	1,38	3,25	9,68	22,97	40,30	79,44	
10^3C_t		11,34	12,16	19,88	29,81	36,26	52,63	
trim	[deg]	-0,03	-0,20	-0,46	-1,39	0,87	3,43	
sink	[mm]	-0,68	1,49	3,46	15,35	20,37	8,16	
squat	[mm]	-0,41	3,56	8,27	29,91	29,48	44,16	

Discussion on resistance and hull shape

After the towing tank tests an analysis of the results was made. If a prediction was made with existing catamarans data the resulting coefficients would have led to under-estimated values of resistance as shown in fig. 4.43. In this figure it is reported the resistance curve of SWAMP at maximum payload in towing tank R_{TT} compared to a predicted resistance $R_{Predicted}$ made with a prediction obtained by using the data of [132]. This means that the project requirements of SWAMP results in

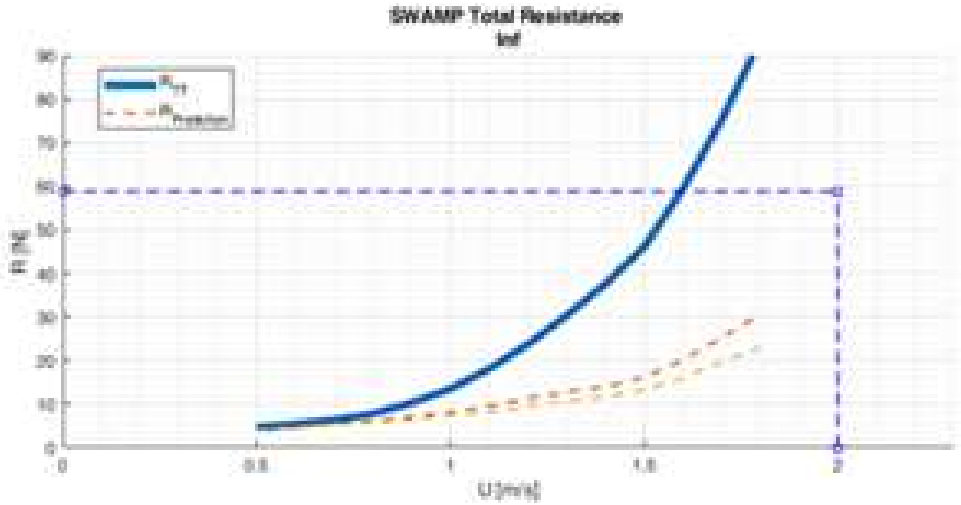

Figure 4.43: R_{TT} *compared to* $R_{Predicted}$

a hull which resistance is higher than the one that could have been possible with an un-constrained design. This kind of analysis suggested to analyse other hull shapes and to see if other hull configurations could lead to a lower resistance.
The first analysis was made by considering a certain number of existing double ended hull data from the Italian towing tank *INSEAN*. As in the case of another (more recent) DEF [157], these hulls shapes, which geometry are reported in fig. 4.44 and which data are summarised in table 4.8, are characterised by higher B/T and higher $L/\nabla^{1/3}$. This means that if we apply the same hull length of SWAMP to these hulls the resulting draft is much lower. These hulls also have a lower L/B ratio resulting in a lower C_B with a consequent hull characterised by lower breadth.
The hulls were used as inverse scaled models to make a comparison analysis withe the resistance

Figure 4.44: *Four INSEAN double ended hull shapes*

of SWAMP but, since the geometry is very different also this analysis resulted unreal.
A rough estimation was made by superimposing the SWAMP resistance with the resistance obtained from scaled models which coefficients were supplied by INSEAN. To make a reasonable comparison the resistance of the models was scaled by using the same $\nabla^{2/3}$ of SWAMP at maximum payload. The results of this rough check showed that the resistance curve of SWAMP is higher than the resistance of the DEF hulls scaled by $\nabla^{2/3}$ value [2].
The analysis was rough and, as shown in table 4.8, the INSEAN models are characterised by lower

[2] From the comparison it was possible to understand that the resistance of SWAMP goes much more with the ratio of ∇ than with the ratio of $\nabla^{2/3}$ (i.e. the wetted surface)

Table 4.8: *The characteristics of SWAMP compared to the INSEAN*

DATA	**SWAMP**	**1960**	**1940**	**1182**	**1156**
L_{pp}	1.2400	96.000	68.400	4.717	4.771
Los	1.2400	99.000	68.400	4.800	4.800
T	0.14	4.090	3.250	0.218	0.204
B	0.2400	15.700	14.600	0.856	1.055
A_w	0.5	1656	938	4.60	3.81
Δ	28.5	3153000	1518000	402	514
L/B	5.167	6.306	4.685	5.607	4.549
$L/\nabla^{1/3}$	4.060	6.774	5.971	6.389	5.993
B/T	1.714	3.839	4.492	3.936	5.163
C_B (Los)	0.6700	0.4830	0.4700	0.4580	0.4960

C_b but this check showed that the resistance of SWAMP can be compared to double-ended hulls and suggested that the adoption of different hull shapes could be possible and modifications in the SWAMP hull shape where investigated.

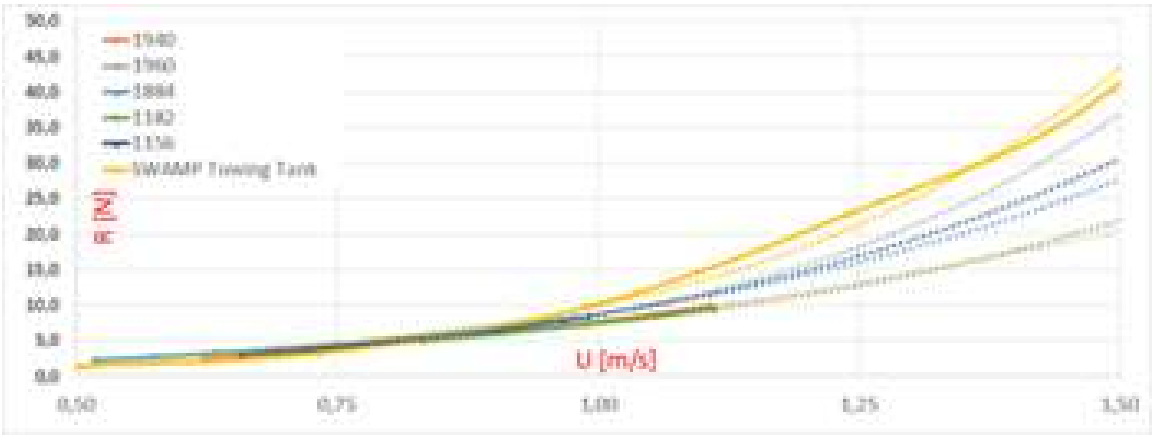

Figure 4.45: *A Rough analysis comparing SWAMP resistance and the four double ended hulls*

Thanks to CFD tools [158], [159], [160] provided at DITEN it was possible to check the possibility of designing a hull with a different shape.
The first step was verifying the capability of the CFD tools of correctly predicting the resistance of the vehicle. An analysis was made to compare the results of the towing tank tests and the results of the CFD analysis on SWAMP hull fig. 4.46.
The CFD analysis was made for 3 different speeds $U = 1.0\,, 1.5\,, 2\,m/s$ at the design weight of $58\,kg$

Figure 4.46: *The qualitative comparison of the bow wave shape between towing tank experiments and CFD analysis at two speeds:* $U = 1m/s$ *and* $U = 1.5m/s$

with a draft of $0.14\,m$. Three rounds of trim correction were made to validate the analysis. The pictures in fig. 4.47 show the comparison between the real model and the CFD wave profile (The picture for the analysis at $U = 1.5\,m/s$ shows the trimmed model).
The results obtained from the comparison are showed in fig. 4.47. From this graphic it can be seen that the CFD slightly under estimates the resistance of SWAMP if compared to the towing tank results. But the percentage error is under 9% and the qualitative trend of the curve is quite perfectly similar with a small hump present at at $1.25\,m/s$.

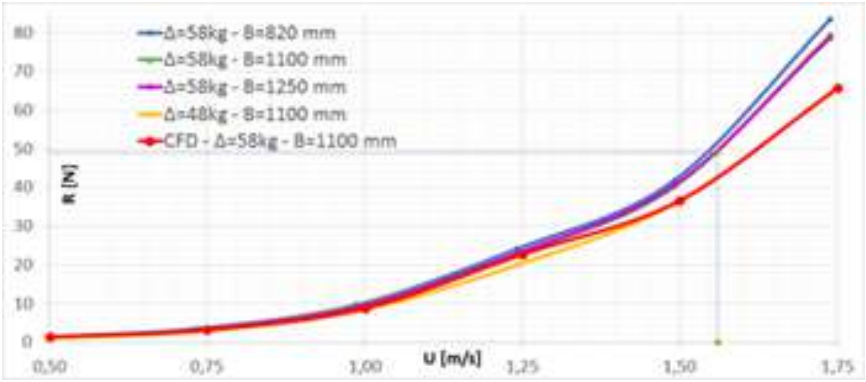

Figure 4.47: *The quantitative comparison of the resistance prediction with CFD and the towing tank results*

The first step was verifying that the CFD analysis could give good results for the design of different hull shapes. Based on the same requirements of the wigley hull then the second step was designing two new hull shapes. These were quite different from the SWAMP wigley one. The lines-plan of the two hulls are reported in fig. 4.48.
The first variant was asymmetric stern-bow trying to create smoother waterlines. As the resistance (mainly wave making) is influenced by the waterline shape of the end(s), slim waterlines were designed. The advantage of this solution could have been the resistance reduction but with a loss in the controllability.
The second variant was asymmetric port-starboard. This is a peculiar shape investigated in different past studies. As an example [155] compared symmetrical and asymmetrical catamarans and the symmetrical form had the lowest delivered power and highest propulsive efficiency, while the asymmetrical form had the highest delivered power and lowest propulsive efficiency. While Utama [141] [161], using data form a split hull test, showed that asymmetrical hulls are found to be

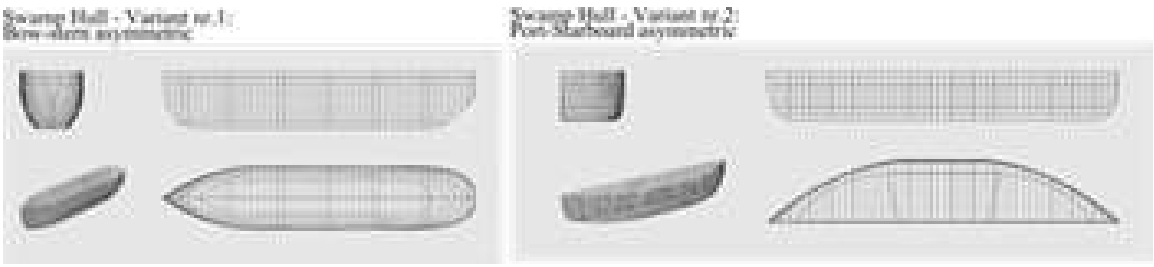

Figure 4.48: *The linesplan of two possible variants of SWAMP hull shape*

less influenced by the interference due to separation and stagger changes.
The characteristics of the two asymmetric hulls are reported in table 4.9. By means of CFD analysis

Table 4.9: *The characteristics of SWAMP compared to the two variants*

DATA	**SWAMP**	**Variant 1**	**Variant 2**
L_{pp}	1.24	1.24	1.24
T	0.14	0.145	0.15
B	0.245	0.245	0.22
A_w	0.5	0.5	0.52
Δ	28.5	28.5	28.5
L/B	5.1	5.1	5.6
$L/\nabla^{1/3}$	4,06	4,06	4,06
B/T	1.714	1.7	1.47
C_B (Los)	0.67	0.65	0.695

on the Variant nr.1 and on two versions (a and b) of the Variant nr.2 interesting results were found. In fig. 4.49 the results of the CFD analysis are reported in the form of the total resistance coefficient

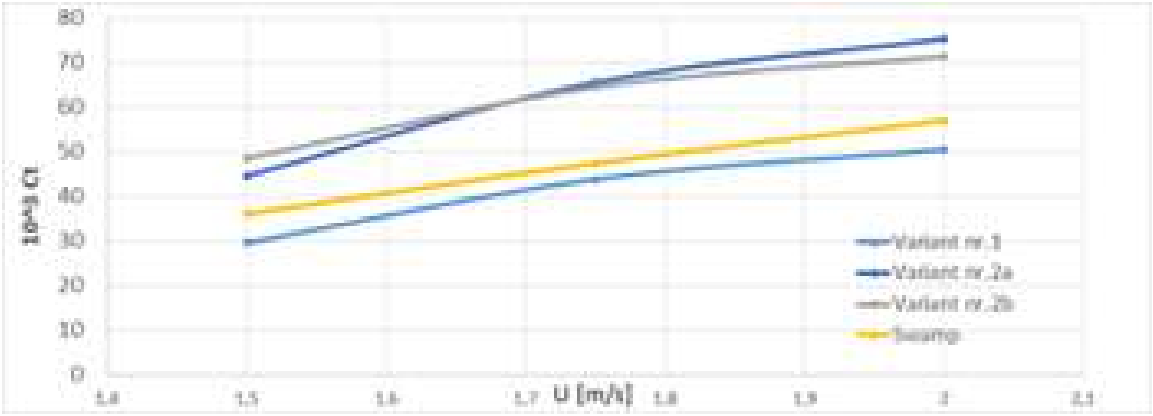

Figure 4.49: *The* $10^3\,C_t$ *curves of SWAMP wigley hull and of the two variants obtained from the CFD analysis*

($10^3\,C_t$). Analysis were performed at three high speeds of $1.5\,m/s$, $1.75\,m/s$ and $2.0\,m/s$. The Variant nr.2 results (in both versions) to have a higher C_t than the SWAMP one. The Variant nr.1 resistance results to be comparable with the SWAMP one.
This analysis was interesting to show how the conflicting requirements of SWAMP are a constrain that leads to a hull shape and choice which must necessarily sacrifice a little hydrodynamic efficiency in favor of operability.

4.5 Stability

SWAMP catamaran shape is advantageous thanks to the unique characteristics in terms of stability. The catamaran solutions resolve some of the big issues of monohulls, and kayaks, which suffer from pitch, roll, and heaving. Since the total width of catamaran is much larger than equal monohull, depending the stability on waterplane section moment of inertia, the multihull stability results much higher.
As mentioned before SWAMP is virtually unsinkable in every condition thanks to the fact that the non-hygroscopic foam completely fills the hull. The transverse stability can be calculated in intact condition and depends on the distance from VCG and the metacentre: GM_t. Even-if the *HSC Code* is used for bigger manned vessels the stability of SWAMP was assessed using the classic criteria through GM, GZ, area under the GZ curve, and the angle at which the maximum GZ occurs; GZ is the righting lever of the stabilising moment. As shown in fig. 4.50 the GZ curve for a

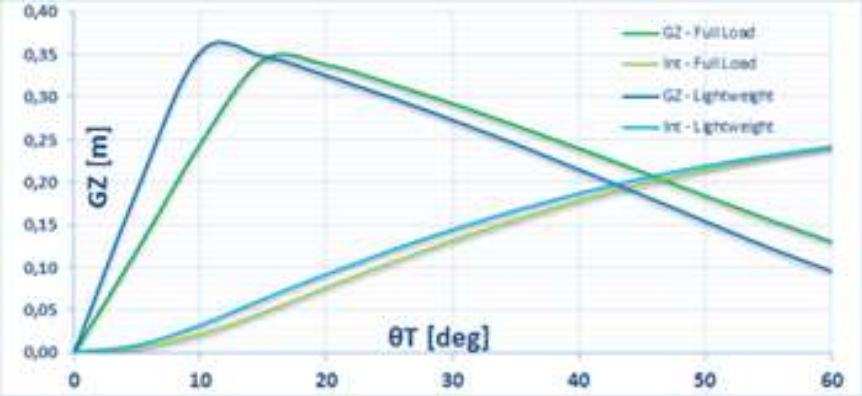

Figure 4.50: *Stability of SWAMP at lightweight and maximum payload*

catamaran tends to be linear over a big range of angles. This happens until one hull begins to emerge from the water, this does not happen in the range of loads of SWAMP. Applying (or increasing) a heeling moment therefore has the effect of reducing the maximum residual GZ value and area under the curve, without affecting the residual GM_T value. The table table 4.10 resumes the values of stability of the catamaran hull at $B = 1100\,mm$ with a the full payload and lightweight stability values. For this analysis the payload was positioned on the deck as a box $0.8\,x\,0.6x\,0.3\,m$. The table also reports a comparison with the stability criteria shown the good matching of the criteria with SWAMP characteristics.

The weighing of SWAMP was assessed by creating a table comprising all the on-board elements, their position and weight. In this way it was possible to identify the position of the Centre of Gravity COG of the vehicle, the weight distribution fig. 4.51 and the stability.
Thanks to the symmetry of swamp hull, of swamp propulsion and weight distribution the loading condition always starts from a balanced vehicle. If care will be taken in loading the vehicle, then it will always float in static condition with a trim approximately $0\,deg$. This is advantageous in case of navigation in extremely shallow water because an initial trim may decrease the operative profile of the vehicle.

Figure 4.51: *The weight and buoyancy distribution at full load*

Table 4.10: *Stability Data*

	Full Payload	Lightweight	
T	0.14	0.09	[m]
Z_b	0.08	0.05	[m]
VCG	0.26	0.27	[m]
KM_T	1.66	2.47	[m]
GM_L	0.58	0.94	[m]
KM_T	1.66	2.47	[m]
GM_T	1.4	2.19	$>$ 0.015 [m]
Comparison with stability criteria			
GZ max	0.34	0.35	$>$ 0.2 [m]
theta max	15	10	$\geq$ 10 [deg]
area 0-30 [deg]	0.13	0.14	$>$ 0.055 [rad*m]
area 30-40 [deg]	0.05	0.04	$>$ 0.03 [rad*m]
area 0-40 [deg]	0.18	0.19	$>$ 0.09 [rad*m]

Its important to report that from the data obtained from the on-board AHRS (attitude and heading reference system) which provides roll, pitch and yaw, attitude and heading information together with the *Hydrostatic curves*, the *Cross Curves* and *Bonjean diagrams* it will be possible to assess the stability of swamp in every loading condition.

The hydrostatic curves are the resume of stabilty characteristics of the vehicle in hydrostatic

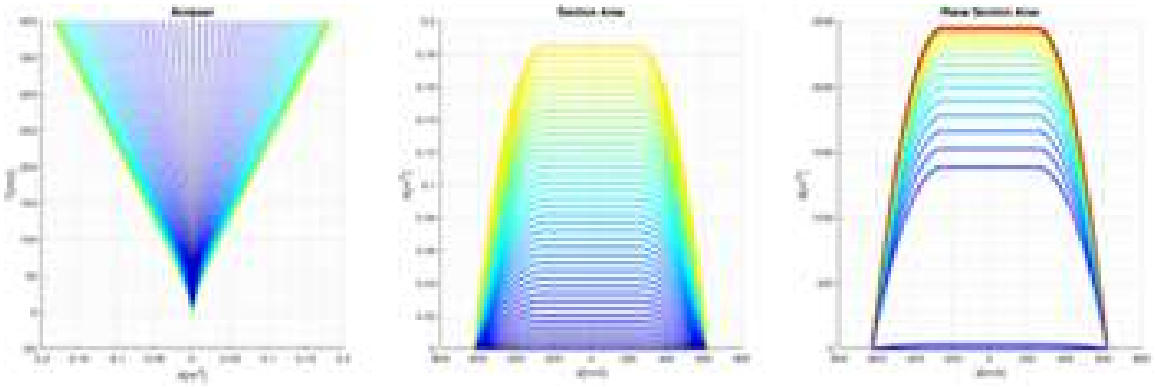

Figure 4.52: *The section areas and transverse aress curves*

condiction. The Cross curves of stability are drawn to define displacement at various angles of heel. They give the distance between Keel K and the perpendicular to the centre of buoyancy Z. KZ is calculated for a range of waterlines and heeling angles, these are known as cross curves of stability and depend only upon the geometry.

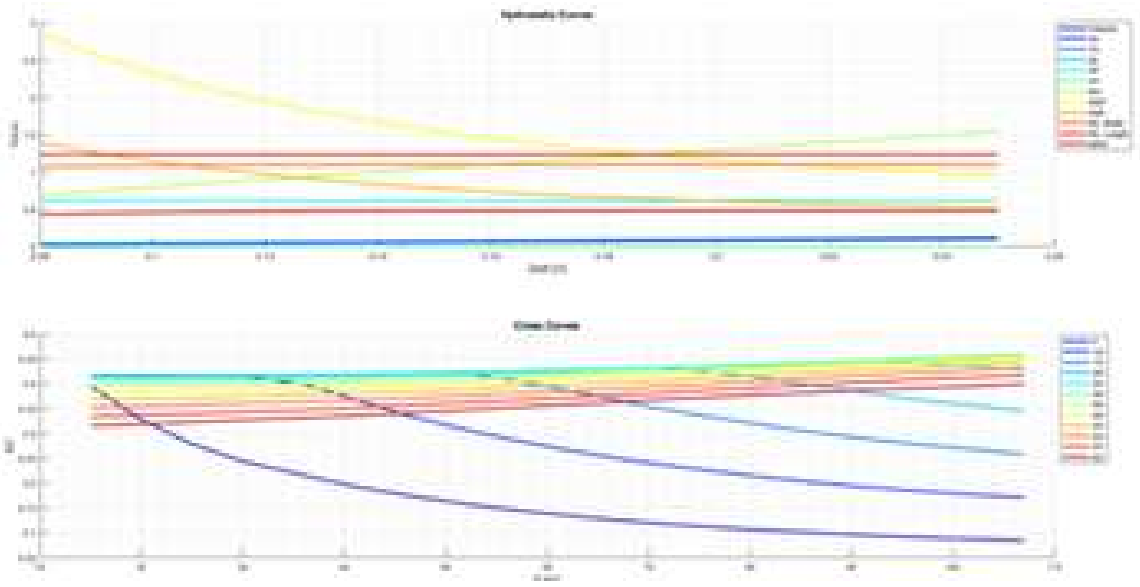

Figure 4.53: *The hydrostatic and the cross curves*

4.6 Propulsion layout and choice

SWAMP was designed around and together the possibility of installing the Pump-Jet Module described in Chapter 5 and in [162]. The commonly used propulsion systems for shallow waters monitoring ASVs are Free-propeller or Ducted-propeller propulsion modules, Waterjet systems, and aerial systems. Screw propelled solutions are subject to damages caused by impacts with obstacles at low depth and therefore not recommended, aerial propulsion, perfect for shallow water, has the disadvantage of having large dimensions that are not suitable for SWAMP design criteria. On the other hand the use of Waterjet propulsion can be considered a suitable choice but it was difficult to couple such a system to the needs of a highly manoeuvrable vessel. The solution adopted was integrating the Waterjet propulsion with a highly steerable solution and the Pump-Jet geometry was chosen. With respect to classical Waterjet propulsion the Pump-Jet is characterised by lower operative speeds, higher structural integrity given by the total integration in the hull and higher manoeuvrability thanks to 360 *deg* steering ability. This kind of system was never adopted before in ASVs.

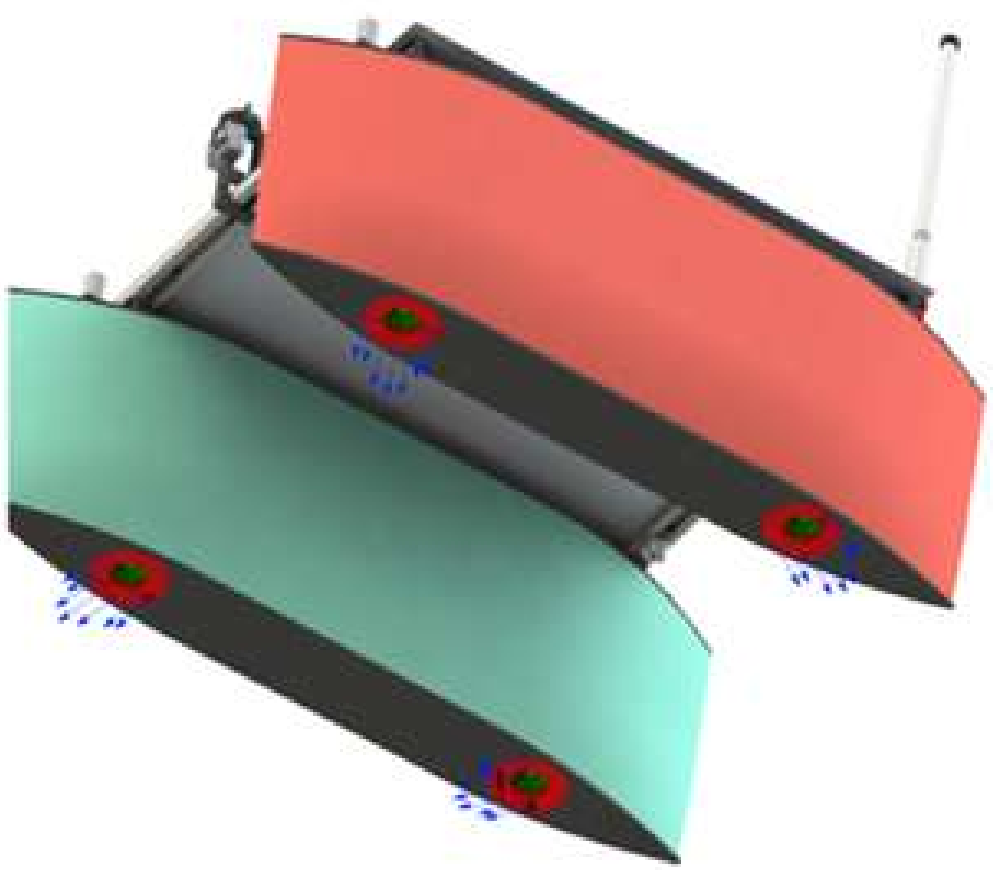

Figure 4.54: *The propulsion layout of SWAMP*

4.7 The modularity concept

Hardware, software and mechanical modularity was one of the main ideas behind the conception of SWAMP structure. The two hulls of SWAMP are two separate modules. Each hull can be composed of more or less sections of lightweight foam, and the operational needs may lead to a reduction of the number of sections, to the increase or modification of the geometry of the sections. Modularity concept is supported by the mechanical solution of the holes drilled in the foam. This solution allows to think the hull as a modular structure where propulsion units, batteries in a various number, sensors and payloads may be positioned or removed from the hull by just pushing into or pulling from the holes. The hardware control system of the SWAMP vehicle is fully modular and it is based on a set of heterogeneous modules contained in watertight canisters. These modules contain computational boards, sensors and the thruster of the vehicle while batteries for power supply are housed into different canisters. Each module composing the hardware control system has got only one connection used for power supply and communicates with the other modules by means of a Wi-Fi radio link at 2.4 GHz. Each of the two hulls composing the complete SWAMP vehicle has got (at least) three modules:

- computational module
- actuation module
- communication module

In this direction modularity led to the extreme; the vehicle can completely be disassembled in just a few steps.
But the modularity exists at two levels in the SWAMP project:

- At a *small scale*: every part constituting the vehicle can be easily removed and/or replaced in few second. In less than 15 minutes the vehicle can be completely dismounted.
- At *large scale*: each hull is a modular vehicle. Each hull can be considered as a single module with its own propulsion, intelligence, communication system and power source. This makes SWAMP a vehicle composed by two vehicles.

The development of modular unmanned vehicles at a *small scale* is something that attracts most of the researchers [163] but few examples really exist that can be said as modular unmanned marine vehicles. In recent years some vehicle like MARTA [164], an AUV for marine archaeology, the WAM-V [165] and P2-ROV [5] reached a good level of modularity.
The development of modular unmanned vehicles at a *large scale* is something that involves few research projects and that is a part of the cooperative control [166]. As explained in [167] the problem of modelling a system of interconnected robots with highly coupled dynamics like the one that exists between the two hulls of SWAMP is an open problem. The study presented in [168] consists of a cluster of modular vehicles that can attach to each other by a connection mechanism. [169] investigates the self-reconfiguration of this modular robotic system by managing the energy consumed heuristic.
The modularity of SWAMP can bring to a fleet of cooperating vehicles that can get together to form a bigger vehicle by means of cooperative algorithms. As an example in [170] a conceptual design of modular vehicles is presented. An hydraulic Propulsion is invented to operate a robot in a fluid environment. The robot moves by routing the fluid through itself. The robot's modules represent sections of a hydraulics network. Each module can move fluid between any of its faces. The modules (network sections) can be rearranged into arbitrary typologies.
This kind of robotic solution can be useful in the self-assembly of large teams of autonomous robotic

boats into floating platforms. In [171] identical self-propelled robotic boats autonomously dock together and form connected structures with controllable variable stiffness. These structures can self-reconfigure into arbitrary shapes limited only by the number of rectangular elements assembled in brick-like patterns.
Assembly studies to reinforce the ideas of a fleet of modular robots with on-board thrusters, active connectors, embedded computers and communication systems will be subject of future studies of SWAMP.

Chapter 5

Propulsion System

5.1 Introduction

As shown in Chapter 2 surveying wetlands is arduous, as the technological solutions currently available for use in in this peculiar environment have proven inadequate. In particular, water sampling and monitoring by using ASV in the very shallow waters, that sometimes characterize swamps, rivers, lakes, and coastal areas, is extremely complicated. While some of these vehicles have been specifically designed to work in shallow waters, nevertheless, as shown in Section 5.2, they usually adopt propulsion units that are unsuitable for operation in extremely shallow waters, namely those between 10 and 15 cm in depth.
The solutions adopted so far are quite classic and more suitable and innovative propulsion units are necessary to increase the operative area of the vehicles in shallow water.
Various uncommon ideas were investigated in the initial phase. The use of the paddle wheels was one of these. This system is no longer used but this is linked to the fact that the adoption of such a solution is complex due to the variable immersion that occurs at sea due to the presence of the waves. A solution of this type would have require an ad-hoc design and a study on the materials to be used but the advantages could have been numerous. Moreover this system is poorly studied from the academic point of view and the design is more empirical than theoretical, even if recently its application at high speed has return to the attention of researchers, as shown in [111]. A paddle wheel system, that includes a wheel for both sides of the vehicle, has already been used in manned applications and it has been found to be exceptionally manageable and with good directional control [172] and [113]. The system is practical because it can guarantee good usability even in the case of amphibious needs of the designed vehicles. But other systems like paddle wheels exist that have already been widely used in amphibious vehicles that provide for the use of wheels, [173] or screw-propelled [114, 174].In [148] the *whale-tail* solution is investigated. In robotic terms the biomimetic solutions like [175] and [176] are of notable interest but also in the naval field they do not disdain alternative solutions, like that of the flapping foil which is widely supported by researches of theoretical type ([177] and [178]). Some tank tests have been carried out on caudal fin thrusters, with efficiencies that have not proven to be high [179] but leave hope for experimentation. Furthermore, the MARIN (Maritime Research Institute Netherlands) has performed numerous tests and calculations on the concept of O-foil [180], with very positive theoretical results. The O-foil system was then tested on the MS Triad in 2013, promising to increase efficiency and reduce consumption up to 50%.
A possible solution could have been the Surface-Piercing Propellers (SPP) that have only the lower half of a disc immersed in the water and therefore they are suitable for shallow drafts. Even if they are usually used for HSC, recently a slow-speed SPP-CPP was investigated as shown in [181], which exploits the fact that SPP beside the thrust generates a large side force too, which enables steering. Nevertheless, SPP have a large propeller disc whose bottom half only is producing thrust and, due to generated side force, have to be used in pairs. A difficult application on a catamaran and lowly

manoeuvrable solution.
As far as the double ended vessels are concerned most of the designer's choice fell on Voith-Schneider propellers (VSP), that have proven themselves as reliable propulsion systems for DEF [157] but these are not suitable to work in very shallow water, because in case of impact with the bottom, the system can irreparably be damaged. For this reason, in some cases the Pump-Jet [182] was used and after investigating the possibility of using various systems like paddle wheels, flapping foil and screw propulsors, the choice for SWAMP fell on the Pump-Jet. While Waterjet systems are widely used, these may only be used as a main propulsion system. On the other hand the steerable Pump-Jet has the advantageous solution of being both a propulsion and a manoeuvring system.
The basic principle of a waterjet system is that water is sucked from beneath the keel of the vessel, then it passes through the axial flow pump where the pressure is increased, then the water, at a high speed, flows out the system again through a nozzle. Thus the thrust is generated in forward direction. It is possible to compare the velocity field of Pump-Jet with the velocity field of low-power water-jet. Low-power Waterjets, and high power ones have a common factor: the high jet velocity. Pump-Jet is a steerable pump-based thruster suitable for shallow water and non-standard applications, which can be used both as a maneuvering aid and as the main thruster. It provides 360 degrees of continuous steering, a compact design, installation flush with the hull, and virtually no risk of damages from grounding or floating debris.
At present, no small-sized (under 1 kW) Pump-Jet-based solution is available on the market, and the available literature on this kind of thruster is very poor. For this reason, in order to develop a propulsion unit based on the Pump-Jet concept for shallow water ASVs, we had to design our system from scratch, from modeling to design and construction. This paper describes a Pump-Jet Module (Pump-Jet Module) (shown in fig. 5.1) built with innovative techniques, together with the mathematical modeling used for designing the system. Design characteristics, production techniques, bollard pull tests and experimental results are reported in this article. This research is intended to pave the way for the application of Pump-Jet technology to lightweight ASVs for extremely shallow water applications.

Figure 5.1: *The modular Pump-Jet thruster for ASV operations in extremely shallow water.*

5.2 Pump-Jet Module Application

The main indications that drove the design of the Pump-Jet Module are that any propulsion system, to be used in extremely shallow waters:

a) has to be able to work on a small vehicle with minimal draft

b) it has to be capable of surviving in the probable event of grounding

c) it has to provide the vehicle a high degree of controllability

d) it must be modular

e) it must be both light and small

ASV propulsion systems often adopt commercial propulsion units. The most common systems used in ASVs for monitoring shallow waters are free or ducted propeller propulsion modules, water jet systems, and aerial systems. A schematic review of these systems is shown in fig. 5.2.

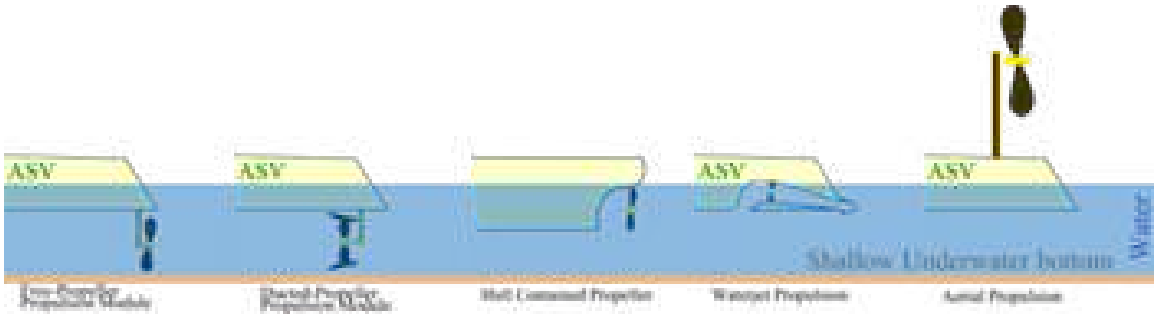

Figure 5.2: *Existing ASV propulsion systems.*

Free propeller modules with a vertical fin supporting the propeller are amongst the most common (e.g., [50,116,183]) and most efficient systems currently available and allow considerable design flexibility. On the other hand, these propellers are extremely liable to damage from collision with obstacles at low depth and they are therefore not recommended. Ducted propulsion modules have the same structure, but the propeller is protected by the presence of the duct (e.g., [48, 184]), in some cases with an azimuth system (also with rim-driven technology [185] and hubless propellers), combining high control capabilities with high thrust at low speed. Ducted systems have similar problems as the above-mentioned free-propellers, in that the unit may be subject to impact with the seabed. Moreover the diameter of the propulsion unit and the need of working well below the free-surface to avoid cavitation and to maintain the efficiency, increase the depth of the vehicles, inibithing the possibile access in extremely shallow environments. For this reason, free propeller thrusters, whose disc is completely contained within the hull (e.g., [84]), offer a partial protection from impact and the possibility of accessing shallower waters, but do not represent a real improvement either in terms of maneuvering or protection.
Aerial propulsion used, as an examble by aerRobotix [76], which may at a first appear to be an excellent alternative for shallow water operations, has the disadvantage of the propeller's large size (compared to the vehicle) and low efficiency, which also involves poor design flexibility and high noise levels, making it unsuitable for protected areas. This kind of propulsion is also used by an other recently developed italian vehicle: the DEVSS The use of water jet propulsion provides a good alternative, especially because the lack of protruding appendages solves the problems of draft and navigation in shallow water (e.g., Sonobot [109, 186]). However, if the system is flush with

the hull, this will result in low maneuvering capacity, thus barring hovering functions. If the solution involves a complex and damage-prone directional system (e.g., [187, 188]) for the nozzle with a reversing bucket to reverse thrust, it will not satisfy the impact-resistance requirement of shallow waters research.
Some interesting amphibious-like solutions such as [189] are currently being employed in the laboratory, and these may prove to be of great interest in the future. Other interesting solutions being used to work underwater in the proximity of the seabed have been proposed in the U-CAT [190,191] and WIEVLE [192] robots; these avoid the risk of damaging the propulsion unit and are suitable for AUVs and ROVs. This range of approaches suggests that various solutions may be adopted to extend the survey ability of ASVs.
A low cost ASV recently studied [193] investigated the possibility of using the screw theory for the propulsion system, which provides good manoeuvrability and amphibious features to the vessel.
In order to combine the ability of working in only a few centimeters of water, combined with satisfactory control abilities the SWAMP ASV design is based on an azimuth thruster. This solution, known as the Pump-Jet, has previously been adopted in ships working in shallow waters, but it has never been adopted in robotic vehicles. Only some AUVs adopt a Pump-Jet based propulsion for the manoeuvrability of the vehicle, and in particular [194] uses a steerable pump-based solution for the manoeuvring.
Vehicles expressly designed to work in shallow and confined waters and in harsh environments may minimize the effects of possible (and probable) impact with the waterway ground by combining a flat bottom with the use of a module. The Pump-Jet Module is suitable for these vehicles and for accessing extremely shallow waters since it satisfies the requirements of reduced immersion, controllability, propulsion intactness, and minimal impact on the environment. The Pump-Jet Module can work in minimum water depths as low as $50\,mm$ without risking damage; the possible impact of the vehicle with outcropping stones, roots, or similar objects that can damage the propulsion system with consequent risk of losing the vehicle is minimized by the Pump-Jet geometry. Since ASVs must be able to access narrow areas for sampling, even in the presence of external disturbances, they should be fully controllable both in station keeping and in path following. For this reason, a propulsion layout based on four azimuth thrusters (like the Pump-Jet Module) is considered a suitable approach.

5.2.1 The Pump-Jet

The Pump-Jet operates on the principle of a vertical axis pump. An impeller sucks in water from beneath the hull, and through the blades, the water is whirled tangentially and radially outward into the casing chamber. The fluid gains both velocity and pressure while passing through the impeller. The outlet nozzles in the steerable casing accelerate the flow, and a jet of water produces thrust horizontally beneath the flat-bottomed hull.
The first prototypes of steerable thrusters with outlets placed in the bottom of watercraft were invented around 1920 [195], but more recent systems were developed around 1975 for military craft. Today, these constitute an alternative either as a main or as an auxiliary propulsion unit. Various manufacturers produce them: Veth [196], Schottel [197], Jastram [198], Tees White Gill [199] and PT. Marine Propulsion Solutions [200]. A schematic reproduction of these products is displayed in fig. 5.3.

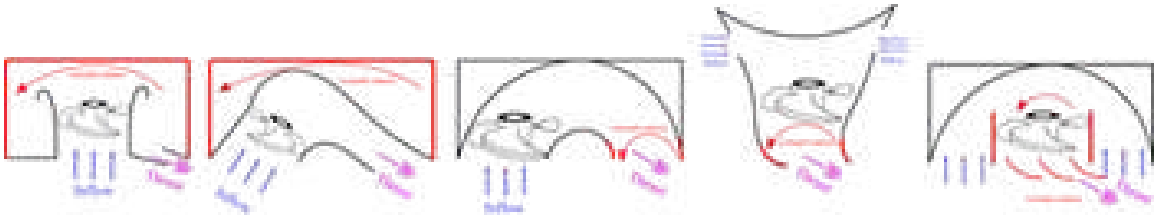

Figure 5.3: *Schematic description of the industrial products. Left to right: Schottel SPJ [197], Veth Compact Jet [196], Jastram Azimuth Grid Thruster [198], Tees T3s Vertical Shaft Unit [199] and PT. Marine Propulsion Solutions [200]*

Each of these manufacturers has developed its own Pump-Jet system with unique characteristics. The main advantage of using Pump-Jet s is maximum thrust at minimum draft. Another advantage claimed by the manufacturers is that effective thrust can be achieved even at higher speeds. Since the Pump-Jet is installed flush with the hull, it does not produce a significant increase in resistance if compared to other systems, and there is no risk of collision with floating debris. This system is suitable for operating in extremely shallow waters, since the risk of damaging the system in case of grounding is very limited. While this system was initially developed as a maneuvering device, currently, it is also used as a main thruster. In addition to all these advantages, most of the manufacturers claim that the system is distinctly low-noise.
Veth produces various versions of the Pump-Jet, but the most space-saving one is the Compact Jet, where the propeller is placed at an angle of 17°, so that greater thrust can be generated when water flows through a hydrodynamic streamlined housing control grid. The entire system, grid plus propeller, is 360° steerable. The whole system is placed on the vertical plane of the vessel, whereby water is sucked in obliquely from under the ship: this makes this solution similar to water jet propulsion.This type of control grid derives its momentum only in overpressure. Veth claims that the system is low-noise. The complexity of the system lies in steering an oblique propeller.

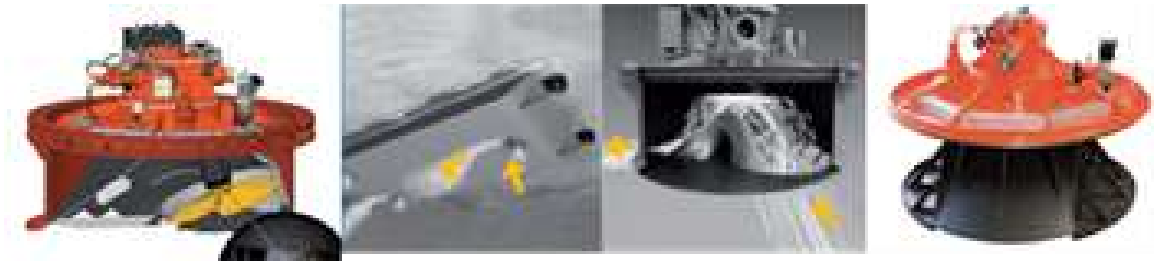

Figure 5.4: *Veth Compact Jet [196]*

The Schottel Pump-Jet (SPJ) differs in part from the Veth-type control grid because the Schottel Pump-Jet is based on the principle of centrifugal pumps, where centrifugal forces ensure that the fluid is pumped through a 360° rotating outlet nozzle. In this system, the pump shaft is coaxial with the azimuth shaft, thus reducing bulkiness. The SPJ owes its success to compact design.

Figure 5.5: *Schottel SPJ [197]*

The Jastram azimuth grid thruster is a special system requiring two openings in the hull. The first, fixed, is used by a propeller that generates a high volume of water at low pressure, which flows towards a second, steerable, opening through a horizontal channel. The actual thrust direction is given by the rotation of this second opening. The Jastram azimuth grid thruster is capable of providing highly accurate dynamic positioning, responsive steering and emergency propulsion. As all the Pump-Jet s it mounted flush to the bottom of the vessel, it has no protruding parts which could be damaged in shallow water. A removable grid protects the horizontally mounted propeller. Smaller parts and sand are washed through the large-volume housing.

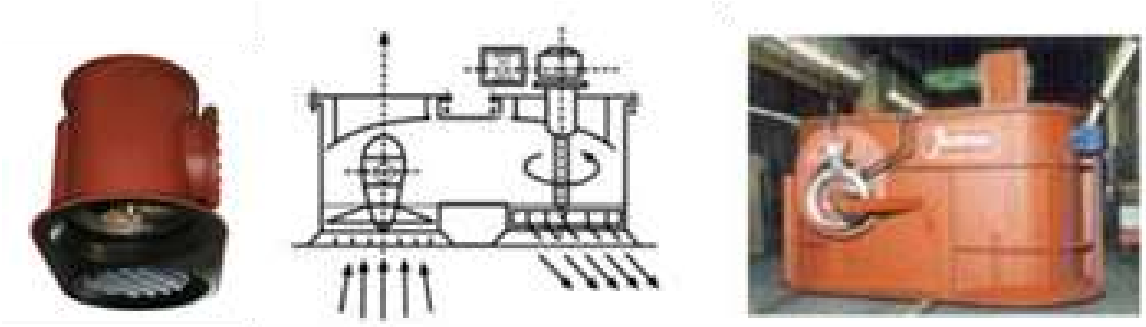

Figure 5.6: *Jastram Azimuth Grid Thruster [198]*

The Tees Vertical Shaft Unit system is a unique piece featuring two water inlets on the sides of the hull pushing water downwards, where a steerable grid pushes the water in the desired direction. The gain in space and the hydraulic advantages are obvious. On the other hand, this system constrains hull shape design and seems to be more suitable as a maneuvering system than as a main thruster.

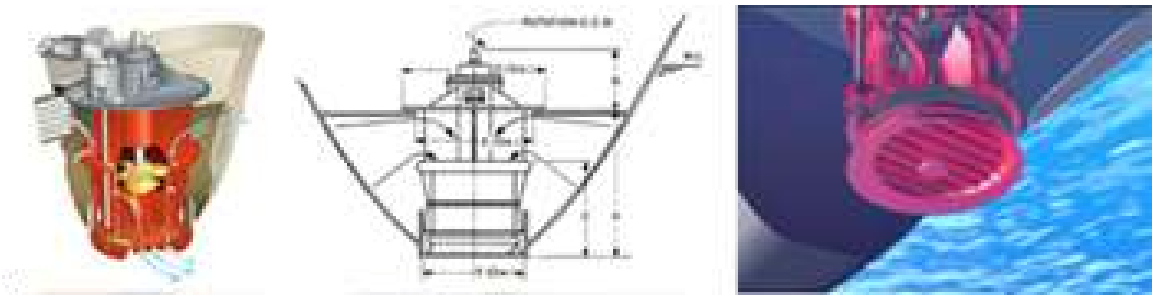

Figure 5.7: *Tees T3s Vertical Shaft Unit [199]*

A variant of the duct system is a horizontally arranged system with suction in the plane with

two to four outflow openings. This system is widely used in inland bow propulsion. A three and-or four channels form is used, the outflow from the vertical propeller is deviated by a vertical rotating component to produce a thrust in one/two directions.
PT. Marine Propulsion Solutions is recognized as one of the world's leading Electric Podded Thruster and Propulsion Systems Manufacturer. It introduces its unique and tailored Azimuthing Pumpjet Thruster Systems for all types of Marine vessels. In particular, as shown in fig. 5.8 and in fig. 5.3, most of the options studied by PT. Marine Propulsion Solutions comprise a system that is conceptually similar to the Tees one and the inverse if compared to the other solutions. Below the vessel there is an external suction with a central steerable jet.

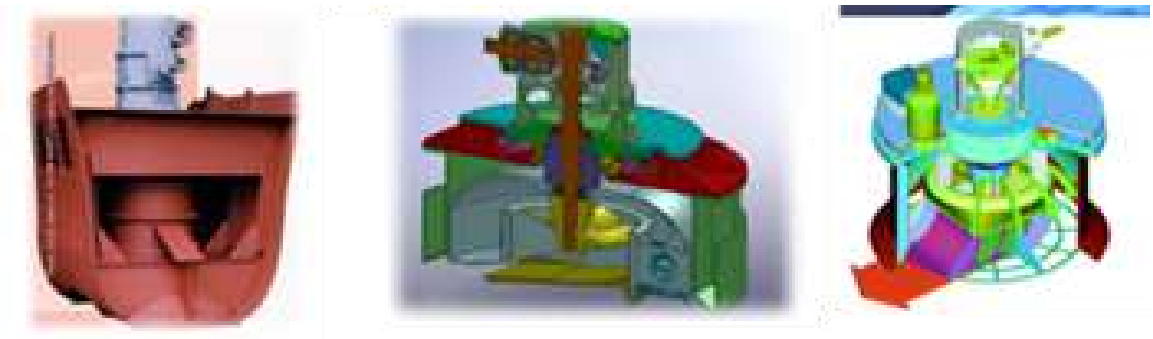

Figure 5.8: *PT. Marine Propulsion Solutions [200]*

Summing up, the Pump-Jet concept is a consolidated design based on the simple application of basic physical laws with acceptable efficiencies. Very few studies exist in the literature on Pump-Jet design and functioning, and they are related to the effects of the Pump-Jet on riverbanks [201] or on the performances of hulls that mount this kind of system [202]

5.3 Pump-Jet Module Design

The geometry of our Pump-Jet Module was inspired by the existing systems mentioned above [203]. Our aim in installing a Pump-Jet Module on an ASV was to prevent damage in case of collision with the bottom, and to reduce a possible additional resistance.

The main idea behind the Pump-Jet Module was to design a watertight module that can easily be dismounted from the ASV for easy transportation and can be employed on different vehicles. For compactness, the control unit is embedded and contained inside the module. The azimuth motor provides continuous feedback on position, guaranteeing high maneuverability with high rotating nozzle speed. As mentioned before and shown in fig. 5.9, the Pump-Jet principle stems from a mixed-flow or centrifugal pump, which produces static pressure that causes water flow to stream out of a steerable nozzle. The (usually vertical) pump sucks in water from under the vessel; the water is channeled through a casing and flows out through a nozzle positioned at the bottom of the unit near the inlet duct. Thrust is produced by conversion of static pressure into kinetic energy and potential energy. When water flows out of the pump, energy is transformed into kinetic energy, which leaves the system at high speed through the nozzle opening. Since thrust is the product of water flow by water velocity, the greatest advantage of the Pump-Jet is that it only requires a very low volume flow to generate a propulsion force. The entire casing is designed to be 360° steerable; the water jet trajectory is relatively short, minimizing frictional losses, and its path through the casing chamber is also relatively short and three-dimensional: this and other factors make the system efficiently compact.

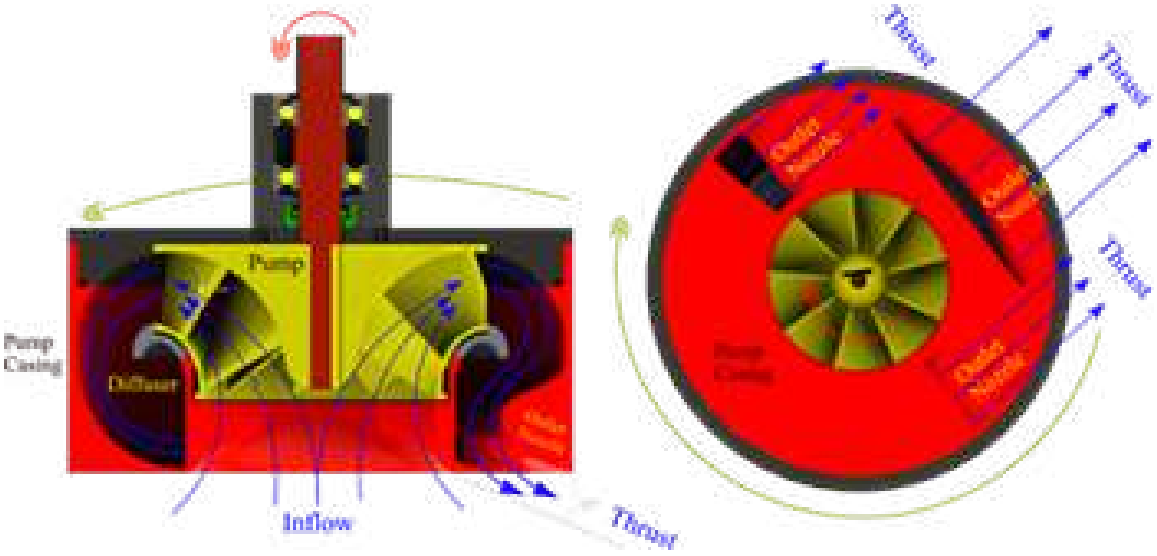

Figure 5.9: *The Pump-Jet operating principle.*

The nozzle area at the bottom of the propulsion unit is approximately one third of the intake area, so water intake velocity is only one fourth of outlet velocity in the nozzles. This is important to minimize the risk of sucking in unwanted bodies in shallow waters. The outlet angle of the water is approximately 15° from horizontal: almost the entire jet thrust is converted effectively into forward thrust. At the same time, in shallow water, the impact on the river/lake bed or sea bed is reduced, and measurements can be carried out with limited disturbance, as the water is expelled almost horizontally from the Pump-Jet Module and rises towards the surface as soon as it leaves the nozzles. The high velocity of the water leaving the nozzles means that the Pump-Jet Module can be used to maneuver vessels at high speed since considerable thrust can be achieved even at high speeds. This is due to the high intake performance of the mixed-flow pump. As far as

construction is concerned, the pump impeller was 3D printed for ease of production, and also because this production method made it possible to test different pumps. For the same reason, the module itself was constituted by a 3D-printed element hosting both the inlet duct and the outlet nozzle (the element governing thrust production), as shown in fig. 5.10. This element is structurally connected to a hollow shaft made in Polyoxymethylene (POM) that houses the bearing for the pump-shaft and is supported by a self-lubricating bushing, in turn hosted by a housing made in POM; this represents the structural element of the thruster. Two Nitrile Butadiene Rubber (NBR) sealing rings, one for the hollow shaft and the other for the pump-shaft, guarantee water-tightness. The housing constitutes the main support for the two brushless electric motors: one drives the pump, and the other governs nozzle steering. The first motor is coaxial with the pump, while the second shaft axis is parallel to the shaft of the pump, and motion is transmitted to the nozzle by mean of two fiber-reinforced plastic gears, where the driven gear is screwed to the hollow shaft, which in turn is screwed to the nozzle. On top of the module's housing, a plastic pipe with a plastic cap is installed, and two NBR O-rings seal the entire module. Inside the volume formed by the plastic pipe, the brushless motor, the control electronics, and the communication system are contained. In this way, the electric power cable is the only additional element entering the module, thus creating a one-piece element.

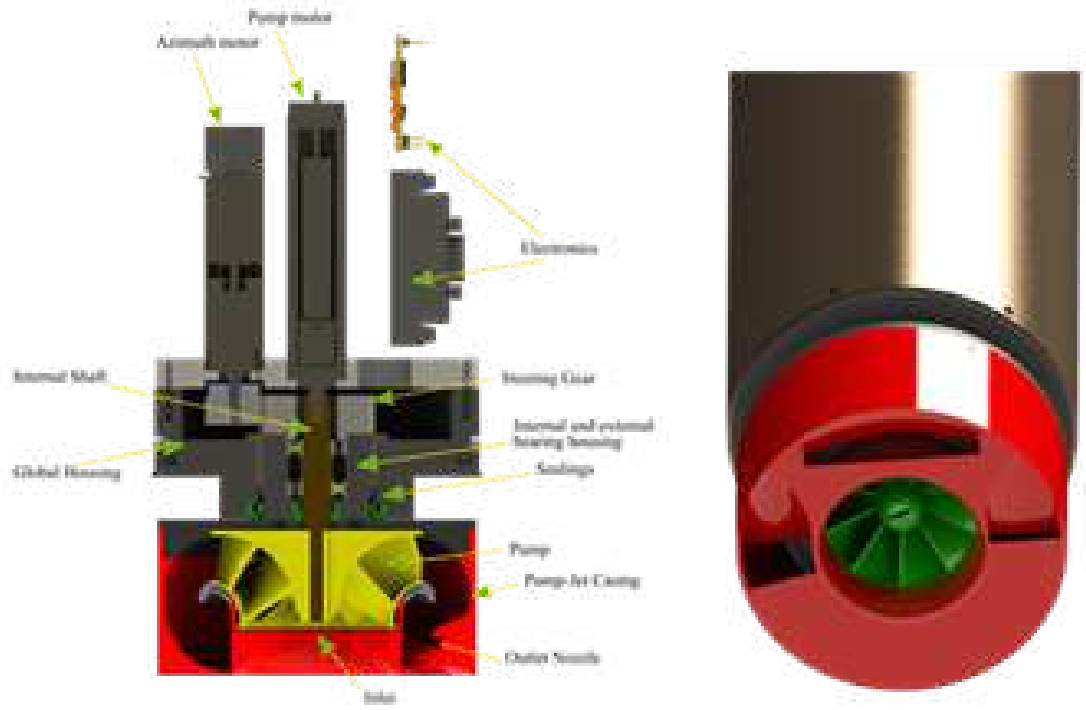

Figure 5.10: *The PJ Module (Pump-Jet Module).*

All the elements were made of lightweight inert plastics, so as not to compromise the samples acquired by the ASV mounting the Pump-Jet Module. A 3D printer was used for building the Pump-Jet Module components, thus allowing us to prototype the system quite rapidly. Moreover, this made it possible, during the testing phase, to modify promptly and test various configurations, and no high-cost mold was necessary for the impeller and the outlet duct.

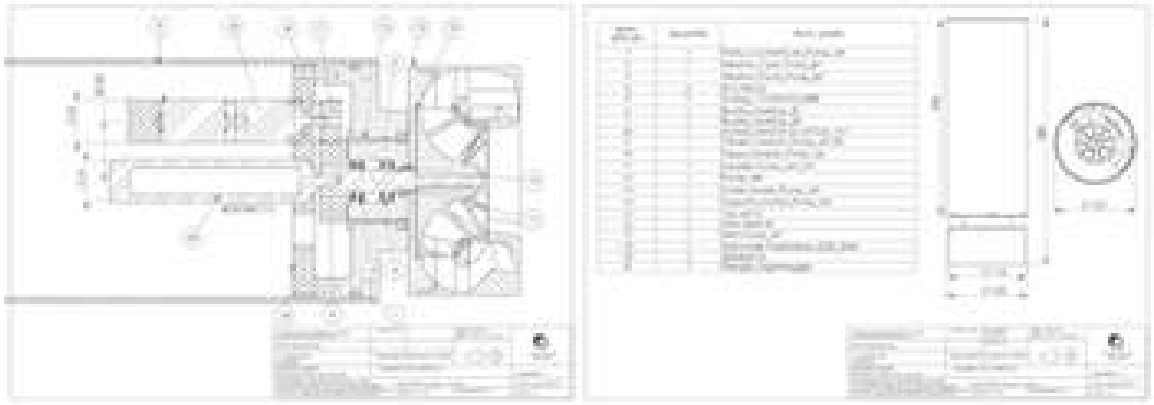

Figure 5.11: *The Pump-Jet Module mechanical drawings*

5.3.1 Pump Design

To start designing the system, the Pump-Jet Module's geometry had to be defined. Based on the ASV's size and thrust needs, the authors used the theory governing mixed-flow pumps to define the geometrical constraints underpinning the entire design.

Geometric Data

The maximum diameter of the Pump-Jet Module was defined based on the following parameters:

- draught of SWAMP,a small-/medium-sized ASV,
- payload of SWAMP,a small-/medium-sized ASV,
- main dimensions SWAMP, a small-/medium-sized ASV,
- required thrust for SWAMP, a small-/medium-sized ASV,

the desired value was identified as $D_p = 120$ mm. A number of geometric characteristics constraining the Pump-Jet Module design were identified; most of these constraints were related to the main diameter D_p (see fig. 5.12), which must make it possible to scale the system for different diameters and choose the one that better matches mixed-flow pump requirements and the geometrical constraints of the vessel.

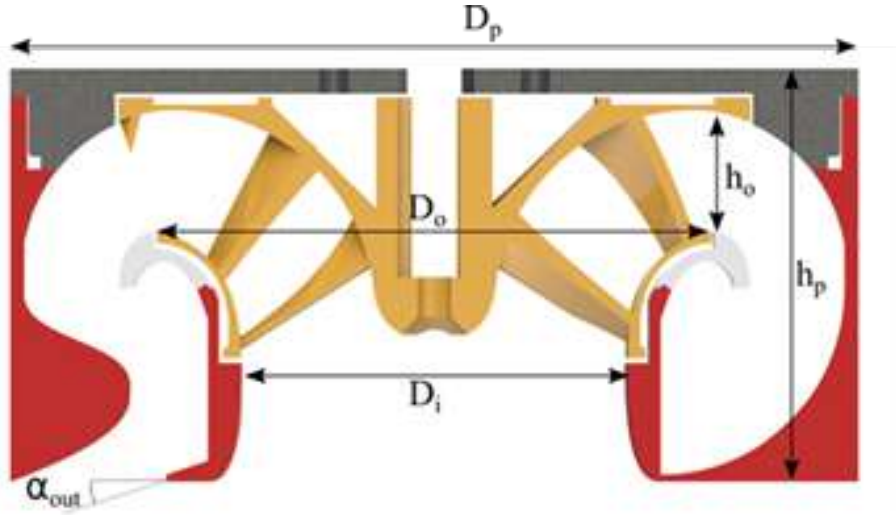

Figure 5.12: *Schematic design of the Pump-Jet Module with the main characteristics.*

To constrain the design, the height of the casing was imposed to be $h_p = D_p/2$ to allow for the future Pump-Jet Module scaling. The inlet diameter of the Impeller was imposed to be: $D_i = D_p\,0.45$, and the maximum outlet diameter of the impeller: $D_o = 0.6\,D_p$, while the height of the impeller outlet was defined as $h_o = 0.2\,D_p$; therefore, the impeller areas were: $A_i = \pi\,D_i^2/4$ and $A_o = 2\,\pi\,D_o/2\,h_o$. These values determined the overall dimensions of the Pump-Jet Module, and D_o was particularly important because, as shown below, this value influences the pump head and the RPM of the impeller, thus constituting a key element in selecting the motor.

The chosen water discharge angle with respect to the Pump-Jet Module bottom was $\alpha_{out} = 15$ deg.

As a final geometric constraint, to achieve the requested outlet area (as shown in fig. 5.13), the discharge nozzle was subdivided into three channels, then the outlet area was calculated by summing up the three areas:

$$A_n = a_{d_{front}} + 2\,a_{d_{side}} \quad (m^2) \tag{5.1}$$

With the latter value all the geometric data were determined.

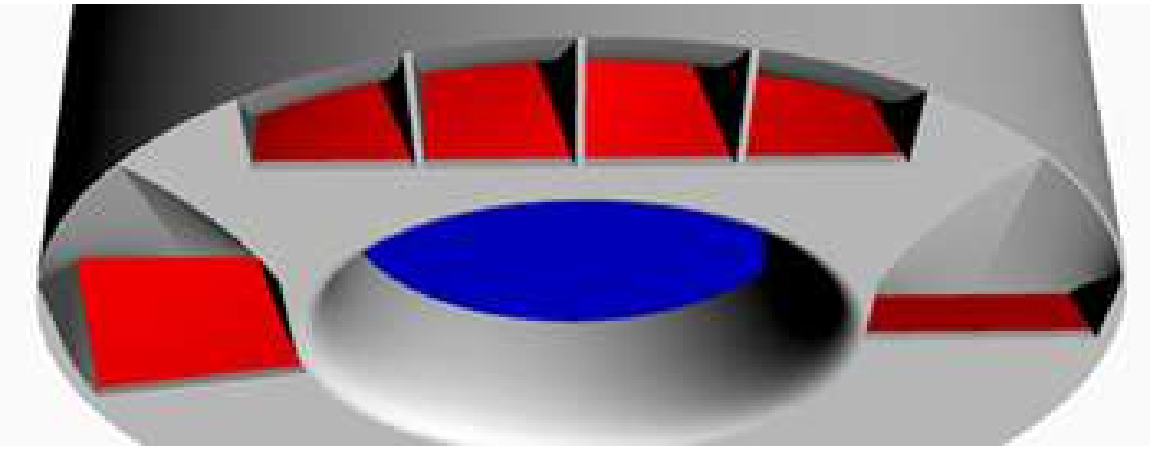

Figure 5.13: *In red, the outlet areas are shown.*

Propulsion Data

The value of the design thrust for the Pump-Jet Module was obtained from the resistance of SWAMP small-/medium-sized ASVs.
The module may be considered as a free-running propeller studied for bollard pull and low speed. The exact amount of thrust has to be validated during moving tests (e.g., in self-propulsion in a towing tank) with the module installed on various ASVs, whose advance speed may influence the exact amount of thrust produced by the module resulting into a thrust deduction factor and/or a wake fraction.
In fig. 5.14 the curve resistance of SWAMP at weight of $58\,kg$ is reported. To take into consideration a possible 20% loss in thrust at speed an added resistance was calculated by multiplying the resistance for a 1.2 factor. The resultant resistance at $1.5\,m/s$, divided for the number of thrusters (i.e. 4), was taken as the required thrust is reported in the same fig. 5.14. The design thrust of the Pump-Jet Module was identified as $T = 12.3\,[N]$.

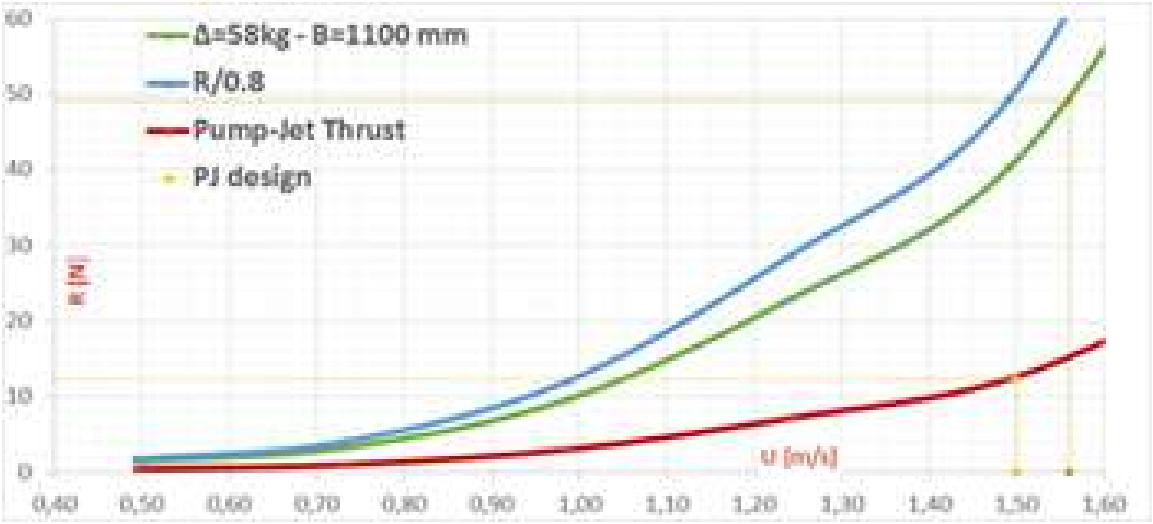

Figure 5.14: *The SWAMP resistance and the Pump-Jet expected thrust value.*

Thrust is roughly originated from water flow multiplied by outlet water velocity. For this reason, all these parameters must be calculated in order to model the thrust unit. The vessel's propulsion thrust derived from the change in momentum taking place when water enters and leaves the jet thruster system [110]. Therefore, the thrust produced by the Pump-Jet system is expressed as follows:

$$T = \rho_w \, A_n \, V_o \, (V_o - V_i) \quad (N) \tag{5.2}$$

where A_n is the discharge area, V_o is the outlet flow speed, and V_i the inlet flow speed. With respect to the output angle, the thrust is:

$$T_\alpha = T/cos\alpha_{out} \quad (N) \tag{5.3}$$

Since the value to be extracted is outlet water velocity V_o, then water flow must also be calculated. To do so, we can use the equation:

$$T_\alpha = (\rho_w \, A_n \, V_o^2)/cos\alpha_{out} \tag{5.4}$$

where V_i is, in first approximation, negligible. This assumption is supposed to work since this value does not substantially influence the value of H_p. During impeller design, a little inflow velocity was assumed possible due to vehicle speed [204]. As mentioned above, case-by-case tests were performed

to evaluate Pump-Jet Module thrust at various ASV velocities. The flow rate at the outlet therefore is:

$$m_f = \rho_w \, A_n \, V_o \quad (kg/s) \tag{5.5}$$

$$Q_o = A_n \, V_o \quad (m^3/s) \tag{5.6}$$

Pump Head

The data calculated above led us to defining the pump head necessary to design the impeller. From the Bernoulli equation:

$$\begin{aligned} &P_i + 1/2 \, \rho_w \, V_i^2 + \rho_w \, g \, H_p = \\ &P_o + 1/2 \, \rho_w \, V_o^2 + \rho_w \, g \, \Delta h + \rho_w \, g \, h_{loss} \end{aligned} \tag{5.7}$$

where H_p is the head associated with the pump and P_o and P_i the outlet and inlet static pressures, which are equal because the atmospheric pressure added to the water column is constant. Δh is the static difference in the head between inlet and outlet, which in this case was null, and h_{loss} is the term associated with the loss of head due to the flow through the system and the pump.

These losses were present in the system; thus, it was necessary to add these values to the pump head calculation. Losses can be calculated as the sum of two factors:

$$h_{loss} = h_o + h_p \quad (m) \tag{5.8}$$

where h_p are the losses due to pump efficiency. h_o, internal losses, is defined as the sum of the losses at the intake and the nozzle (also due to 3D machining imperfections):

$$h_o = h_i + h_n + h_{man} \quad (m) \tag{5.9}$$

The h_{loss} value was added as a η_{loss} coefficient to the value of the pump head.

This allowed to calculate the total head of the pump:

$$H_p = (\frac{V_o^2}{2\,g} - \frac{V_i^2}{2\,g})/\eta_{loss} \tag{5.10}$$

Using this value, we could identify the pump type by calculating the pump specific speed:

$$N_s = n \sqrt{Q_o}/H_p^{0.75} \tag{5.11}$$

as shown in fig. 5.15.

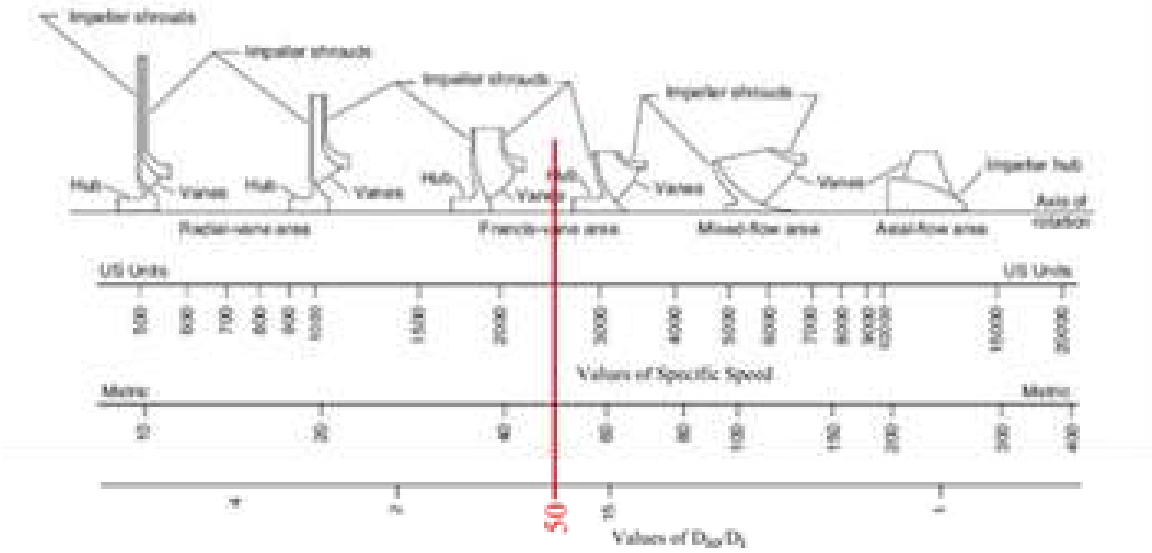

Figure 5.15: *The choice of the impeller type as a function of the specific speed.*

In addition, the brake power associated:

$$P_{pump} = \frac{\rho_w \, g \, Q_o \, H_p}{\eta_p \eta_m \eta_r} \tag{5.12}$$

Since the motors that the authors pre-identified for the Pump-Jet Module design had a maximum operating speed of 1200 RPM, then our $metric \, N_s = 50$, then the pump was a mixed flow pump of the type reversible Francis turbine. The consequent ratio D_o/D_i was chosen to be 1.5, which gave us the inlet/outlet ratio $e = 0.68$.

Impeller Design

Mixed flow pumps borrow characteristics from both radial flow and axial flow pumps. As liquid flows through the impeller of a mixed flow pump, the impeller blades push the liquid out away from the pump shaft and to the pump suction at an angle greater than 90 deg. In Francis pump impellers, design factors, requiring Euler's triangles to be known, are important and are obtained from experimental designs and data. Various ratios are used and can be found in the literature [205].

To design the impeller vane layout, the following parameters are required:

- Meridian velocities at inlet and outlet
- Impeller outside diameters
- Impeller vane inlet and outlet angles
- Velocity triangles to be drawn for several streamlines (minimum of three streamlines)

Following the design procedure suggested by [206,207], the authors found a time-saving procedure for designing the Francis pump for rapid prototyping. This involved:

- Selection of the inlet and outlet diameter of the pump impeller and the various geometric data
- Meridian flow analysis resulting in the surface of revolution
- Calculation of blade angles from hub to tip based on free vortex theory
- Geometrical transformation of each surface of revolution into a plane with flow angles

- Reverse transformation of cascade geometry and flow data to the back-to-back intersections on the surfaces of revolution

The velocity triangles of the inlet and outlet of the impeller are shown in fig. 5.16 with their reference names.

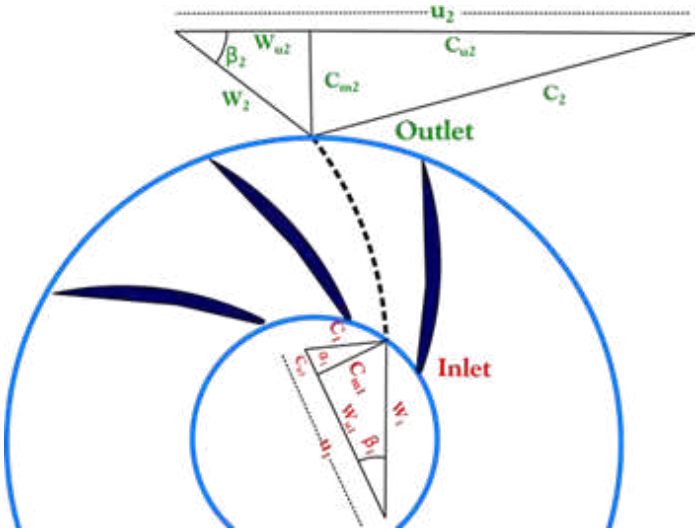

Figure 5.16: *The pump reference triangles.*

The main design elements are listed below:

- The vane discharge angle β_2 was the most important design element since all theoretical characteristics were determined by the vane angle alone. All design constants depended on β_2. This value was fundamental for determining pump design since normal head and capacity increase when β_2 increases. This angle should be between 15° and 35° in order not to affect efficiency appreciably.

- $K_u = u_2/\sqrt{2\,g\,H_p}$ is a speed constant used for calculating impeller diameters when RPM and pump head H_p are defined as in our case. Smaller pumps require a higher value of K_u to compensate losses.

- $D_m^2 = (D_{2o}^2 + D_{2i}^2)/2$ is the mean effective diameter, which, for mixed flow pumps, divides the flow throughout the impeller into two equal parts.

- The capacity constant $K_{m2} = c_{m2}/\sqrt{2\,g\,H}$ value is important since it is obtained from experimental data. Differences from these data may lead to leakages and losses.

- Entrance velocity $c_{m1} = Q/A1$ is supposed to be the velocity just ahead of the vanes. This depends on $K_{m1} = c_{m1}/\sqrt{2\,g\,H}$. Usually, depending on the impeller approach, c_{m1} is equal to the velocity through the impeller eye or slightly lower.

- The minimum number of vanes z_{blades} required is six for low β_2 and large pumps. Smaller impellers and impellers with smaller head require fewer vanes, but for our experiment, we chose three different numbers of vanes: 8, 9, and 10, to lower the slip factor. The number of vanes depends on β_2. The lower β_2, the lower the number of vanes.

Pump Geometric Parameters

The various geometric design parameters for developing the mixed-flow pump were obtained from [205] and its experiment-based coefficients. The graph in fig. 5.17 was used to obtain the diameter ratio $e_m = D_i/D_m$ value of 0.65. This value allowed us to calculate all the inlet geometry data as follows: tip diameter (and radius) of impeller $D_{1t} = D_i$, mean diameter (and radius) of the blade $D_{1m} = D_p\,0.3$, and the inlet root diameter (and radius) $D_{1r} = \sqrt{-2\,D_{1m}^2 + D_{1t}^2}$, which divides the flow into equal parts.

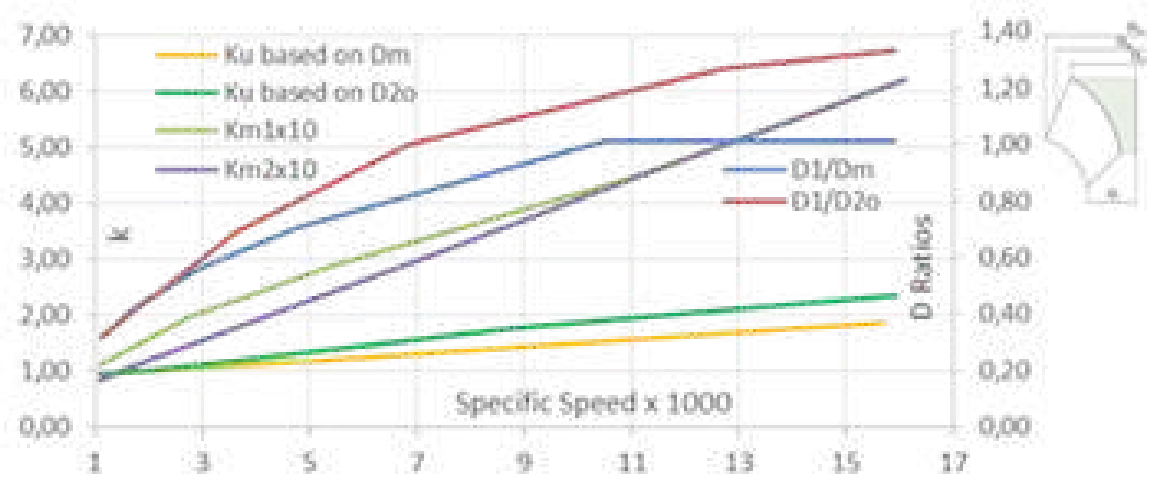

Figure 5.17: *Guiding parameters obtained from experimental data.*

fig. 5.17 was also used to obtain the outlet geometry data as follows:

Tip diameter (and radius) at the outlet from $e = D_i/D_{2t}$, mean diameter (and radius) at the outlet $D_{2m} = D_i/e_m$, and the root diameter (and radius) at the outlet $D_{2r} = \sqrt{2\,D_{2m}^2 - D_{2t}^2}$.

Blade heights can also be calculated: the blade height inlet was derived from initial geometrical analysis and was $l_i = D_p\,0.15$, while blade height at the outlet can be calculated as $l_o = l_i\,(D_{2m}/D_{2t})$.

With all these data, based on geometric considerations, it is possible to calculate and design the internal $2D$ layout of the Pump-Jet Module. A Matlab® code was expressly created for this purpose).

Velocity Triangles

The impeller of the Pump-Jet Module system was designed using velocity triangles.

The area of the inlet was obtained from:

$$A_{1m} = 2\,pi\,R_{1m}\,li \tag{5.13}$$

Thus, the axial velocity is:

$$c_{m1} = Q_o/(A_{1m}) \tag{5.14}$$

and

$$c_1 = c_{m1} \tag{5.15}$$

The radial velocity is:

$$u_{1m} = 2\,\pi\,n_{prog}/60\,R_{1m} \tag{5.16}$$

If the liquid enters the impeller without a tangential component, the whirl component c_{u1} is low

(zero or 0.1), in our case, we imposed:

$$c_{u1} = 0.1 \tag{5.17}$$

Then, we can calculate the component:

$$w_{u1m} = u_{1m} - c_{u1} \tag{5.18}$$

In addition, the resulting velocity:

$$w_{1m} = \sqrt{c_1^2 + u_{1m}^2} \tag{5.19}$$

This can also be done for the outlet where the area is obtained:

$$A_{2m} = 2\,pi\,R_2 m\,lo \tag{5.20}$$

Thus, meridian velocity at the outlet:

$$c_{m2} = Q_o/(A_{2m}) \tag{5.21}$$

Radial velocity is:

$$u_{2m} = 2\,\pi\,n/60\,R_{2m} \tag{5.22}$$

The tangential component of absolute velocity at the outlet can be calculated from:

$$c_{u2m} = (H_p\,g + u_{1m}\,c_{u1})/(u_{2m}) \tag{5.23}$$

Then, we can calculate the component:

$$w_{u2m} = u_{2m} - c_{u2} \tag{5.24}$$

and:

$$c_{2m} = \sqrt{c_{m2}^2 + c_{u2m}^2} \tag{5.25}$$

The resulting velocity:

$$w_{2m} = \sqrt{c_{m2}^2 + w_{u2m}^2} \tag{5.26}$$

Fluid slip due to the difference in pressure and velocity between the trailing and leading faces of impeller blades is important in radial impellers. A deviation in the angle at which the fluid leaves the impeller from the impeller's vane has to be taken into consideration. This value is evaluated through the Stodola equation. The Stodola [208] slip value comes close to the exact correction number if the number of vanes exceeds six and β_2 is small, then the correction factor is:

$$\sigma = 1 - \frac{\pi * sin(beta_{2m})}{z_{blades} * (1 - (c_{m2}/u_{2m})\,cot\beta_{2m})} \tag{5.27}$$

and:

$$c'_{u2m} = \sigma * c_{u2m} \tag{5.28}$$

By applying this correction, the vane entrance angle is calculated:

$$\beta_{1m} = atan(c_{m1}/w_{u1m}) \tag{5.29}$$

The vane outlet angle is calculated:

$$\beta_{2m} = atan(c_{m2}/w_{u2m}) \tag{5.30}$$

Based on the above-mentioned dimensions, the values obtained are those summarized in Table table 5.1:

Table 5.1: *Results.*

Thrust T	12.25	(N)
Pump Nominal Speed n	1185	(RPM)
Pump Head H_p	1.70	(m)
Number of Impeller Blades z_{blades}	9	
Metric Specific Speed N_s	47	
US Units Specific Speed $N_{s_{gpm}}$	2430	
Speed Constant K_u	0.88	
Head Coefficient ψ_p	0.39	
Diameters Ratio Di/Dm	0.65	
Capacity Constant 1 K_{m1} 10	3.02	
Capacity Constant 2 K_{m2} 10	1.22	
Vane Entrance Angle β_{1m}	39.5	(deg)
Vane Outlet Angle β_{2m}	21.3	(deg)

Pump 3D Drawing

Based on these data, obtained for various sections, the vanes were drawn by means of a 3D computer graphics software. A sequence of the drawings phases is reported in fig. 5.18. This phase was important also for the fact that the final version of the pump had to be 3D printed and this requires a perfectly defined *.stl* format model. The impeller was drawn using the velocity triangles

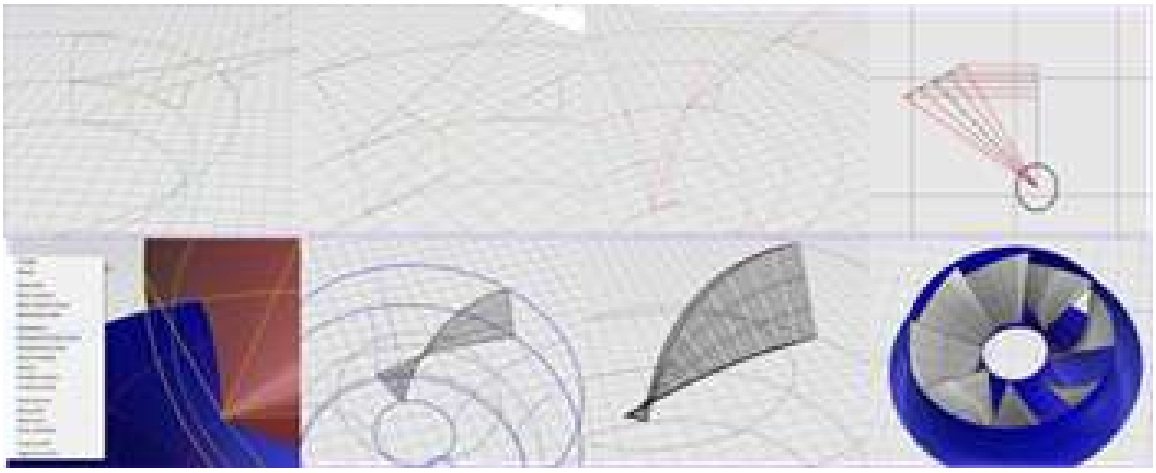

Figure 5.18: *Phases of the drawings of the pump for the Pump-Jet Module*

fig. 5.19 and by applying results to the various sections of the vanes when the obtained chord was divided into equal intervals.
The blade section of the mixed flow pump impeller blade was designed using the mean stream line theory [209, 210] from the radius of curvature of mean stream line and the chord length of blade section at the hub obtained from the calculation of the meridian and peripheral velocity components. The design was carried out in solid modelling software. The calculations were done using the following governing equations. With the mean stream line method when extended to other sections of the blade resulted in the complete blade profile.
Due to the small dimensions, and the necessity of robustness related to the 3D printing process, the no wing profile was applied to the blades and just a thickness of 1mm was applied. A the leading edge a smooth curvature was applied. The resulting velocities and blade inlet and outlet angles were obtained from the velocity triangles. An example of the angles used to draw the 3D model of the pump is shown in fig. 5.19.

Figure 5.19: *Inlet, outlet, and intermediate section meridian triangles for the design of the impeller.*

Casing Design and Drawing

To design the casing fig. 5.20, the fundamental parameter was the outlet area A_n, which was determined during the first design stages as the equilibrium value between the possible pump head with a 120-mm diameter and the expected motor RPM. Since the outlet of this system was subjected

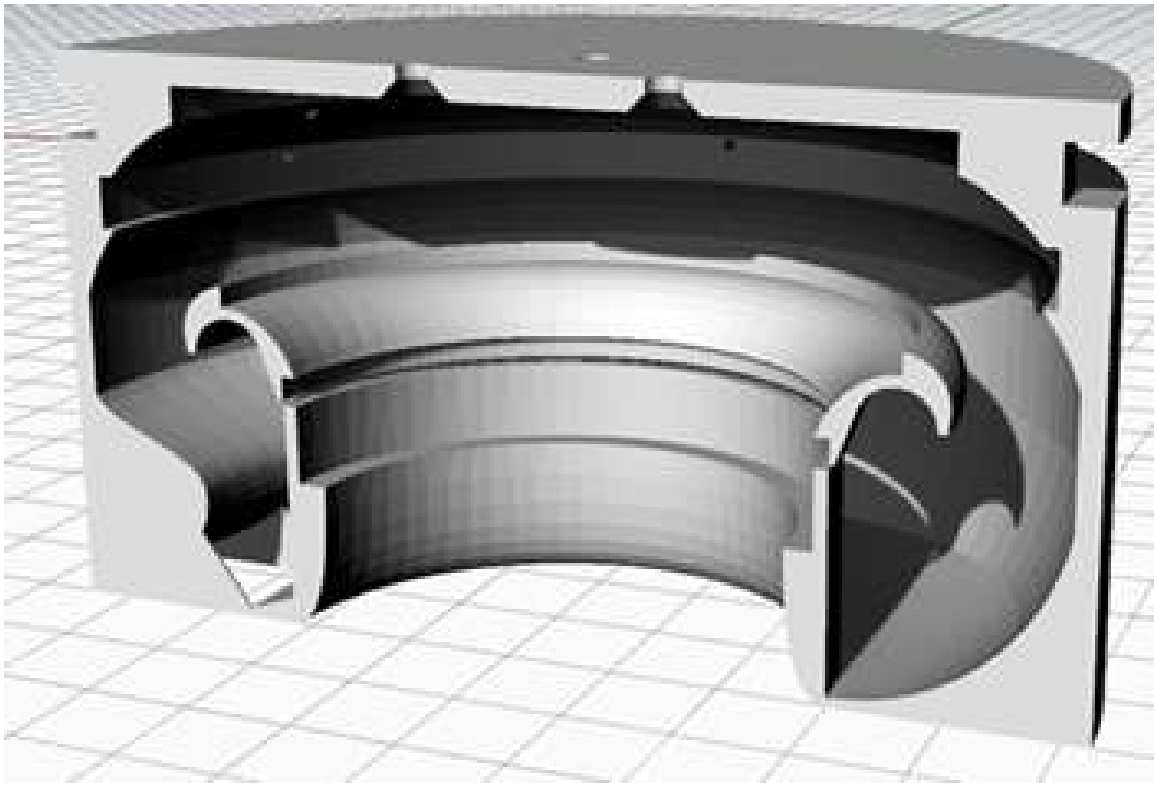

Figure 5.20: *The casing of the Pump-Jet Module*

to a sudden change in the water flow section, a consequent and localized head loss was present and can be calculated with the formula:

$$h_n = k_n V_o^2/(2g) \tag{5.31}$$

where V_o is the average outlet speed and k_n a dimensionless parameter (so-called coefficient of localized resistance), which depends, essentially, on the geometric configuration and is between 0.9 and one for sharp edge outlets such as those that can be encountered in the outlet of a Pump-Jet Module. This value was used to initially determine the pump head. To design the casing, we followed the criterion of removing any possible sharp edge and took into consideration that the rotatory component of the pump impeller induces on the flow creates a jet that is a bit asymmetrical. Therefore, to obtain the desired area A_n, we provided three openings: one was central in the frontal part of the Pump-Jet Module, and two were on the sides. The two side openings were non-symmetrical, as shown in fig. 5.13, and the geometry of the outlet nozzles was obtained after several tests made by varying the geometry of the outlets. The dissemination of these tests is reported in Section 5.5.

5.3.2 Motors' Layout and Choice

The expected power consumption for the Pump-Jet Module was obtained from Equation (5.12) and is shown in fig. 5.21. By considering a pump efficiency equal to 0.75, 0.95 mechanical efficiency (for the bearing efficiency and the sealing frictional resistance) and neglecting the relative rotative efficiency, the brake pump power can be achieved. Assuming a motor efficiency of 0.85, the expected maximum electric power at the design point was around 90 W. Considering this value, the chosen

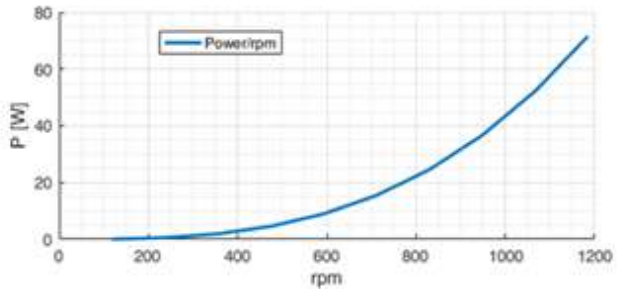

Figure 5.21: *The expected Pump-Jet Module power consumption.*

motor for the Pump-Jet Module impeller was the Maxon Ec-4pole with a 14:1 reduction gear. It is a highly efficient and reliable 36-V brushless motor with a 120-W power supply. It has an excellent working point around 1185 RPM at 90 W.
The chosen azimuth motor was the Faulhaber 2232-BX with a 59:1 reduction, which guaranteed 0.85 Nm and a rotational speed of 492 deg/s. This means that the azimuth system can be steered 360 degrees in less than one second. A note is interesting whit this data: the commonly used steerable propulsion systems have a slow dynamics resulting in a azimuth speed really slow if compared to the Pump-Jet Module one. As an example the Jastram system turning rate for the grid is up to 180 degrees in 8 seconds. The commonly used navigation, guidance and control systems for ASV consider a slow dynamics of the azimuth [211]. In the case of SWAMP innovative control techniques may be investigated. Taking this into consideration novel algorithms can be studied.
This motor has an integrated absolute encoder that allows constant information on the exact thruster position. The Faulhaber 2232-BX motor, together with the 59:1 reduction coupled with the gear reduction of 2:1, provides the exact position of the thruster with precision well below 0.1 deg and permits continuous rotation in any direction. Table 5.2 lists the characteristics of the chosen brushless motors.

Table 5.2: *Motor.*

Parameters	**Pump Motor**	**Azimuth Motor**	
Type	Maxon Ec-4Pole	Faulhaber 2232-BX4	
Nominal power	123	13	(W)
Nominal voltage	36	24	(V)
Nominal speed	16,700	4840	(RPM)
Nominal torque (max. cont)	63.1	14.6	(mNm)
Nominal current (max. cont)	3.43	0.54	(mNm)
Stall torque	1130	61.7	(mNm)
Max. efficiency	89	74	[%]
Reduction Ratio	14	59	: 1
Max. continuous torque	2.4	9	(Nm)
Max. efficiency	89	74	%
Total weight	239	140	(g)
Nominal reduced speed	1193	82	(RPM)
Nominal reduced torque	883	861	(mNm)

5.3.3 Hardware Control System and Power Supply

As illustrated in fig. 5.22, the motors with the corresponding encoder with the controllers ESCON Module 50/5 were all installed in the Pump-Jet module. The controller is a small-sized, powerful four-quadrant PWM servo controller for highly efficient control of brushless EC motors up to 250 W.

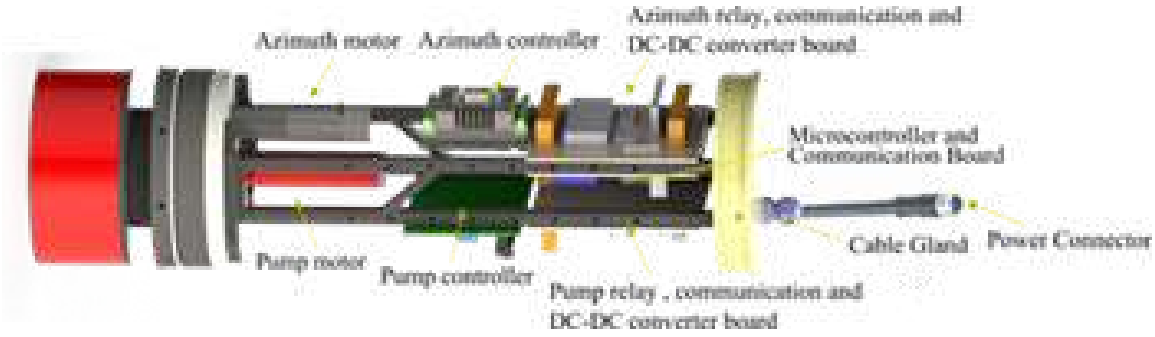

Figure 5.22: *The Pump-Jet Module electronics*

For the azimuth brushless DC-motors with absolute encoders, the Faulhaber MCBL3006S-AES was chosen. This system has overload protection for electronics and the motor and self-protection from overheating and over-voltage. The controller together with the motor's absolute encoder allowed for a positioning resolution of 4096 steps per revolution; this means, if we consider the reduction gear, 483,328 steps for a 360 deg rotation.
The Magnetic absolute encoder, SSI, works on 4096 lines per revolution on a single rotation. This means that for the reduced system it is necessary, when the motor is turned on, to perform an "homing" procedure that allows the Faulhaber controller to exactly know its position, a reed sensors based on magnetic system was implemented. The $0\,deg$ position is thus implemented at the turn-on by making this procedure.
The actuation module is based on a Huzzah ESP8266 board, which is an Arduino-like microcontroller board with Wi-Fi capabilities. The Huzzah also offers considerable I/O expandability with 9 GPIO (General Purpose Input Output) I/O digital channels, 1 analog input channel, and 2 UARTs (Universal Asynchronous Receiver-Transmitter) serial I/O channels. Additional digital, analog, serial, etc., I/O channels can easily be added to the board thanks to the presence of one I2C and one SPI bus interface. The actuation module communicates with the SWAMP control system through a Wi-Fi link, with the servo controller of the propulsive motor through an RS-232 serial channel, and with the servo controller of the azimuth motor through an additional SPI D/A channel. Power on/off, enable/disable, and fault signals are managed by means of the GPIO channels. One of the main objectives of this propulsion unit was to provide a completely closed module that communicates with each control unit without requiring a cable. With this in mind, the power supply of the module came from an external source (e.g., the battery of the ASV). Alternatively, in a modular approach, the power supply could be installed inside the module, thus creating a completely closed module that only communicates with the external world through a Wi-Fi connection, but does not require an external power supply or communication cables. For this purpose, the canister of the module was bulky enough to be able to house a battery module.
The cap of the module is provided with a cable gland and the cable the exit from the module terminates with a M12 Binder series ip68 male connector that is used for the connection to the power supply.
The adoption of azimuth propulsion and the 360 deg rotation capability requires robust guidance techniques. The problem of avoiding singular configurations of azimuth thrusters was addressed

in [212]: these configurations may cause poor maneuverability and temporary loss of control, a circumstance that is recovered very slowly if the steering system is slow. This is avoided using the Pump-Jet Module high steering speed, and the adoption of the MCBL3006S-AES control system was suitable for controlling the Pump-Jet Module. To guarantee that ASVs adopting a Pump-Jet Module are able to satisfy specific operational requirements (path following, station keeping, vehicle following), suitable guidance and control schemes need to be developed and implemented. This should be done in combination with the development of suitable thrust control mapping also related to data quality since collected data could be affected by abrupt maneuvers, rough azimuth changes, or jerky motion.

5.4 Pump-Jet Module Construction and 3D Printing

The physical construction of the Pump-Jet Module was entirely carried out at the CNR-INM laboratories. Pictures of the manufacturing process are shown in figs. 5.23 to 5.26.
3D printing allowed us to carry out the above-mentioned tests on the various openings of the Pump-Jet Module, and while in this article, the authors only report on the final design of the Pump-Jet Module, various pumps and nozzles were designed and tested.
The pump impellers were built using a desktop filament 3D printer in PLA (Polylactic Acid) and ABS (Acrylonitrile Butadiene Styrene) for the testing phase, and the final version was built in PETG (Polyethylene Terephthalate), a non-hygroscopic, robust material.
Various casings were designed and printed in ABS since this material is non-hygroscopic and robust. Thickness was slightly adjusted between the first version and the final versions to take into consideration the behavior of the 3D printer's layered structure.

Figure 5.23: *The 3d printing of the hydraulic parts of Pump-Jet Module.*

As described in Section 5.3, the Pump-Jet Module was made out of plastics like HPDE, POM, and PVC. Non-rotational elements were constructed using a CNC mill-machining machine, while all the rotational parts (except from commercial parts like self-lubricating gears, self-lubricating bearing, and metallic bearing) were made in plastic by means of a lathe machine.

Figure 5.24: *The manufacturing of the mechanics of the Pump-Jet Module.*

The electronic and electric cards have been designed and built specifically for the Pump-Jet Module. These include the communication and power boards of the two motors and the power management board, the on-board microcontroller board and the wifi communication system.

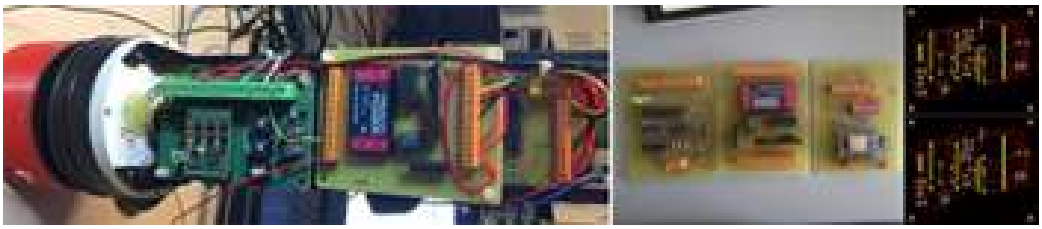

Figure 5.25: *The manufacturing of the electronic part of the Pump-Jet Module.*

The whole Pump-Jet is close by a PVC pipe and sealed with two oring, one on the lowest part and one on the top cover.

Figure 5.26: *The Pump-Jet Module final layout*

5.5 Experimental Tests and Calibration

Direct validation of bollard thrust tests was performed in a small pool at the CNR-INM laboratory in Genova to measure thrust and torque delivered by the impeller. Tests were performed at different stages during the design process using an ad-hoc low-cost system for the measurement of thrust exerted by marine thrusters. The system, shown in fig. 5.27, is constituted by an aluminum fulcrum lever in which the thruster was positioned on one side and a load cell with a strain gauge and its amplifier positioned on the other. The load cell (-10 to 10 kg) was connected to an Arduino Due micro-controller, which was used to record the acquired data and manage the Maxon Servoamplifier 4-Q-EC - DECV 50/5 that was used to command the motor. Data were recorded on an SD card, and the output string was defined as follows: date; thrust (g); motor speed, current, voltage; Hz and RPM from the motor's hall sensors; driving reference Voltage (V).

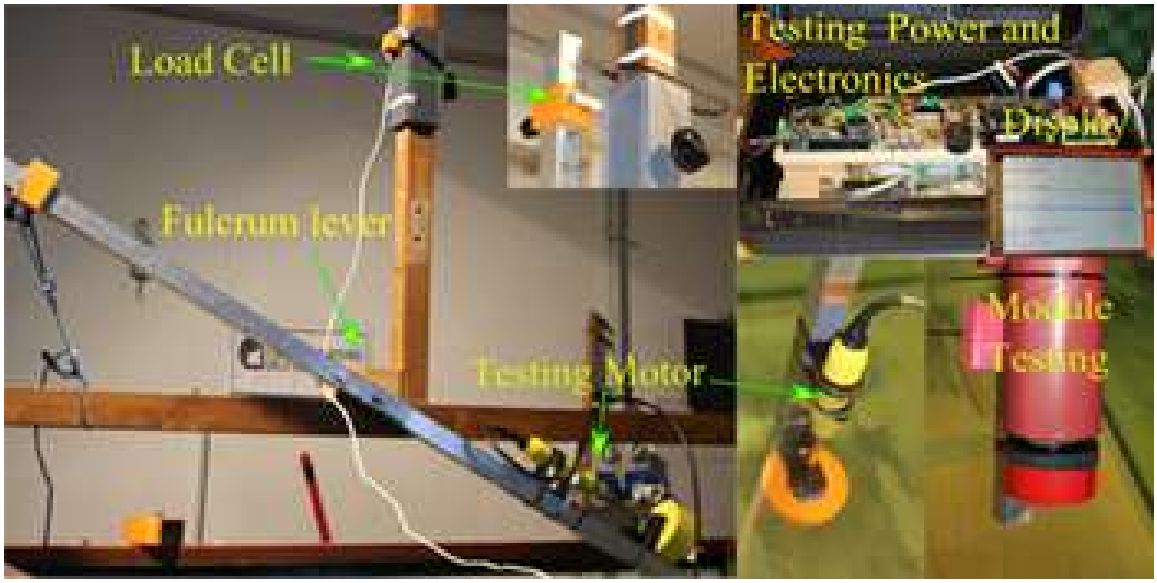

Figure 5.27: *The fulcrum lever testing-rig.*

The driving reference voltage was used to command the system. This voltage is also used when the module is mounted on the ASV, and the command is given via Wi-Fi.
Bollard thrust tests were performed with the propulsion unit in forward direction and with various steering angles. Table table 5.3 summarizes the tests performed on the Pump-Jet Module system. Tests where performed on the Pump-Jet alone and on the entire Pump-Jet Module. The diameter of both the Pump-Jet and of the impeller was varied. Tests were done with the variation of the diameter of the impeller, the number of blades, and the outlet geometry. Tests were also performed at different depths, but no significant variation was recorded.

Figure 5.28: *Examples of different configurations tested - Top: various central outlet designs - Middle: Tests modifying continuously the side outlets - Bottom: Various Pump-Jet configurations*

As shown in fig. 5.28, 3D printing allowed to modify quickly and test a significant number of outlet sections and impellers.

Table 5.3: *Characteristics.*

D_p	D_o	Configuration	Nozzle Configuration
110	65	$z_{blades=8}$ Small Nozzle Opening	Symmetrical Outlet
110	77	$z_{blades=8}$ Large Nozzle Opening	Symmetrical Outlet
120	77	$z_{blades=8}$ Small Nozzle Opening	Symmetrical Outlet
120	77	$z_{blades=8}$ Large Nozzle Opening	Symmetrical Outlet
120	77	$z_{blades=8}$ Varying Lateral Outlet Opening	Asymmetrical Outlet
120	77	$z_{blades=8}$ Varying Central Outlet Opening	Asymmetrical Outlet
120	77	$z_{blades=8}$ Varying Lateral Outlet Opening	Asymmetrical Outlet
120	77	$z_{blades=8}$ Varying Central Outlet Opening	Asymmetrical Outlet
120	77	$z_{blades=8}$ Varying Central Outlet Opening	Asymmetrical Outlet
120	77	$z_{blades=8}$ with Flow Straightener	Asymmetrical Outlet
120	77	Varying z_{blades} : 8 , 9 , 10	Asymmetrical Outlet
120	80	$z_{blades=9}$	Asymmetrical Outlet
120	80	$z_{blades=9}$ at Various Angles	Asymmetrical Outlet

5.5.1 Initial tests

A series of initial tests was performed to verify the functionality of the Pump-Jet.
The tests were performed by installing the various geometries on the testing rig and driving the impeller with the motor of a propulsion unit of another UMV.

The important part at the beginning was also to find a suitable matching between the required thrust and the outlet geometry.
The first tests gave low values of thrust but increasing the nozzle opening and modifying asymmetrically the side openings the thrust increased too, up to the expected value.
Various tests were performed also for the choice of the motor.This was done by modifying the impeller diameter. The optimum was found with a perfect matching with an EC 4pole maxon motor with a 14:1 reduction of which a copy was present in the CNR-INM laboratory.

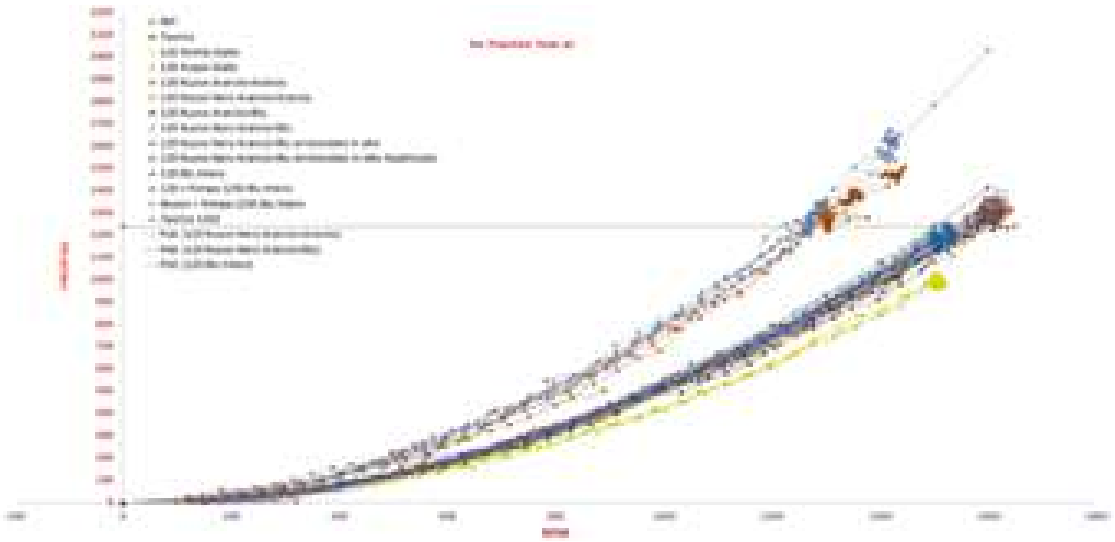

Figure 5.29: *The results of the long series of tests performed on the Pump-Jet geometry*

Some tests were performed by increasing the number of blades of the impeller z_{blades}. Results of the long series of tests is summarised by the graphic in fig. 5.29.

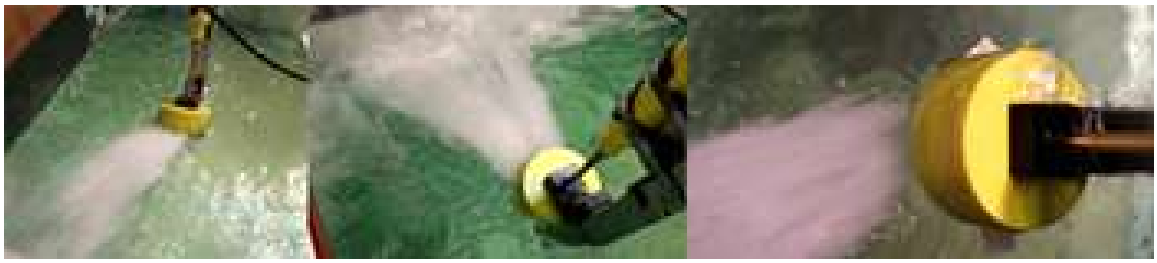

Figure 5.30: *PJ jet during tests*

5.5.2 Final tests

This section describes tests conducted in the final configuration of the Pump-Jet Module. Testing results reported here were produced with a diameter of $D_p = 120$ mm, a $z_{blades} = 9$ impeller with an external mean diameter of $D_{2m} = 80$ mm, and an asymmetrical outlet geometry with a symmetrical central nozzle and asymmetrical lateral nozzles with a ratio of 1 : 3 between one side's and the other side's outlet section area. The bigger outlet was the one that was directly invested in due to the positive speed of the rotational component of the fluid flow produced by the impeller. The ratio between pump inlet and outlet areas was about 2.5 with 2200 mm^2 at the inlet and 900 mm^2 at the outlet.

Fixed angle tests

While a huge number of data were obtained by varying some of the above-mentioned parameters, in this section, we provide graphs of the results of bollard pull thrust tests in the final configuration of the Pump-Jet Module thruster. The main results are reported in the thrust vs. motor RPM graph in fig. 5.31, where the experimental results are compared with theoretical expected values. This graph shows that results matched satisfactorily. This graph is important since this curve

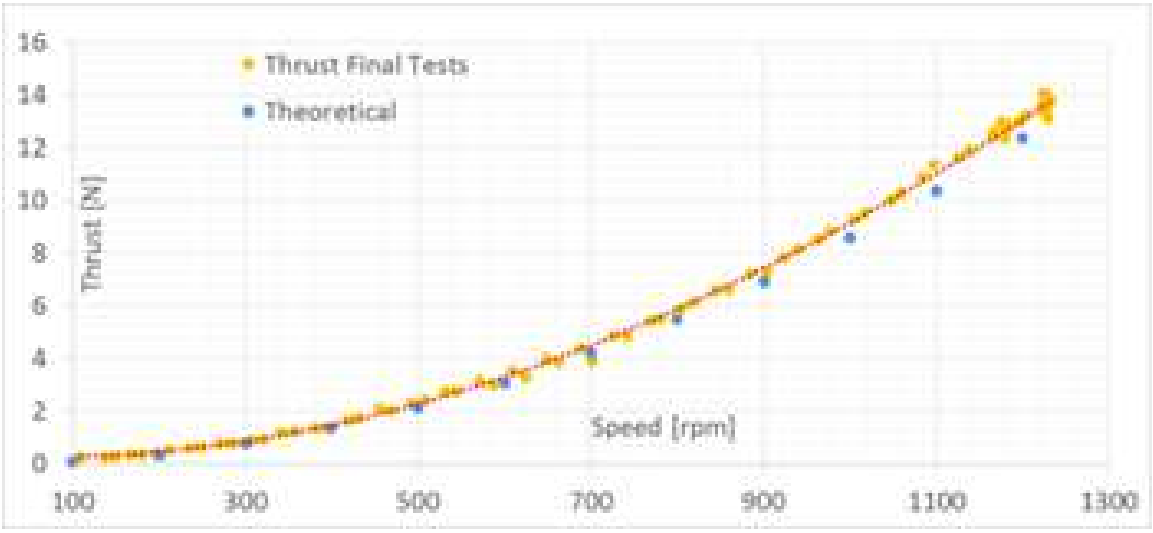

Figure 5.31: *Results of bollard pull thrust tests: thrust vs. motor RPM.*

was used from the control unit to create a match between thrust and reference voltage value used to command the motor, which is strictly related to the motor's RPM. For the same tests, *power vs. motor RPM* values are shown in fig. 5.32 and *power vs. thrust* values are shown in fig. 5.33, indicating that the maximum achievable power was around 105 W for a thrust of about 13.5 N. This power value was less than the 120 W that could be supplied by the motor. This means that, in the case of necessity, the motor can supply much more thrust than the design one. In fig. 5.34 it is shows a continuous acquisition of 90 second of thrust around the design value of 12.3 N with a standard deviation of 0.26 and a speed of the motor of 1179 RPM with a standard speed deviation of 9.67. For the same test the Power absorption at this thrust value was recorded and it is shown in fig. 5.35. This indicates that power consumption was about 96.7 W with a standard deviation of 4.33. These results are in accordance with expected values listed in Table table 5.1.

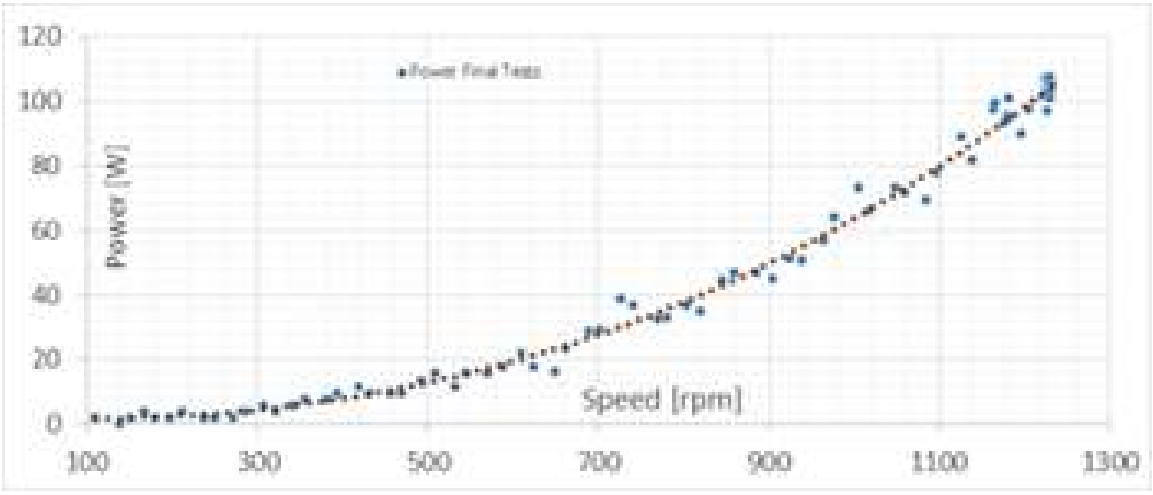

Figure 5.32: *Results of bollard pull thrust tests: power vs. motor RPM.*

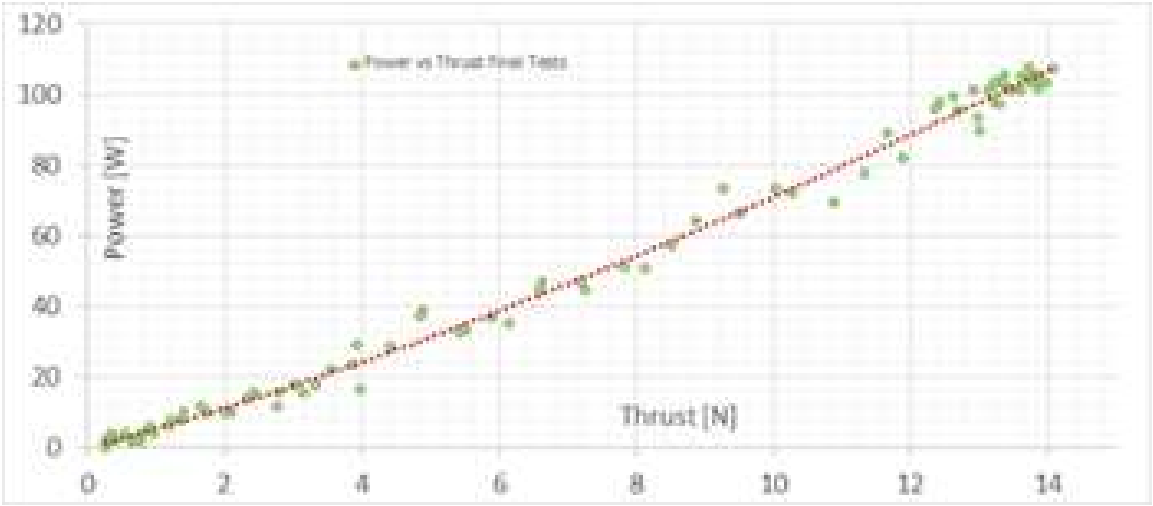

Figure 5.33: *Results of bollard pull thrust tests: power vs. thrust.*

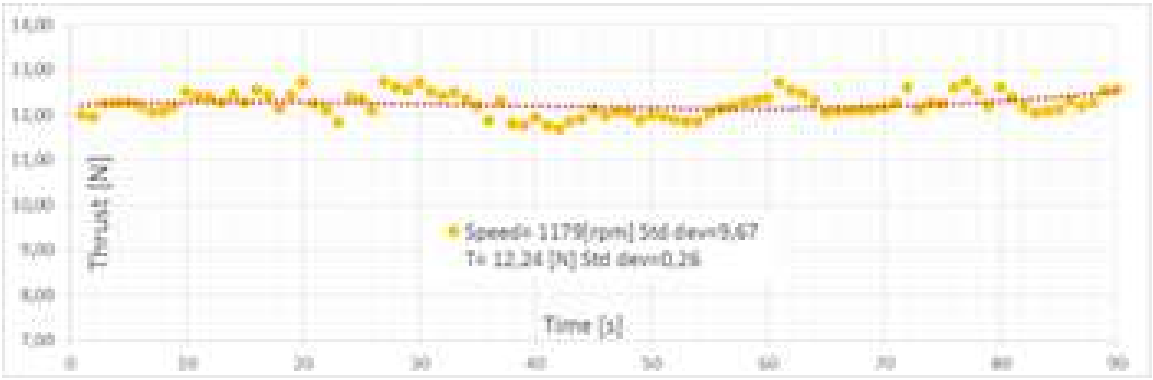

Figure 5.34: *Results of bollard pull thrust tests at design RPM.*

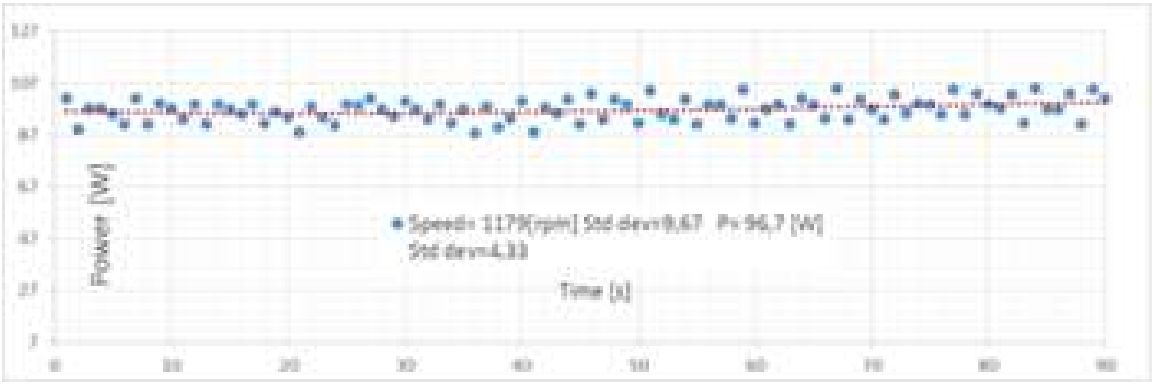

Figure 5.35: *Results of bollard pull thrust tests: power vs. thrust.*

Bollard Pull Tests at Different Steering Angles

Tests were performed at various angles. The results of these tests showed the exact angles at which the thruster yielded maximum thrust. The final assembly of the Pump-Jet Module implemented for the tests is shown in fig. 5.36.

Figure 5.36: *The Pump-Jet Module prepared for the testing phase.*

If α_0 is the steering angle when $\alpha = 0$, which is defined as the angle that divides the central outlet into equal parts, as shown in fig. 5.37, since the rotation caused by the impeller naturally induces a tangential component as part of the outlet flow (visible in fig. 5.30); as a consequence, thrust reaches its maximum value at an angle that is not zero. The results of these tests are shown in the figure below.

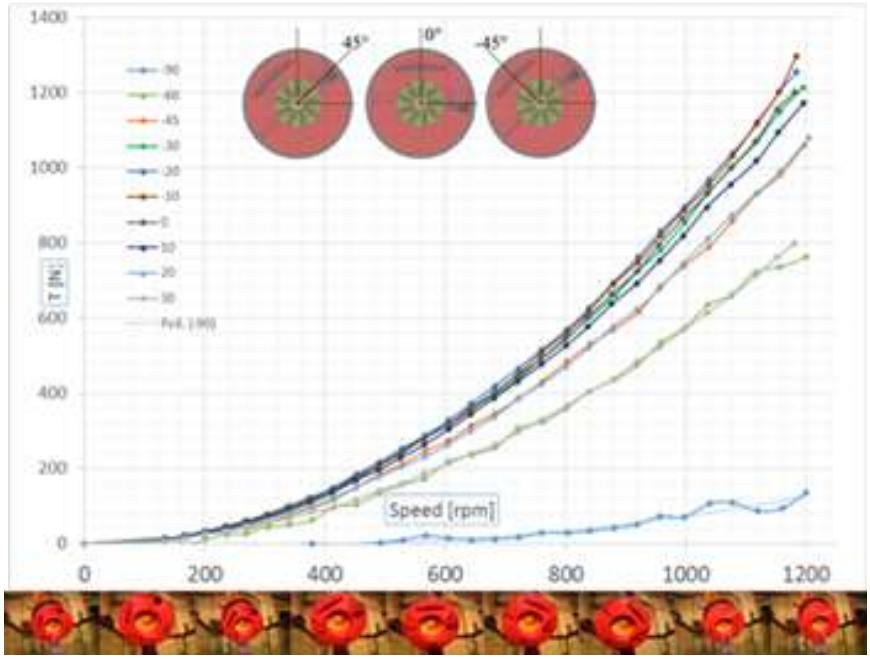

Figure 5.37: *Results of bollard pull thrust tests: thrust vs. RPM at different angles.*

Tests were performed from -90 deg–$+90$ deg at 5 deg steps, but for clarity, only some of the data are shown in fig. 5.37. Using a mono-component load cell, we measured the forward thrust component X_t in the x direction (ahead of the motion of the vehicle when $\alpha = 0$). Maximum thrust

T_{max} was set at -10 deg; this means that thrust had a non-0 Y_t component in the y direction when $\alpha = 0$. This component can be checked by performing tests at $+90$ deg and -90 deg. While at $+90$ deg, it was not possible to measure any thrust since the cell was unloaded, at -90 deg, X_t was clearly non-zero. In this way, we were able to determine whether it was possible to correct the thrust angle through the values of this X_{t-90}.
The fig. 5.38 shows two thrust curves at -45 deg and at -60 deg. These were compared with thrust curves at zero multiplied by the cosine of α, which is the value of X_t at an angle $\alpha \neq 0 \, or \, 180$. By comparing this curve with the -45 deg and -60 deg curves obtained during the tests, we determined that superimposing the values was not possible. However, when the above-mentioned angle correction was applied, the resulting curves were reasonably superimposable on the original curves. Since the following curves were superimposable when paired: -60 deg and $+30$ deg, -45 deg and $+20$ deg, -30 deg and 0 deg, and -20 deg and -10 deg, the new α_0' can easily be identified. For the Pump-Jet Module, the above-mentioned correction was taken into consideration when designing control strategies, and α_0' was set at $\alpha = -15$.

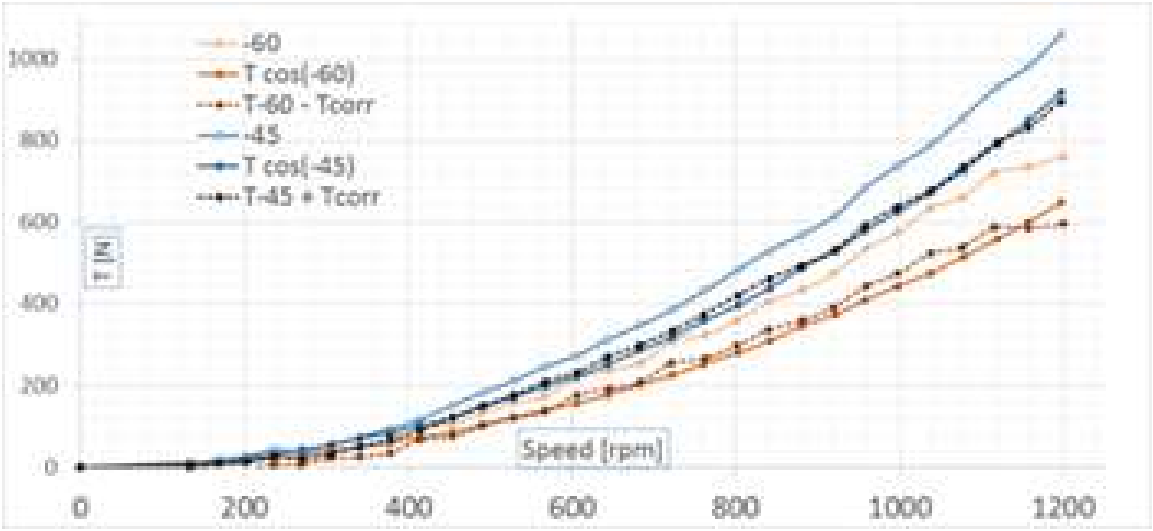

Figure 5.38: *The application of angle correction.*

The final characteristics of a Pump-Jet Module

Test results were satisfactory, and after calibration of the outlet nozzle geometry, the system met the initial requirements. A summary of the main characteristics of the system is provided in Table table 5.4.

Table 5.4: *Characteristics.*

Nominal Thrust	(N)	12.3
Nominal Power Consumption	(W)	95
Maximum Thrust	(N)	14.5
Maximum Power Consumption	(W)	125
Steerable Angle	(deg)	360 Continuous Rotation
Absolute Position Precision	(deg)	$\leq$0.01
Nominal Draft	(mm)	100
Minimum Draft	(mm)	35
Operating speed	(m/s)	1.5
Diameter	(mm)	120
Height	(mm)	300
Weight	(kg)	2.0
Operating Voltage	(V)	36–24

5.5.3 A Comparison with existing systems

By adopting the equations used for designing the Pump-Jet Module, it was possible to estimate the expected power consumption of a larger version to compare the module with existing, more powerful large-sized systems. The system's efficiency and power consumption seemed to be in accordance with the parameters given by industrial manufacturers.

In fig. 5.39, the Pump-Jet Module ratio between thrust (kN) and Power (kW) is compared with industrial Pump-Jet units; the value of the T/P ratio is shown in the ordinate and the value of power (kW) in the abscissa. This graph shows that the T/P ratio of Pump-Jet Module was a bit higher than the equivalent ratio in larger versions. Conversely, small compact systems usually present problems related to scaling and losses due to finishing and manufacturing, which in general lead to lower thrust and power values.

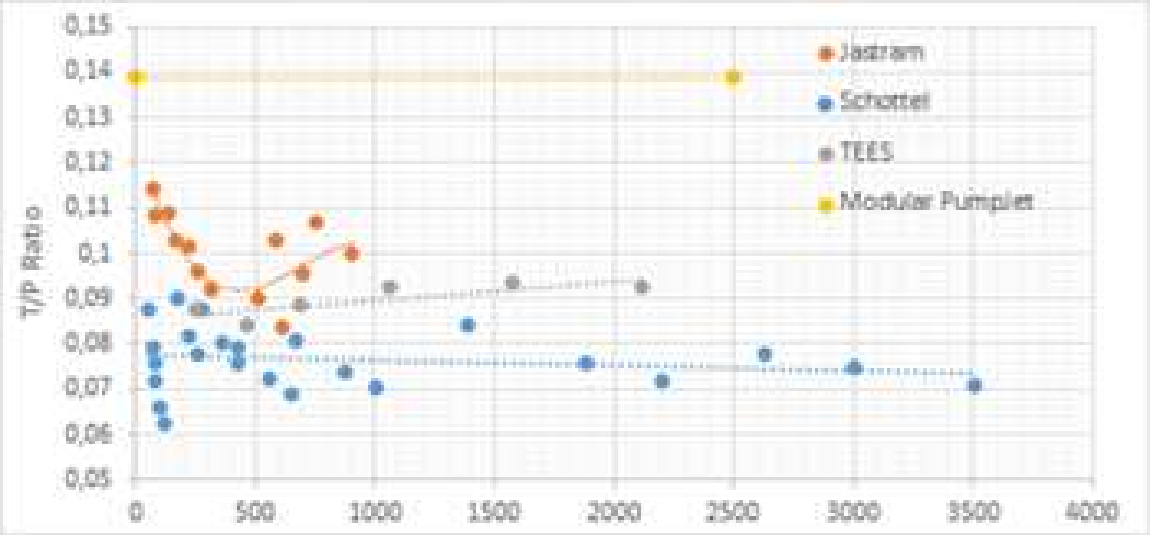

Figure 5.39: *The comparison between Pump-Jet Module estimation and the existing solutions.*

5.6 The SWAMP thrust layout

5.6.1 The four SWAMP thrusters

Bollard thrust tests were performed on the 4 Pump-Jet of SWAMP to measure the delivered thrust and power of the impeller using the above described test rig. This allowed to characterise the propulsion units by defining the thrust vs RPM and the consequent power vs RPM curves that, as far as the control is concerned, results into a driving reference voltage [V] to be applied to the main motor.
The four Pump-Jet Module thrusters test results at the maximum thrust angle are reported in fig. 5.40. These tests show a very good matching between all the thrusters results for what regards *thrust vs RPM* and a quite good matching for what regards *power vs RPM* curves.

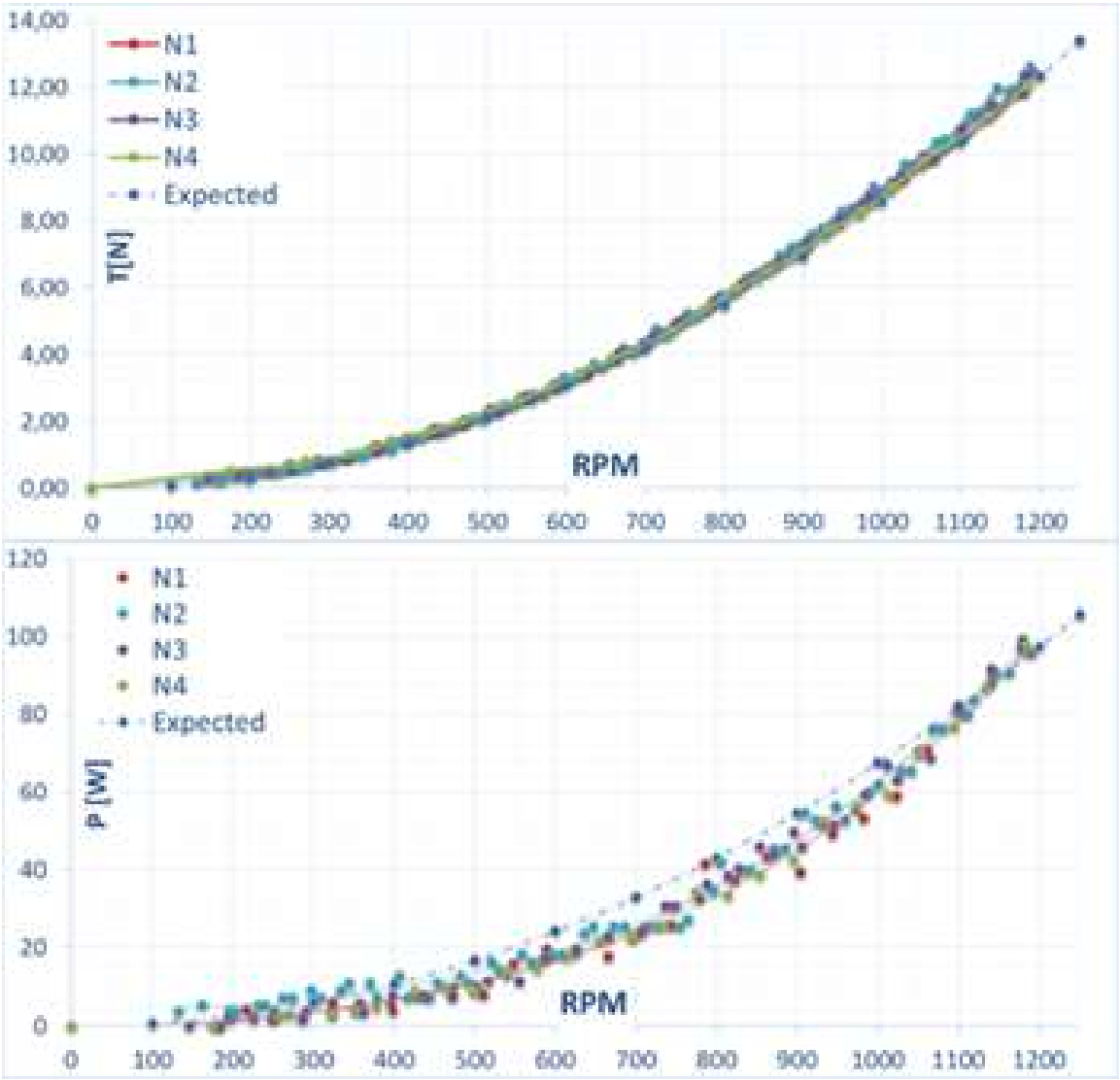

Figure 5.40: *The four Pump-Jet Module bollard pull Thrust vs RPM and Power Vs RPM graphics*

5.7 Thrust Layout

The four thrusters are mounted on SWAMP inside the holes drilled in the foam as shown in fig. 5.42 The cylinder shape of the Pump-Jet Module is designed to be easily installed on the

Figure 5.41: *SWAMP front section with the Pump-Jet modules*

vehicle in an ease way. As mentioned the main advantage of Pump-Jet system is the fact that this propulsion is flush with the hull as shown by the section reported in fig. 5.41, thus minimising the risks of damages due to possible grounding.

Figure 5.42: *The Pump-Jet Module inside the hull. It is clear how flush with the hull they are*

The functioning of the Pump-Jet Module, widely described in the previous sections, operates on the principle of a vertical axis pump: the impeller sucks-in water from below the hull, gains both velocity and pressure. The water is directed to an external volute and pushed towards outlet nozzles present in the 360 *deg* steerable casing. The nozzles accelerate the flow and a jet of water produces thrust horizontally beneath the flat-bottomed hull. The outlet angle of the water is 15° away from horizontal: almost the entire jet thrust is converted effectively into forward thrust. At the same time, there is less impact in shallow water with river/lake bed or sea water bed with less disturbance in the measurements carried-on, as the water is expelled almost horizontally from the Pump-Jet Module and rises towards the surface as soon as it leaves the nozzles.

Two commands are used to control the Pump-Jet Module: the thrust command and the angle command. The thrust is applied in the form a percentage $(0 - 100\%)$ of the RPM at the maximum thrust as shown in table 5.5, while the angle is applied as a value in the interval $[-\pi, \pi]$ which is the mapping of the 360 *deg* on the 495411 *steps* counted by the absolute encoder. The angle is controlled

Table 5.5: *Thrust Reference Map and the Angle Reference Map*

THRUST COMMANDS			POSITION COMMANDS	
Command	Speed	Thrust	Command	Angle
[%]	[RPM]	[N]	[steps]	[deg]
10%	119	0.1	-495411	-360
15%	178	0.3	-433485	-315
20%	237	0.5	-371558	-270
25%	296	0.8	-309632	-225
30%	356	1.1	-247706	-180
35%	415	1.5	-185779	-135
40%	474	2.0	-123853	-90
45%	533	2.5	-61926	-45
50%	593	3.1	0	0
55%	652	3.7	61926	45
60%	711	4.4	123853	90
65%	770	5.2	185779	135
70%	830	6.0	247706	180
75%	889	6.9	309632	225
80%	948	7.8	371558	270
85%	1007	8.8	433485	315
90%	1067	9.9	495411	360
95%	1126	11.0	743117	540
100%	1185	12.2	990822	720

through the absolute encoder present on the steering motor that allows to know the position of the thruster with precision much less than 0.1 *deg* and to continuously rotate in any direction. The rotational rate of the steering is about 490 $[deg/sec]$ with a complete rotation in less than 1 second that results in a very responsive control unit.

5.7.1 Forces and moments

The forces and moments produced by the Pump-Jet Module are referred to the vehicle's coordinate system. As shown in fig. 5.41 the four Pump-Jet Module thrusters are positioned on SWAMP inside holes machined in HDPE foam plates. Each hole centre is placed on the longitudinal axis (x) at a distance of 0.350 m from mid-ship. Through the structure the forces are transmitted to the hull. Each hole position on the transverse axis depends on the distance between the two hulls and is $S/2$, that for the design breadth, is 0.400 m.
The adoption of four Pump-Jet Module positioned as shown in fig. 5.43 guarantees a high degree of controllability with the possibility of providing highly accurate dynamic positioning and path following.
Considering the vehicle as a rigid body with three degrees of freedom: two translations, the forward

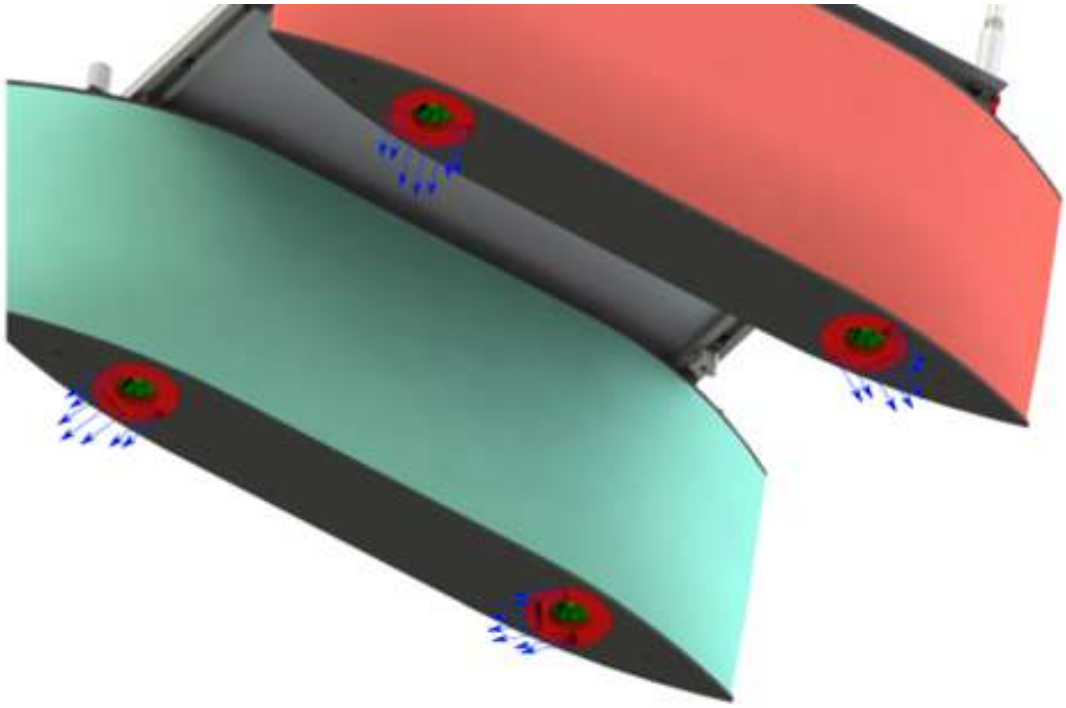

Figure 5.43: *The four azimuth thrusters functioning on SWAMP hull*

motion along the longitudinal axis x_{0G} and the drift motion along the transverse axis y_{0G}, and the rotation ψ about the vertical axis (Yaw). The rigid body equations in earth fixed and body fixed system are:

$$\begin{cases} X_0 = \Delta \ddot{x}_{0G} \\ Y_0 = \Delta \ddot{y}_{0G} \\ N_0 = I_{zz} \ddot{\psi} \end{cases} \quad \begin{cases} X = \Delta(\dot{u} - vr - x_G r^2) \\ Y = \Delta(\dot{v} + ur + x_G r^2) \\ N = I_{zz}\dot{r} + \Delta(\dot{v} + ru) \end{cases} \tag{5.32}$$

Being u,v and r the forward, drift and rotational speeds of the body in the body fixed coordinates system and Δ and I_{zz} the mass constants.
In the equilibrium equation 5.33 the global forces and moments acting on SWAMP are a sum of external disturbances: wind , current [1], internal forces of the hull and a sum of forces X_T, Y_T and

[1] waves are, at the moment, not considered for SWAMP coastal and lacustrine nature

moments (N_T) produced by the thrusters:

$$\begin{cases} X = X_{Hull} + X_T + X_{wind} + X_{current} + X_{waves} \\ Y = Y_{Hull} + Y_T + Y_{wind} + Y_{current} + Y_{waves} \\ N = N_{Hull} + N_T + N_{wind} + N_{current} + N_{waves} \end{cases} \tag{5.33}$$

Each Pump-Jet Module is constituted by two motors:

- **Azimuth motor** controlling the orientation α_i of the thrust exerted by the i-th jet, assumed equal to 0 when the thruster pushes along the surge direction. For simulation purposes, the controlled motor is assumed to have a first-order dynamics with time constant t_α, i.e. $\frac{1}{1+t_\alpha s}$

- **Pump motor** controlling the thrust T_i^{PJ} exerted by the i-th jet. The pump motor is assumed to have time constant equal to zero.
  Each Pump-Jet is positioned at $\underline{p}_i^{PJ} = \left[l_i^{PJ}, b_i^{PJ}, 0\right]^T$ with a rotation matrix that is $R_{PJ_i,b} = I$ with respect to the body fixed reference system.
  The resulting rotation matrix between the Pump-Jet thrust and the body fixed reference system is:

$$\begin{pmatrix} \cos\alpha_i & -\sin\alpha_i & 0 \\ \sin\alpha_i & \cos\alpha_i & 0 \\ 0 & 0 & 0 \end{pmatrix} \tag{5.34}$$

Given T_i^{PJ} as the generic thrust always positive and $\alpha_i = (0, 2\pi]$ the generic angle and thrust configuration of SWAMP can be seen in fig. 5.44.
The contribution to the external force and torque given by each Pump-Jet is:

$$\underline{\tau}_i^{PJ} = \begin{pmatrix} X_i^{PJ} \\ Y_i^{PJ} \\ N_i^{PJ} \end{pmatrix} = \begin{pmatrix} \cos\alpha_i \\ \sin\alpha_i \\ -b_i^{PJ}\cos\alpha_i + l_i^{PJ}\sin\alpha_i \end{pmatrix} T_i^{PJ} \tag{5.35}$$

The thrusters forces acting on SWAMP are then the forces and moment produced by the Pump-Jet Module. The thrust configurations reported on the local coordinates system of the vehicle is summarised as:

$$\begin{pmatrix} X_T \\ Y_T \\ N_T \end{pmatrix} = \begin{pmatrix} X_T^{PJ} \\ Y_T^{PJ} \\ N_T^{PJ} \end{pmatrix} = \begin{pmatrix} X_1^{PJ} + X_2^{PJ} + X_3^{PJ} + X_4^{PJ} \\ Y_1^{PJ} + Y_2^{PJ} + Y_3^{PJ} + Y_4^{PJ} \\ N_1^{PJ} + N_2^{PJ} + N_3^{PJ} + N_4^{PJ} \end{pmatrix} \tag{5.36}$$

From the above equation it is possible to see that there are infinite configurations of the thrusters position for every task being station keeping, path following or vehicle cooperation. Whit this configuration the system results redundant respect to a complete failure of one or more thrusters.
Referring to [213], in the case of SWAMP, denoting with

$$\begin{aligned} X_i^{PJ} &= T_i \cos\alpha_i \\ Y_i^{PJ} &= T_i \sin\alpha_i \\ i &= 1..4 \end{aligned} \tag{5.37}$$

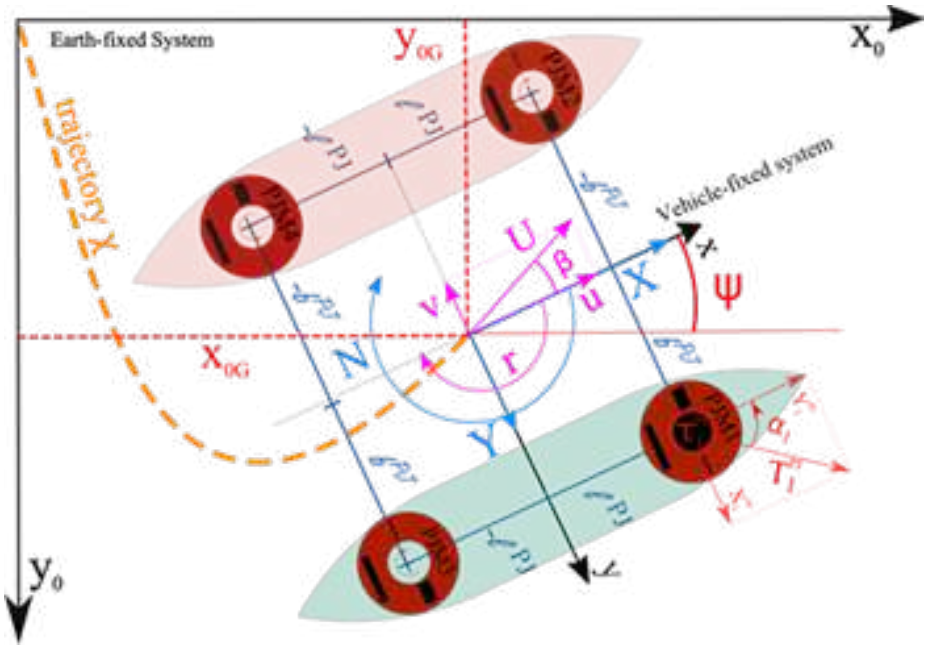

Figure 5.44: *The reference system for the thrust allocation of SWAMP vehicle*

the extended thrust vector $\underline{\chi}^{PJ}$ is defined as

$$\underline{\chi}^{PJ} = \left[X_1^{PJ}\, Y_1^{PJ}\, X_2^{PJ}\, Y_2^{PJ}\, X_3^{PJ}\, Y_3^{PJ}\, X_4^{PJ}\, Y_4^{PJ}\right]^T \tag{5.38}$$

and the generalised force for the Pump-Jet system is computed as:

$$\underline{\tau}^{PJ} = B\underline{\chi}^{PJ} \tag{5.39}$$

where

$$B = \begin{pmatrix} 1 & 0 & 1 & 0 & 1 & 0 & 1 & 0 \\ 0 & 1 & 0 & 1 & 0 & 1 & 0 & 1 \\ b^{PJ} & l^{PJ} & b^{PJ} & -l^{PJ} & -b^{PJ} & l^{PJ} & -b^{PJ} & -l^{PJ} \end{pmatrix} \tag{5.40}$$

Each Pump-Jet thrust is assumed to be positive and lower than a maximum value as it follows:

$$\begin{aligned} X_i^{PJ}\cos\alpha_i + Y_i^{PJ}\sin\alpha_i &\leqslant T_i^{MAX} \\ X_i^{PJ}\cos\alpha_i + Y_i^{PJ}\sin\alpha_i &\geqslant T_i^{min} \\ \alpha_i = atan2\left(Y_i^{PJ}, X_i^{PJ}\right) & \\ i = 1..4 & \end{aligned} \tag{5.41}$$

Being $\alpha_{i,0}$ the current orientation of the i-th Pump-Jet and $\Delta\alpha$ the maximal angle variation in the sampling period, the following constraints hold

$$\begin{cases} X_i^{PJ}\sin\left(\alpha_{i,0} - \Delta\alpha\right) - Y_i^{PJ}\cos\left(\alpha_{i,0} - \Delta\alpha\right) \leqslant 0 \\ -X_i^{PJ}\sin\left(\alpha_{i,0} + \Delta\alpha\right) + Y_i^{PJ}\cos\left(\alpha_{i,0} + \Delta\alpha\right) \geqslant 0 \end{cases} \quad i = 1..4 \tag{5.42}$$

Thrust allocation in selected working configurations

Specific Pump-Jet configurations are selected corresponding to typical working modes such as, for instance, *station-keeping* and *forward/backward surge transfer*. In these cases, the Pump-Jet orien-

tation angles are constrained in pre-defined sectors and, according to the positive thrust physical constraint, suitable sub-sets of actuators are allocated to generate the desired directional force and torque. In the research of an equilibrium, in case of *station keeping* the sum of forces and moment should be 0.
Naming X_R, Y_R, N_R the resulting external forces and moment acting on the vehicle:

$$F_R = \begin{pmatrix} X_R \\ Y_R \\ N_R \end{pmatrix} = \begin{pmatrix} X_{wind} + X_{current} \\ Y_{wind} + Y_{current} \\ N_{wind} + N_{current} \end{pmatrix} \tag{5.43}$$

Four equilibrium equations are present:

$$F_R = \begin{pmatrix} X_R + X_T \\ Y_R + Y_T \\ N_R + N_T \end{pmatrix} = \begin{pmatrix} 0 \\ 0 \\ 0 \end{pmatrix} \tag{5.44}$$

The thrust allocation matrix id est the mapping of the required forces on the thrusters present on-board is then:

$$F_R = B\underline{\chi}^{PJ} : \begin{cases} g_1(\underline{\chi}) \ : \ X_R + X_1 + X_2 + X_3 + X_4 = 0 \\ g_2(\underline{\chi}) \ : \ Y_R + Y_1 + Y_2 + Y_3 + Y_4 = 0 \\ g_3(\underline{\chi}) \ : \ \begin{array}{l} N_R + X_1^{PJ} b^{PJ} + Y_1^{PJ} l^{PJ} + X_2^{PJ} b^{PJ} + Y_2^{PJ}(-l^{PJ}) + \\ X_3^{PJ}(-b^{PJ}) + Y_3^{PJ}(l^{PJ}) + X_4^{PJ}(-b^{PJ}) + Y_4^{PJ}(-l^{PJ}) = 0 \end{array} \\ g_4(\underline{\chi}) \ : \ X_1^2 + Y_1^2 - (\tau_1^{PJ})^2 = 0 \\ g_5(\underline{\chi}) \ : \ X_2^2 + Y_2^2 - (\tau_2^{PJ})^2 = 0 \\ g_6(\underline{\chi}) \ : \ X_3^2 + Y_3^2 - (\tau_3^{PJ})^2 = 0 \\ g_7(\underline{\chi}) \ : \ X_4^2 + Y_4^2 - (\tau_4^{PJ})^2 = 0 \end{cases} \tag{5.45}$$

The equations $g_{4:7}(\underline{\chi})$ are used, known the equations (5.37), to remove trigonometric functions from the problem.
The problem has more incognitos than equations. To find a solution and to minimise the required parameters (e.g. thrust or power consumption) an optimum problem has to be solved. An objective function has to be found and the minimum of the surface of possible solutions has to be identified. To do this the method of lagrangian multiplier can be used.
The Lagrange multiplier method allows to reduce the stationary points of a function in n variables and m boundary constraints $g(\underline{\chi}) = 0$, said objective, to those of a third function in $n+m$ variables not bound, called Lagrangian:

$$\Lambda(\underline{\chi}, \lambda) = f(\underline{\chi}) + \lambda \cdot g(\underline{\chi}) = f(\underline{\chi}) + \sum_{j=1}^{m} \lambda_j g_j(\underline{\chi}), \tag{5.46}$$

that is, introducing as many new scalar variables λ as there are the constraints that are called multipliers.
That means that, given the above defined $g(\underline{\chi})_j$:

$$\nabla f(\underline{\chi}) + \sum_{j=1:7}^{m} \lambda_j * \nabla g(\underline{\chi})_j \tag{5.47}$$

As an example the function to be optimised can be:

$$f(\underline{\chi}) = \sum_{i=1:4}^{n} \frac{X_i^2 + Y_i^2}{(T^{MAX})^2} \tag{5.48}$$

Where, to reduce the thrust, T_{MAX} is the sum of the maximum allowable thrust of the four Pump-Jet and is $T_Max = \sum T_i^{MAX}$.

The general DP-Thrust allocation problem can be summarised as minimising a cost function including a quadratic approximation of the power consumption as well as a penalty for variations in the extended thrust vector that is intended to reduce wear-and-tear in the thrusters.

Chapter 6

Power and electronics

The idea at the base of the architecture of the hardware control system of SWAMP was to remove as much as physical connections as it was possible. In marine robots the cables connecting the sub-systems greatly influence the design.
The connections represent one of the weakest points in UMV. Each well done connection is constituted by: a couple of underwater or water resistant connectors on one side, a suitable connecting cable covered by HDPE coating, a couple of underwater or water resistant connector on the other side.
Marine connector's cost is high. As an example in ROVs and AUVs the cost of underwater connectors can double the cost of the total of the propulsion units. Moreover every connector represents a place from where water can enter into the canisters where precious sensors and electronics are hosted. In addition the weight of underwater cables is not negligible.
With this in mind the idea of removing cables was investigated. Wireless power transfer finds application in the industry and its application in robotics was studied by [214]. In [215] a solution was studied to replace external cables with a wireless connection. In this case the cableless system led to various advantages including simplified motion planning, fewer self-collisions, and use of 3D-sensing for collision detection that greatly outweigh any loss in reliability.
In the SWAMP architecture the communication cables were removed by replacing it with Wi-Fi. The only on-board cable is available for transferring the power coming from the on-board batteries to the users. Future developments will lead to the complete removing of the cables. The use of multiple distributed Wi-Fi modules is novelty for ASV. Something similar regarding the sensors was recently investigated by [87]
All the modules were produced in the CNR-INM laboratories from the circuits, the production of the motherboards, the assembling, the connection and the construction of the canisters. All the modules are contained into PVC pipes closed by POM-made caps with side o-ring and tested underwater a 1 m depth.

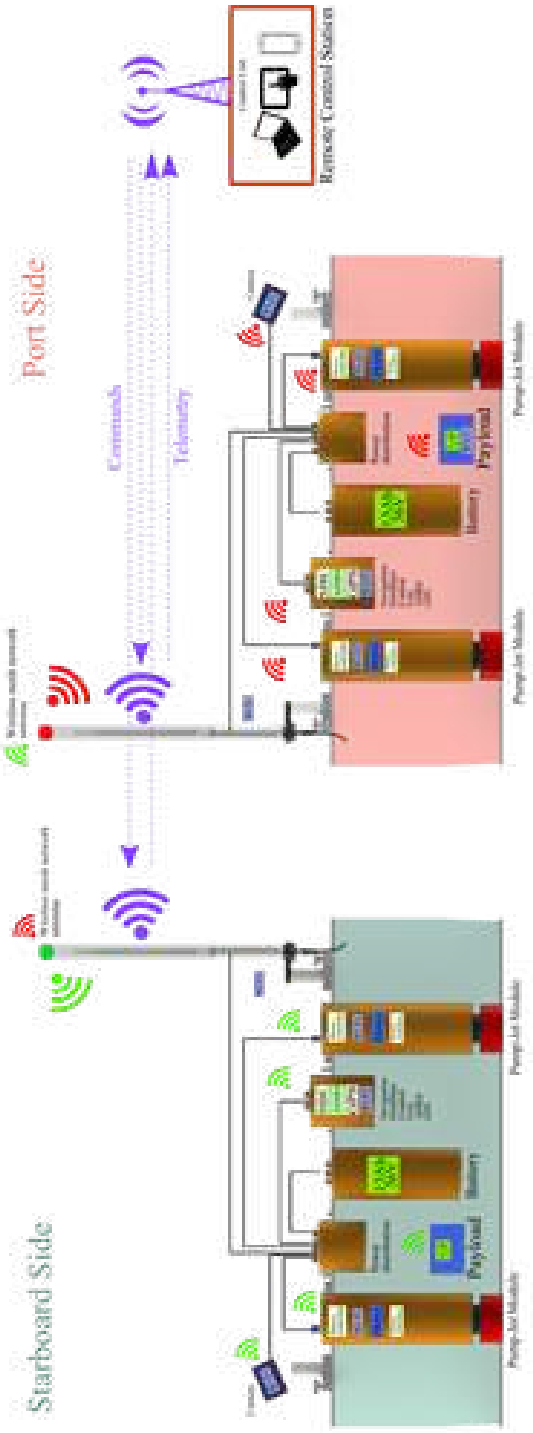

Figure 6.1: *The hardware control system and the electric scheme of SWAMP*

In a future development it is foreseen to endow the hardware control system modules with an internal power supply (like a battery) eliminating all cables, so reducing at a minimum the costs for water proof connectors and the complexity of the cabling.
Thank to the modularity of such a system additional modules can be easily added (e.g. computational, actuator, sensor, etc. modules).

6.1 Hardware control system

The hardware control system of the SWAMP vehicle is fully modular and it is based on a set of heterogeneous modules contained in watertight canisters. These modules contain computational boards, sensors and actuators for the control of the vehicle while batteries for power supply are housed into different canisters. Each module composing the hardware control system has got only one connection used for power supply and communicates with the other modules by means of a Wi-Fi radio link at 2.4 GHz. Each of the two hulls composing the complete SWAMP vehicle has got (at least) three modules:

- A computational module

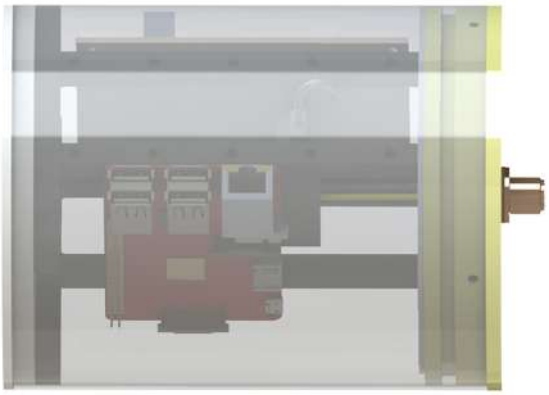

- An actuation module (Pump-Jet Module)

- A communication module

6.1.1 The computational module (CM)

The computational module is based on a Raspberry Pi 3.0 model B SBC (Single Board Computer) running the Raspbian OS (Operating System). Raspberry Pi boards are inexpensive but very powerful computers based on ARM processors. The Raspbian OS is a derived version for ARM processors of the Debian OS (a GNU/Linux-based OS). On the computational module runs the control system software of each single hull because each hull is designed for working as a single vehicle. When the SWAMP vehicle is in the complete configuration (i.e. the two hulls are physically connected together) one of the two computational modules becomes the master and the other one becomes the slave. Inside the computational module canister also is present the basic navigation sensor constituted by a Microstrain 3DM-GX3-35 which characteristics are reported in fig. 6.2. It is a high-performance, miniature AHRS (attitude heading reference system) with GPS that combines Micro Electro-Mechanical Systems (MEMS) sensor technology and a highly sensitive embedded GPS receiver. It incorporates a triaxial accelerometer, triaxial gyro, triaxial magnetometer, temperature sensors, and a dedicated 32 bit processor running a sophisticated fusion algorithm to provide orientation, inertial, and GPS measurements. Data from the GPS receiver is time synchronized with the inertial sensors and all inertial and GPS data are available as custom user packets (either by polling or continuous stream). This system is a miniature AHRS with GPS with digitally filtered data. that communicate with the Raspberry Pi board by means of USB 2.0 / RS-232 serial connection.
The sensor has to be calibrated before use by applying a correction coming from the magnetometers present onboard.

Figure 6.2: *The characteristics of the on-board AHRS and GPS sensors*

The computational module of each hull, by means of the Wi-Fi link, can communicate with the computational module of the other hull (e.g. for coordinating their maneuvers), with its actuation module and, by means of the communication module, with the pilot console. The actuation module is based on a Huzzah ESP8266 board which is an Arduino-like microcontroller board with Wi-Fi capabilities. The Huzzah has also got a good I/O expandability with 9 GPIO (General Purpose Input Output) I/O digital channels, 1 analog input channel and 2 UARTs (Universal Asynchronous Receiver-Transmitter) serial I/O channels. Additional digital, analog, serial, etc. I/O channels can be easily added to the board thanks to the expandability guaranteed by the presence of one I2C and one SPI bus interfaces.
This module is 125 mm diameter, 150 mm high and weighs 0.95 kg.

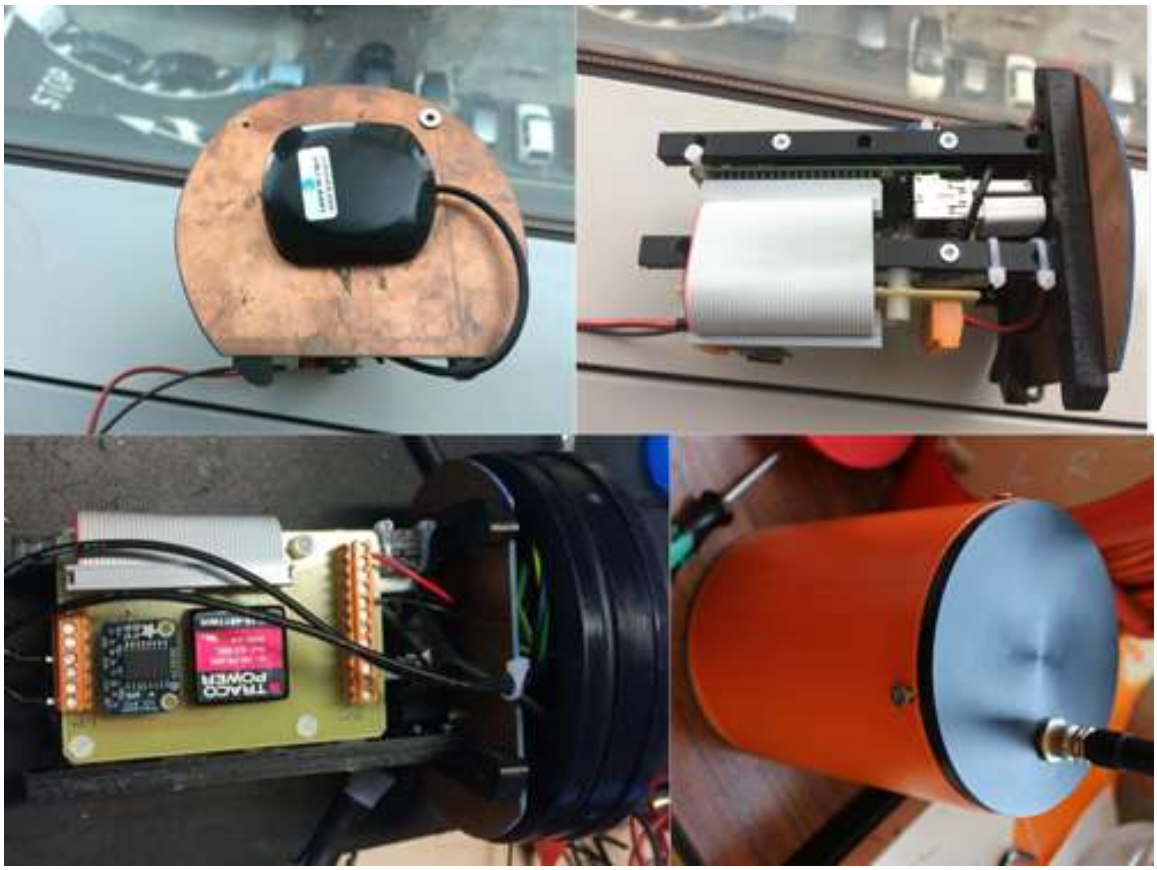

Figure 6.3: *The assembly and construction of the computational module*

The actuation module (AM)

As listed in the Chapter 5, the actuation module is constituted by the two motors:

- The main motor, the Maxon Ec-4pole with its ESCON Module 50/ controller. The ESCON Module Motherboard (in the following, "ESCON Module MoBo") is available as an alternative to developing an own motherboard. All required connections are already in place and designed as screw-type terminals.
- The azimuth motor, the Faulhaber 2232-BX with the Faulhaber MCBL3006S-AES controller. The controller is a small-sized, powerful 4-quadrant PWM servo controller for the highly efficient control of brushless EC motors up to approximately 250 W. This system has overload protections for electronics and motor, self-protections from overheating and overvoltage. The controller together with the motor's absolute encoder allows for a positioning resolution of 4096 steps per revolution, this means, if we consider the reduction gear, 483328 steps for a 360 deg rotation.

The controlling and communication module is also contained in the canister. It is based on another Huzzah ESP8266 microcontroller board. The actuation module communicates by means of the Wi-Fi link with SWAMP control system, by means of one RS-232 serial channel with the servocontroller of the propulsive motor and by means of an additional SPI D/A channel with the servocontroller of the azimuth motor. In this way the Pump-Jet Module can communicate via Wi-Fi with the central unit of one hull or the other in function of the actual configuration or in function of the operational requirements. Power on/off, enable/disable and faults signals are managed by means of the GPIO channels.
This module is 125 mm diameter, 400 mm high and weighs 2.6 kg.

Figure 6.4: *The assembly of the Pump-Jet Module*

The communication module

While wireless networks are widely used for the tele-operation of marine robots resulting reliable, on the other hand the integration of wireless communication into SWAMP required careful consideration, since the risks and potential loss of reliability had to be evaluated.
The communication module is an Ubiquiti Bullet M2HP working at 2.4 GHz that can works both in AP (Access Point) mode and in SA (Station Adapter) mode depending on which mode is working the computational mode of the single hull (either master or slave).
The network created on-board the SWAMP vehicle is a wireless mesh network (WMN) that is a communications network made up of radio nodes organized in a mesh topology. A mesh refers to rich interconnection among devices or nodes. Wireless mesh networks often consist of mesh clients, mesh routers and gateways.
Wireless WDS Mesh Network Mesh Network is a topology that has a full bidirectional connectivity between his nodes. In this mode every node in network (access point) hasn't only a way to other nodes, but they can access to other network with other nodes. Mesh has some modes such as full mesh, partial mesh or hybrid mesh. Mesh network is advantageous since it has roaming ability, full coverage, redundancy and it is fault tolerant between the links.
The on-board system can be setup into two modes: wireless WDS mesh with mesh interface and wireless WDS mesh with bridge interface.
Thank to the modularity of such a system additional modules can be easily added (e.g. computational, actuator, sensor, etc. modules) communicating Wi-Fi and without the need of a wired connection.
This module is 40 mm diameter, 500 mm high and weighs 0.95 kg.

Figure 6.5: *The assembly and construction of the communication module*

6.2 Low-level Control architecture

The basic idea is to have a vehicle made up of N modules (control modules, actuators, sensors, etc.) which communicate via a Wi-Fi connection using the 192.168.29.0 network.

- The Access Point (AP) of the Wi-Fi network which is installed on-board SWAMP, has an IP address: 192.168.29.1
- The Station Adapter (SA) of the Wi-Fi network, which is installed near the control station on the ground or on the support boat, has as IP address: 192.168.29.2.
- Computational Module (CM) - Module based on a Raspberry Pi card on which it runs a Microstrain 3DM-GX3-35 sensor acquisition program. The CM of the SWAMP vehicle has an IP address of 192.168.29.101
- Actuator Module (AM) - Arduino board based modules. There's one for every propulsion block of SWAMP. These modules are used to operate the actual propeller and the azimuth motor. The 4 AM modules have an IP address between 192.168.29.201 and 192.168.29.204 and receive the commands on the UDP port 2968.

Communication protocol of the AM modules

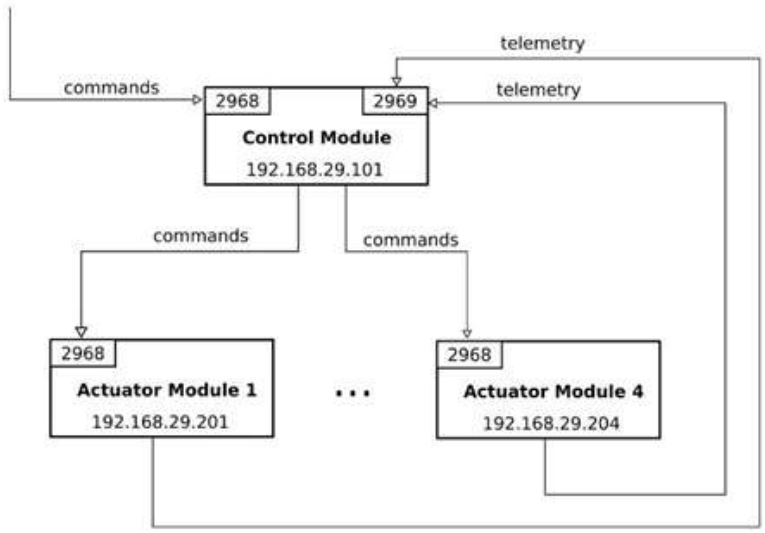

Figure 6.6: *The Logical communication scheme*

The command packets sent to the AM modules are ASCII strings derived from the C programming language (that is alphanumeric sequences of characters terminated with the character "0"). The commands are sent via a datagram-type network connection.
Following is the list of commands and the description of telemetry.

- Command COMMAND_MOTOR_POWER_OPCODE == 1002
  Example: "1002 <engine number> <0/1>"
  The engine number can be 0 == THRUST_MOTOR or 1 == AZIMUTAL_MOTOR.
- COMMAND_MOTOR_ENABLE_OPCODE command == 1003
  Example: "1003 <engine number> <0/1>"
  The engine number can be 0 == THRUST_MOTOR or 1 == AZIMUTAL_MOTOR.
- COMMAND_MOTOR_SET_REFERENCE_OPCODE command == 1004
  Example: "1004 <engine number> <reference value>"
  The motor number can be 0 == THRUST_MOTOR or 1 == AZIMUTAL_MOTOR.

In the case of THRUST_MOTOR the reference value is a number included in the interval [0,100000] (i.e. 0 - 100% expressed in thousandths) and indicates the RPM.
In the case of AZIMUTAL_MOTOR the reference value is the number of steps corresponding to the position you want the engine to reach and is a number included in the interval [-2147483648,2147483647].

- COMMAND_AZIMUTAL_MOTOR_SET_MAX_SPEED_OPCODE command == 1005
  Example: "1005 100"
  This command is used to set the maximum motor rotation speed expressed in RPM.
- Command COMMAND_AZIMUTAL_MOTOR_GO_HOME_OPCODE == 1007
  Example: "1007"
  This command is used to return the azimuth motor to the home position (0).
- COMMAND_ENABLE_DEBUG_LOGGING_OPCODE command == 10000
  Example: "10000 <0/1>"
  It is used to enable or disable debug logging. By default the program of the AM has debug logging enabled. It is recommended to disable it in normal operating conditions because it generates a lot of output that slows down the system and degrades performance.
- COMMAND_ENABLE_TELEMETRY_OPCODE command == 10001
  Example: "10001 <0/1>"
  Used to enable / disable telemetry sending. By default the program AM sends telemetry (described below).
- Command COMMAND_CHANGE_TELEMETRY_IP_ADDRESS_AND_UDP_PORT_OPCODE == 10002
  Example: "10002 201 2970"
  It is used to change the IP address and UDP port at which the AM program send telemetry.

All the commands developed for the architecture of SWAMP can be used in an ease way by a computer connected to the network. The commands can be sent from a C-program, from Matlab, Simulink or other programming tools in an ease way.
Below is reported an example of commands sent via Matlab to the starboard bow thruster Pump-Jet number 1, address 192.168.29.201. In this case the motors are enabled and a 50% of Pump RPM provides thrust at an angle of 45 deg:

```
m1 = udp('192.168.29.201',2968);   % User Datagram Protocol of Pump − JetModule1
fopen(m1)                          % Open the communication
fwrite(m1,'1002 0 1')              % Power On Pump motor
fwrite(m1,'1002 1 1')              % Power On of the Azimuth motor
fwrite(m1,'1003 0 1')              % Enable Pump motor
fwrite(m1,'1003 1 1')              % Enable Azimuth motor
fwrite(m1,'1007')                  % Homing
fwrite(m1,'1005 7000')             % Azimuth speed rotation 7000 RPM
fwrite(m1,'1004 1 41284')          % Rotate 45 deg the Azimuth motor
fwrite(m1,'1004 0 50000')          % Pump motor speed (50000/100000) 50%
fwrite(m1,'1003 0 0')              % Unable Pump motor
fwrite(m1,'1003 1 0')              % Unable Azimuth motor
fwrite(m1,'1002 0 0')              % Power Off of the Pump motor
fwrite(m1,'1002 1 0')              % Power Off of the Azimuth motor
fclose(m1)                         % Close the communication socket
```

Communication protocol of the Microstrain 3DM-GX3-35 sensor acquisition program

On the CM runs a 3DM-GX Microstrain sensor acquisition program. The commands and packages of Telemetry received / sent by this program are ASCII strings derived from the programming language C (that is alphanumeric sequences of characters terminated with the character "0"). These strings are made up of values separated by spaces. The data is sent via a datagram-type network connection.
By default the program sends telemetry data to IP address 192.168.29.100 on UDP port 2969. It is also possible to have the telemetry sent to multiple recipients.
Following is the list of commands and the description of the telemetry.

- COMMAND_ENABLE_DEBUG_LOGGING_OPCODE command == 10000
  Example: "10000 <0/1>"
  This command enables / disables debug logging. By default the Microstrain 3DM-GX3-35 sensor acquisition program has the logging of debug enabled. It is recommended to disable it under normal operating.
- COMMAND_INSERT_TELEMETRY_IP_ADDRESS_AND_UDP_PORT == 10001
  Example: "10001 <least significant byte of the IP address> <UDP port>"
  This command adds a new recipient to the set of recipients which to send the telemetry.
- COMMAND_REMOVE_TELEMETRY_IP_ADDRESS_AND_UDP_PORT == 10002
  Example: "10002 <least significant byte of the IP address> <UDP port>"
  This command removes a recipient from the set of recipients to whom send telemetry.

As for the telemetry package sent by the aforementioned program, the fields present are the following, The firts number is the identification number of the sender (it is the least byte significant of the IP address of the CM):

1) Identification number of the sender
2) yaw (6 decimal places)
3) pitch (6 decimal places)
4) roll (6 decimal places)
5) latitude (8 decimal places)
6) longitude (8 decimal places)
7) heightAboveEllipsoid (6 decimal places)
8) heightAboveMSL (6 decimal places)
9) horizontalAccuracy (6 decimal places)
10) verticalAccuracy (6 decimal places)
11) llhPositionValidFlags (uint16)
12-14) scaledAccel [X, Y, Z] (6 decimal places)
15-17) scaledGyro [X, Y, Z] (6 decimal places)
18-20) scaledMag [X, Y, Z] (6 decimal places)
21-29) orientMatrix [X] [Y] (6 decimal places)
30) northVelocity (6 decimal places)
31) eastVelocity (6 decimal places)
32) downVelocity (6 decimal places)
33) speed (6 decimal places)
34) groundSpeed ..(6 decimal places)
35) heading (6 decimal places)
36) speedAccuracy (6 decimal places)
37) nedVelocityValidFlags (uint16)
38) headingAccuracy (6 decimal places)
39) utcTimestamp (uint64)
40) utcTimeValidFlags

Note that also in this case at the end of the string, to facilitate the eventual display of data in a terminal, before the '0' character were inserted the characters "n".

6.3 Power

Power is provided by modules containing Lithium-ion Rechargeable cell batteries with a Nominal Voltage of $36\,V$ and with a nominal capacity of $13\,Ah$. One battery module fig. 6.7 is installed on each hull in a watertight canister easily replaceable.

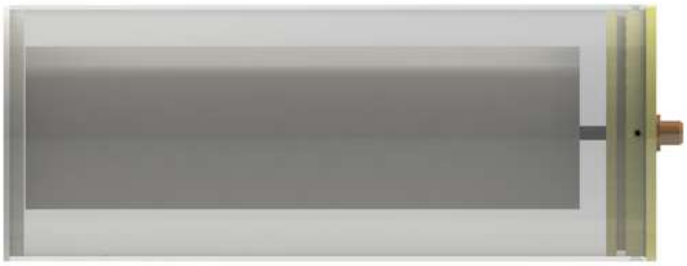

Figure 6.7: *The battery module design*

Each battery is connected to a power distribution unit fig. 6.8 that is used for turning-on and off the vehicle and splits the power to various users.

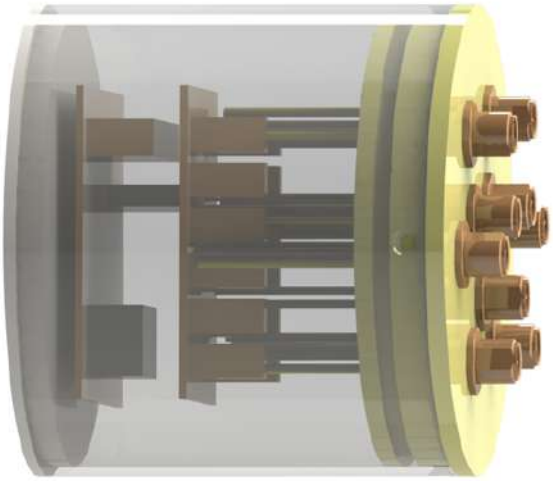

Figure 6.8: *The power distribution and power-on module*

With the resistances obtained during the towing tank tests in the standard configuration $B = 1100$ at maximum payload $\Delta = 58\,kg$ in deep waters it was possible to dimension the power required and foresee various usage profiles of the vehicle. The choice of the batteries was done with the idea of a minimum of endurance of $2\,hour$ and a maximum of $6\,hour$. This depending on the usage of the SWAMP ASV and on the requirements of the mission.
Due to the on-board presence various users running at various Voltages a series of industrial DC-DC converter had to be chosen. Depending on the current and power needs of the single devices. Users at 5V, 12V, 24V, 36V are present on-board as reported in table 6.1.
From these data it was also possible to extract the power required by the systems. Considering the extreme case of operation at the maximum power of all the systems on board, the table 6.1 was created. It reports the power need of the on-board installed systems for one single hull. In the last two columns the current [A] and the power [W] resulting from the application of the DC-DC is

Table 6.1: *The on-board power needs of the various sources*

	Different Voltage				Battery Voltage	
	$5V$	$12V$	$24V$	$36V$	$36V$	
	$[W]$	$[W]$	$[W]$	$[W]$	[A]	[W]
Thruster Bow				90	2.5	90.0
Thruster Stern				90	2.5	90.0
Azimuth Bow			7.2		0.2	7.2
Azimuth Stern			7.2		0.2	7.2
Wi-Fi bow thruster	2.5				0.1	2.5
Wi-Fi stern thruster	2.5				0.1	2.5
CPU Raspberry PI3	12.5				0.3	12.5
Wi-Fi Bullet			24		0.7	24.0
Microstrain 3DM-GX3-35	0.8				0.0	0.8
Wi-Fi cameras	10				0.3	10.0
Relais	10.5	1.2	2.4		0.4	14.1
CPU Raspberry PI3 sensors module	12.5				0.3	12.5
Sonar		1.2			0.0	1.2
CTD		2.94			0.1	2.9
Laser pointer	0.05				0.0	0.1
Camera	5				0.1	5.0
Tot	56.4	5.3	40.8	180	**7.8**	**282**

reported. The total power consumption of a single hull is, at the maximum continuous power, $7.8\,A$ at $36\,V$ with a resulting power of $282\,W$.

The battery

Lithium-ion battery packs have a high round-trip efficiency and present lower volume, weight, temperature sensitivity and maintenance of lead-acid batteries.
The choice has fallen on Li-ion first of all for their lightness in relation to classical Lead acid batteries. Moreover they are more suitable for harsh environments (both hot and cold), even if they loose efficiency at low temperatures this loss is much less than with the classical batteries. Moreover, the discharge rate affects the performance of lead acid batteries. At -20 °C, a Lithium battery that delivers a 1C current (one times its capacity), can deliver more than 80% of its energy when the Gel or AGM batteries will deliver 30% of their capacity.
In standard environment Li-ion batteries have an efficiency that is around 99% and can fastly be charged to 100% of capacity or less without capacity losses. The latter capacity is also thanks to the fact that the discharge curve of Li-ion batteries is essentially flat, meaning that a 20% charged battery will provide nearly the same output voltage as an 80% charged battery.
Each hull of SWAMP has its own battery pack. They are composed by sets of cells with a voltage of $3.7\,V$ and a capacity of $2.6\,Ah$. The batteries are composed in 10 batteries in series giving a resultant voltage of $37\,V$ put in 5 parallel sets giving a resultant capacity of $13\,Ah$. The summarising of the characteristics of the batteries and of the cells is reported in table 6.2.
As shown in fig. 6.9, unlike lead-acid batteries, it is considered practical to regularly use 90% or

Table 6.2: *Each hull's battery pack features. The main characteristics are reported in* ***Bold*** *and are: Voltage, Power, Capacity, Life Cycles, Discharge and Weight*

Battery Pack			Cells	
Series	**1**	#	**10**	#
Parallel	**1**	#	**5**	#
Nominal voltage	**37**	**V**	**3,7**	**V**
Nominal capacity	**13**	**Ah**	**2600**	**mAh**
Power	**481**	**Wh**	**9,62**	**Wh**
Internal resistance	≤ 150 m Ω			
Life cycles	**> 800 cycles @ 1C 100% DOD**			
Monthly self-discharge	<3%			
Charge efficiency	100% @ 0.5C			
Discharge efficiency	96 - 99% @ 1C			
Peukert constant	**1,1**	**k**		
Depth of Discharge: DOD	**90%**			
Depth of Discharge Limit	**1,3**	**[Ah]**		
Charge voltage	**42,0**	**V**	**4,2**	**V**
Charge mode	0,2 at 42V		0,2	2,75
Charge current	1 A		1300	mA
Maximum charge current	≤ 6 A		2600	mA
Charge limit voltage	42 +/- 0.1 V			
Direct current	10 A			
Maximum current	15 A (<5min)		5200	mA
Discharge limit voltage	**28**	**V**	**2,75**	**V**
Charge temperature	0 ° C to 45 ° C @ 60 +/- 25% Relative humidity			
Discharge temperature	-20 ° C to 60 ° C @ 60 +/- 25% Relative humidity			
Storage temperature	0 ° C to 40 ° C @ 60 +/- 25% Relative humidity			
Humidity	5% ≤ RH ≤ 85%			
Cell and Method	18650 / 10S6P			
Plastic container	PVC			
Dimensions	mm 76 x 70 x 300 h		18,4 x 65	
Weight	**3**	**kg**	**47**	**g**

more of the rated capacity of a lithium battery bank, and occasionally more use the 100% DoD of the batteries.

Figure 6.9: *The usability percentage of Li-ion [216]*

But for the chosen standard quality LiFePo4 battery pack a Dod of 90% and 1C discharge rate was indicated as a threshold. With this the number of cycles remains well above 800 with a capacity that remains above 90%. This number of cycles can be greatly increased by reducing the depth of discharge (DoD). And in the standard usability of SWAMP the DoD will always remain well above 90%.

Keeping the Depth of Discharge (DOD) below the maximal limit of 100% and ideally at 95% DoD then threes standard limit-missions were planned and the results are reported in table 6.2.

The three missions are reported considering a continuous payload power absorption of about $90\,W$. The first mission considers only high speed operational speed (e.g. in adverse current), the second mission may be considered the standard mission and involves high speed transfers and low speed data acquisitions and the third considers intermediate speeds for transfer and sampling with a longer endurance. In the table the State of charge (SOC) value is calculated and reported and this value is also reported in fig. 6.10. The SOC is defined as the percentage of the releasable capacity relative to the battery nominal capacity [217, 218].

For shallow water lower speeds are requested to maintain the time, reduced endurance shall be considered due to the higher resistance coefficients. Additional power batteries may easily be installed

Table 6.3: *The results of the standard mission's power supply analysis*

Mission Type 1										
U	$time$	P_{prop}	I_{prop}	P_{Users}	P_{tot}	I_{tot}	P_{Wh}	$I^n * t$	C_{Fin}	SOC
[m/s]	[min]	[W]	[A]	[W]	[W]	[A]	[Wh]	Ah	Ah	0
0	0	0	0,0	88	0	0	0	0	13	1
1,5	100	171	4,3	88	259	6,5	433	12	1,1	0,08
Mission Type 2										
U	$time$	P_{prop}	I_{prop}	P_{Users}	P_{tot}	I_{tot}	P_{Wh}	$I^n * t$	C_{Fin}	SOC
[m/s]	[min]	[W]	[A]	[W]	[W]	[A]	[Wh]	Ah	Ah	0
0	0	0	0,0	88	88	0	0	0,0	13	1
1,5	12	171	4,3	88	259	6,5	52	1,4	11,6	0,89
1,2	24	74	2,0	88	162	4,3	84	0,9	10,7	0,82
0,5	156	17	0,5	88	105	2,9	315	6,8	3,9	0,3
1,2	168	74	2,2	88	162	4,7	347	1,0	2,9	0,22
1,5	180	171	5,3	88	259	8	399	1,8	1,1	0,08
Mission Type 3										
U	$time$	P_{prop}	I_{prop}	P_{Users}	P_{tot}	I_{tot}	P_{Wh}	$I^n * t$	C_{Fin}	SOC
[m/s]	[min]	[W]	[A]	[W]	[W]	[A]	[Wh]	Ah	Ah	0
0	0	0	0,0	88	0	0	0	0,0	13	1
1	30	40	1,0	88	128	3,2	64	1,7	11,3	0,87
0,8	210	24	0,6	88	112	3	400	9,4	1,9	0,15
1	240	40	1,1	88	128	1,8	464	0,9	1	0,08

on board of SWAMP in case of higher power consumption, long missions or additional payloads that required a high on-board power.

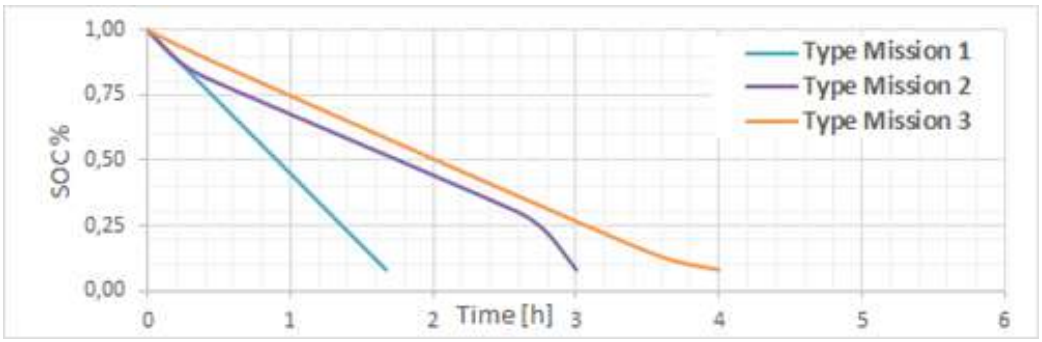

Figure 6.10: *The State Of Charge of the batteries during the three planned mission*

Anyway the three missions above described are limit cases of long-endurance missions in which all the on-board users are at the maximum power and the vehicle is continuously moving. Experience suggests that the missions will last longer.
In total 4 battery packs were built but just a couple per time are used. The construction of these modules is reported in fig. 6.11. Each module is 125 mm diameter, 310 mm high and weighs 3.4 kg.

Figure 6.11: *Battery assembly*

The power distribution module

The only function of the power distribution module is to re-distribute the power produced by the battery. The concept behind this module is to reduce the number of connections to unplug when a battery has to be changed.
The module is constituted by a number of ip68 female and male connectors where the users are connected. All the connectors used on-board are of the type M12-S male/female cable connectors to be mounted on a panel or free.These connectors have 3+PE contacts, moulded on cable, IP68, PUR black, 4 x 1.50 mm^2 and are produced by Binder.
One of the connectors is the switch-on / switch-off connector that is used to power-on SWAMP.
Each hull has its own power distribution module fig. 6.12. Each module is 125 mm diameter, 120 mm high and weighs 0.85 kg.

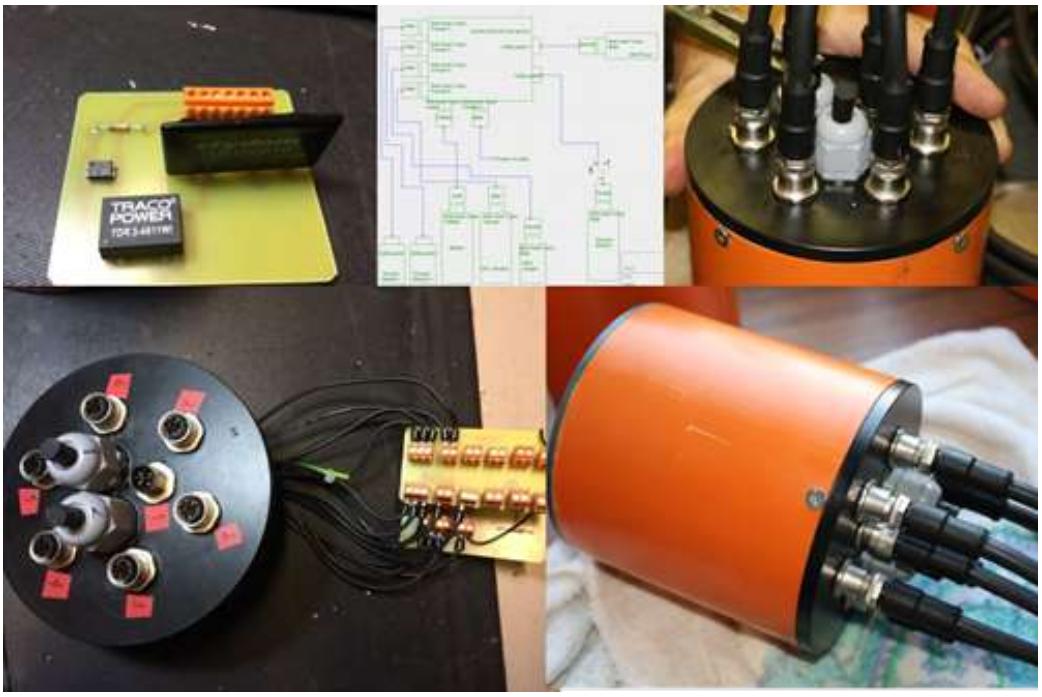

Figure 6.12: *Power distribution assembly*

6.4 The basic NGC system

Single vehicle NGC system, both as catamaran or single hull vessel, consists of a dual-loop hierarchical guidance and control architecture of the class presented in [219]. As shown in Figure

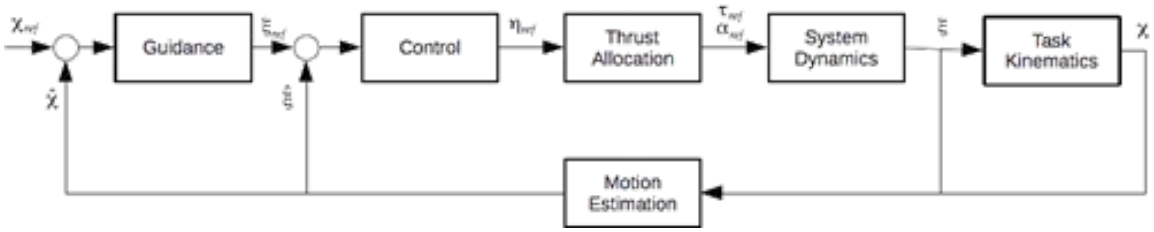

Figure 6.13: *Navigation Guidance and Control architecture*

6.13, the outer guidance loop manages the kinematics interactions between the vehicle and the environment at task function level and generates the reference linear and angular velocities for the control module. The inner control loop handles system dynamics, implementing a velocity servo-loop for surge, sway, yaw respectively, to generate the desired surge and sway forces and yaw torque. Motion estimation is based on (partial) knowledge of system dynamics and extended Kalman filtering techniques, as discussed in [220], where basic guidance and control algorithms, including straight line-following, are presented. Advanced techniques for generic path-following and multi-vehicle cooperative guidance, e.g. vehicle-following, are presented in [221] and [222], respectively.
Thanks to NGC system modularity, it is only needed to tune parameters of the guidance, control and motion estimation algorithms and to design and implement the Thrust Allocation module, that is specific of each vessel class.

6.5 Distributed control

During the design of SWAMP hardware architecture a special attention was focused on Multi-Robot Systems (MRS), intended as those robotic systems obtained via composition of different separately controlled sub-systems. These can cooperate when it is required to cooperate in executing a common assigned task but can work independently or independently with a common strategy in function of the requirements.
In this context, as shown by [223], which main research objective has been the design of a modular, computationally distributed, functional and algorithmic architecture facing with the problem of controlling complex robotic systems, an MRS can be obtained either by a physical connection, i.e. by physical or electro-mechanical assembling that involves sub-systems (this is the case of the two SWAMP hull connected by the transverse bars), or by the composition of systems that may be the direct consequence of the specific task to be performed as may be the case of the two unconnected hulls asked to move an object in a cooperative way. These concepts are illustrated in fig. 6.14.

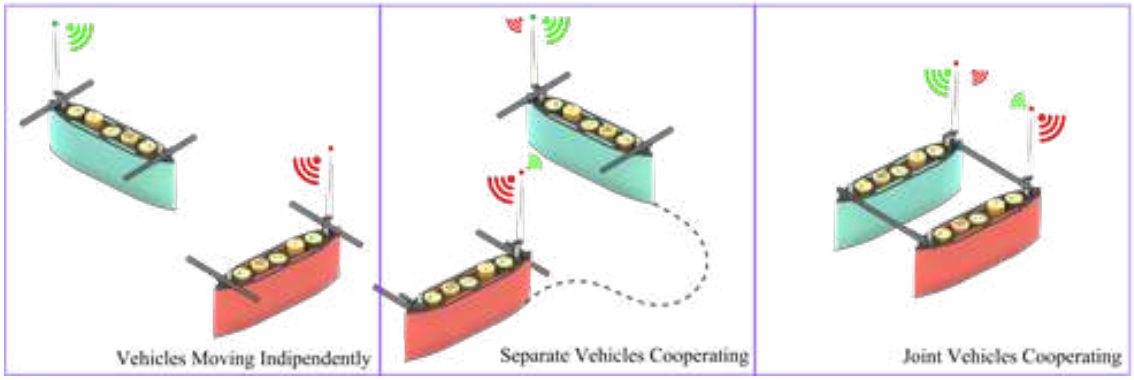

Figure 6.14: *The possible cooperating scenario of SWAMP with physical link separated*

But the distributed control and the modularity may become helpful also to comply with standards of redundancy.
The redundancy is to have two or more sensors or systems required to perform a function so that the redundant unit can take over from the failed unit without unacceptable interruption of the function. This is the special case of SWAMP where two hulls with separated intelligence, separated power sources, highly controllable thrusters, separated and taking-over communication systems result highly redundant. The transfer of failures between redundant subsystems is avoided by the complete separation of the redundant systems.
A schematic explanation of this redundancy is reported below:

- Fault of one of the communication systems:
  i) consequence: No consequence exists
  ii) Solution: The other hull's communication system takes over the duties of the one in default

- Loss of control system on one hull
  i) consequence: No consequence exists
  ii) Solution: The other hull's control system takes over the duties of the one in default

- Fault of one thruster on one hull:
  i) Consequence: Small - Loss of thrust symmetry.
  ii) Solution: The vehicle is over-actuated. The fault of one thruster is not a problem thanks to the fact that the vehicle is highly controllable also with 3 thrusters.

- Fault of one thruster on each hull
  i) Consequence: Medium - Possible loss of thrust symmetry.
  ii) Solution: The vehicle is over-actuated. The fault of one thruster on each hull is not a problem thanks to the fact that the vehicle is highly controllable also with just 2 thrusters. Ad-hoc fault strategies have to be studied

- Fault of two thrusters on one hull
  i) Consequence: Medium - Total loss of surge thrust symmetry.
  ii) Solution: The vehicle is over-actuated. The fault of two thruster on the same hull may become a problem of control. Ad-hoc fault strategies have to be studied

- Fault of a battery on one hull
  i) Consequence: Medium - Total loss of surge thrust symmetry.
  ii) Solution: The vehicle is over-actuated. The fault of two thrusters on the same hull may become a problem of control. Ad-hoc fault strategies have to be studied

In general, full stop and restart of the system are not complied in redundancy and the SWAMP vehicle is based on systems which are immediately available for use since they are always turned on during normal functioning.
As an example in the highest standard level of Dynamic Positioning, namely the *DP-3* (shown by DNV-GL rules [224]) any loss of position may not occur in the event of a single fault in any active or static component or system, including complete loss of a compartment.
Any active component or systems on-board like generators, thrusters, switchboards, DP control computers, sensors have to be redundant. Moreover any components has to be one watertight compartment preventing from flooding. And in case of flooding this event should not damage the redundant elements. This should happen also in any case of fire.
Two fully redundant power and thruster systems each capable of maintaining position and heading if the other fails. As listed above the SWAMP design can also make use of multiple systems each providing partial redundancy such that the vessel can maintain position with all combinations of independent systems that survive any defined fault.

Chapter 7

Field Tests

In this chapter the tests performed on the assembled SWAMP vehicle are reported. The vehicle has been extensively tested in laboratory and in real environment.
In particular a series of field tests have been conducted together with some experiments related to various aspects of applications.
After the first initial tests in Genova Pra and Genova Harbour the robot was used in an experiment of citized engagment in robotic during the *Festival della Comunicazione* in Camogli (GE) Italy. After these tests the robot was used in an other real environment in Croatia both for producing a Map of the sea bottom both for the testing on the functioning of the vessel itself. The final test was done on the Roia (Roja) River for the application of robotics in the mapping of a river. In this final test the robot proved to be constructed with the right specifications.

7.1 Assembly: The SWAMP vehicle

In this section it is described the assembly of the new Unmanned Marine Vehicle SWAMP. The vehicle itself is studied as an inspection vehicle but it can be equipped with different types of sensors in order to make it flexible and adaptable to various applications such as sampling of water or objects, underwater manipulation, cooperation with underwater vehicles or with other underwater or surface vehicles, mapping of underwater ground and detection of vegetation lying on the seabed.
As mentioned in Chapter 6 all the modules were produced in the CNR-INM laboratories from the circuits, the production of the motherboards, the assembling, the connection and the construction of the canisters.
Before assembling the vehicle every element subjected to external loads had to be pressure-tested. All the modules which are contained into PVC pipes closed by POM-made or PVC caps with side o-ring were tested underwater. This kind of test was useful to ensure that the vehicle, even if a surface one, was all water-pressure-resistant. Every pressure canister is provided with at least one O-rings. Tests where performed for a pressure equivalent to 1 m of underwater depth that stands for 0.1 bar of pressure and a consequent load of 1 Pa.
Every element was scantled with a FEM analysis thus the pressure test is only required to assess the good behaviour of the sealing.
The images of the tests are reported in fig. 7.1. The vehicle assembly is easy: all the modules are inserted in their holes. In the design configuration and for the perfect balancing of the vehicle the central holes are for the installation of the batteries, the fore and aft holes are for the installation of the thrusters and the remaining holes are for the installation of the Computational Module and the Power distribution Module and for the installation of the sensors.
The assembly of the vehicle is reported in fig. 7.2. The procedure is quite easy, all the elements are inserted in holes. The motors absolute sensors requires that the Pump-Jet Module does not turn when they are mounted. This means that they have to be fixed to the hull. The fixing is done

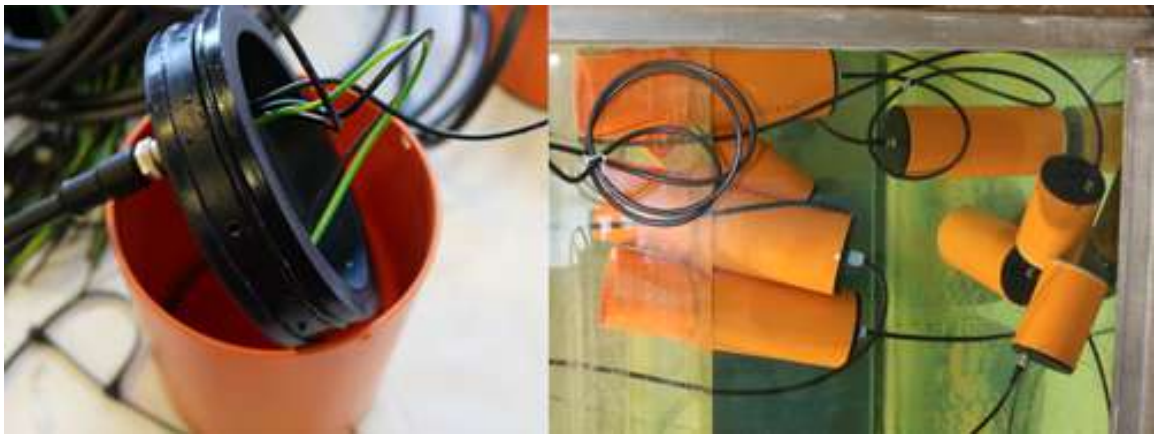

Figure 7.1: *SWAMP elements water pressure tested*

Figure 7.2: *SWAMP assembly procedure and the final installation*

with an couple of clamps that are blocked by one bolt. The only other elements that needs to be

Figure 7.3: *The clamp for blocking the motor's rotation*

blocked, for evident reasons, is the Computational Module where the gyro is present. Here a 3D printed block is used that allows the ease blocking of the rotation without impeding the moving of the module.
For the coupling of the hulls as shown in fig. 7.2 the two transverse bars are used. A panel, a structure, or what-else can be installed in the "hole" created by the two hulls.
It is important to note that the installation of the elements inside the hull is just a matter of few minutes that is the necessary time for connecting the powering cables. In this sense SWAMP is a real "back-pack" vehicle. This characteristic finds its application in continental, inland and coastal waters that are generally not easy to access and data related to these areas may not exist at all.

7.2 Bench funtional tests

Functional tests are standardly performed for every single part of the vehicle. In figs. 7.4 to 7.6 are shown the bench tests performed on the various elements. Functioning tests were especially made for testing the Communication architecture of the vehicle's on-board systems. Tests were made on the maximum required power and on the integration of all the on-board systems. Tests were also made on the functioning of the motors, of the onboard sensors, on the functioning of hardware control architecture, on the batteries and power distribution functioning.
In fig. 7.4 it is reported the phase of integration of the sensors.

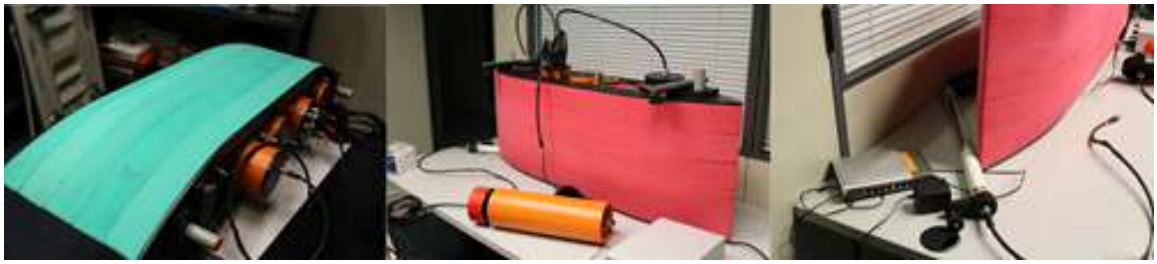

Figure 7.4: *Integration tests, communication tests*

In fig. 7.5 it is reported the phase of software architecture testing by using all the commands described in and applying to the motors modules and to the Computational Module.

Figure 7.5: *Software architecture testing*

In fig. 7.6 it is reported the phase of propulsion testing in the pool of CNR-INM. In particular,

Figure 7.6: *Propulsion testing and calibration*

for the motors, it was important to verify the homing position that allows to apply a correction to exactly orient the thrust vector with a maximum at the 0 deg as defined in Section 5.7. As an example of the tests performed, in fig. 7.7 is reported the surge speed $u\,[m/s]$ recorded by the AHRS during functioning tests in the pool. The vehicle moves forward and backward continuously. Two

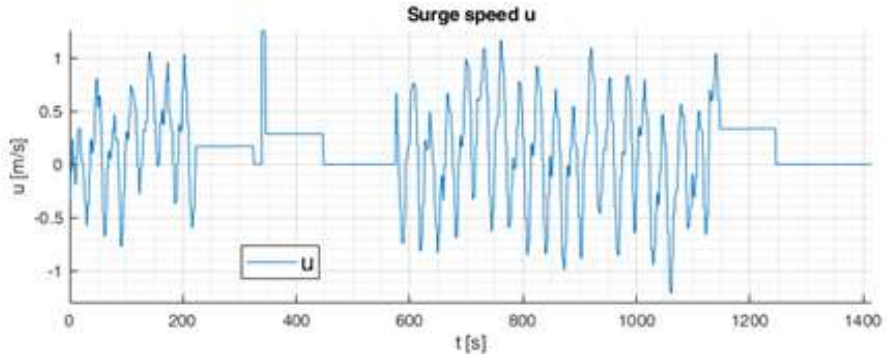

Figure 7.7: *The results of surge speed during reversing speed tests in the small CNR pool*

commands are used to control the Pump-Jet Module: % of the RPM for the thrust and the angle for the azimuth. The thrust is applied in the form a percentage $(0 - 100\%)$ of the RPM at the maximum thrust. while the angle is applied as a value from $-\pi to + \pi$ which is the mapping of the 360 *deg* on the 495411 *steps* counted by the absolute encoder.
As specified in the Chapter 4 the fine calibration of SWAMP weight-buoyancy is made by using standard lead elements inserted in the holes drilled in the foam. The calibration is not difficult thank to symmetric configuration of the vessel.
One of the most important passages was made for the calibration of the Microstrain Gyro. Careful attention is always taken in avoiding the presence of sources such as coils, magnets, and ferrous metal structures but these sources are hard to avoid and so a field calibration of the magnetometer after final installation was necessary. Since this sensor is the only native payload for the navigation of SWAMP, this phase was quite important to avoid the presence of errors in the data of navigation (e.g. heading).
Following the Hard & Soft Iron Calibration manual of the producer [225] the software to collect and process the magnetic vectors into calibration coefficients was used. The software collected the X, Y and Z axis magnetic vectors directly from the 3DM-GX3 in real time for further processing, data points wer uploaded on the IMU. With the software it was possible to verify the success of calibration.

7.3 Sea trials

For the sea trials the SWAMP vehicle was controlled using a software architecture similar to the one already developed in [84, 226–228].
A practical model where practical basically stands for consistent, from the point of view of the degree of accuracy, with the quality in terms of noise and sampling rate of the measurements provided by the proprio-ceptive sensors available onboard the platform, i.e. GPS (when on surface), AHRS.

7.3.1 Tests in Genoa Harbour

The first functional tests were conducted in the scenario of the Genoa Harbour.
Here the functioning of the vehicle in real environment was tested for the first time. Since portability and logistics were important constraints in the design of the vehicle also these aspects had to be checked. In fig. 7.8 is depicted the transport of swamp in the CNR-INM van, its mounting on the floating pier of the Genova harbour and the deployment from an height of almost $1\,m$ above the sea surface.

Figure 7.8: *The logistics of SWAMP*

The at sea trials were conducted, as shown in fig. 7.9, by securing the vehicle with a Dyneema rope to ensure that in case of failure the vehicle could be recovered.
The first tests gave good results and all the systems functioning were assessed without any mechanical or electrical faults.
Since a key step in environmental monitoring is to acquire data and map on the locations and their

Figure 7.9: *First functioning tests in Genoa Harbour at the "Riparazioni Navali" where CNR-INM has an access to the sea.*

characteristics to better perform assessment of change over time it was necessary to have a precise GPS positioning. Tests were also necessary to verify the good functioning of the GPS present on the Microstrain platform.

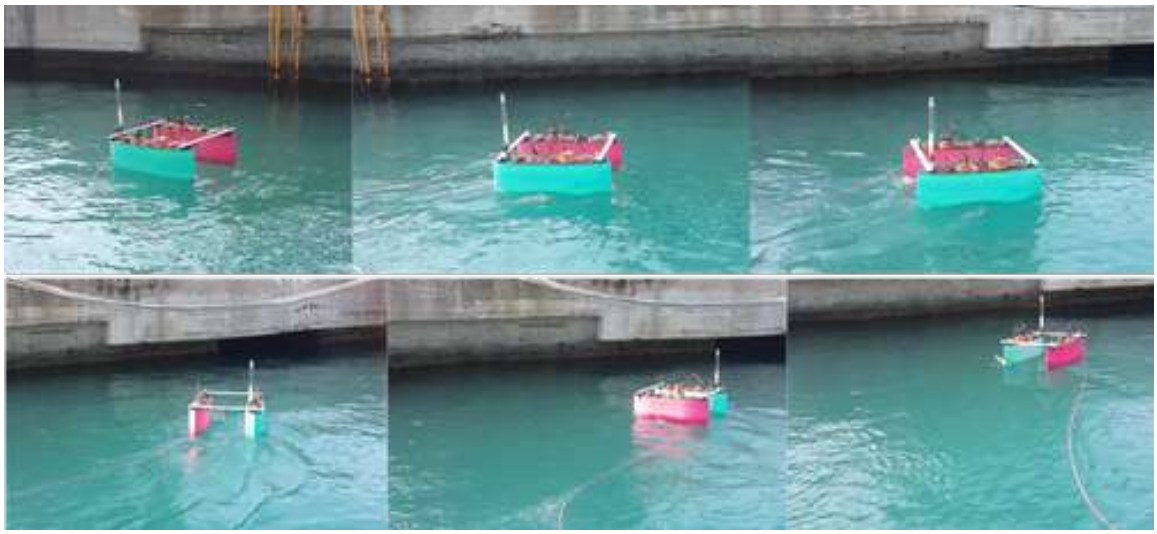

Figure 7.10: *SWAMP manoeuvring and high speed first tests*

7.3.2 Functioning Tests in Genova Pra

A second set of functioning tests were performed in Genova Pra location.
Also these tests were performed with the aim of evaluating the functioning of all the on-board systems of SWAMP.

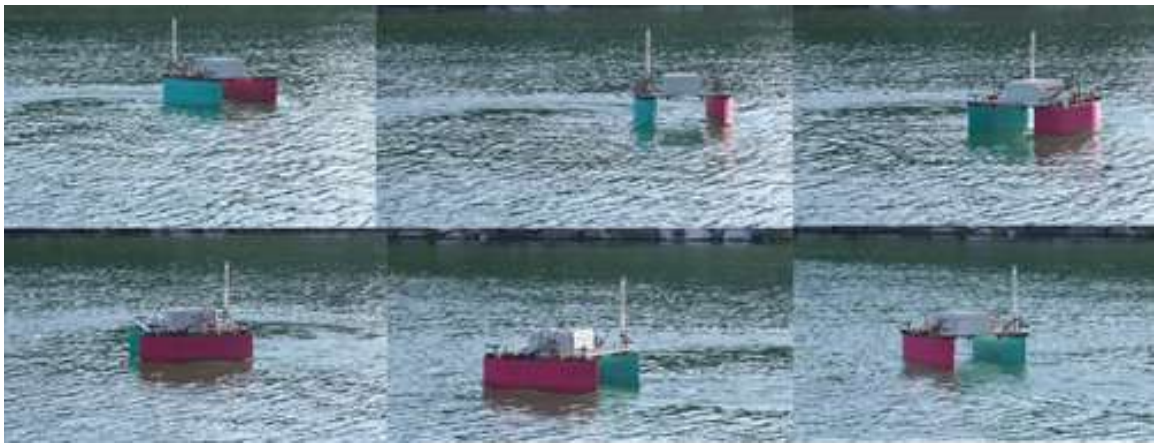

Figure 7.11: *SWAMP tests in Pra*

Tests were conducted by using a control that mapped the two bow thrusters to steer synchronously with an angle that varied from −90 to +90 deg. The stern thrusters were turned off. This kind of configuration was functional to the following tests performed in Camogli in the framework of the *Communication Festival*.

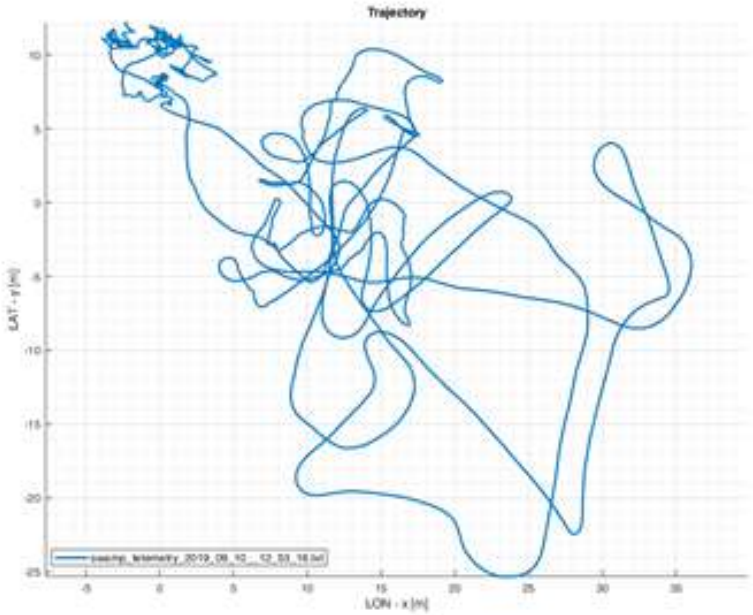

Figure 7.12: *All the SWAMP tests in Pra - LAT-LON data*

One of the significant tests is reported in fig. 7.13. The vehicle was guided by giving a almost constant 90 deg thrust port or starboard.
Data in the figures are the Gps data normalised in x [m] and y [m] reported on a squared map. The angles α of the thrusters and T^{PJ} the thrust commanded by $RPM_{\%}$, the percentage amount of RPM commanded to the thrusters (e.g. bp = BowPort thruster).

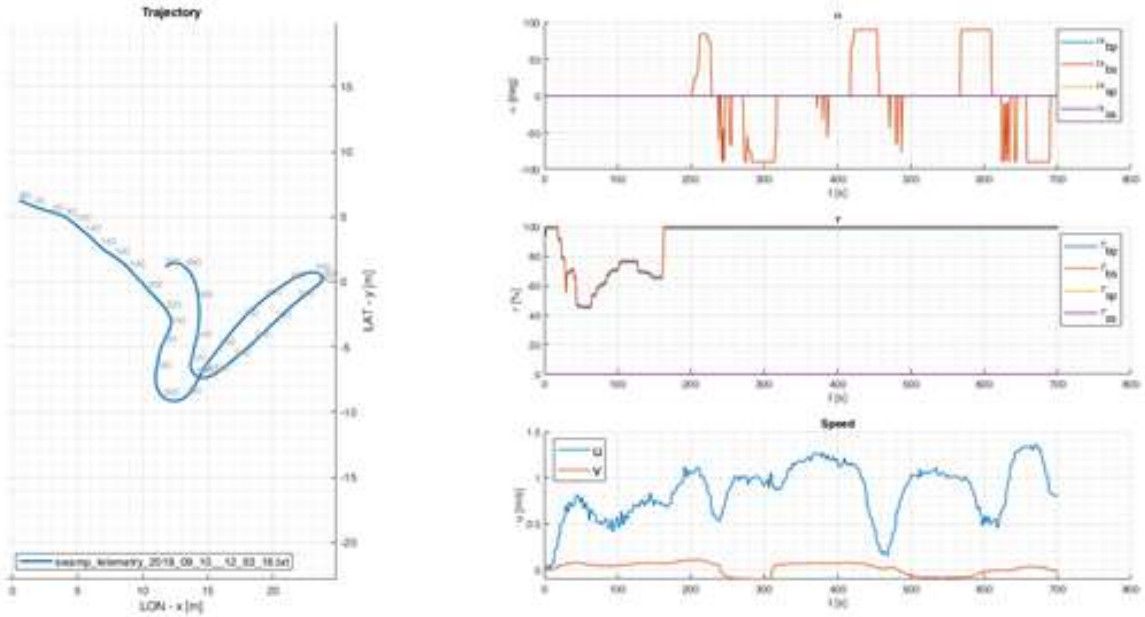

Figure 7.13: *SWAMP tests in Pra - LAT-LON data - The thrusters Angles and Thrust Actuation - Surge (u) and Sway (v) speeds - First part*

In fig. 7.14 the values of pitch, roll and yaw are reported. No significant variations in pitch and roll were recorded with the augmenting of thrust.

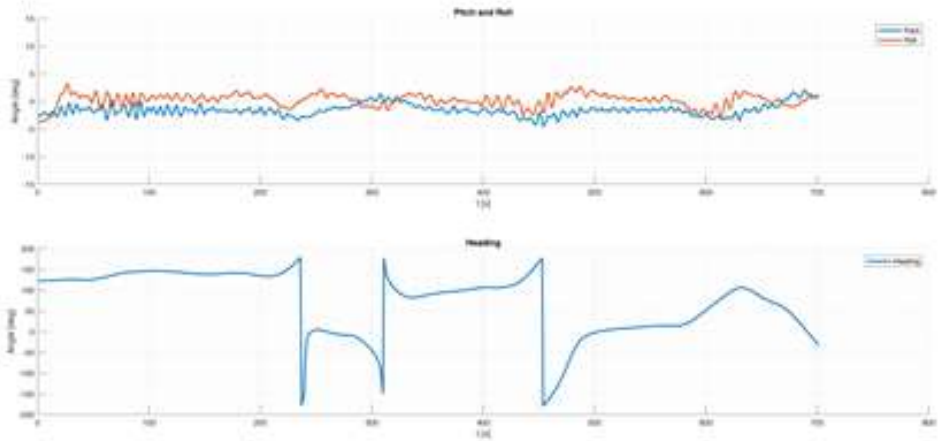

Figure 7.14: *SWAMP tests in Pra - Pitch & roll and Yaw - First part*

Another test is reported in fig. 7.15 where the vehicle is pushed by two thrusters at maximum reference $RPM_{\%}$. After a short rectilinear trajectory the vehicle is suddenly turned right and next the trajectory is again corrected towards a straight line.

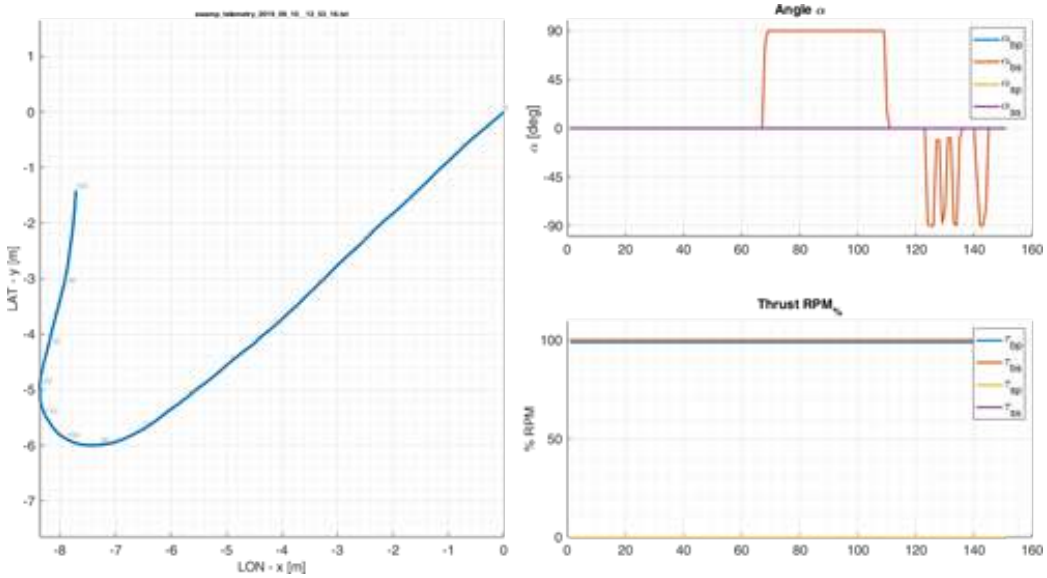

Figure 7.15: *SWAMP tests in Pra - LAT-LON data - The thrusters Angles and Thrust Actuation - Second part*

With the vehicle with small payload the two thrusters allowed the vehicle to reach up to $1.20\,m/s$ thus validating the functioning of the Pump-Jet also at speed. This is shown in fig. 7.16.

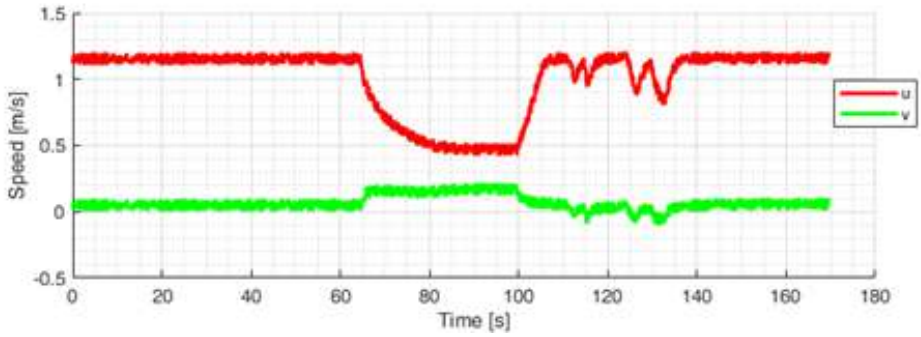

Figure 7.16: *SWAMP tests in Pra - Surge (u) and Sway (v) speeds - during the test - Second part*

Interesting is also the test reported in fig. 7.17, where the full ahead with two motors can be checked.

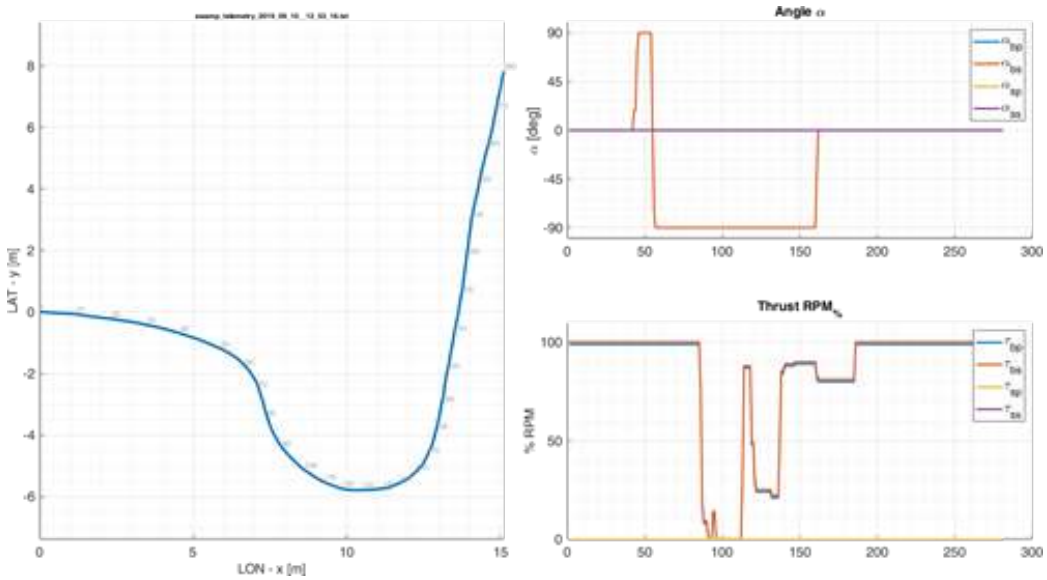

Figure 7.17: *SWAMP tests in Pra - LAT-LON data - The thrusters Angles and Thrust Actuation - Third part*

Also here the vehicle reached the velocity of $1.20\,m/s$ as reported in fig. 7.18.

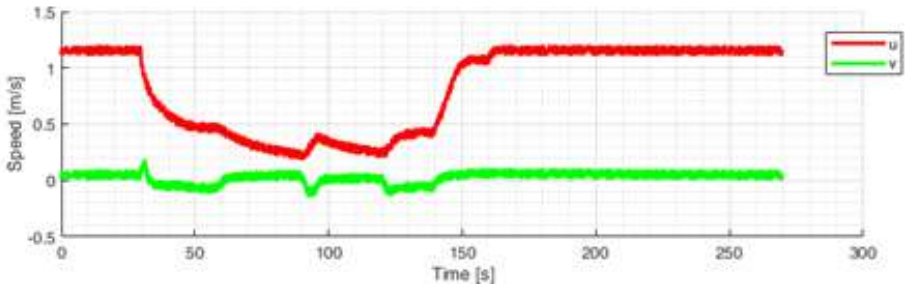

Figure 7.18: *SWAMP tests in Pra - Surge (u) and Sway (v) speeds - during the test - Third part*

An interesting test was done on the impacting (crashing) fig. 7.19 of the vehicle against a pier and against a rock. The tests were not planned before but the result was to assess the impact ability of the hull and the possibility of working close to the shore without worries.

Figure 7.19: *The SWAMP crash-test*

Sonar Tests

During these tests a sonar was mounted inside the port hull of SWAMP. The sonar object of the test is an ECS400 sonar Echologger with single beam, compact and light, which works at a frequency of 200 kHz. The peculiarity of this sonar is the possibility of having not only the value of the range in output but the entire acoustic signal of return.
The sonar was positioned inside one of the holes drilled in the hull and was layed on top of the 8 mm thick HDPE plate that constitutes the bottom of SWAMP hull. This is a protected place contained inside the hull.
The battery for powering and the electronics for the acquisition of the data and for the communication of this sensor are positioned inside the white box that can be seen in fig. 7.11. In this set-up the sonar communicates with a Raspberry Pi 3 that sends data via the on-board Wi-Fi to the telemetry pack.
One of the objectives of this test was to evaluate if the presence of the HDPE plate on the bottom could influence the sonar ability to perform a bathymetry.
Before the tests in Genova Pra some preliminary tests were performed in the CNR-INM pool in Genova. The results of these tests are reported in fig. 7.20. The picture shows that the the presence of a 8 mm thick plate of HDPE does not influence the functioning of the sonar. The recorded data are influenced with a constant value of delay. By applying a constant correction related to this delay to the recorded data the bathymetry value can be acquired in a repetible way.
This means that the HDPE hull can be used to protect the sonar also in very shallow water. In

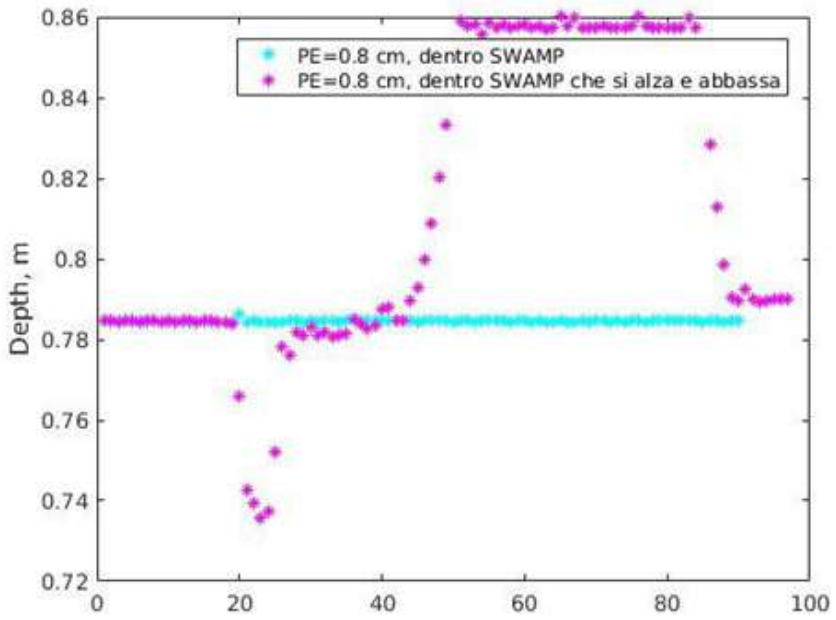

Figure 7.20: *Sonar test results in the pool. Magenta, the sonar data with SWAMP rising. Ligthblue with SWAMP static*

fig. 7.20 the sonar records approximately 0.78 m Ligthblue with SWAMP staticly floating in the pool. The Magenta data, show the data recorded by the sonar with SWAMP lifted of 0.08 m.

7.3.3 Tests in Camogli

The idea of the tests performed in Camogli during the *Festival della Comunicazione, September 14-15, 2019* was both to assess the usability and functioning of the vehicle and to perform the first experiment of *Marine Robotics*, *citizen Engagement* and *Machine Learning*.

Figure 7.21: *SWAMP at the Festival della Comunicazione, September 14-15, 2019*

During the Festival the researchers of CNR-INM installed a driving position on the *Rivo Giorgio* pier and positioned two gates (composed by four buoys) in the stretch of sea in front of the pier. The large number of people that visited the booth had to pilot the robot using a Joypad in order to make it pass through the two gates by making a S-shaped path. The thrust and direction used to move SWAMP was given by two of the four Pump-Jet Module azimuth thrusters composing the propulsion layout of SWAMP. The more or less successful trajectories were recorded and a Neural Network trained an Artificial Intelligence to learn how to make a similar trajectory. After a few manual trajectories the Artificial Intelligence was activated and the robot successfully made the S-shaped path without any problem and with different external disturbances and starting positions. The robot learnt from the people! After two days of navigation in the midst of bathers and under a scorching sun SWAMP proved to be suitable for working in very shallow water highly manoeuvrable. But, also proved to be a suitable tool also for working within the people integrating the robotics into the social ambient.

Imitation Learning

The learning system developed for the SWAMP by CNR-INM group [229–231] and adopted during the experiment is a *Reservoir Computing* technique [232] which is a computational framework suited for temporal/sequential data processing as the data from the telemetry of SWAMP are. It is derived from several recurrent neural network models. The Reservoir Computing consists of a reservoir for mapping inputs into a high-dimensional space and a readout for pattern analysis from the high-dimensional states in the reservoir. The reservoir is fixed and only the readout is trained

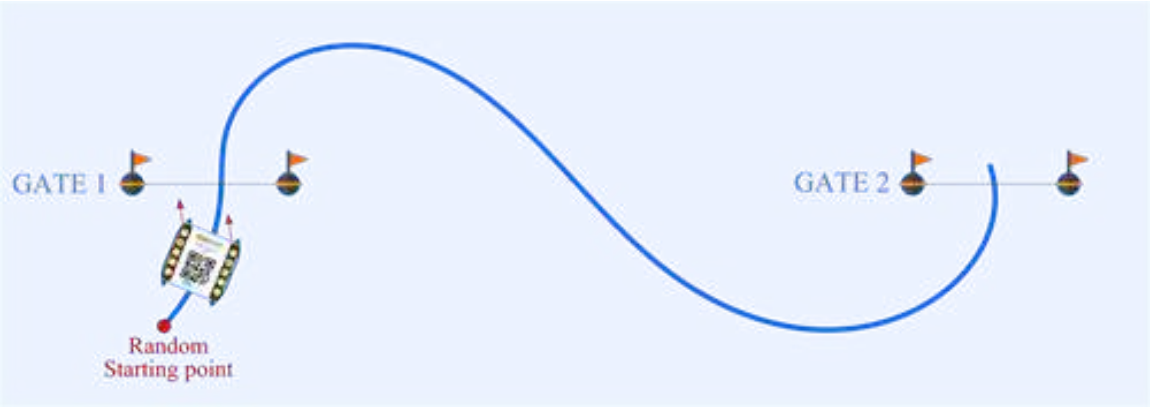

Figure 7.22: *The goal of the experiment*

with a simple method such as linear regression and classification fig. 7.23 [1]. The major advantage of reservoir computing compared to other recurrent neural networks is fast learning, resulting in low training cost.

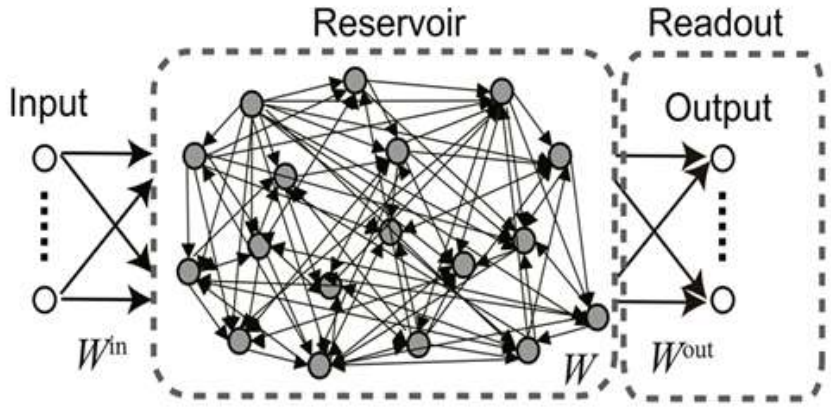

Figure 7.23: *RC frameworks where the reservoir is fixed and only the readout weights are trained. A conventional RC system with an Recurrent Neural Network-based reservoir [233] as in Echo-State Networks [234]*

Another advantage is that the reservoir without adaptive updating is amenable to hardware implementation using a variety of physical systems, substrates, and devices. In fact, such physical reservoir computing was chosen for the SWAMP architecture.

The goal

As said before the goal of the experiment was to drive the vehicle through two gates in the same direction as shown in fig. 7.24. To allow people to drive the vehicle a Joypad Logitech F310 was adopted.
As shown in the same figure, and following the data of table 5.5, the Joypad levers were mapped in the following way:

- The right lever was used to steer the Pump-Jet angles. α was limited in the interval $[-\pi/2, \pi/2]$. The angles was applied to the two bow thrusters while the stern thrusters were turned off.

[1] Courtesy of [232]

- The left lever was used for powering the Pump-Jet. The percentage of RPM was used to command the amount of thrust T_i^{PJ}, as shown in Chapter 5. The thrusts was applied to the two bow thrusters while the stern thrusters were turned off.

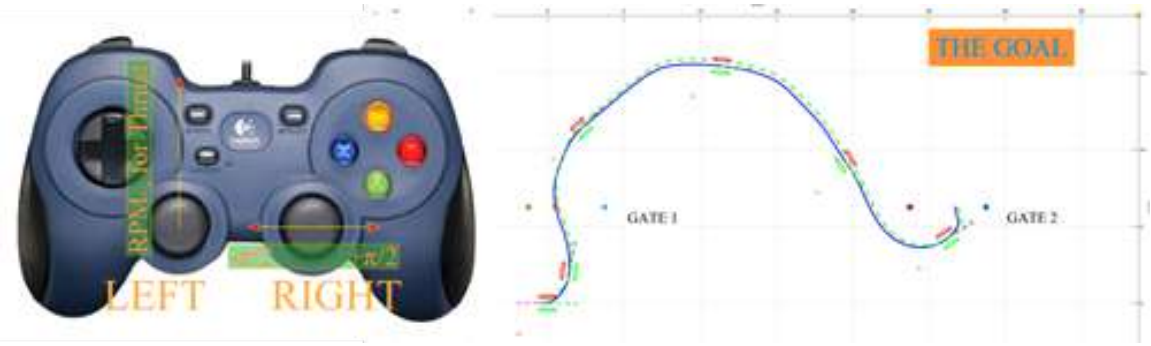

Figure 7.24: *The mapping of the commands on the Logitech Joypad and the goal of the experiment*

The simulations

Figure 7.25: *The simulator of SWAMP in the Camogli environment*

In order to test the ability of the Imitation Learning to train the system, the first tests were carried out using the simulator (fig. 7.25) whose description is reported in Chapter 8. In the simulator used to describe the SWAMP manoeuvrability the use of a Joypad was implemented. The neural network was trained by using the trajectories made by the researchers of CNR piloting the vehicle in simulation.
An example of the training sets is reported in fig. 7.26. In the tests the piloting starts in [0 0]. The pilot drives the vehicle through the green gate and the data are recorded from this moment to the moment in which the vehicle passes through the red gate. The trajectories obtained from the manual piloting of the simulator were then used for the training of the AI.

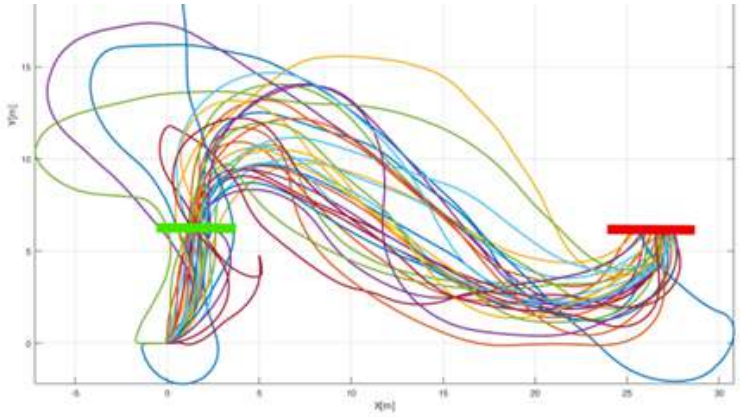

Figure 7.26: *The training sets for the simulated tests*

The training was done by letting the neural network learn the values of position (x [m], y [m]) and heading (ψ [rad]) and the commands given by the pilot in terms of applied α and T_i^{PJ}.
After a relatively small number of training sets the network learned how to pilot the vehicle through the two gates.
The AI test was carried out by manually piloting the vehicle for the initial part of the manoeuvre (few

seconds) and then applying the control made with the AI. The results of the successful trajectories piloted by the AI are reported in fig. 7.27 . Some of the trajectories are standard S-shaped paths. In these figures it can be seen that all the trajectories are different from each other. This means that the AI does not copy the same trajectories but always performs a different control to reach the final goal.
In the figure some examples of different trajectories are reported. In these cases some external disturbances were applied. Some of the disturbances were applied at the starting of the vehicle with a different starting heading, in some other cases the disturbances were applied during the trajectories with wind gusts, current and ,also, external disturbances applied by the operator with a Joypad moving the stern thrusters.
Simulation results are provided to show the good behavior of the algorithm. An example is the light-blue trajectory in the right corner that succeeds to reach the goal even-if the simulator passes in a place where no training trajectories is present (see fig. 7.26).

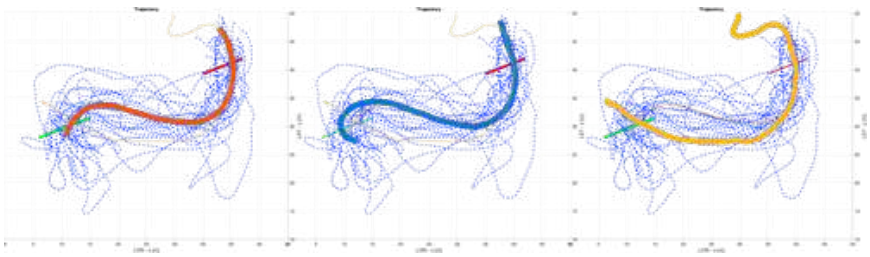

Figure 7.27: *The results of the simulations made with the artificial intelligence piloting the SWAMP simulator*

Moreover, the commands given by the AI are smoother than the commands given by the human pilot as shown in fig. 7.28. In fact, while human tends to use the maximum thrust and angles the AI uses less power and has a less nervous use of the angle of actuation.

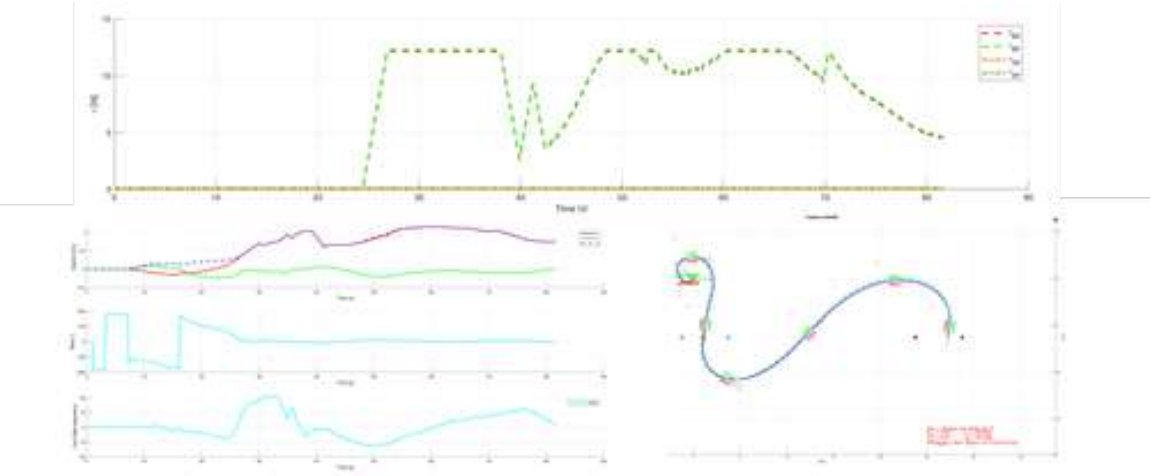

Figure 7.28: *One of the simulations of SWAMP algorithm with the data of the commands applied by the artificial intelligence*

The (successful) imitation learning experiment

Given the good results of the simulations, the Camogli experiment was done by letting people piloting the SWAMP vehicle from a gazebo mounted on the pier fig. 7.29.

Figure 7.29: *The Camogli setup*

Most of the people succeeded in piloting SWAMP through the gates of the goal. This allowed to train the neural network to make its own path to reach the goal.

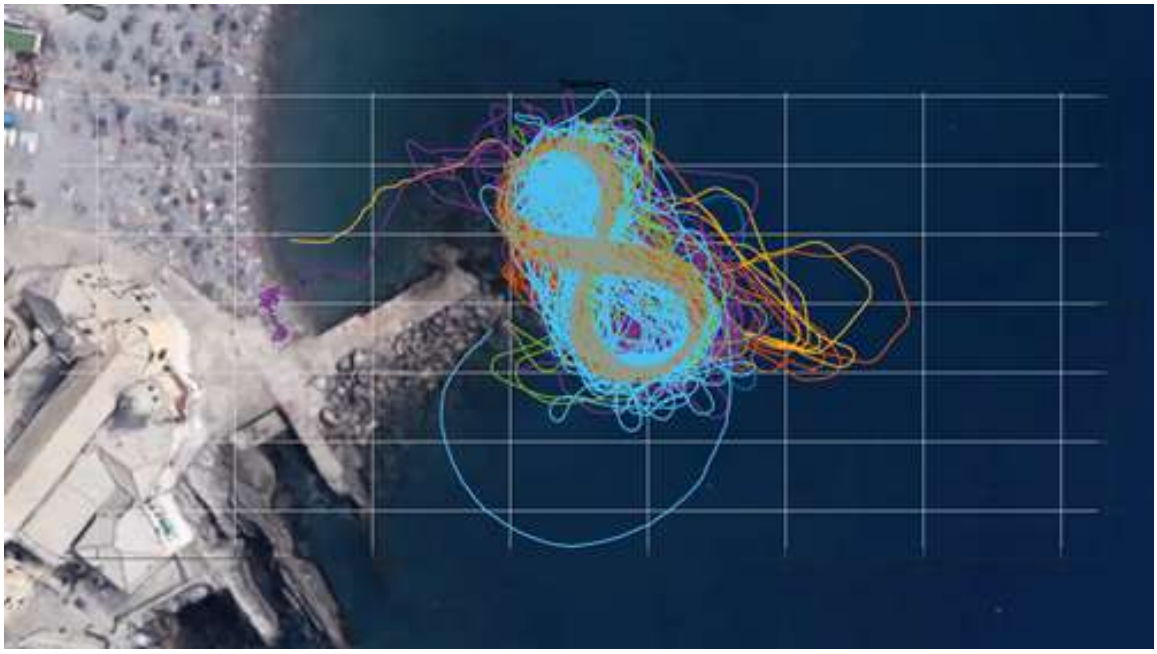

Figure 7.30: *The paths of SWAMP during the learning experiment. In the figure an 8 is depicted to show che main paths of the vehicle.*

In general the vehicle was guided by giving an almost constant 90 deg thrust port or starboard, few people really drove the vehicle by managing the intermediate angles. In general people did not proportion the thrust amount but they always used the full throttle.
In fig. 7.31 is reported a set of tests performed in Camogli where it is possible to see this kind of driving. Here can be appreciated the 8-shaped path for passing through the gates.

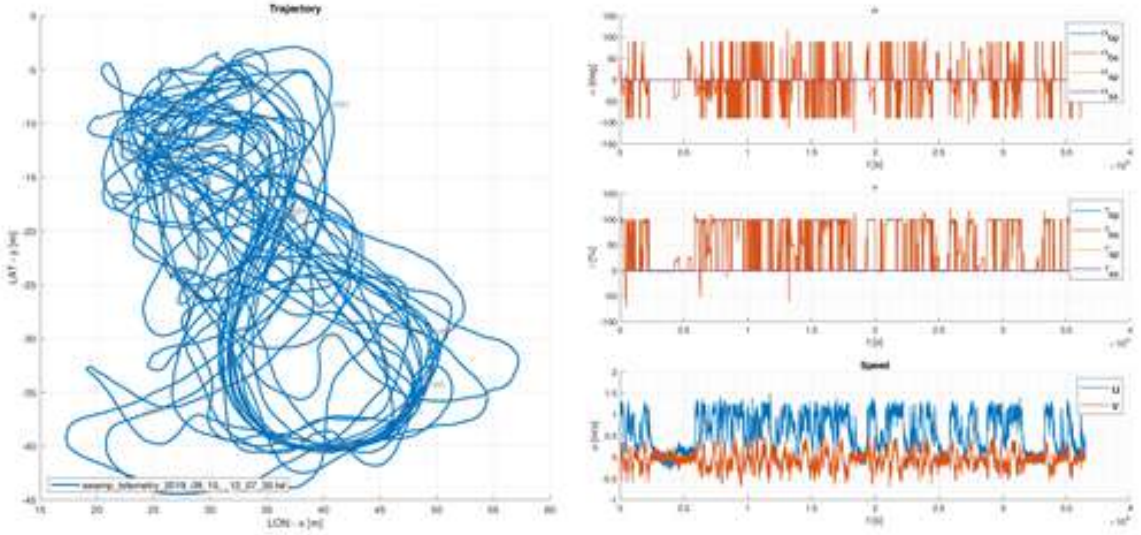

Figure 7.31: *The paths of SWAMP during the learning experiment and the commands given by the pilots second day*

Each time the pilots started their "mission" a recording started too. All the "missions" ended as long as SWAMP passed through the gates, or close to it.
The trajectories used for the training are reported in fig. 7.32. From the same picture, among all the trajectories that were used for the training, some interesting examples are shown.

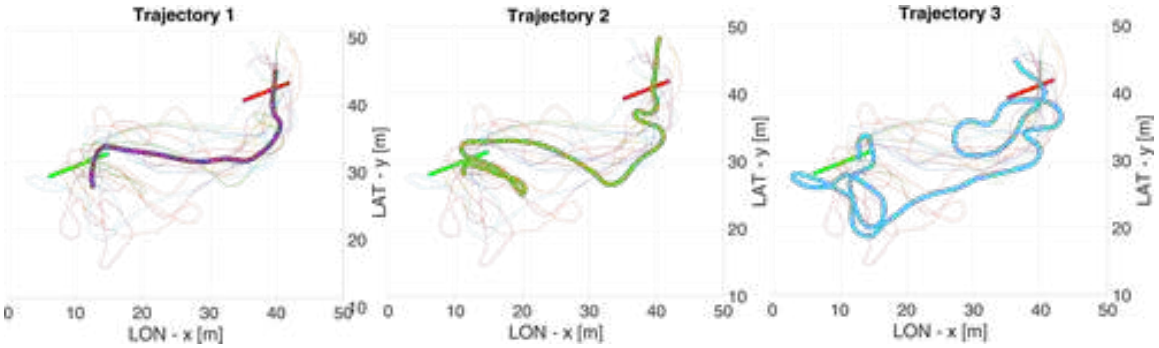

Figure 7.32: *Some examples of the training trajectories*

The first trajectory is quite standard one, while the other two trajectories is quite chaotic and shown how among all the trajectories not all of them where really successful at first but where anyway used for the training.

Figure 7.33: *The successful result of the AI*

The results achieved by the Artificial Intelligence are reported in fig. 7.34. The first trajectory on left is a "standard" trajectory where the pilot started as if he had to drive to make the S-Path and the AI took the control in few seconds. After a perfect trajectory the AI achieved the goal of making SWAMP pass through the gate. The pictures of this result are reported in fig. 7.33.This experiment was made with an adverse sea state with waves that were not present during the pilot's tests. This is also shown by the pictures in fig. 7.33.
The second trajectory is also a "standard" where the AI achieved the result of making SWAMP pass through the gate. The difference from the first test was that the pilot started a bit inclined with respect to (and if compared to) the training trajectories. The AI corrected the path and passed through the gate also in this case.
But the mostly successful trajectory is the third one. In this case the pilot started from a position where the training trajectories haven't been. Moreover with respect to the usual passages through the Start, the vehicle started its trajectory in the reverse direction. Nevertheless the AI drove the vehicle through the second gate again. The results showed how the artificial intelligence does not copy the human being but learns from him to solve problems. In this case, as explained before, the AI learned from the GPS position and Heading how to drive the vehicle through the commands to be sent to the azimuth thrusters. As shown in the results of the simulations fig. 7.28 the control

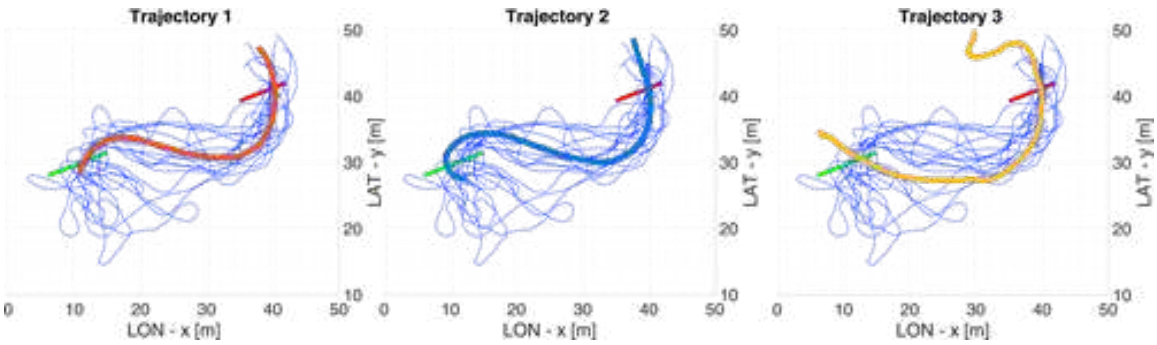

Figure 7.34: *Three of the trajectories performed by SWAMP with the AI piloting the vehicle. In Blue the training trajectories are reported*

made by the AI is also smoother than the one made by the human operator. This is also shown by the results of the tests. In particular in the fig. 7.35 a comparison is shown of this difference. The human operator basically drives the robot through constant on-off type thrusts and uses the angles at the maximum excursion. On the other hand the AI not only uses less nervous and jerky thrust than the human operator but lower excursion angles by varying in a smooth way its applied value.

This is especially shown in the first example.

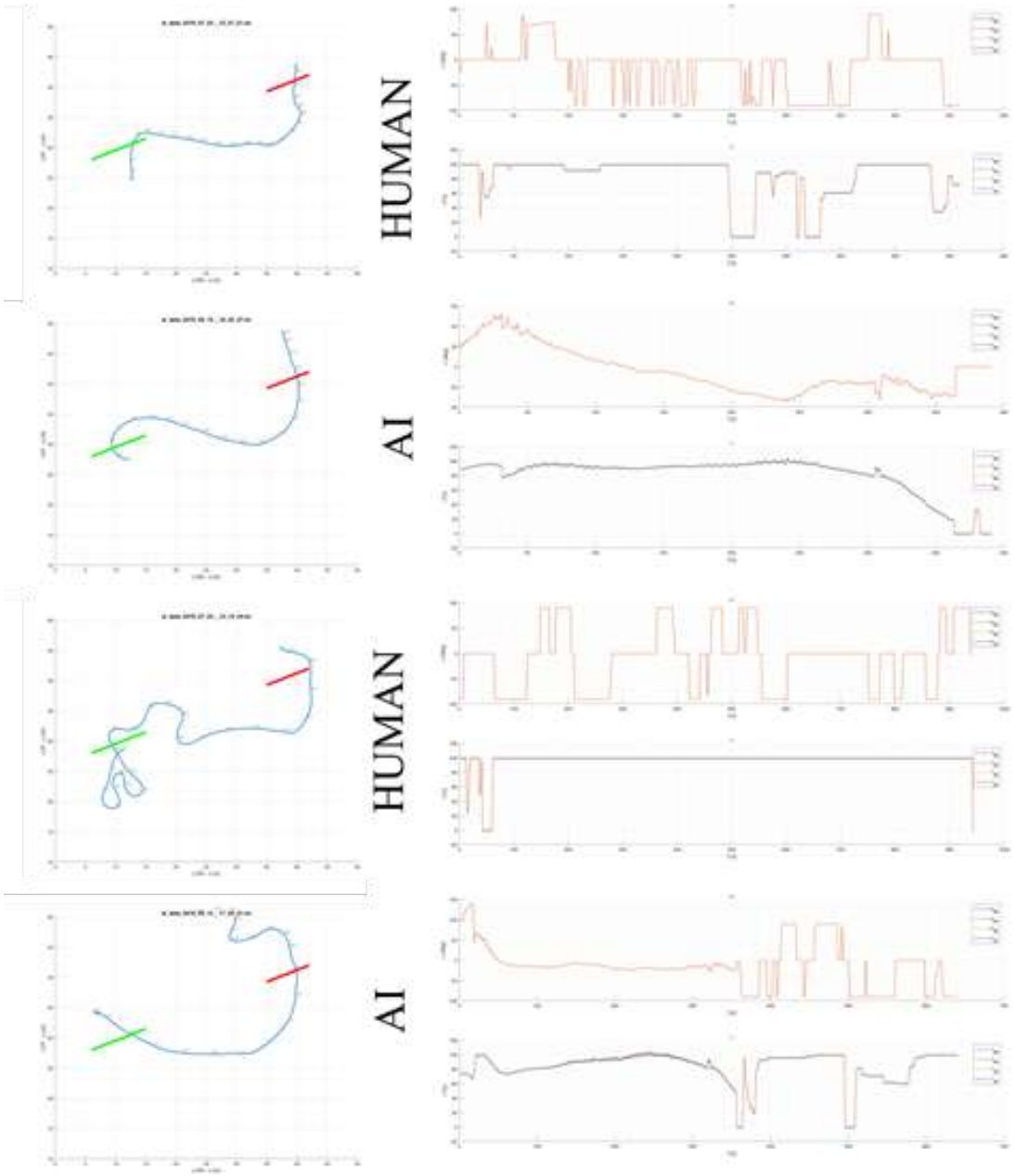

Figure 7.35: *Two comparisons of the commands given by human operator and by the AI*

A lesson was learnt during the tests in Camogli.The communication system has always to be turned on, in-fact it happened that the vehicle loss the communication due to a power-off of the generator and it crashed against the rocks that form the shore of the Camogli's pier. Luckily no problem happened to the vehicle thanks again to the presence of the soft structure of the hull.

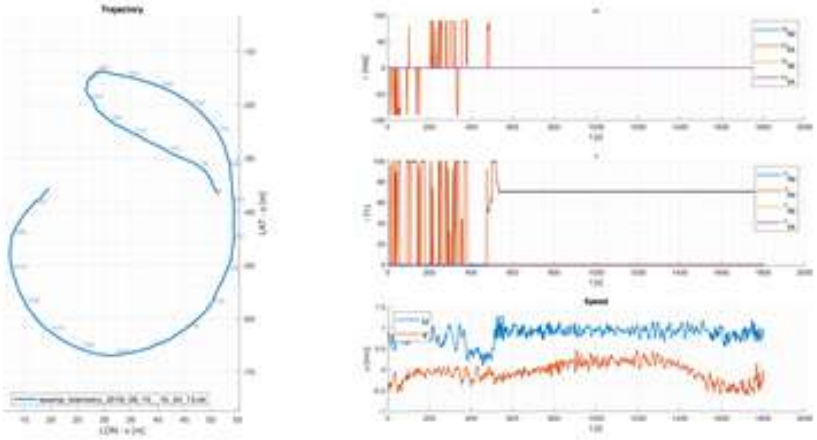

Figure 7.36: *The trajectory where the vehicle crashed against the rocks at speed*

Another advantage of the use of a soft structure for the vehicle's hull is related to the fact that the vehicle moved in the middle of the bathers without scaring them. This was also thanks to absence of protruding and dangerous thrusters.
In this direction this aspect in addition to the experiment of citizens involved in teaching to a "learning robot" was another step-over to bring marine robotics in the middle of the population.
A dead-reckoning system has to be implemented on-board.

7.3.4 Tests in Towing Tank

After the AI experiment the vehicle was again reported in the Towing tank facility of the Univesità di Genova fig. 7.37 to carry on some propaedeutic tests for the following tests of Biograd Na Moru.
Tests were conducted also to prepare the following self-propelling tests and one test was conducted also in self-propelling.

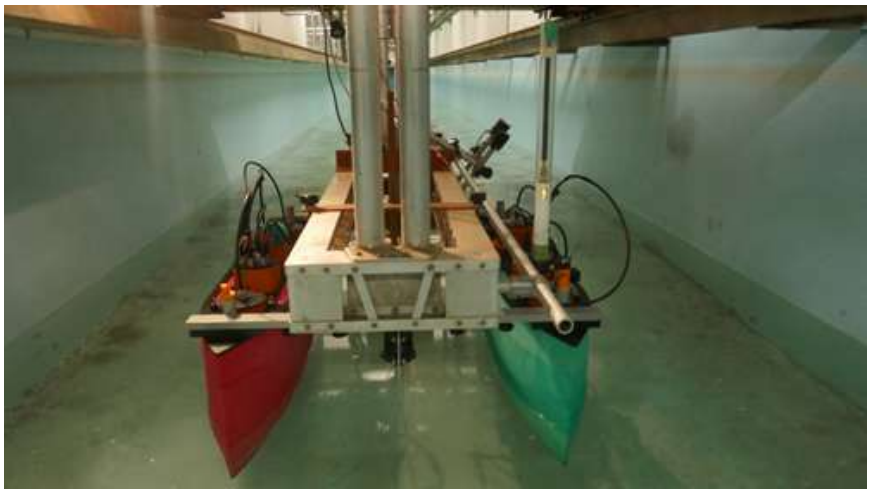

Figure 7.37: *SWAMP assembled in the towing tank*

Bollard Pull Tests

During the tests the vehicle was attached to the load cell described in Chapter 4 to record the thrust of the 4 Pump-Jet Module when mounted inside the hull. The results are reported in figs. 7.38 to 7.40.
In the first test fig. 7.38 the thrusters were tested alone in the tank giving results that are in accordance to what expected, even-if a small variability between the 4 thrusters is recorded. This may be due to the testing facility that involved the adoption of the model bonded by the model-driving devices.
In the second test fig. 7.39 the thrusters were tested in pairs in the tank giving results that are in

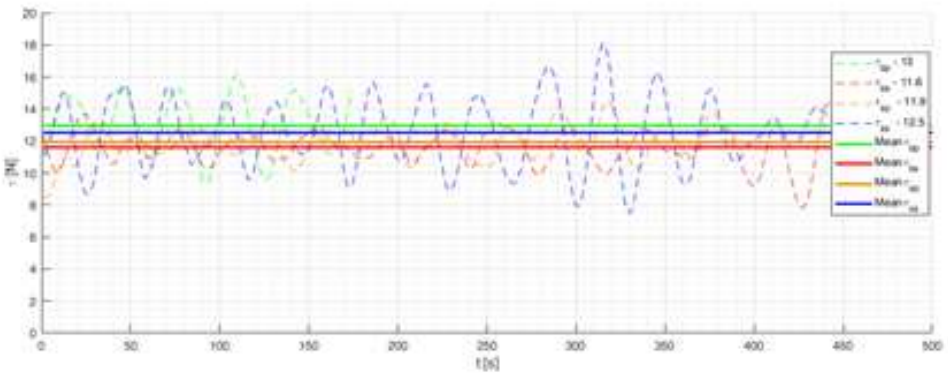

Figure 7.38: *The results the Bollar Pull tests of the single Pump-Jet Module s tested alone*

accordance to what expected, even-if a small variability between the couples is presented. This may be due to the testing facility that involved the adoption of the model bonded by the model-driving devices. Particular attention was to be taken on the thrusters coupled on the same hull i.e. the

Port thrusters and the Starboard thrusters. Non particular influencing effect was recorded. Further analysis are required at speed.

In the third test fig. 7.40 the thrusters were tested all together resulting in a thrust that is

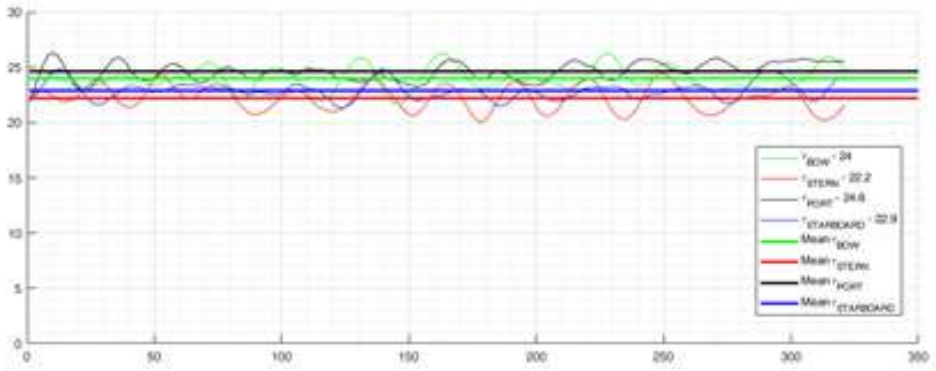

Figure 7.39: *The results of the Bollar Pull tests of the Pump-Jet Module s coupled in pairs*

in accordance to the theoretical one. In the graphic on the top is reported the recording of the thrusters at different actuation percentage and in the bottom graphic the curve interpolating the test results is reported together with the theoretical curve and the values of the interpolated value.

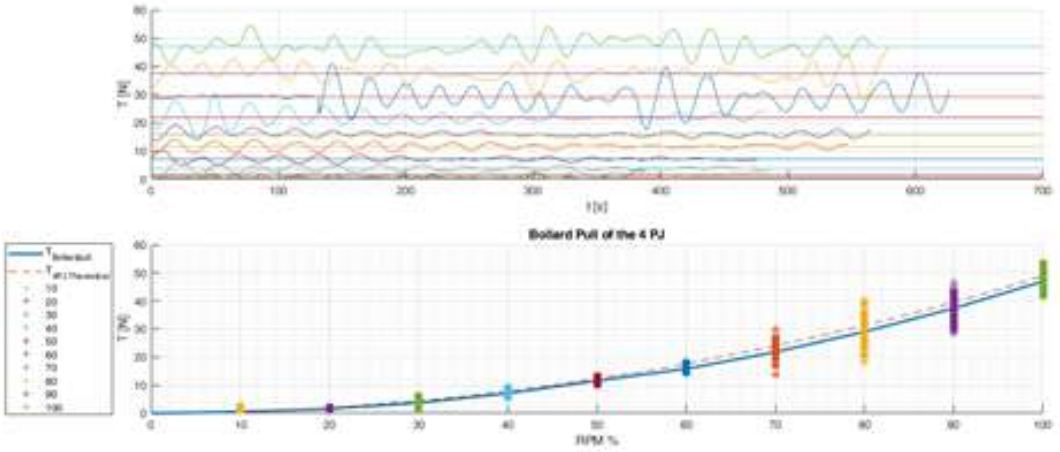

Figure 7.40: *The results of the bollard-pull tests of the four Pump-Jet Module s together. All the points reported in the bottom graphic represent the fluctuation of thrust as reported in the top one*

Self-propelling test

As mentioned one first test was conducted on the self-propelling of the vehicle. In the self-propulsion test fig. 7.41, the model is towed and during the test the propulsion unit is turned on providing thrust.These kind of tests are usually performed to evaluate the values the propulsive qualities of a vessel. These are evaluated also with experimental tests which results are the *thrust deduction factor* t, the *wake fraction* w the propulsive efficiency η_P. While w is fundamental for the design of classical propeller, the correspondent value for the Pump-Jet should still be found. On the other hand the t value is the value that is used to find an equilibrium of forces at constant velocity.

The thrust deduction factor is described by the equation:

$$t = 1 - \frac{R_t - F_D}{T_{bollardpull}} \tag{7.1}$$

being F_D the towing force recorded by the dynamo-meter and $T_{bollardpull}$ the thrust the propulsion units are expected to provide to the model in absence of the thrust deduction. Based on this equation the factor of thrust deduction is determined by the results of resistance obtained during the towing tests described in Chapter 4 and the propulsion tests carried out above on the thrusters mounted on the hull. The procedure is

- choosing a propulsive speed and verifying the resistance of the model R_t
- applying a $RPM_{\%}$ command proportional to the expected value of $T_{bollardpull}$ required
- running the model in the towing tank and verifying the difference between the resistance and the thrust that is recorded by the load cell in form of F_D

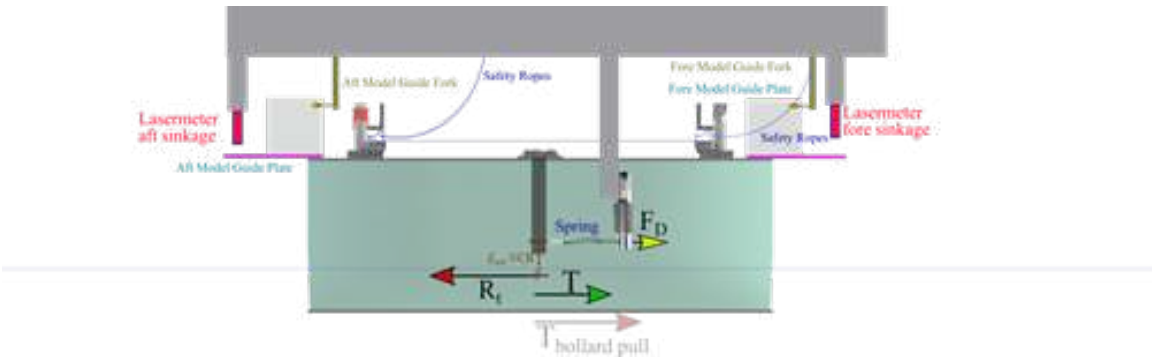

Figure 7.41: *Scheme of the self-propelling tests*

One exploration test was conducted in the towing tank at $1\,m/s$. The recorded data are reported in fig. 7.42.

Figure 7.42: *The results of the first self-propelling tests*

- A towing experiment was conducted at 1 m/s with a resultant resistance of about12.4 N.
- In the second test the two Bow thrusters were turned on at 70% and a $1 - t = 0.68$ was recorded

- In the second test the two Stern thrusters were turned on at the same 70% and a $1-t=0.68$ was recorded similar to the one recorded in the previous test conducted with the two Bow thrusters. This shows that (apparently) no or small influence on the value of $1-t$ is given by the position of the thrusters (be they fore or aft). This has to be verified in further tests.
- In the final test the two stern thrusters were turned on at 85% to nullify the thrust deduction obtained in the previous tests

It has to be considered that this test, that depends on the speed of the model, also depends on the running attitude that may differ considerably between various conditions even if in the case of SWAMP a perfect pitch and roll balance is always researched. Further tests will be conducted.

7.3.5 Tests in Biograd Na Moru

The last tests reported in this thesis are those carried on in Biograd Na Moru in Croatia within the Breaking the Surface international interdisciplinary field workshop of maritime robotics and applications.

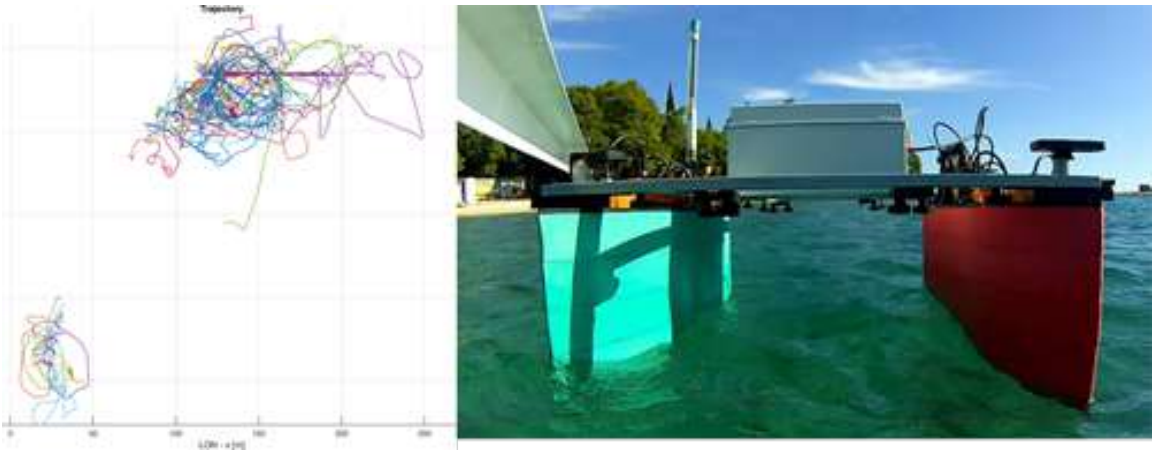

Figure 7.43: *The ensemble of the tests conducted in Biograd Na Moru*

In Biograd Na Moru extensive tests were conducted. In particular, a set of steady-state ahead-reverse motions, circles and zig-zag manoeuvres have been performed in order to verify the vehicle drag and to identify inertia parameters. Moreover these tests were important for starting to evaluate the loss of thrust of the four Pump-Jet when mounted on the vehicle moving in the water thus calculating the thrust deduction factor Moreover in this tests a sea-bed reconstruction was made by using a single-beam echosounder.
In this thesis the results of some tests are reported, in particular:

- Turning Circle
- Self-Propulsion ahead and astern
- Seafloor map reconstruction

The testing condition was with SWAMP at a $48kg$ total weight.
For the tests the basic navigation, guidance and control system was composed by a set of modules that can be flexibly interconnected in such a way to online select the desired or most proper configuration for the specific mission. The implemented modules range from low-level velocity controller for linear and angular degrees of freedom, up to advanced guidance algorithms for generic path-following execution.
For the first tests general theoretical model of the vehicle hydrodynamics was considered and simplifications have been performed on the basis of reasonable assumptions and the consistency and quality of the parameter estimates.

Turning Circle tests

For the turning circle tests the thrusters are commanded by giving the inverse direction to the bow and stern thrusters as shown in in a configuration shown in fig. 7.44.

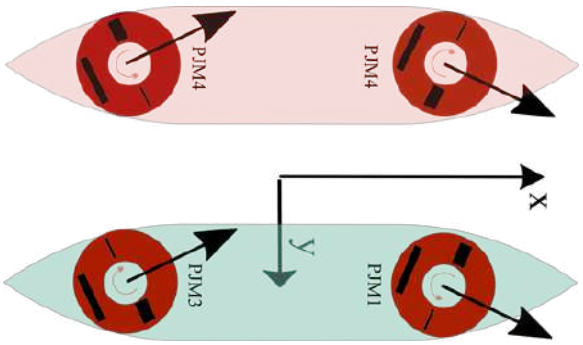

Figure 7.44: *The thrust configuration for the turning circle tests*

In fig. 7.45 the first test related to turning circle is reported. The angle of the thrusters is positioned at an 30 deg and the thrust is 60% for all the thrusters.
The tactical diameter D_t recorded is almost 9 m and the advance speed was almost 1 m/s.

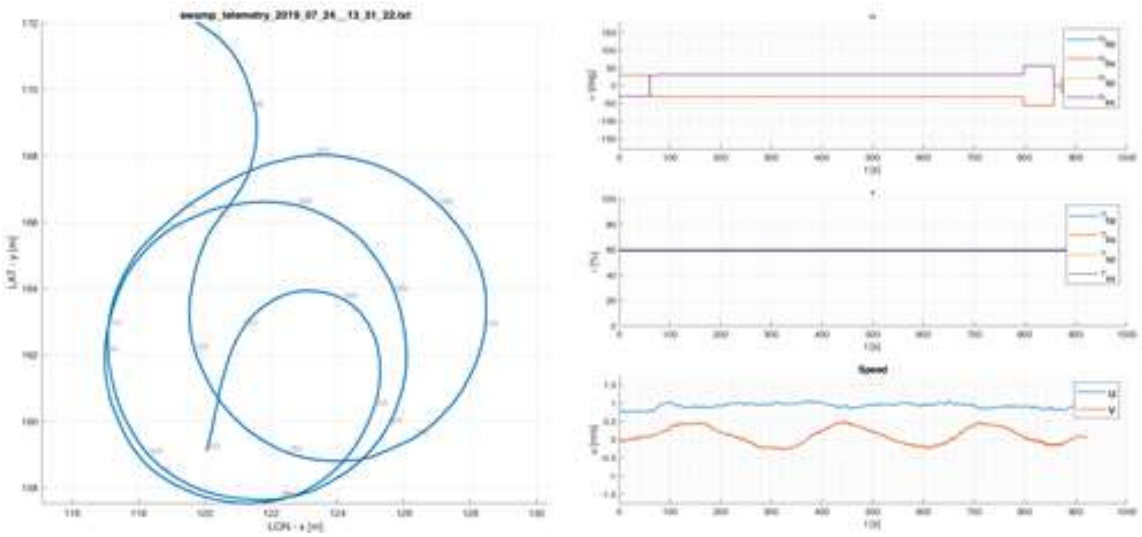

Figure 7.45: *Turning Circle Test # 1*

The heading, pitch and roll [2] are reported in fig. 7.46.

[2]The roll is always around 5 deg because no initial correction was applied to the sensor installed in the foam

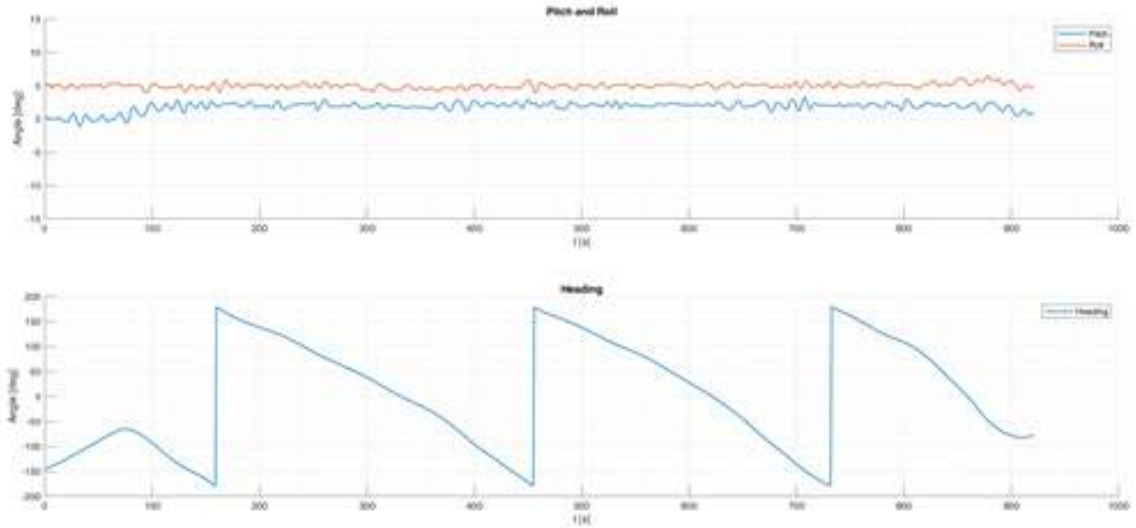

Figure 7.46: *Turning Circle Test # 1 - Pitch Roll Heading*

In fig. 7.47 the second test related to turning circle is reported. The angle of the thrusters is positioned at 30 deg and the thrust is 60% for all the thrusters. The angle is reversed at a certain point and an 8-Shaped trajectory was obtained.
Also in this case the tactical diameter D_t recorded is almost 9 m and the advance speed was almost 1 m/s.

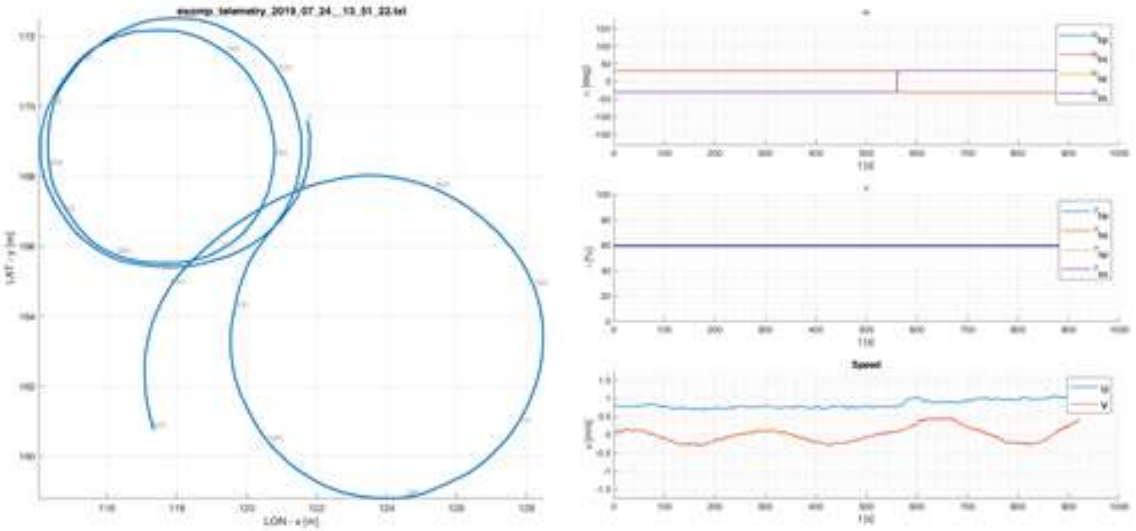

Figure 7.47: *Turning Circle Test*

The heading of this second test is reported in fig. 7.48.

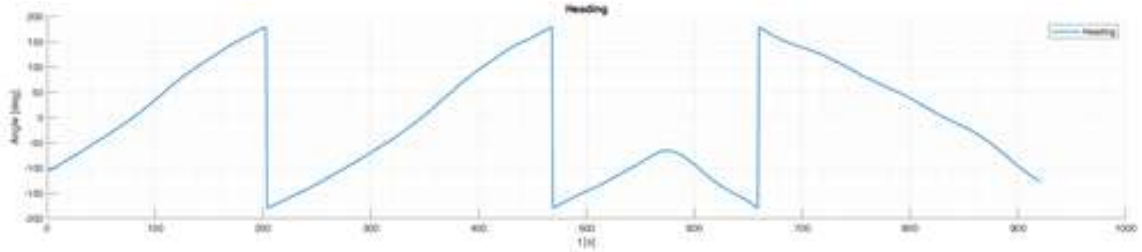

Figure 7.48: *Turning Circle Test # 2*

In fig. 7.49 the third test related to turning circle is reported. The angle of the thrusters is positioned at 60 deg and the thrust is 60% for all the thrusters.
Also in this case the tactical diameter D_t is recorded and the value is less than 2 m. The advance speed in this case was almost 0.5 m/s.

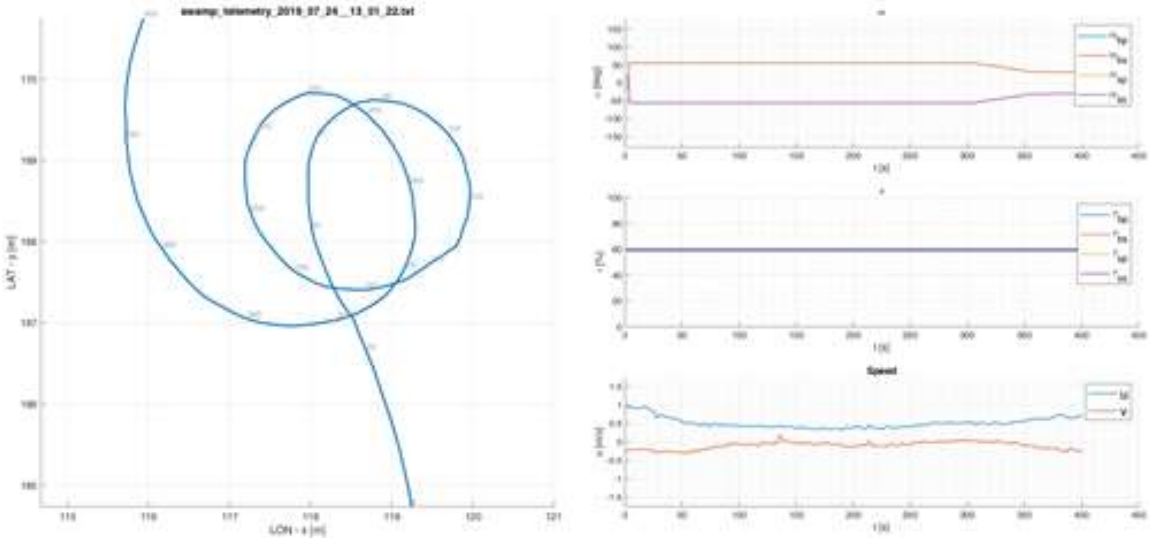

Figure 7.49: *Turning Circle Test # 2 - Heading*

In fig. 7.49 the heading of this last test is reported

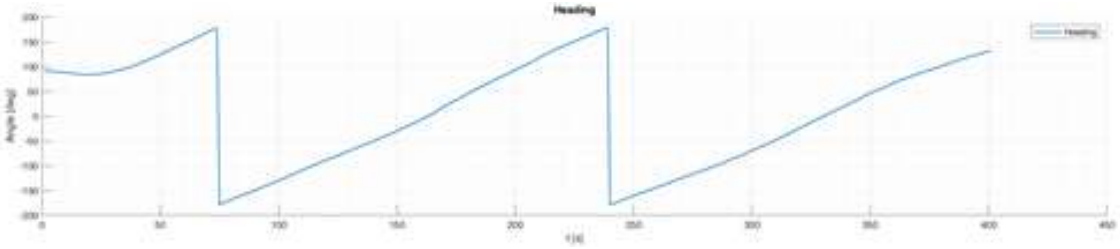

Figure 7.50: *Turning Circle Test # 3*

Self propelling at Sea

As mentioned, the self-propulsion test at sea were conducted in Biograd. In this case the idea was to evaluate or trying to evaluate the *thrust deduction factor* t. As said, the thrust deduction factor is described by the equation:

$$t = 1 - \frac{R_t - F_D}{T_{bollardpull}} \tag{7.2}$$

but in this case it was evaluated with another procedure due to lack of measuring devices that could give the possibility of recording the F_D. In this case it was possible to record the speed achieved by the vehicle at a certain $RPM_{\%}$ applied.
In this case the procedure was the following:

- a $RPM_{\%}$ was assigned to the four thrusters in forward or reverse motion
- the speed was recorded
- in function of the recorded speed and from the data obtained during the towing tank tests a resistance R_t associated to that speed was found
- by knowing the amount of thrust that the 4 Pump-Jet Module should have produced at the assigned $RPM_{\%}$ it was possible to assess the difference between the thrust that the propulsion units should have produced $T_{Bollardpull}$ and the real one called $R_{\%}$, namely the resistance associated to that $RPM_{\%}$. The ratio between these values is $1 - t$.

$$1 - t = \frac{R_{\%}}{T_{bollardpull}} \tag{7.3}$$

In this case various tests were conducted with the vehicle self-propelling with the thrusters at different $RPM_{\%}$: [30 40 50 60 70 80 90 100] in ahead $\alpha_{thruster} = 0\,deg$ and reverse motion $\alpha_{thruster} = 180\,deg$. The complete set of tests is reported in fig. 7.51

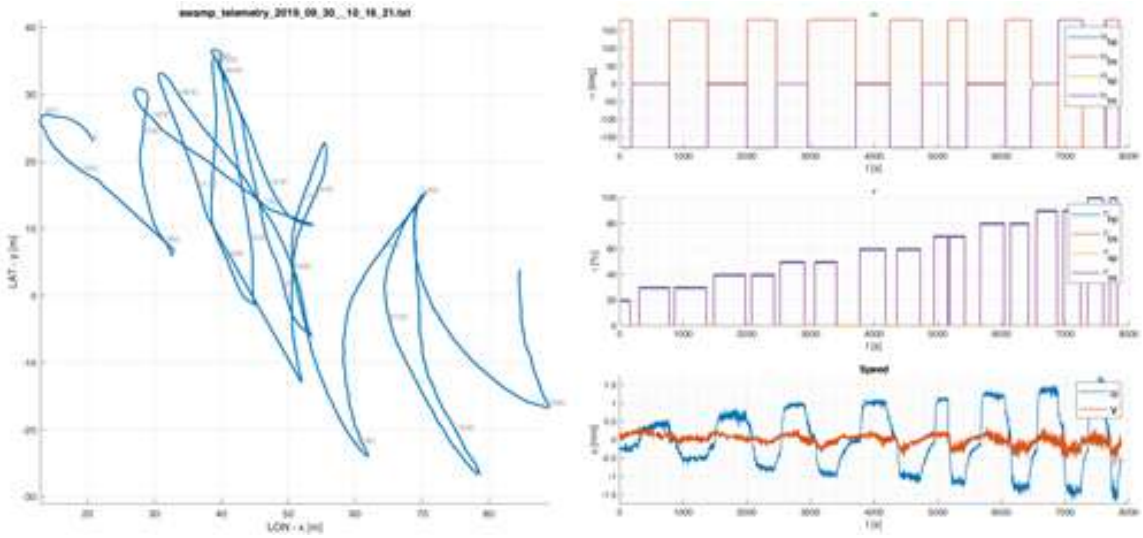

Figure 7.51: *The data recorded for the Self propelling at sea tests*

of these data only the most linear, thus interesting, parts were taken as reported in fig. 7.52. Each of the parts is associated to a medium speed recorded by the AHRS+GPS mounted on-board.

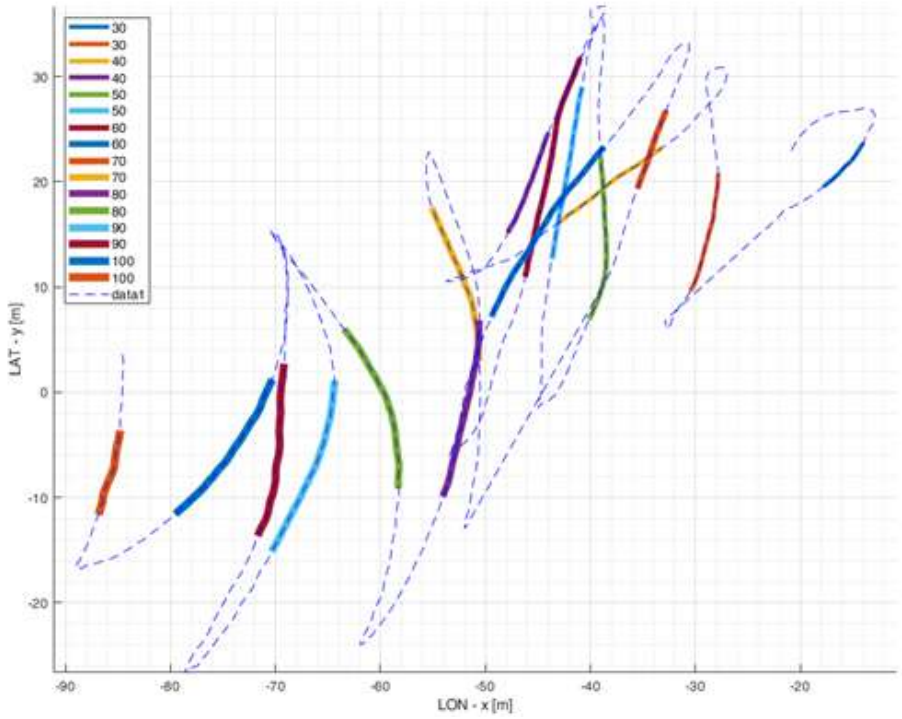

Figure 7.52: *The data taken for the analysis of the self-propulsion*

From the speed data recorded and shown in fig. 7.53 the medium value of speed in function of the $RPM_{\%}$ applied was extracted.

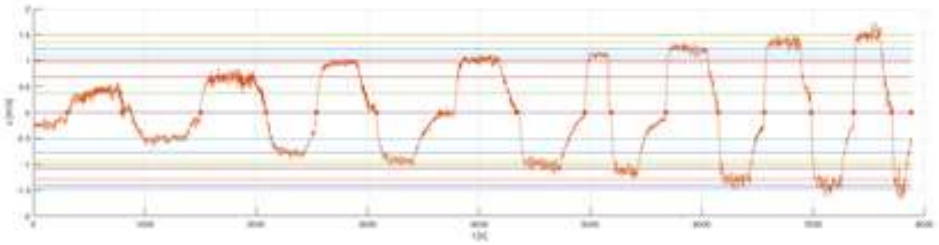

Figure 7.53: *The data recorded for the Self propelling at sea tests*

The speed reached by SWAMP in function of the $RPM_{\%}$ applied both in forward and reverse motion is reported fig. 7.54 with the interpolation curve between the two values.

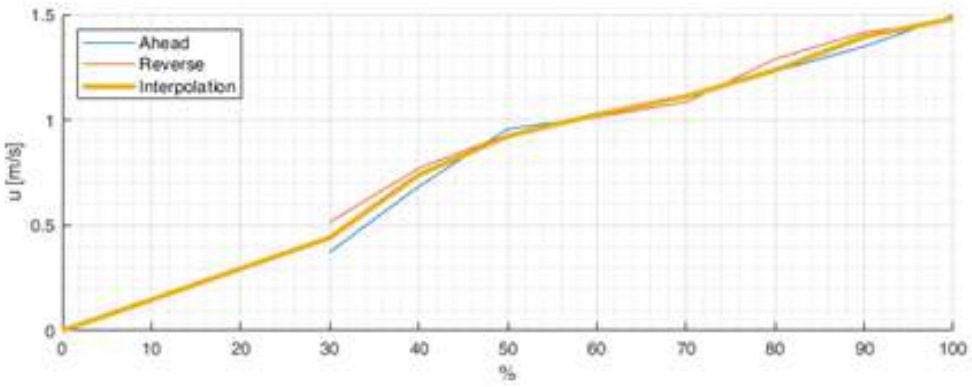

Figure 7.54: *The data recorded for the Self propelling at sea tests*

The results of the analysis is reported below and the procedure to calculate $1-t$ is:

- Choose a speed
- Extract the resistance at that speed
- Find the $RPM_{\%}$ applied to arrive at that transfer speed
- Find the Thrust that should be produced by the thrusters at that $RPM_{\%}$
- The difference between this Thrust and the Thrust really produced (= Resistance) is the value used to calculate $1-t$

This procedure is summarised in the fig. 7.55.

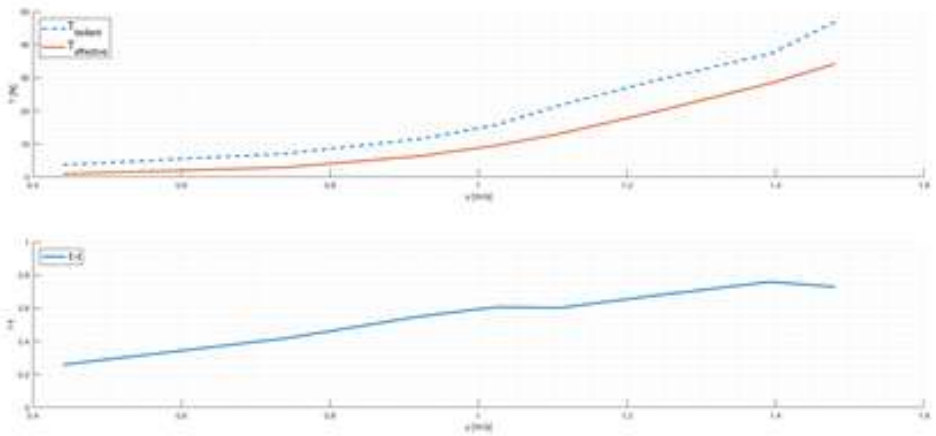

Figure 7.55: *The results of the calculation of* $1-t$

The results of this calculation are reported in fig. 7.56, where it is possible to see that, for the data extracted in the tests in Biograd, we have a high value of $(1-t)$ at low value of $RPM_{\%}$, this means that at low speeds and at low RPM the Pump-Jet loose a huge quantity of thrust.

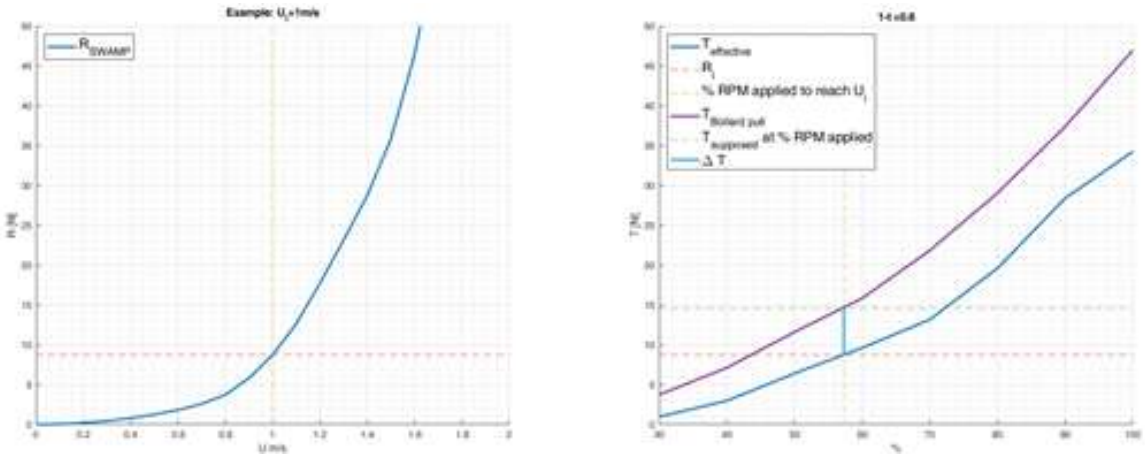

Figure 7.56: *The values of* $1-t$

With four Pump-Jet Module at high speeds (and around the design RPM) we have $(1-t) = 0.75$ which is a value that is in the range of $1-t$ values that are usually obtained for ship propeller, while at low RPM and low speed a greater loss is recorded with $(1-t)$ that reaches (small) values

around 0.3.
Therefore substantially, it is reasonably better to use 2 thrusters rotating at an higher speed than to use 4Pump-Jet Module at low speed.
Also these results have to be validated by additional tests. It is possible that the Pump-Jet Module works better at low speeds but it is probably a question of RPM so it will be necessary make more self-propulsion tests in the towing tank. The tests will be important even with only 1 Pump-Jet Module at various regimes.
One note regarding these tests is also related to the Pitch and Roll recorded during the tests and especially at low speeds. In the tests, as shown fig. 7.57, the pitching and rolling of the vehicle were important due to the presence of external disturbances like waves that may have affected the results. Also for this reason further tests are required.

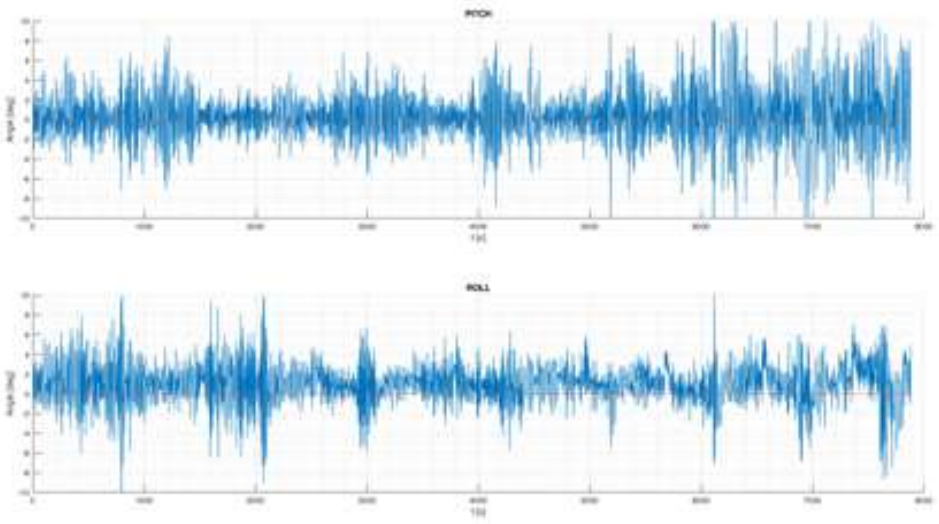

Figure 7.57: *The disturb in Pitch an Roll recorded during the tests*

Bathymetry test

Another test reported in this session is the mapping test by using the single beam echosounder mounted inside the foam hull of SWAMP. This test was very important to verify the ability of the vehicle to host inside and not outside the sonars thus reducing the number of protruding elements and protecting the same from any external impact.
The sonar the compact echosounder ECHOLOGGER ECS400, with log of backscatter data as well as altitude already presented in this section and used in the past for Posidonia mapping the same environment [107, 107].The acoustic Frequency was set to 200 KHz a suitable frequency to work in range 0.15 m to 100 m.
For the test it was necessary to set up and integrate the raspberry used for communicating Wi-Fi with the vehicle and to acquire the echologger together with precise GPS data. The results, that were successful, are reported in figs. 7.58 and 7.59

Figure 7.58: *The GPS data reported on Q-GIS map*

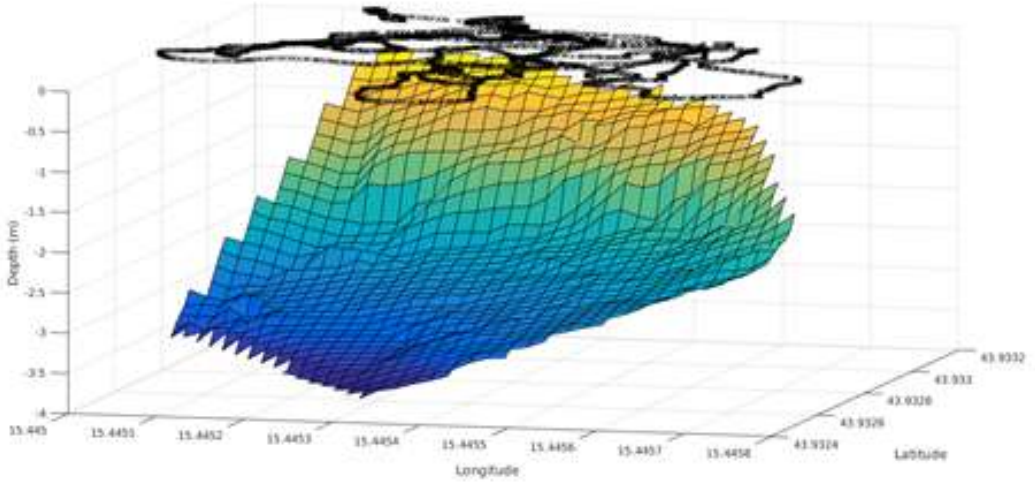

Figure 7.59: *The reconstruction of the bathimetry*

7.3.6 The Roia River

Since portability, modularity and applications in really harsh environment were the driving requirements in the construction of SWAMP a real harsh environment application is reported in these pages.
The final test was done on the Roia (Roja) River for the application of robotics in the mapping of a river. In this final test the robot proved to be constructed by correctly matching the initial requirements. Indeef it proved to be suitable for the difficult to access areas.
In this section it is depicted the transportation and operations carried on over the Roja river. SWAMP worked in the wetlands at the estuary of the river in Ventimiglia passing in the middle of the plants and of the rebris transported by the river. SWAMP was lately transported by car at Airole where it was transported dismounted by hand to the river, mounded and put in action. In there SWAMP worked in the middle of the stream also in presence of strong current, rocks obvious impacts with the shore. The hull perfectly responded to these impacts, the sonar for the bathimetry was protected by the soft structure also in extremely shallow waters and in the presence of the rocks.
The notions reported in Chapter 3 can be conveyed by a single set of still images figs. 7.60 to 7.66, which convey their meaning or essence more effectively than a mere verbal description. In this case *a picture is worth a thousand words.*

Figure 7.60: *SWAMP in the middle of the wetland at the estuary of Roia River*

Figure 7.61: *SWAMP in the middle of the wetland at the estuary of Roia River*

Figure 7.62: *SWAMP transported in the canyon of Roia River*

Figure 7.63: *SWAMP passing a fast place of the river*

Figure 7.64: *SWAMP passing a fast place of the river*

Figure 7.65: *SWAMP passing a fast place of the river*

Figure 7.66: *SWAMP on the Roja river*

Chapter 8

SWAMP Manoeuvrability simulator

8.1 Manoeuvrability Equations

A simulator was developed for the manoeuvrability of SWAMP that was used to test control algorithms, to train the Artificial Intelligence for the Imitation Learning tests and to try to emulate the behaviour of SWAMP.

8.1.1 Introduction

Given the absence of manoeuvrability models for small-size catamaran vehicles it was necessary to adopt an existing solution that could somehow emulate the operation of SWAMP in all the maneuvering conditions (i.e. low and higher speed). The final goal of the simulator was adopting a system that could be used for the qualitative simulation of SWAMP manoeuvres, for the manual piloting with a Joypad and for the application of control algorithms to be lately calibrated at sea. For this reason the adopted model was not created to perfectly describe the maneuverability of SWAMP but to function as a testing system that could describe the behaviour of a manoeuvring catamaran.
Nowadays the existing experimental and theoretical approaches allow the manoeuvrability of big ships with standard monohulls to be reasonably well predicted in the open sea navigation without experimental model tests. This has become possible also thanks to the development of lumped-parameters mathematical models such as Mathematical Modeling Group (MMG) one, since the force components can be reasonably determined based upon theoretical and experimental approaches. However such models are usually not suitable to describe the manoeuvring at lower speeds. Even though the consequences of a bad prediction can be of a greater magnitude order there are still few applicable works related to the manoeuvring prediction in low speed navigation and in restricted waters.
In the choice of a model that could describe SWAMP manoeuvrability it was necessary to adopt a solution that could embrace all the operational situations of the vehicle. These include 0 and low speed and higher speeds (that for SWAMP means Froude numbers from 0 to 0.5) and to take into account both the operational cases a model where the hull forces could be predicted in all the conditions was chosen.
The solutions were few and the one that was chosen for SWAMP is the *Unified mathematical model for ocean and harbour manoeuvring* [235] based on the MMG. In the case of a normal-sized ship this system gives reasonable results while its adoption for SWAMP, given the absence of experimental data, was chosen only for the possibility of embracing a wider range of operational speed. The choice of the Unified mathematical model for ocean and harbour manoeuvring was done also to eliminate any possible singularity during simulations. An adaptation and a brutal calibration knowing that this could lead to uncertainties was made. It was decided to sacrifice precision for the seeking of usability.

However the validation and calibration gave reasonable results even though the model has still to be validated with a targeted campaign of experimental test.

8.1.2 Motions equations

The vehicle is considered as a rigid body coincident with its COG and with 3 degrees of freedom: two translations, *Surge* and *sway*, and a rotation, the *Yaw* motion. The other 3 motions are considered negligible for the purposes of coastal navigation.
The Co-ordinate system is shown in fig. 8.1, where u represents forward (surge) velocity, v the lateral (sway) velocity and r turning velocity, respectively at mid-ship ($L_{pp}/2$). X and Y represent hydrodynamic force components at mid-ship in x, y axis directions, respectively. N is the force moment around z axis.
The position and the motions of the COG $[x_{oG}(t)\ y_{oG}(t)\ \psi(t)]$ is evaluated during the manoeuvring time with respect to a fixed system with North reference [1]. In particular, it is possible to consider the fixed system coinciding with the integral system at the initial instant. The mobile system is used to calculate the actions on the hull and to solve the equations of Manoeuvrability. No positional-type forces acting on the hull is considered.
The description of the fixed and local system is depicted in fig. 8.1 where the local system coincides with $[L_{pp}/2\ y_{0_G}\ z_{0_G}]$. The absolute velocity U of the COG is always tangent to the trajectory and

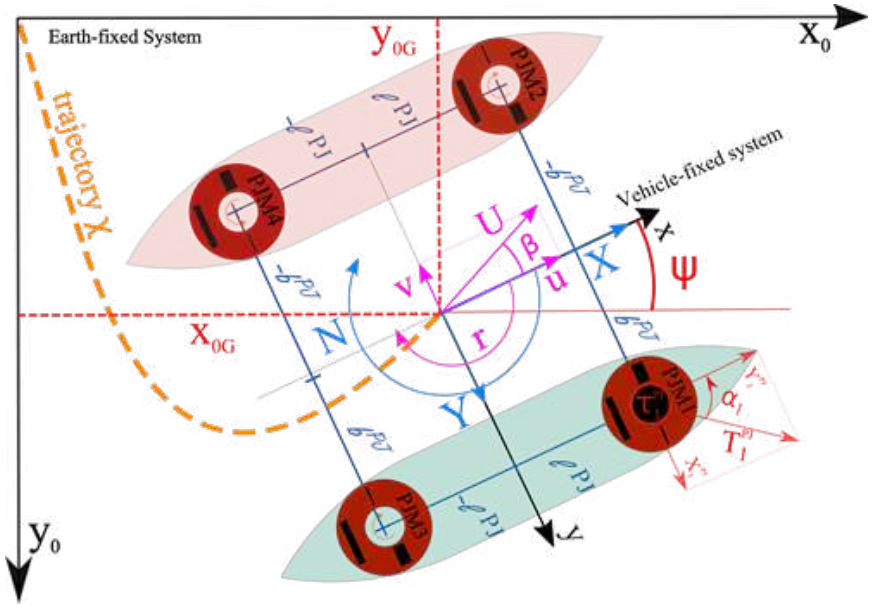

Figure 8.1: *Reference system*

its components are $u = U \cdot \cos\beta$ (surge speed), $v = -U \cdot \sin\beta$ (sway) and $r = \frac{d\psi}{dt}$ (angular velocity). The *drift angle* β is the angle formed between the vehicle bow and the velocity vector.
The manoeuvrability equations allow to obtain these velocities through the evaluation of the forces acting on the vehicle at every instant and their integration allows to calculate the position of *COG* (x_{oG}, y_{oG}, ψ).
To derive the temporal coordinates of the centre of gravity it is necessary to impose the form of the

[1] ψ represents the angle formed by the vehicle bow with the fixed reference. ($\psi >$ 0 when the bow rotates to the starboard side)

equations of dynamic equilibrium. The vehicle as a rigid body in the plane:

$$\begin{cases} X_0 = M \cdot \ddot{x}_{oG} \\ Y_0 = M \cdot \ddot{y}_{oG} \\ N = I_z \cdot \ddot{\psi} \end{cases} \tag{8.1}$$

Where: X_0, Y_0, N are the components of the forces and the moment. $M = \Delta$ is the mass of the vehicle, I_z is the mass moment of inertia with respect to the vertical axis and. Knowing the exact value of the components X_0 and Y_0 and N it is possible to solve the equilibrium equations. But it is not possible to obtain this value instant per instant, so it is better to bring these equations into the mobile reference since this allows the problem to be simplified.
Thus the forces are obtained in the x and y directions:

$$\begin{cases} X = X_0 \cdot \cos\psi + Y_0 \cdot \sin\psi \\ Y = Y_0 \cdot \cos\psi - X_0 \cdot \sin\psi \end{cases} \tag{8.2}$$

Similarly the velocities can be obtained in the x and y directions:

$$\begin{cases} \dot{x}_{oG} = u \cdot \cos\psi - v \cdot \sin\psi \\ \dot{y}_{oG} = v \cdot \cos\psi + u \cdot \sin\psi \end{cases} \tag{8.3}$$

And deriving the latter from the accelerations:

$$\begin{cases} \ddot{x}_{oG} = \dot{u}\cos\psi - \dot{v}\sin\psi - (u\sin\psi + v\cos\psi) \cdot \dot{\psi} \\ \ddot{y}_{oG} = \dot{u}\sin\psi + \dot{v}\cos\psi + (u\cos\psi - v\sin\psi) \cdot \dot{\psi} \end{cases} \tag{8.4}$$

By simplifying the differential *Equations of motion in the Body System* centered in a geometric reference system are obtained:

$$\begin{cases} X = M \cdot (\dot{u} - v \cdot \dot{\psi} - x_G \cdot r^2) \\ Y = M \cdot (\dot{v} + u \cdot \dot{\psi} + x_G \cdot \dot{r}) \\ N = I_z \cdot \dot{r} + M \cdot x_G(\dot{v} + r \cdot u) \end{cases} \tag{8.5}$$

Where u(t), v(t), r(t) are the unknowns.[2] With these equations the forces are referred to the vehicle system and not dependent on the route or position. The internal forces are therefore linked to the hydrodynamics of the hull (to the relative flows between hull and fluid) and to external actions. In general, the most influential external forces are generated by the manoeuvring and propulsion systems that in the case of SWAMP are coincident.
The other factor considered in the present simulator are current and wind forces.
It can, therefore, be said that the forces:

$$\begin{cases} X = X_{Hull} + X_T + X_{wind} + X_{current} \\ Y = Y_{Hull} + Y_T + Y_{wind} + Y_{current} \\ N = N_{Hull} + N_T + N_{wind} + N_{current} \end{cases} \tag{8.6}$$

[2]Note that the mixed components with products of velocities (e.g. $r \cdot u$) representing the centrifugal components that allow to take into account the fact that the mobile system rotates with respect to the fixed system are present

The forces and the moment resulting on the hull are function of the 6 influencing variables: the velocities of the mobile system and their derivative.

$$\begin{cases} X = X(u, \dot{u}, v, \dot{v}, r, \dot{r}) \\ Y = Y(u, \dot{u}, v, \dot{v}, r, \dot{r}) \\ N = N(u, \dot{u}, v, \dot{v}, r, \dot{r}) \end{cases} \tag{8.7}$$

Taylor series expansion in the point [3] where a cause intervenes and disturbs the simple straight rectilinear motion of the vehicle is used in order to solve a problem of this type.
In the case of linearising the problem and taking into account only the degree 1 terms, the above equations become:

$$\begin{cases} -X_u(u - U) + (M - X_{\dot{u}}) \cdot \dot{u} - Mv \cdot r = 0 \\ -Y_v \cdot v + (M - Y_{\dot{v}}) \cdot \dot{v} - (Y_r - Mu) \cdot r - Y_{\dot{r}} \cdot \dot{r} = 0 \\ -N_v \cdot v - N_{\dot{v}} \cdot \dot{v} - N_r \cdot r + (I_z - N_{\dot{r}}) \cdot \dot{r} = 0 \end{cases} \tag{8.8}$$

Where the terms $X_u, X_{\dot{u}}, Y_v, Y_{\dot{v}}, Y_r, Y_{\dot{r}}, N_v, N_{\dot{v}}, N_r, N_{\dot{r}}$ are the derivatives of the forces in Taylor's expansion called *Hydrodynamic Derivatives* whose value depends on the shape of the hull. It is possible to derive some of them from the experimental tests.
The linearised 8.8 are the most simplified equations, the linear ones. In general, the most complicated equations take into account a greater number of terms of Taylor's expansion and are those of the non-linear models. When significant deviations from the conditions around which the expansion is made non linear therms are present. In order to calculate the *Non-linear forces* there are other mathematical models besides the SNAME one (Taylor's expansion), among them there is the one proposed by the Japanese group that is named the Mathematical Model for Manoeuvring Ship Motion (MMG Model), this model considers a limited number of derivatives:

$$\begin{cases} (M - X_{\dot{u}}) \cdot \dot{u} = M \cdot (v \cdot r + x_G \cdot r^2) + X \\ (M - Y_{\dot{v}}) \cdot \dot{v} + (M \cdot x_G - Y_{\dot{r}}) \cdot \dot{r} = -M \cdot ur + Y \\ -(M \cdot x_G + N_{\dot{v}}) \cdot \dot{v} + (I_{zz} - N_{\dot{r}}) \cdot \dot{r} = -Mx_G \cdot ur + N \end{cases} \tag{8.9}$$

These equations can be solved by calculating the accelerations $(\dot{u}, \dot{v}, \dot{r})$ from which the velocities are obtained through numerical integration (u,v,r) and by integrating again the result it is possible to calculate the path of the vehicle (x,y,ψ).
A model based on the studies of the MMG was used to develop the present simulator where, since the steady hydrodynamic force are considered proportional to the square of fluid velocity, the basic structures of hydrodynamic force components of ship hull (X_H, Y_H and N_H) are basically described as the sum of products of velocity components (u, v and r).

The MMG model

The MMG model is widely used in the preliminary study of manoeuvrability and several methods have been developed for the prediction of hydrodynamic coefficients once the main characteristics of a vessel are known (cross-flow model, polynomial model, Fourier expansion model, tabular manoeuvring model and RANS-based CFD model [236]).
The operative profile of SWAMP embraces all the values between 0 speed to cruise speed thus considering both low speed manoeuvrability and cruise speed manoeuvrability.

[3] The closer to this point, the higher the precision. The higher the degree of the polynomial, the better the results

In low speed operations the forward speed is reduced to 0 and sway and turning velocities relatively increased due to the side thrust. This makes it difficult to predict the force components by adopting the high speed manoeuvring models because the drift angle β and the non-dimensional turning rate r' become extremely larger. β reaches 90° and r' goes to $\pm\infty$ when the forward speed is zero.
There are various methods that could be used but the objective of the SWAMP simulator was to find the most rapid way of emulating the real vehicle manoeuvrability. The methods of Kose [237], and Yumuro [238] allow to predict the hydrodynamic coefficients for vessels with a high β, but require the use of experimental tests for their evaluation. The Karasuno [239] method, on the other hand, makes it possible to calculate the coefficients also for large β. However, the method is very complicated and not generalized. Kang [240] has developed a method for predicting hydrodynamic forces that encompasses both low and high speeds. This versatility is achieved by applying the Kijima [241] method for predicting forces around the cruising speed ($\beta < 30°$) and the Karasuno method for low-speed forces ($\beta > 30°$). However this method does not take into consideration 0 speed that obviously occurs with SWAMP double ended hull.
In general most of the models are based on cross-flow drag [242] with more or less accurate analysis, e.g. in Karasuno [243] that take into consideration the vorticity effects occurring in transverse motions.
The model presented for lateral force and yaw moment by [244] adopts the cross-flow drag expressed as the integration of lateral drag in longitudinal direction 8.10:

$$\begin{cases} Y_{HNL} = -\frac{\rho}{2}\int_{-L/2}^{L/2} C_D(x)d(x)\,|v+rx|\,(v+rx)dx \\ N_{HNL} = -\frac{\rho}{2}\int_{-L/2}^{L/2} C_D(x)d(x)\,|v+rx|\,(v+rx)xdx \end{cases} \tag{8.10}$$

The important parameter of these expressions is the cross flow drag coefficient C_D that depends

Figure 8.2: *Cross-Flow drag Concept [245]*

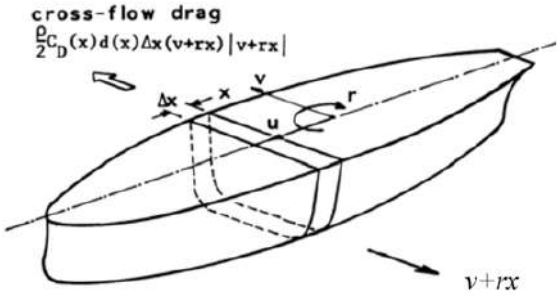

on the geometrical characteristics of the vessel.
Cross flow drag allows to work on a model that is more flexible than those where it has to be switched from high to low speed.
Yoshimura adopted a unified mathematical model that can be used to well describe the manoeuvring motion from ocean going to low speed manoeuvring since it has the same linear coefficients. In this modelling, the characteristic of course stability and initial turning is kept the same as the conventional mathematical model.
The merit of this model is firstly that the course keeping quality of ship coincides with those of the conventional mathematical model. Moreover there are few coefficients or parameters which make it easier for the manoeuvring prediction in a design stage as the coefficients for non-linear force are only four, the above described C_D and two correction factors of lateral velocity due to yawing and the resistance coefficient.
This model allows the simulation from ocean going to harbour manoeuvring even in the forward

speed is zero. The Yoshimura model allows to have acceptable results for the whole speed range while other MMG models, even if using equations studied for angles $-90° \leq \beta \leq 90°$ are not applicable in case of null speed where hull forces depending on the dimensionless rotation speed: $r' = \frac{r \cdot L}{\sqrt{u^2+v^2}}$ cannot be calculated. This term tends to infinity when the vehicle velocity $U = \sqrt{u^2 + v^2}$ tends to 0 and leads to very marked discontinuity in terms X'_H, Y'_H and N'_H which imply substantial changes in the manoeuvring terms.

The coordinate system in the Yoshimura model is the one shown in 8.1, the equations used are the 8.9 [4]. Where the forces X, Y and the moment N are divided into hull, propeller, current and wind forces as described in equation 8.6.

For the forces X_{Hull}, Y_{Hull} and Z_{hull} [235] uses the following dimensionless formulations:

$$\begin{aligned} X'_H &= X_H / \frac{\rho}{2} LdU^2 = a'_1 u' + a'_2 v' r' \\ Y'_H &= Y_H / \frac{\rho}{2} LdU^2 = b'_1 v' \left|u'\right| + b'_2 r' u' + Y'_{HN} \\ N'_H &= N_H / \frac{\rho}{2} L^2 dU^2 = c'_1 v' u' + c'_2 r' \left|u'\right| + N'_{HN} \end{aligned} \tag{8.11}$$

where, $u' = u/U, v' = v/U, r' = r(L/U)$

And the coefficients are described in function of the: the resistance coefficient, $X'_0 = X'_{0(F)} + \left(X'_{0(A)} - X'_{0(F)}\right)(\beta|/\pi)$ (where $X'_{0(F)}$ and $X'_{0(A)}$ are the resistance coefficient of ahead and astern); the Cross-Flow drag coefficient C_D; the Correction factor for yaw C_{rN}; and the Correction factor for lateral force C_{rY}. The latter coefficients are introduced in the Yoshimura model and allow to simplify the expression of the non linear force components induced by lateral drag of hull:

$$\left.\begin{aligned} Y_{HN} &= -\left(\tfrac{\rho}{2}\right) dC_D \int_{-L/2}^{L/2} \left|v + C_{rY} rx\right| \left|\left(v + C_{rY} rx\right) dx \right. \\ N_{HN} &= -\left(\tfrac{\rho}{2}\right) dC_D \int_{-L/2}^{L/2} \left|v + C_{rY} rx\right| \left(v + C_{rY} rx\right) \cdot x \cdot dx \end{aligned}\right\} \tag{8.12}$$

And the final equations are:

$$\begin{aligned} X'_H =& X_H / \left(\frac{\rho}{2}\right) LdU^2 = \left\{X'_{0(F)} + \left(X'_{0(A)} - X'_{0(F)}\right)(\beta/\pi)\right\} u' + \left(m'_y + X'_{vr}\right) v' r' \\ Y'_H =& Y_H / \left(\frac{\rho}{2}\right) LdU^2 = Y'_v v' \left|u'\right| + \left(Y'_r - m'_x\right) r' u' - C_D \int_{-1/2}^{1/2} \left|v' + C_{rY} r' x'\right| \left(v' + C_{rY} r' x'\right) dx' \\ N'_H =& N_H / \left(\frac{\rho}{2}\right) L^2 dU^2 = N'_v v' u' + N'_r \cdot r' \left|u'\right| - C_D \int_{-1/2}^{1/2} v' + C_{rY} r' x' \left| \left(v' + C_{rY} r' x'\right) x' dx' \end{aligned} \tag{8.13}$$

The linear derivatives $m'_y + X'_{vr}$, Y'_v , $Y'_r - m'_x$, N'_v, N'_r are derived, from coefficients that can be found in literature. An example is [246] or the blunt body ship's coefficient in [241]. While the other coefficients can be derived from models, calculations or literature.

In the case of SWAMP, knowing and accepting the uncertainties that this may lead, the coefficients were derived from [246]. The coefficients were applied to the monohull and then doubled to obtain the values for a catamaran.

[4] In which the terms $Y_{\dot{r}}$ and $N_{\dot{v}}$ are usually considered null as non-influential

8.1.3 The simulator

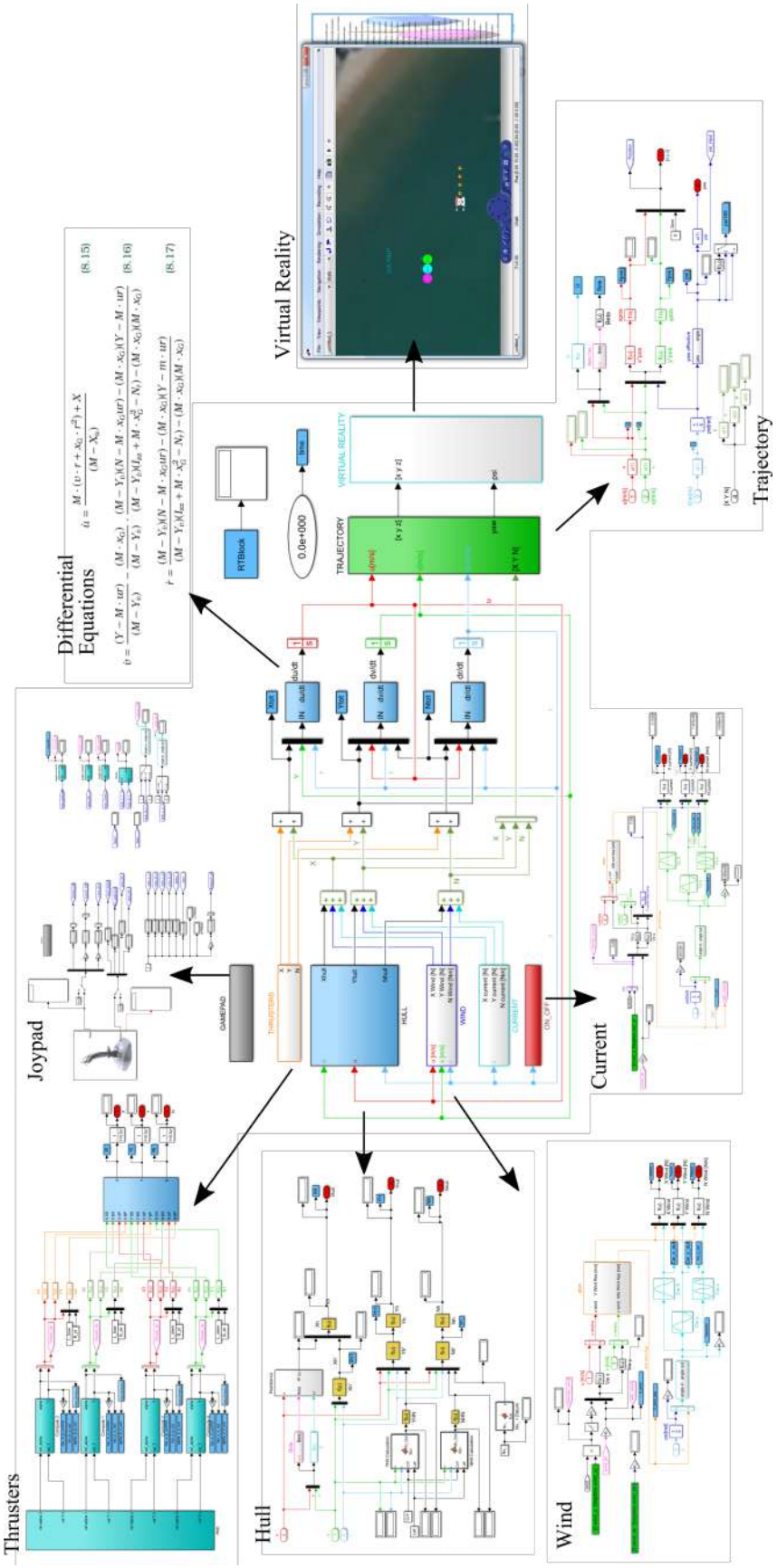

Figure 8.3: *The SWAMP simulator*

The simulator was developed by using Simulink® ambient through the use of subsets, each of which represents an on-board system or a physical phenomenon agent on SWAMP. All subsets are connected by a network of connections and logical processes.
Various blocks are present. The internal forces are calculated in the *Hull block* used for calculating the $(X_{Hull}, Y_{Hull}, N_{Hull})$. The external forces are calculated by the *Thrusters block* that provides the values of (X_T, Y_T, N_T) in function of the equations described in Chapter 5 and by applying the $(1-t)$ recorded during the open water tests. and the external disturbances are calculated in the *Wind block* $(X_{wind}, Y_{wind}, N_{wind})$ and in the *Current block* $(X_{current}, Y_{current}, N_{current})$ by adopting the formulas suggested by $DNV-GL$ rules.
The integrator blocks are used to numerically solve the differential equations 8.1.3 and to calculate the speeds and next the positions computed by the *Trajectory block*. The trajectories are converted, together with the other parameters, into input signals that are the output of the simulator and the input for the *Virtual Reality* ambient developed with the V-Realm Builder of Matlab® and Simulink®. The Virtual reality was used to pilot the simulator of SWAMP with the same Logitech Joypad used during the Camogli experiment. A *timer function block* was used to peace the time and render the Virtual Reality synchronised with the real time.

The differential equations

The manoeuvrability equations used by Yoshimura are the 8.9. The simulator deals with solving the differential equations integrating them numerically for each step of the process. To make them integrable, the equations must be written in the form:

$$\begin{cases} \dot{u} = \frac{M\cdot(v\cdot r + x_G\cdot r^2)+X}{(M-X_{\dot{u}})} \\ \dot{v} = \frac{(Y-M\cdot ur)}{(M-Y_{\dot{v}})} - \frac{(M\cdot x_G)}{(M-Y_{\dot{v}})}\cdot\frac{(M-Y_{\dot{v}})(N-M\cdot x_G ur)-(M\cdot x_G)(Y-M\cdot ur)}{(M-Y_{\dot{v}})(I_{zz}+M\cdot x_G^2-N_{\dot{r}})-(M\cdot x_G)(M\cdot x_G)} \\ \dot{r} = \frac{(M-Y_{\dot{v}})(N-M\cdot x_G ur)-(M\cdot x_G)(Y-m\cdot ur)}{(M-Y_{\dot{v}})(I_{zz}+M\cdot x_G^2-N_{\dot{r}})-(M\cdot x_G)(M\cdot x_G)} \end{cases} \tag{8.14}$$

The equations 8.1.3 are integrated within the simulator to obtain the velocities: u, v, r. Then, from the velocities, the trajectories are integrated to obtain the position and the heading of the vehicle x_{pos}, y_{pos}, Yaw.

$$\begin{cases} u = \int \dot{u}\, dt \\ v = \int \dot{v}\, dt \\ r = \int \dot{r}\, dt \end{cases} \rightarrow \begin{cases} \psi = \int r dt \\ \dot{x}_0 = u * cos(\psi) - v * sin(\psi) \\ \dot{y}_0 = u * sin(\psi) + v * cos(\psi) \end{cases} \rightarrow \begin{cases} H_{eading} = \psi \\ X_{pos} = \int \dot{x}_0 dt \\ Y_{pos} = \int \dot{y}_0 dt \end{cases} \tag{8.15}$$

M is mass, I_{zz}, the inertia moment about z and $X_{\dot{u}}, Y_{\dot{v}}, N_{\dot{v}}$ are the added inertia and represent the forces due to accelerations. For SWAMP simulator, with the vehicle at its maximum weight the following values were derived. Mass and Inertia were calculated from CAD and stability calculations. The added mass and inertia were derived from [247] and [248] that suggest the added mass in x to be 5% of the mass, the added mass in y to be 40% of the mass and the added moment of inertia to be 50% of the total inertia:

M	I_{zz}	$X_{\dot{u}}$	$Y_{\dot{v}}$	$N_{\dot{r}}$
$[kg]$	$[kg\,m^2]$	$[kg]$	$[kg]$	$[kg\,m^2]$
58	7.88	-2.9	-23.2	-3.94

Hull Forces

The hull forces are calculated in this block, thanks to ad-hoc embedded-function blocks, in the form:

$$\begin{aligned} X_H &= \left(\frac{\rho}{2}\right) Ld \left[\left\{X'_{0(F)} + \left(X'_{0(A)} - X'_{0(F)}\right)(\beta/\pi)\right\} uU + \left(m'_y + X'_{vr}\right) L \cdot vr\right] \\ Y_H &= \left(\frac{\rho}{2}\right) Ld \left[Y'_v|u| + \left(Y'_r - m'_x\right) L \cdot ru - \left(\frac{C_D}{L}\right) \int_{-L/2}^{L/2} |v + C_{rY} rx| \left(v + C_{rY} rx\right) dx\right] \\ N_H &= \left(\frac{\rho}{2}\right) L^2 d \left[N'_v vu + N'_r L \cdot r|u| - \left(\frac{C_D}{L^2}\right) \int_{-L/2}^{L/2} |v + C_{rY} rx| \left(v + C_{rY} rx\right) x dx\right] \end{aligned} \tag{8.16}$$

The resistance coefficient X'_0 was derived from the towing tank tests on the SWAMP hull, while C_D was derived from the expression $C_D = -0.0591 * (L_{wl}/d) + 1.848$ and C_{rN}, C_{rY} were derived from regressions present in [235] and also the linear derivatives $m'_y + X'_{vr}$, Y'_v , $Y'_r - m'_x$, N'_v, N'_r were obtained from the coefficients that can be found in the same publication.
The value of N'_r was corrected by reducing its value of 5% to calibrate the coefficient in compliance with the results obtained from the turning circle tests in the first sea-trials.
The coefficients are resumed in the following table:

$m'_y + X'_{vr}$	Y'_v	$Y'_r - m'_x$	N'_v	N'_r	C_D	C_{rY}	C_{rN}
0.168	-0.54	0.066	-0.226	-0.135	1.325	0.942	0.2000

Shallow Water Correction

For vessels that manoeuvre at low speeds in shallow and restricted waters, the vehicle is subject to phenomena that cause changes to the flows that surround the hull and change its manoeuvring characteristic. As mentioned in Chapter 4 for shallow water we mean those waters in which the ratio between the depth of the water h and the immersion of the vehicle T are in a ratio that is $h/T \leq 3$.
In the case of manoeuvrability at low speed it is very important to know what the effect of the shallow backdrop is on the manoeuvre because an error in the evaluation could be critical for the vehicle. In this simulator a correction was applied just to the resistance, in function of the results obtained in the towing tank. Further development will increase the capacity of the simulator to predict also a manoeuvrability influenced by shallow water.

Wind Force

The wind forces are obtained from the wind loads formulas suggested by DNV-GL [224] and calculated using the following formulas.

$$\begin{aligned} X_{wind} &= \frac{1}{2}\rho_{\text{air}} V^2_{\text{wind}} A_{F,\text{wind}} * (-0.7 * \cos(\alpha_{wind})) \\ Y_{wind} &= \frac{1}{2}\rho_{\text{air}} V^2_{\text{wind}} A_{L,\text{wind}} * (0.9 * \sin(\alpha_{wind})) \end{aligned} \tag{8.17}$$

$$\text{dir} = \begin{cases} \alpha_{wind}\ if\ 0 \leq \alpha_{wind} \leq \pi \\ 2\pi - \alpha_{wind}\ if\ \pi \leq \alpha_{wind} \leq 2\pi \end{cases} \tag{8.18}$$

$$N_{wind} = Y_{wind} * \left(x_{L,\ \text{air}} + 0.3 * \left(1 - 2 * \frac{dir}{\pi}\right) * L_{pp}\right) \tag{8.19}$$

Where:
α_{wind}= wind coming from direction

$A_{F,\text{wind}}$ = frontal projected wind area
$A_{L,\text{wind}}$ = longitudinal projected wind area
$x_{L,\text{ air}}$ = longitudinal position of the area center of $A_{L,\text{wind}}$
The wind intensity is calculated by applying the relative speed and angle with respect to the incoming speed and direction of the vehicle.

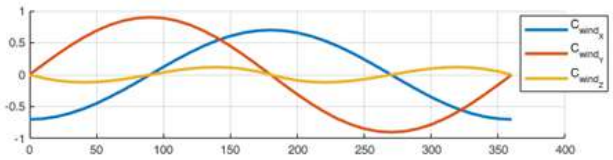

Figure 8.4: *The wind coefficients*

Current Force

The current forces are obtained from the current loads formulas suggested by DNV-GL [224] and calculated using the following formulas.

$$\begin{aligned} X_{current} =& \frac{1}{2}\rho_{\text{water}} * V^2_{\text{current}} * A_{F,\text{current}} * (-0.18 * \cos(\alpha_{current})) \\ Y_{current} =& \frac{1}{2}\rho_{\text{water}} * V^2_{\text{current}} * A_{L,\text{current}} * (0.6 * \sin(\alpha_{current})) \end{aligned} \tag{8.20}$$

$$\text{dir} = \begin{cases} \alpha_{current} \; if \; 0 \leq \alpha_{current} \leq \pi \\ 2\pi - \alpha_{current} \; if \; \pi \leq \alpha_{current} \leq 2\pi \end{cases} \tag{8.21}$$

$$N_{current} = Y_{current} * \left(x_{L,\text{current}} + \max\left(\min\left(0.4 * \left(1 - 2 * \frac{dir}{\pi} \right), 0.25 \right), -0.2 \right) * L_{pp} \right) \tag{8.22}$$

$\alpha_{current}$ = current coming from direction
$A_{F,\text{current}}$ = frontal projected current area
$A_{L,\text{current}}$ = longitudinal projected current area
$x_{L,\text{current}}$ = longitudinal position of the area center of $A_{L,\text{current}}$
The current intensity is calculated by applying the relative speed and angle with respect to the incoming speed and direction of the vehicle. This formulation is used to assess the Dynamic Position

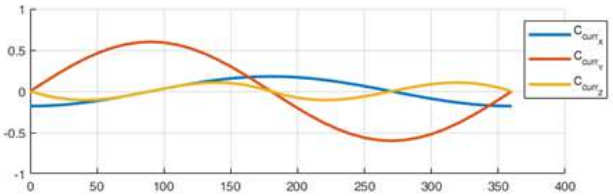

Figure 8.5: *The current coefficients*

and does not take into consideration the quadratic form of the forces when the speed increases. It was decided to use this kind of formulation to easily apply an external disturbance during the simulations. The 0.18 coefficient value of the $X_c current$ was calibrated for SWAMP simulator.

Pump-Jet Module thrusters block

The block for the thrusters module is used to drive the vehicle.
The thrust actions on SWAMP are the sum of the Pump-Jet Module's actions:

$$\begin{pmatrix} X_T \\ Y_T \\ N_T \end{pmatrix} = \begin{pmatrix} X_T^{PJ} \\ Y_T^{PJ} \\ N_T^{PJ} \end{pmatrix} \tag{8.23}$$

To model the azimuth thrusters it is necessary to distinguish between the two components along x and y axis and of the resulting moment. An example of Pump-Jet azimuth thrusters is reported in [249].
Given T_i^{PJ} as the generic thrust always positive and $\alpha_i = (0, 2\pi]$ the generic angle and thrust configuration of SWAMP can be seen in Fig.8.6
In table 8.1 the commands used to pilot each module are reported. Each module's thrust block input is a percentage of the maximum RPM and the output is a thrust value T_i^{PJ}. The input for the Azimuth block is an angle in *deg* and the output is an angle α_i in *rad*.

Table 8.1: *The mapping of the command of SWAMP thrusters*

Command	$RPM_{\%}$	10	20	30	40	50	60	70	80	90	100
Speed	RPM	118.5	237	355.5	474	592.5	711	829.5	948	1066.5	1185
T_i^{PJ}	[N]	0.12	0.49	1.10	1.95	3.05	4.39	5.98	7.81	9.88	12.20
Command	[deg]	-360	-270	-180	-90	0	90	180	270	360	
α_i	[rad]	-2π	$3/2\ \pi$	$-\ \pi$	$-\ \pi/2$	0	$\pi/2$	π	$3/2\ \pi$	$2\ \pi$	

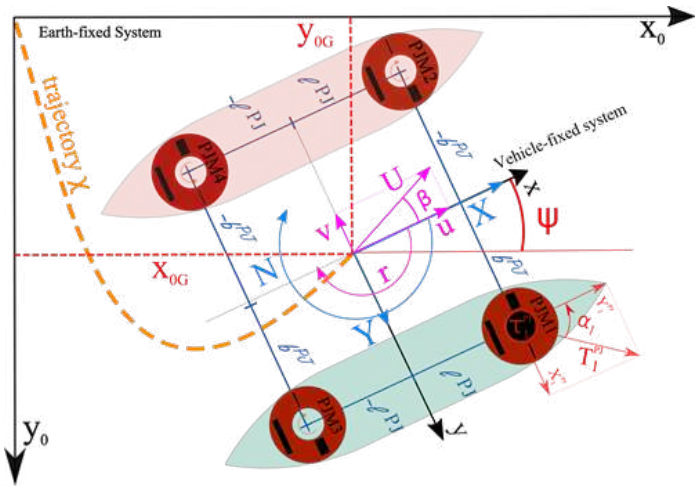

Figure 8.6: *The reference system for the thrust allocation of SWAMP vehicle*

The thrusters forces acting on SWAMP are then reported on the local coordinates system of the vehicle and the contribution to the external force and torque given by each Pump-Jet Module is:

$$\tau_i^{PJ} = \begin{pmatrix} X_i^{PJ} \\ Y_i^{PJ} \\ N_i^{PJ} \end{pmatrix} = \begin{pmatrix} \cos\alpha_i \\ \sin\alpha_i \\ -b_i^{PJ}\cos\alpha_i + l_i^{PJ}\sin\alpha_i \end{pmatrix} T_i^{PJ} \tag{8.24}$$

And the total forces acting on SWAMP are then:

$$\begin{pmatrix} X_T^{PJ} \\ Y_T^{PJ} \\ N_T^{PJ} \end{pmatrix} = \begin{pmatrix} t_{11} & t_{12} & t_{13} & t_{14} \\ t_{21} & t_{22} & t_{23} & t_{24} \\ t_{31} & t_{32} & t_{33} & t_{34} \end{pmatrix} \begin{pmatrix} T_1^{PJ} \\ T_2^{PJ} \\ T_3^{PJ} \\ T_4^{PJ} \end{pmatrix} \tag{8.25}$$

Where:

$$\begin{aligned} t_{1i} &= cos\alpha_i \\ t_{2i} &= sin\alpha_i \\ t_{3i} &= -b_i^{PJ}\, cos\alpha_i + l_i^{PJ}\, sen\alpha_i \end{aligned}$$

In the final version of the simulator the value of $(1-t)$ is applied based on the curves obtained in the self-propelling tests at sea.

The thrusters layout configuration provides the values mapping: 1 = "bs" bow starboard thruster, 3 = "ss" stern starboard thruster, 2 = "bp" bow port thruster, 4 = "sp" stern port thruster. The resulting forces and moments are the sum of the components:

$$\begin{pmatrix} X_T^{PJ} \\ Y_T^{PJ} \\ N_T^{PJ} \end{pmatrix} = \begin{pmatrix} X_{bs} + X_{ss} + X_{bp} + X_{sp} \\ Y_{bs} + Y_{ss} + Y_{bp} + Y_{sp} \\ N_{bs} + N_{ss} + N_{bp} + N_{sp} \end{pmatrix} \tag{8.26}$$

Then, depending on the thruster chosen as shown below:

$$\text{Bow Starboard Thruster} : \begin{cases} X_{bs} = T_{bs}^{PJ} * cos\alpha_{bs} \\ Y_{bs} = T_{bs}^{PJ} * sin\alpha_{bs} \\ N_{bs} = Y_{bs} * L_B + X_{bs} * B_{sb} \end{cases} \tag{8.27}$$

$$\text{Stern Starboard Thruster} : \begin{cases} X_{ss} = T_{ss}^{PJ} * cos\alpha_{ss} \\ Y_{ss} = T_{ss}^{PJ} * sin\alpha_{ss} \\ N_{ss} = Y_{ss} * L_S + X_{ss} * B_{sb} \end{cases} \tag{8.28}$$

$$\text{Bow Port Thruster} \begin{cases} X_{bp} = T_{bp}^{PJ} * cos\alpha_{bp} \\ Y_{bp} = T_{bp}^{PJ} * sin\alpha_{bp} \\ N_{bp} = Y_{bp} * L_B + X_{bp} * B_{pt} \end{cases} \tag{8.29}$$

$$\text{Stern Port Thruster} \begin{cases} X_{sp} = T_{sp}^{PJ} * cos\alpha_{sp} \\ Y_{sp} = T_{sp}^{PJ} * sin\alpha_{sp} \\ N_{sp} = Y_{sp} * L_S + X_{sp} * B_{pt} \end{cases} \tag{8.30}$$

Where $L_S = -0.35$, $L_B = 0.35$, $B_{pt} = 0.4$, $B_{sb} = -0.4$, are the distances in x and y of the thrusters' center from the origin.

The Joypad

The mapping of the basic controls of the thrusters is reported in Table 8.2.
As shown in Table 8.2 and in Fig. 8.7 the Joypad levers were mapped in the following way:

- The right lever was used to steer the Pump-Jet angles. α was limited in the interval $[-\pi/2, \pi/2]$. The angles was applied to the two bow thrusters while the stern thrusters were turned off.
- The left lever was used for powering the Pump-Jet. The percentage of RPM ($RPM_{\%}$) was used to command the amount of thrust T_i^{PJ}. The thrust was applied to the two bow thrusters

Table 8.2: *The mapping of the command of SWAMP thrusters*

Command	$RPM_{\%}$	20%	40%	60%	80%	100%
Speed	RPM	237	474	711	948	1185
T^{PJ}	[N]	0.49	1.95	4.39	7.81	12.2
Left Pad		0.2	0.4	0.6	0.8	1
Command	[deg]	-90	-45	0	45	90
Signal	[pos]	-123853	-61927	0	61927	123853
α_i	[rad]	- $\pi/2$	- $\pi/4$	0	$\pi/4$	$\pi/2$
Right Pad		-1	-0.5	0	0.5	1

while the stern thrusters were turned off.

Figure 8.7: *The mapping of the commands on the Logitech Joypad*

The training for the experiment in Camogli was done by letting the neural network to learn the values of position (x [m], y [m]) and heading (ψ [rad]) and the commands given by the pilot: α mapped on $joy_{angle}(k)$ and $RPM_{\%}$ mapped on $joy_{thrust}(k)$.

8.1.4 Examples of simulations

The Matlab® model was implemented and used to train the AI for the testing of the Camogli experiment before the construction of SWAMP.
To validate the mathematical model various simulations where done with the aim of checking the absence of singularities. The model was then used to test the training of the artificial intelligence control as reported in chapter 7.

Turning Circle

Some examples of the simulations performed is reported in figs. 8.8 to 8.10.
The first simulation reported is the one of fig. 8.8 where an 8-shaped manoeuvre was performed. The actuators are positioned at 30 deg on the bow and -30 deg on the stern and after half simulation inverted.

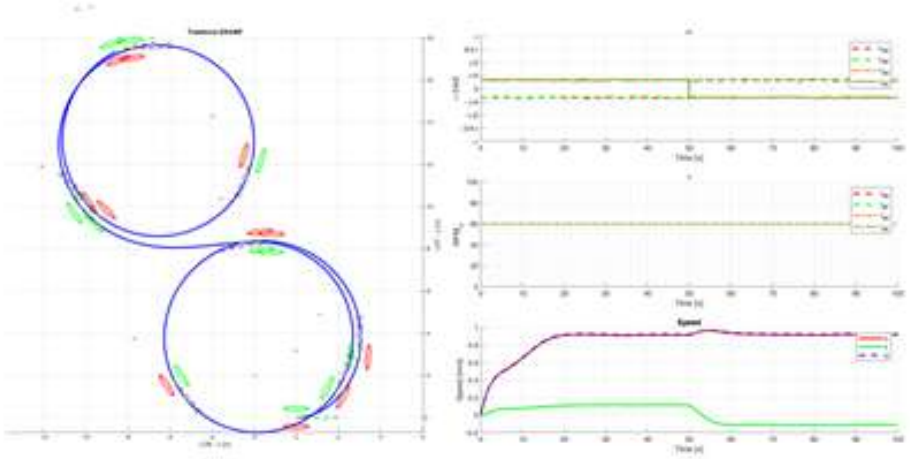

Figure 8.8: *Double circle simulation*

The results of the simulations in terms of speeds is reported in fig. 8.9

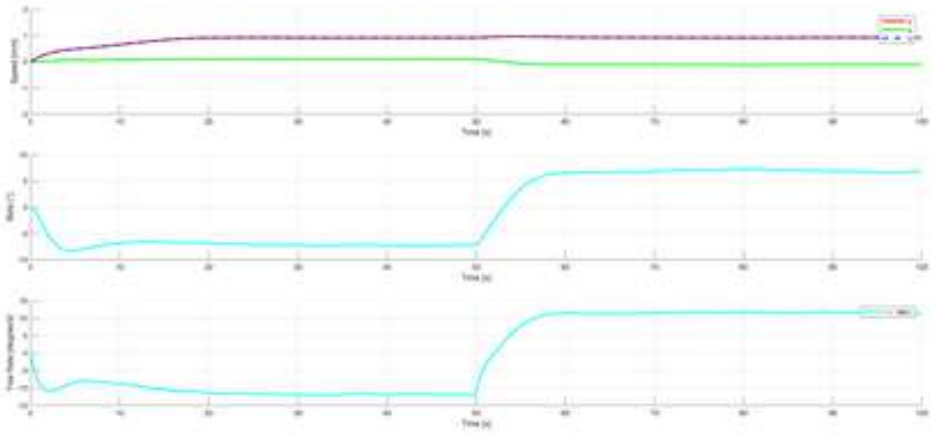

Figure 8.9: *Speeds during the double circle simulation*

While the graphic of the forces and moments acting on the vehicle are reported in fig. 8.10:

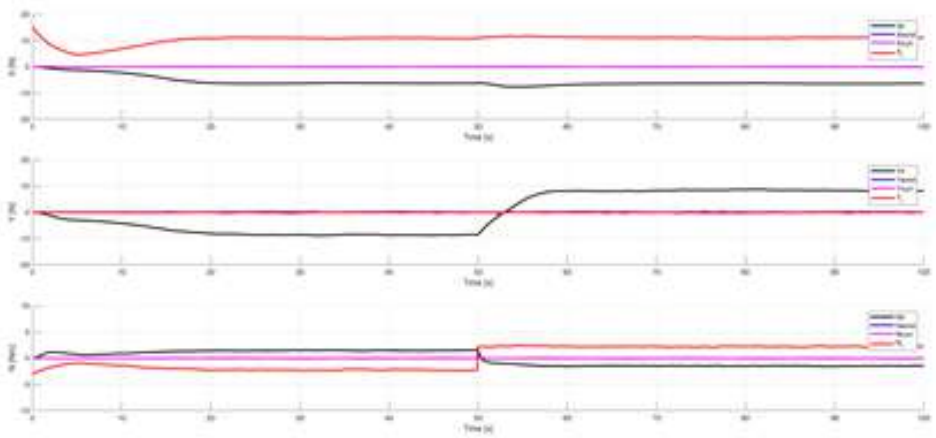

Figure 8.10: *Forces during the double circle simulation*

These data are quite smooth and no singularity was recorded (after the initial tune-up). Looking at the simulations it was possible to compare the results with the one obtained in the sea trials. It is possible to report the results of the same type of trajectory, with the same amount of thrust performed in Biograd. In fig. 8.11 the circle obtained with the simulator (blue line) is superimposed to the circle obtained in the sea trials (red line) at the same angle and amount of thrust ($RPM_{\%} = 60$ and $|\alpha_i| = 30$ deg).

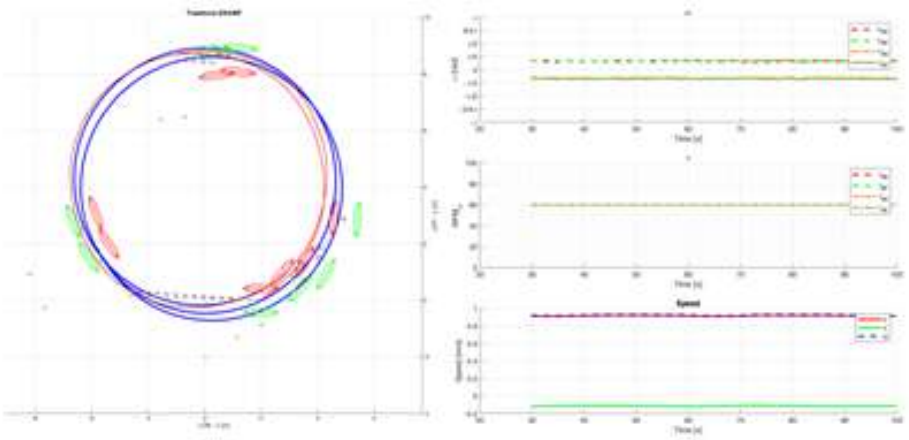

Figure 8.11: *The circle tests conducted in Biograd Na Moru*

From the results it is possible to see that the results are quite similar and further analysis will increase the reliability of the simulator. Some improvements to the mathematical model may be expected by the use of inverse system identification methods based on the sea trial results, such as those presented in [250] and [251].

Zig Zag 20 deg - 20 deg

Another example of simulation is reported in figs. 8.12 to 8.14. In this simulation to the model a control is applied that maps the same thrust (direction and intensity) to the stern thrusters to perform a $-20\,deg$ to $+20\,deg$ zigzag test.

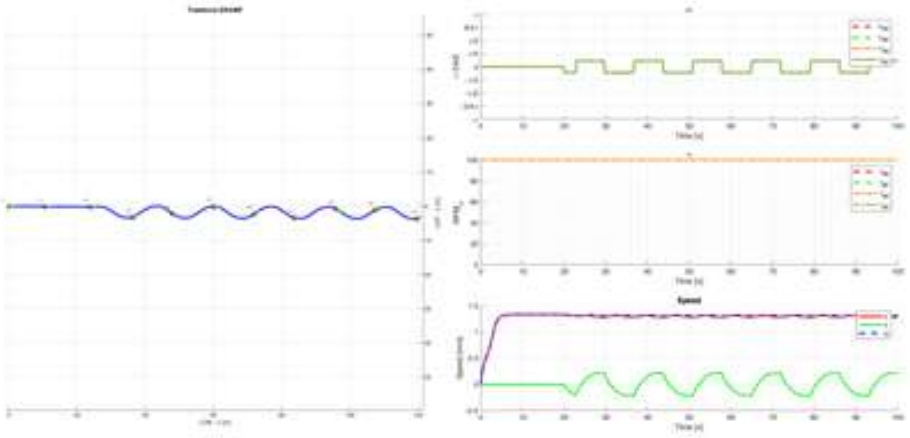

Figure 8.12: *The zig-zag simulation*

In fig. 8.13 the actuating angle of the thrusters is shown together with the Yaw angle. From these simulations it is possible to see how the vessel produces a zigzag path. The recorded overshoot is almost 10 deg.

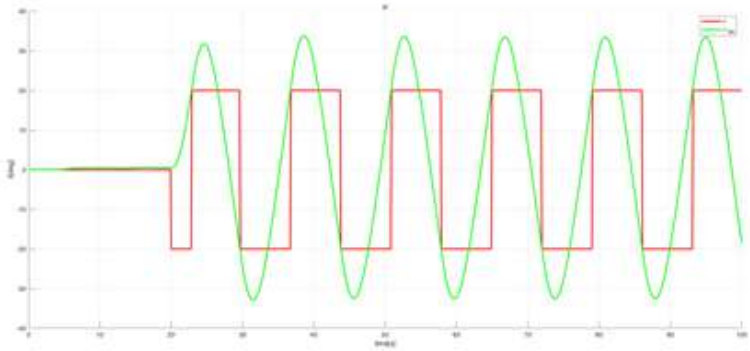

Figure 8.13: *Reference system*

The forces acting on the hull are reported in fig. 8.14.

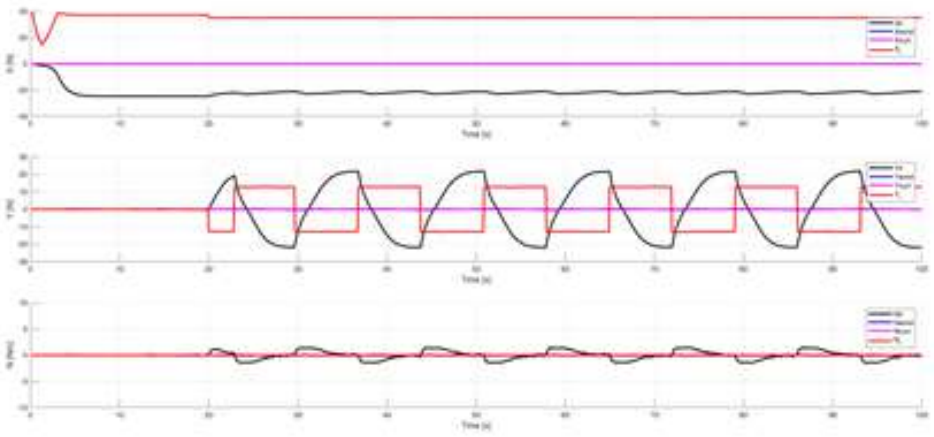

Figure 8.14: *Forces acting on the hull*

Chapter 9

Conclusions

9.1 Essence

The present thesis was born from the interest that arouses the investigation into the requirements for an Autonomous Surface Vehicle, able to access very shallow waters, that I made some years ago. The result of that interest is the work made during my Ph.D. period whose physical representation is a robot named SWAMP which is characterised by various new concepts. The vehicle was conceived, designed and constructed on the basis of the ideas developed during the experiences I have had in the last years. The project is based on concepts arising both from the air-cushion vehicles technology and from marine robotics knowledge, and it relies on the experiences I have had in participating in missions in remote and difficult areas, such as Ny Alesund on the Kongsfjord, in the Svalbard archipelago.

In these years I have made an image of how I wanted to bring new concepts in the robotics and which were the new concepts that I wanted to introduce in an ASV and I tried to bring them into the Ph.D project and into my doctoral thesis.
SWAMP prototype is the physical result of the application of these concepts to a specific project.

On an ontological level the essence [1] of SWAMP is not the machine equipped with subsystems but a set of subsystems that form a vehicle. The two aspects are very different. Two things are fundamental within this concept, the very concept of vehicle (from the lat. vehicŭlum, der. of vehĕre "to carry") and the communication system. Everything else composing SWAMP is not superfluous but is not fundamental.

[1] For Aristotle the essence is the property or set of properties that make an entity or substance what it fundamentally is, and which it has by necessity, and without which it loses its identity

The concept of vehicle means that a system for creating the movement (propulsion) is required and a structure that "bonds" the subsystems is required. This does not mean that this structure must necessarily be material. SWAMP is like a "being" composed of various organs (the individual modules) that interact and cooperate with each other: cooperation can also lead them to coordination, that is, they can also decide to give the command to one of them for a certain time (as in the case of two cooperating monohulls that form a catamaran).

The aspects of practical nature are on a lower level than the main ontological concepts. These aspects are anyway of great importance since are based on a focused approach. The use of soft structures, the adoption of the concept of modularity and the use of improved actuation systems are the new concepts that have driven the practical design of SWAMP. These, together, make the robot suitable to work in an ideal way in its operational environment and scenario.

The practical technological results that characterise the design of SWAMP follow specific requirements and combine concepts of robotics with concepts of naval architecture and marine engineering, aspects that are not always united. These aspects are used, for SWAMP, with the aim of designing a robot suitable to give an added value to the concept of Ecorobotics. This paradigm involves the integration of ecological approaches and robotics to develop technological tools for environmental monitoring. The Robotics applied to environmental sciences is intended to help the human to improve the precision and the quality of the data gathering that allow to better understand the functioning of the Earth with the final scope of preserving it.

9.2 The technological results

The SWAMP vehicle was conceived under the basic idea of a modular, portable and re-configurable robot that is at the base of the recent robots designed at CNR-INM like Proteus [4, 5] and e-URoPe [106].
The vehicle was purposely designed to work in extremely shallow waters, down to only a few centimeters in depth to extend the survey possibility in the peculiar ambient represented by Wetlands.
A set of operational requirements were listed in the initial stage of the project and by following these concepts, a "requirement based design" was carried on by adopting new design concepts.

Among the new concepts introduced in this thesis, a new soft and light structure, able to withstand external loads and to protect the sensors and payloads, was designed and adopted. As far as we know, this is the first application of a soft sandwich foam hull. The most similar solution is [121] made with rigid foam and fibreglass.
The use of this concept allowed to adopt an extremely modular structure characterised by the adoption of low weight modules. Each module can be easily dismounted from the vehicle. But the real idea is that all these modules can be replaced easily by another module. In this direction the robot is a platform that is constituted by a set of sub-modules:

- Structural Modules
- Hull sections
- Thrust modules
- Communication modules
- Sensors modules
- Powering modules
- Control unit modules

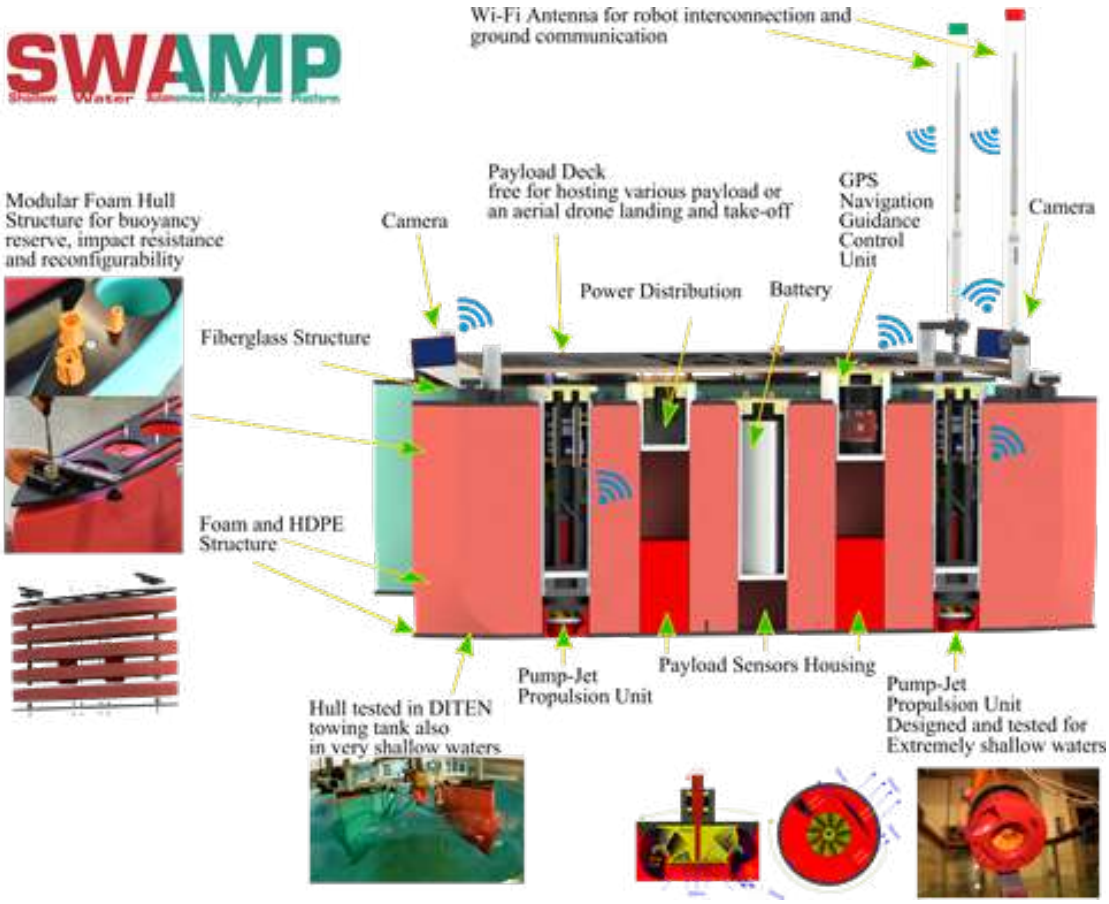

Figure 9.1: *SWAMP (Shallow Water Autonomous Multipurpose Platform) peculiarities*

Its nature exists only when these modules are put together but every single part of the vehicle can be modified. This can be done by modifying the hull shape, by modifying the thrust units, by modifying the powering, sensors, communication and control unit module. The installation of the new modified element on-board is easy.
The idea at the base of the modular architecture of SWAMP was to remove as much as physical connections as it was possible. In marine robots the cable connecting the sub-systems greatly influence the design and the cost of a vehicle. In a future development it is foreseen to endow the modules with an internal power supply (like a battery) eliminating all cables, so to extreme the concept of modularity. Thanks to the modularity of such a system, additional modules can be easily added (e.g. computational, actuator, sensor, etc. modules), with the idea of removing the communication cables all the element can be substituted (at least only the communication system should exist for the existence of the SWAMP concept).

A newly-designed modular thruster was developed to extend the operative area in extremely shallow water. The system is based on the Pump-Jet, a solution never adopted before in marine robotics. Four complete thrusters were designed, and then constructed, starting from basic equations by re-evaluating existing pump design. Test results were satisfactory, and after calibration of the outlet nozzle geometry, the system met the initial requirements.

Another Naval Architecture aspect of this thesis is related to the tests in a towing tank in very shallow waters to characterise the whole operational scenarios that SWAMP will face. These are the first tests of this kind, carried out on a prototype at full scale of a marine robot.

As a final result the robot design met all the requirements outlined in the Chapter 3:
the vehicle and its control unit are portable, its dimensions comply with small size and shallow waters and the vehicle is easily deployable. The vehicle structure can withstand to external loads and impacts and the propulsion system is suitable for working in extremely shallow water. Moreover the vehicle is highly modular and re-configurable from hardware and software point of view. This concept is important not only to comply with the different tasks to carry on but also for the requirements coming from the same mission. The vehicle is fully controllable thanks to four azimuth thrusters.

SWAMP is addressed to perform various missions. Among these four main typologies are identified. The first is the *Multi-parameter monitoring platform* composed of deployable underwater multi-parameter probes and air parameters probes possibly deployable with an aerostat. This is addressed to monitor vast coastal strips and difficult to access environments. Following the researches carried on in the Kongsfjorden [4], SWAMP can be used to estimate the biological potentials that contribute to the carbon cycle in Svalbard Archipelago, where icebergs and glaciers, as well as shallow waters near the coast, represent a significant risk to the safety of manned ships. A second typology usable also in this environment such as in wetlands is a *Sampling platform* with a surface water sampling system or with an underwater sampling system to be deployed that is able to host various liters of sampled water. SWAMP is able to answer the request for a *Morpho-bathymetric platform* with different kind of sensors to be mounted in the hull under free water surface or in direct contact with water. This can be used for river-bed mapping also in small mountain rivers presenting shallow waters and possible impacting with the shore or rocks. A shallow water vessel can be used also for the monitoring of Posidonia meadows in coastal areas [107].
For multi-robot environmental assessment SWAMP can become a *Aerial drone landing and take-off platform*. This can be done thanks to the presence of enough space for the take off and landing given by the flat main deck thanks to the fact that all the power and electronics are contained in the hull. Where, anyway, space exists also to host sensors as shown in Chapter 7

9.3 Future developments

For its innovative nature SWAMP will be the base for a series of studies and developments: from propulsion, to control to sensors, to structures to at-field applications. Future developments include full identification in every loading condition. This, together with the detailed design of the vessel will allow, by knowing the actual configuration, to fully control SWAMP in most of the loading conditions.
The most interesting aspect of SWAMP control will be the development of distributed control architectures with conflicting or cooperating control units.
From a mechanical point of view future developments include the use of different hull shapes coupled with the actual structure by just modifying some sections of the foam.
As far as the SWAMP interaction with sensors is concerned, the study of the capacity of sensors to work through the foam structure of SWAMP, in order to always protect them, will be investigated.
Open research topics will be:

1. Mechanics: Pump-Jet Module newer and lower cost versions
2. Structure: Extend the concept of soft structure
3. Simulation: SWAMP Digital Twin with an extended simulator
4. SWAMP conventional (cooperative) NGC system & Thrust Allocation / Dynamic Positioning (TA/DP)
    - Control

- Guidance
- Station-Keeping
- Line-Following
- Path-Following
- Thrust Allocation
- Vehicle cooperation

5. Increase SWAMP Autonomy Level [39, 40]
6. Machine Learning-based GC systems
7. SWAMP intelligent sensor packages
    - seabed classification in shallow water
    - acoustics in shallow waters
    - vision
    - combined acoustics&vision

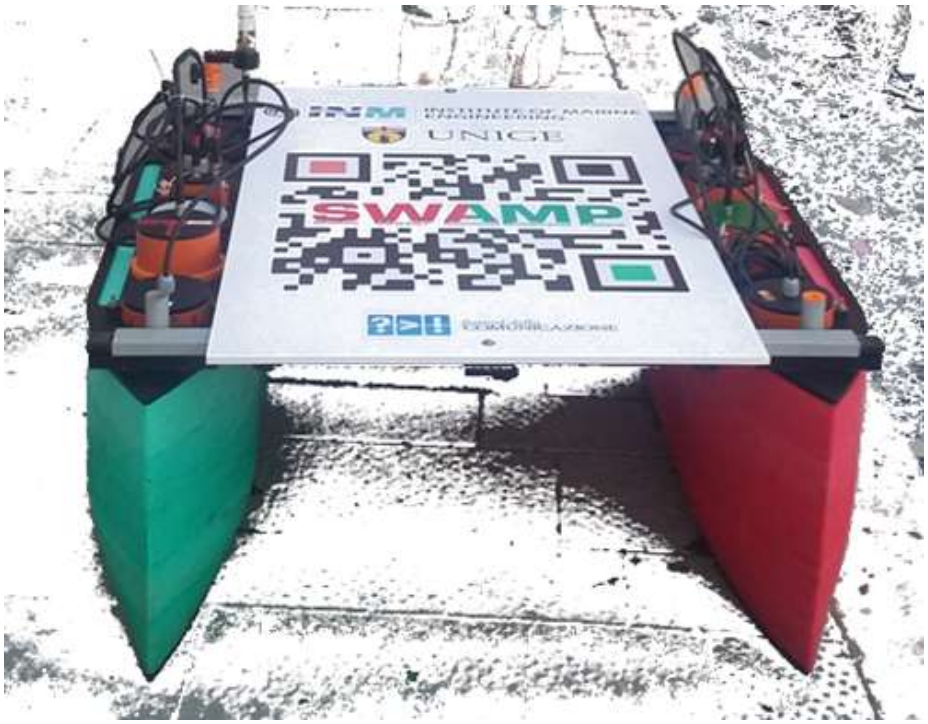

Acknowledgements

The work is the topic of the Ph.D work carried on at DITEN University of Genova by Angelo Odetti in the framework of the XXXII Cycle of the Ph.D in *Scienze e Tecnologie per l'Ingegneria Elettrica, l'Ingegneria Navale e i Sistemi Complessi per la mobilità*. A number of individuals has been fundamental for their, input and ongoing support in helping to design, build and test the SWAMP vehicle.
A first special thanks goes to Gabriele Bruzzone and Massimo Caccia for having supported the research topics of this thesis also with insights and continuous ideas. A second special thanks goes to Michele Viviani for having pushed me to start this Ph.D. and for his infinite support (and patience) during the development of this work with its aptitude in analising the problems.
The last but not least special thanks goes to Marco Altosole for the enthusiastic approach with which he supported the design and developement of Pump-Jet Module and of the actual and future developments of the SWAMP vehicle.
Moreover two persons have been of great inspiration for this work: Marco Mastrangeli for its innovative ideas at the base of the soft-hull concepts adopted in SWAMP and Stefano Sanguineti for the insights related to harsh environment bathymetries.
A general thanks goes to CNR-INM and Univeristà di Genova people, not only for having supported me in the research but also for their work, in particular thanks go to:

- Marco Bibuli, for the implementation of the NGC of SWAMP for the field trials and for the help in the towing tank tests
- Gabriele Bruzzone, also co-relator of this thesis for the conception of the modular HSC architecture and the design and construcion of electronics
- Giorgio Bruzzone for the mechanical support especially in the construction of Pump-Jet Module and the design of SWAMP layout
- Giuseppe Camporeale for its support in the design and construction of the testing design rig
- Stella De Robertis and Jeffrey Earp for their help with the English language
- Alberto Ferrari for its work and support in the towing tank tests
- Roberta Ferretti, for the implantation and tests of the sonar inside the hull of SWAMP
- Mauro Giacopelli for its support in the design and construction of the testing design rig for the propulsion units, for the help in the construction of SWAMP hull and the support during towing tank tests
- Edoardo Spirandelli for its work in the design and construction of the electronics and electrical systems
- Sergio Talocchi for its work and support in the towing tank tests
- Diego Villa for its CFD simulations on the SWAMP hull
- Enrica Zereik, for the implementation of the NGC of SWAMP

This thesis is the sum of some documents and articles developed during the doctorate and of further and extended results reported in this documents. The main articles are the following:

i A New Concept of Highly Modular ASV for Extremely Shallow Water Applications
Odetti A. , Altosole M. , Bruzzone G., Viviani M. , Caccia M.
The 12th IFAC Conference on Control Applications in Marine Systems, Robotics, and Vehicles (CAMS 2019) and the first workshop on Robot Control (WROCO 2019) will be held jointly at KAIST in Daejeon, Korea from 18th until 20th September 2019

ii Design and Construction of a Modular Pump-Jet Thruster for Autonomous Surface Vehicle Operations in Extremely Shallow Water.
Odetti, A., Altosole, M., Bruzzone, G., Caccia, M., and Viviani, M. (2019).
Journal of Marine Science and Engineering, 7(7), 222.

iii Wetlands Monitoring: Hints for Innovative Autonomous Surface Vehicles Design,
Odetti, A. and M. Altosole and M. Caccia and M. Viviani and G. Bruzzone,
Technology and Science for the Ships of the Future. Proceedings of NAV 2018: 19th International Conference on Ship and Maritime Research, 1(1),1014–1021,2018, IOS Press

iv An Advanced Guidance and Control System for an Unmanned Vessel with Azimuthal Thrusters
M. Bibuli, Ga. Bruzzone, Gi. Bruzzone, M. Caccia, G. Camporeale, D. Chiarella, R. Ferretti, M. Giacopelli, A. Odetti, A. Ranieri, E. Spirandelli, E. Zereik
(2018, October) In Proceedings of the International Ship Control Systems Symposium (iSCSS) (Vol. 2, p. 4).

Videos of SWAMP in operation can be found in the following hyperlink or link:
SWAMP LAUNCH - https://youtu.be/XkET5mSaIcQ
SWAMP & CNR-INM Team @ BTS 2019 - https://youtu.be/ccKQ4c03yIo
SWAMP learning from humans - https://youtu.be/nozHpp1TneQ
SWAMP @ SEADRON - https://youtu.be/c7N0wzRAy5c
SWAMP on the Roia River - https://youtu.be/cedv-E-M79U

List of Symbols

The next list describes several symbols that will be later used within the body of the document

$(1+k)$	Form factor
$(1-t)$	Thrust deduction factor
α	Pump-Jet steering actuation angle $[deg]$
α	Pump-Jet steering actuation angle [deg]
α_0	Pump-Jet steering actuation initial angle [deg]
α_0	Pump-Jet steering actuation initial angle $[deg]$
α_0'	Pump-Jet actual steering actuation initial angle [deg]
$\alpha_{current}$	wind coming from direction
α_{out}	Outlet angle with respect to the bottom [deg]
α_{wind}	wind coming from direction
β_2	Vane discharge angle [deg]
β_{1m}	Vane entrance angle [deg]
β_{2m}	Vane outlet angle [deg]
Δ	SWAMP displacement $[kg]$
η_m	Mechanical efficiency
η_p	Pump efficiency
η_r	Relative rotary efficiency
∇	SWAMP underwater volume $[m^3]$
ψ_p	$1/2\,Ku^2$ head coefficient speed constant
ρ_{air}	Air density: 1.226 [kg/m^3]
ρ_w	Water density: 1025 [kg/m^3]
σ	Slip factor
τ	Generic Pump-Jet thrust
A_i	Impeller inlet area [m^2]
A_M	Midship section area $[m^2]$
A_w	Wetted surface area $[m^2]$
A_{1m}	Inlet area [m^2]
A_{2m}	Outlet area [m^2]
A_d	Nozzle discharge area [m^2]
$A_{F,\text{current}}$	frontal projected wind area
$A_{F,\text{wind}}$	frontal projected wind area
$A_{L,\text{current}}$	longitudinal projected wind area
$A_{L,\text{wind}}$	longitudinal projected wind area
A_o	Impeller outlet area [m^2]
ASV	Autonomous Surface Vehicle
AUV	Autonomous Underwater Vehicle
B	Vehicle breadth $[m]$
C_B	$\nabla/(Lwl * Bwl * T)$; Block Coefficient
C_f	Coefficient of frictional resistance [ITTC'57 correlation]
C_M	$AM/(Bwl * T)$; Coefficient of the midship section
C_P	$\nabla/(AM * Lwl)$; Prismatic longitudinal coefficient
C_r	Residuary resistance Coefficient
C_t	Total resistance coefficient
C_t	SWAMP resistance coefficient
C_W	$WPA/(B * L)$; Water-plane coefficient
c_{2m}	Axial component ad outlet [m/s]
C_{Fin}	Residual Battery Capacity
c_{m1}	Entrance velocity [m/s]
c_{m1}	Inlet area [m^2]
c_{m2}	Meridian velocity at outlet [m/s]
c_{u1}	Axial component ad inlet [m/s]
c_{u2m}	Tangential component of velocity at outlet [m/s]
Cb	Block coefficient: $\frac{\nabla}{L*B*d}$
d	Vehicle draft $[m]$
D_i	Inlet diameter of the impeller $[m]$
D_m	$\sqrt{D_{2o}^2 + D_{2i}^2}/2$ is the mean effective diameter $[m]$
D_o	Outlet diameter of the impeller $[m]$
D_p	Diameter of the Pump-Jet Module $[m]$
D_t	Tactical Diameter [m]
D_{1m}	Mean diameter of the blade $[m]$
D_{1r}	Root diameter $[m]$
D_{1r}	Root radius $[m]$
D_{1t}	Tip diameter of impeller $[m]$
D_{2m}	Mean diameter at outlet $[m]$
D_{2r}	Root diameter at outlet $[m]$
D_{2r}	Root radius at outlet$[m]$
D_{2t}	Tip diameter at outlet $[m]$
$Demihull$	Catamaran Vehicle Monohull
DOD	Battery Depth of discharge
$EXSW$	Extremely shallow Water
Fn_H	Depth Froude Number $[\sqrt{V/gh}]$
Fn_L	Froude Number $[\sqrt{V/gL}]$
g	Gravity acceleration: 9.81 [m/s^2]
g	Acceleration due to gravity [9.81ms-2]
GM_L	Longitudinal metacentric height [m]

GM_T	Transverse metacentric height [m]
GZ	Righting arm [m]
h	Water depth $[m]$
h/T	ratio between water depth and vessel draft
h_o	Height of the impeller outlet $[m]$
H_p	Pump head $[m]$
h_i	Losses due to intake $[m]$
h_{loss}	Losses of pump head $[m]$
h_{man}	Losses due to manufacturing imprecision $[m]$
h_n	Losses due to nozzle $[m]$
I_{prop}	Propulsion Current
I_{tot}	Total Electrical Current
k_u	Speed constant
KM_L	Longitudinal Distance from the keel to the metacentre [m]
KM_T	Transverse Distance from the keel to the metacentre [m]
L	Vehicle length $[m]$
L	Length of model on waterline [m]
l_i	Blade height at inlet $[m]$
l_o	Blade height at outlet $[m]$
LCB	Longitudinal center of buoyancy [m]
LCG	Longitudinal center of gravity [m]
m_f	Mass flow rate of the jet [kg/s]
n	Main motor speed [RPM]
N_s	Specific pump speed
NGC	Navigation Guidance and Control
p_i	Inlet pressure [Pa]
p_o	Outlet pressure [Pa]
P_{prop}	Propulsion Power
P_{Pump}	Pump power [W]
P_{tot}	Total Electrical Power
P_{Users}	User's Power
P_{Wh}	Total Power over time
Q_o	Volumetric flow rate of the jet [kg/s]
r	Rotational Speed about z axis [rad/s]
r_i	Impeller radius $[m]$
R_R	Residuary resistance [N]
R_T	Total resistance [N]
R_t	Total resistance [N]
R_{1m}	Mean radius of the blade $[m]$
R_{1t}	Tip radius of impeller $[m]$
R_{2m}	Mean radius at outlet $[m]$
R_{2t}	Tip radius at outlet $[m]$
$RPM_{\%}$	The 0 to 100 % RPM for commanding the thrusters
S	Separation between catamaran demihull centre-lines [m]
SOC	Battery State of charge
T	Vehicle immersion $[m]$
T_i^{PJ}	Pump-Jet thrust [N]
T_α	Pump-Jet thrust at α angle [N]
$T_{bollardpull}$	Thrust in bollard pull tests
U	SWAMP absolute speed [m/s]
u	Surge Speed[m/s]
u_{1m}	Radial velocity at inlet [m/s]
u_{2m}	Radial velocity [m/s]
USV	Unmanned Surface Vehicle
v	Sway Speed [m/s]
V_i	Pump-Jet jet inlet speed [m/s]
V_o	Pump-Jet jet outlet speed [m/s]
VCG	Vertical center of gravity [m]
W_s	SWAMP Wetted surface $[m^2]$
w_{1m}	Resulting velocity at inlet [m/s]
w_{2m}	Resulting velocity at outlet [m/s]
w_{u1m}	Tangential resulting velocity at inlet [m/s]
w_{u2m}	Tangential resulting velocity at outlet [m/s]
X, Y, N	Total forces and moment
x_t	Pump-Jet position along x aboard SWAMP $[m]$
$X_{current}, Y_{current}, N_{current}$	Current forces and moment
$X_{hull}, Y_{hull}, N_{hull}$	Hull forces and moment
$x_{L,\text{air}}$	longitudinal position of the area center of $A_{L,\text{wind}}$
X_T, Y_T, N_T	Thrusters forces and moment
$X_{wind}, Y_{wind}, N_{wind}$	Wind forces and moment
y_t	Pump-Jet position along y aboard SWAMP $[m]$
Z_b	Vertical centre of Buoyancy [m]
z_{blades}	Number of vanes

Bibliography

[1] A. Sander and M. Wolfgang, "The rise of robotics," *BCG Perspectives. https://www. bcgperspectives. com/content/articles/business_ unit_ strategy_ innovation_ rise_ of_ robotics*, 2014.

[2] B.-M. Batalden, P. Leikanger, and P. Wide, "Towards autonomous maritime operations," in *2017 IEEE International Conference on Computational Intelligence and Virtual Environments for Measurement Systems and Applications (CIVEMSA)*. IEEE, 2017, pp. 1–6.

[3] M. Dunbabin and L. Marques, "Robotics for environmental monitoring [from the guest editors]," *IEEE Robotics & Automation Magazine*, vol. 19, no. 1, pp. 20–23, 2012.

[4] G. Bruzzone, A. Odetti, and M. Caccia, "Remote data collection near marine glacier fronts - unmanned vehicles for autonomous sensing, sampling in the north pole," *Sea Technology*, vol. 59, no. 3, pp. 22–26, 2018.

[5] A. Odetti, G. Bruzzone, M. Caccia, E. Spirandelli, and G. Bruzzone, "P2-rov a portable/polar rov," in *OCEANS 2017-Aberdeen*. IEEE, 2017, pp. 1–6.

[6] R. Céréghino, J. Biggs, B. Oertli, and S. Declerck, "The ecology of european ponds: defining the characteristics of a neglected freshwater habitat," in *Pond Conservation in Europe*. Springer, 2007, pp. 1–6.

[7] D. B. Scott, J. Frail-Gauthier, and P. J. Mudie, *Coastal wetlands of the world: geology, ecology, distribution and applications*. Cambridge University Press, 2014.

[8] E. Van den Bergh, A. Garniel, R. K. Morris, and A. Barendregt, "Conservation of tidal freshwater wetlands in europe," *Tidal Freshwater Wetlands*, pp. 241–252, 2009.

[9] W. Mitsch and J. Gosselink, "Wetlands. hoboken," 2007.

[10] P. A. Keddy, *Wetland ecology: principles and conservation*. Cambridge University Press, 2010.

[11] M. L. Kirwan and J. P. Megonigal, "Tidal wetland stability in the face of human impacts and sea-level rise," *Nature*, vol. 504, no. 7478, p. 53, 2013.

[12] K. L. Erwin, "Wetlands and global climate change: the role of wetland restoration in a changing world," *Wetlands Ecology and management*, vol. 17, no. 1, p. 71, 2009.

[13] P. Wadhams, *A Farewell to Ice: A Report from the Arctic*. Oxford University Press, 2017.

[14] M. E. Assessment, *Ecosystems and human well-being: wetlands and water*. World Resources Institute, 2005.

[15] W. J. Mitsch, B. Bernal, A. M. Nahlik, Ü. Mander, L. Zhang, C. J. Anderson, S. E. Jørgensen, and H. Brix, "Wetlands, carbon, and climate change," *Landscape Ecology*, vol. 28, no. 4, pp. 583–597, 2013.

[16] R. Lal, "Soil carbon sequestration to mitigate climate change," *Geoderma*, vol. 123, no. 1-2, pp. 1–22, 2004.

[17] I. R. Geijzendorffer, T. Galewski, A. Guelmami, C. Perennou, N. Popoff, and P. Grillas, "Mediterranean wetlands: a gradient from natural resilience to a fragile social-ecosystem," in *Atlas of Ecosystem Services*. Springer, 2019, pp. 83–89.

[18] Ramsar, *Convention on Wetlands of International Importance especially as Waterfowl Habitat*. Director, Office of International Standards and Legal Affairs., UNESCO, feb 1971, uN Treaty Series No. 14583. As amended by the Paris Protocol, 3 December 1982, and Regina Amendments, 28 May 1987.

[19] R. Sites, https://www.ramsar.org/sites-countries/ramsar-sites-around-the-world.

[20] E. Union, *Directive 2000/60/EC of the European Parliament and of the Council of 23 October 2000 Establishing a Framework for Community Action in the Field of Water Policy, OJ L 327, 22.12.2000, 1*, 2000.

[21] I. L. Decree, "152/06," *Testo unico ambientale. Modificato e integrato con il d.lgs. 4/2008 e con il d.lgs. 128/2010*, 2006.

[22] W. Brack, V. Dulio, M. Ågerstrand, I. Allan, R. Altenburger, M. Brinkmann, ..., and F. J. Hernández, "Towards the review of the european union water framework directive: Recommendations for more efficient assessment and management of chemical contamination in european surface water resources," *Science of The Total Environment*, vol. 576, pp. 720 – 737, 2017. [Online]. Available: http://www.sciencedirect.com/science/article/pii/S0048969716322860

[23] N. Voulvoulis, K. Arpon, and T. Giakoumis, "The eu water framework directive: From great expectations to problems with implementation," *Science of The Total Environment*, vol. 575, pp. 358 – 366, 2017. [Online]. Available: http://www.sciencedirect.com/science/article/pii/S004896971632157X

[24] H. Daniel, A. Borja, J. Carstensen, L. Carvalho, M. Elliott, C. Feld, A. Heiskanen, R. Johnson, J. Moe, D. Pont, A. Solheim, and W. van de Bund, "The european water framework directive at the age of 10: A critical review of the achievements with recommendations for the future," *Science of The Total Environment*, vol. 408, no. 19, pp. 4007 – 4019, 2010. [Online]. Available: http://www.sciencedirect.com/science/article/pii/S0048969710005462

[25] S. Behmel, M. Damour, R. Ludwig, and M. Rodriguez, "Water quality monitoring strategies — a review and future perspectives," *Science of The Total Environment*, vol. 571, pp. 1312 – 1329, 2016. [Online]. Available: http://www.sciencedirect.com/science/article/pii/S0048969716314243

[26] P. T. Vives, *Inventory, assessment and monitoring of Mediterranean Wetlands: Mapping wetlands using Earth Observation techniques*, 2008.

[27] S. Rapinel, E. Fabre, S. Dufour, D. Arvor, C. Mony, and L. Hubert-Moy, "Mapping potential, existing and efficient wetlands using free remote sensing data," *Journal of Environmental Management*, vol. 247, pp. 829 – 839, 2019. [Online]. Available: http://www.sciencedirect.com/science/article/pii/S0301479719308990

[28] X. Y., T. W., J. L., G. Y., and M. L., "Survey on the novel hybrid aquatic–aerial amphibious aircraft: Aquatic unmanned aerial vehicle (aquauav)," *Progress in Aerospace Sciences*, vol. 74, pp. 131 – 151, 2015. [Online]. Available: http://www.sciencedirect.com/science/article/pii/S0376042114001122

[29] M. J. Stealey, A. Singh, M. A. Batalin, B. Jordan, and W. J. Kaiser, "Nims-aq: A novel system for autonomous sensing of aquatic environments," in *2008 IEEE International Conference on Robotics and Automation*, May 2008, pp. 621–628.

[30] M. Mastrangeli and A. Odetti, "www.softhull.com," 2013.

[31] F. Bandini, D. Olesen, J. Jakobsen, M. Kittel, C. Marie, S. Wang, M. Garcia, and P. Bauer-Gottwein, "Bathymetry observations of inland water bodies using a tethered single-beam sonar controlled by an unmanned aerial vehicle." *Hydrology & Earth System Sciences*, vol. 22, no. 8, 2018.

[32] R. Raygosa-Barahona, M. Á. Garcia-Terán, C. Enriquez, and E. Olguín-Díaz, "Experimental evaluation of an autonomous surface craft for shallow-water bathymetry," *Marine Technology Society Journal*, vol. 51, no. 4, pp. 59–67, 2017.

[33] M. S. Fennessy, A. D. Jacobs, and M. E. Kentula, "An evaluation of rapid methods for assessing the ecological condition of wetlands," *Wetlands*, vol. 27, no. 3, pp. 543–560, 2007.

[34] E. Maltby, *Functional assessment of wetlands: towards evaluation of ecosystem services*. Elsevier, 2009.

[35] M. Zasso, "Relazione n. 01/10," in *Ricostruzione dei profili di velocità per la restituzione di misure correntometriche condotte in condizioni di piena*. ARPAV, Dipartimento Regionale per la Sicurezza del Territorio, Alberto Luchetta, U.O. Rete Idrografica Regionale, Italo Saccardo, 2010, pp. 1–22.

[36] G. Zappala, G. Bruzzone, G. Caruso, and M. Azzaro, "Development of an automatic sampler for extreme polar environments: first in situ application in svalbard islands," *Rendiconti Lincei*, vol. 27, no. 1, pp. 251–259, 2016.

[37] V. Bertram, "Unmanned surface vehicles–a survey," *Skibsteknisk Selskab, Copenhagen, Denmark*, pp. 1–14, 2008.

[38] E. Othman, "A review on current design of unmanned surface vehicles (usvs)," *Journal of Advanced Review on Scientific Research*, vol. 16, no. 1, pp. 12–17, 2015.

[39] M. Schiaretti, L. Chen, and R. R. Negenborn, "Survey on autonomous surface vessels: Part i-a new detailed definition of autonomy levels," in *International Conference on Computational Logistics*. Springer, 2017, pp. 219–233.

[40] ——, "Survey on autonomous surface vessels: Part ii-categorization of 60 prototypes and future applications," in *International Conference on Computational Logistics*. Springer, 2017, pp. 234–252.

[41] H. I. Moud, A. Shojaei, and I. Flood, "Current and future applications of unmanned surface, underwater, and ground vehicles in construction," in *Proceedings of the Construction Research Congress*, 2018, pp. 106–115.

[42] V. A. Jorge, R. Granada, R. G. Maidana, D. A. Jurak, G. Heck, A. P. Negreiros, D. H. Dos Santos, L. M. Gonçalves, and A. M. Amory, "A survey on unmanned surface vehicles for disaster robotics: Main challenges and directions," *Sensors*, vol. 19, no. 3, p. 702, 2019.

[43] L. Robotics, https://www.liquid-robotics.com/.

[44] Teledyne, http://www.teledynemarine.com, 2019.

[45] Searobotics, "Searobotics," https://www.searobotics.com/, 2019.

[46] Maribotics, https://www.maribotics.com/, 2019.

[47] J. Curcio, J. Leonard, and A. Patrikalakis, "Scout-a low cost autonomous surface platform for research in cooperative autonomy," in *Proceedings of OCEANS 2005 MTS/IEEE.* IEEE, 2005, pp. 725–729.

[48] J. Wang, W. Gu, and J. Zhu, "Design of an autonomous surface vehicle used for marine environment monitoring," in *2009 International Conference on Advanced Computer Control.* IEEE, 2009, pp. 405–409.

[49] M. L. Seto and A. Crawford, "Autonomous shallow water bathymetric measurements for environmental assessment and safe navigation using usvs," in *OCEANS 2015-MTS/IEEE Washington.* IEEE, 2015, pp. 1–5.

[50] A. Martins, H. Ferreira, C. Almeida, H. Silva, J. M. Almeida, and E. Silva, "Roaz and roaz ii autonomous surface vehicle design and implementation," in *International Lifesaving Congress 2007*, 2007.

[51] G. Ferri, A. Manzi, F. Fornai, F. Ciuchi, and C. Laschi, "The hydronet asv, a small-sized autonomous catamaran for real-time monitoring of water quality: From design to missions at sea," *IEEE Journal of Oceanic Engineering*, vol. 40, no. 3, pp. 710–726, 2015.

[52] M. Dunbabin, A. Grinham, and J. Udy, "An autonomous surface vehicle for water quality monitoring," in *Australasian conference on robotics and automation (ACRA).* Citeseer, 2009, pp. 2–4.

[53] G. Hitz, F. Pomerleau, M.-E. Garneau, C. Pradalier, T. Posch, J. Pernthaler, and R. Siegwart, "Design and application of a surface vessel for autonomous inland water monitoring," *IEEE Robotics & Automation Magazine*, vol. 19, 2012.

[54] F. Raimondi, M. Trapanese, V. Franzitta, A. Viola, and A. Colucci, "A innovative semi-immergible usv (si-usv) drone for marine and lakes operations with instrumental telemetry and acoustic data acquisition capability," in *OCEANS 2015-Genova.* IEEE, 2015, pp. 1–10.

[55] J. Grenestedt, J. Keller, S. Larson, J. Patterson, J. Spletzer, and T. Trephan, "Lorca: A high performance usv with applications to surveillance and monitoring," in *2015 IEEE International Symposium on Safety, Security, and Rescue Robotics (SSRR).* IEEE, 2015, pp. 1–6.

[56] C. Specht, E. Świtalski, and M. Specht, "Application of an autonomous/unmanned survey vessel (asv/usv) in bathymetric measurements," *Polish Maritime Research*, vol. 24, no. 3, pp. 36–44, 2017.

[57] K. T. Suhari, K. S. Apryandika, and M. Rahmawati, "The small hydrography marine boundary boat (shumoo) for mapping bathymetry of shallow water area," in *Proceedings of The 1st Geomatics International Conference (GEOICON) 2016 "Utilization of Satellite Technology for Natural Resources Exploration*, 2016.

[58] K. Suhari, H. Karim, P. H. Gunawan, and H. Purwanto, "Small rov marine boat for bathymetry surveys of shallow waters-potential implementation in malaysia," *International Archives of the Photogrammetry, Remote Sensing & Spatial Information Sciences*, vol. 42, 2017.

[59] Geomar-USV, http://www.geomar-usv.com/features.html, 2019.

[60] Tecdron, "Cyberjet-185," http://www.tecdron.com/wp-content/uploads/2014/06/CYBERJET-185.pdf, 2019.

[61] Dotocean, "Calypso," https://www.dotocean.eu/products/autonomous-systems/calypso/, 2019.

[62] Teledyne, "Z-boat," http://www.teledynemarine.com/Lists/Downloads/Teledyne%20Marine%20Vehicles%20Comparison%20Brochure_110617_SPREADS%206.pdf/, 2019.

[63] P. Kimball, J. Bailey, S. Das, R. Geyer, T. Harrison, C. Kunz, K. Manganini, K. Mankoff, K. Samuelson, T. Sayre-McCord, F. Straneo, A. Traykovski, and S. Hanumant, "The whoi jetyak: An autonomous surface vehicle for oceanographic research in shallow or dangerous waters," *2014 IEEE/OES Autonomous Underwater Vehicles (AUV)*, pp. 1–7, 2014.

[64] P. Mahacek, T. Berk, A. Casanova, C. Kitts, W. Kirkwood, and G. Wheat, "Development and initial testing of a swath boat for shallow-water bathymetry," in *OCEANS 2008.* IEEE, 2008, pp. 1–6.

[65] C. Kitts, P. Mahacek, T. Adamek, K. Rasal, V. Howard, S. Li, A. Badaoui, W. Kirkwood, G. Wheat, and S. Hulme, "Field operation of a robotic small waterplane area twin hull boat for shallow-water bathymetric characterization," *Journal of field Robotics*, vol. 29, no. 6, pp. 924–938, 2012.

[66] S. Zaghi, C. Leotardi, R. Muscari, G. Dubbioso, M. Diez, and R. Broglia, "Rans hydrodynamic characterization of a usv swath configuration including design optimization," in *18th Numerical Towing Tank Symposium NuTTS2015, Cortona, Italy*, 2015.

[67] S. Brizzolara, T. Curtin, M. Bovio, and G. Vernengo, "Concept design and hydrodynamic optimization of an innovative swath usv by cfd methods," *Ocean Dynamics*, vol. 62, no. 2, pp. 227–237, 2012.

[68] S. Brizzolara, M. Bovio, A. Federici, and G. Vernengo, *Hydrodynamic design of a family of hybrid SWATH unmanned surface vehicles.* Sea Grant College Program, Massachusetts Institute of Technology, 2011.

[69] Searobotics, "Hycat," https://www.searobotics.com/images/products/asvs/sr-surveyor/SR-Hycat-SpecSheet.pdf, 2019.

[70] OCEANALPHA, "Esm-30," https://www.oceanalpha.com/product-item/esm30/, 2019.

[71] Clearpathrobotics, "Heron," https://www.clearpathrobotics.com/heron-unmanned-surface-vessel/, 2019.

[72] D. F. Carlson, A. Fürsterling, L. Vesterled, M. Skovby, S. S. Pedersen, C. Melvad, and S. Rysgaard, "An affordable and portable autonomous surface vehicle with obstacle avoidance for coastal ocean monitoring," *Hardwarex*, p. e00059, 2019.

[73] S. Bertram, C. Kitts, D. Azevedo, G. Del Vecchio, B. Hopner, G. Wheat, and W. Kirkwood, "A portable asv prototype for shallow-water science operations," in *OCEANS 2016 MTS/IEEE Monterey*. IEEE, 2016, pp. 1–6.

[74] J. Bayer, "The duckling project: Design and manufacturing of autonomous surface vehicles for various application areas," 2017.

[75] M. H. B. M. Idris, M. A. A. B. C. Kamarudin, M. I. Sahalan, Z. B. Z. Abidin, and M. M. Rashid, "Design and development of an autonomous surface vessel for inland water depth monitoring," in *2016 International Conference on Computer and Communication Engineering (ICCCE)*. IEEE, 2016, pp. 177–182.

[76] P. Duranti, G. Lollino, M. Arattano, M. Rinaldi, O. Giustolisi, J. Marechal, and E. Grant, *CatOne, Multitask Unmanned Surface Vessel for Hydro-Geological and Environment Surveys*. Springer International Publishing, 2015, vol. 3, pp. 647–652.

[77] A. Cuppens, G. Menesse, E. Caligaris, O. Marecos, and G. Wyseure, "A low-cost, open-source autonomous surface vehicle as a multipurpose waste stabilization pond monitoring platform," *Journal of Water, Sanitation and Hygiene for Development*, vol. 9, no. 1, pp. 172–180, 2019.

[78] A. Valada, P. Velagapudi, B. Kannan, C. Tomaszewski, G. Kantor, and P. Scerri, "Development of a low cost multi-robot autonomous marine surface platform," in *Field and service robotics*. Springer, 2014, pp. 643–658.

[79] A. Vasilijevic, B. Buxton, J. Sharvit, N. Stilinovic, D. Nad, N. Miskovic, D. Planer, J. Hale, and Z. Vukic, "An asv for coastal underwater archaeology: The pladypos survey of caesarea maritima, israel," in *OCEANS 2015-Genova*. IEEE, 2015, pp. 1–7.

[80] W. Wang, L. A. Mateos, S. Park, P. Leoni, B. Gheneti, F. Duarte, C. Ratti, and D. Rus, "Design, modeling, and nonlinear model predictive tracking control of a novel autonomous surface vehicle," in *2018 IEEE International Conference on Robotics and Automation (ICRA)*. IEEE, 2018, pp. 6189–6196.

[81] N.-H. Tran, T.-C. Nguyen, V.-T. Tran, V.-C. Nguyen, and T.-N. Nguyen, "The design of an viam-usvi000 unmanned surface vehicle for environmental monitoring applications," in *2018 4th International Conference on Green Technology and Sustainable Development (GTSD)*. IEEE, 2018, pp. 33–37.

[82] B. Bayat, N. Crasta, A. Crespi, A. M. Pascoal, and A. Ijspeert, "Environmental monitoring using autonomous vehicles: a survey of recent searching techniques," *Current opinion in biotechnology*, vol. 45, pp. 76–84, 2017.

[83] W. for a sustainable Mediterranean region, https://medwet.org/, 2019.

[84] M. Caccia, M. Bibuli, R. Bono, G. Bruzzone, G. Bruzzone, and E. Spirandelli, "Unmanned surface vehicle for coastal and protected waters applications: The charlie project," *Marine Technology Society Journal*, vol. 41, no. 2, pp. 62–71, 2007.

[85] M. Caccia, M.and Bibuli, R. Bono, G. Bruzzone, G. Bruzzone, and E. Spirandelli, "Unmanned marine vehicles at cnr-issia," *IFAC Proceedings Volumes*, vol. 41, no. 2, pp. 3070–3075, 2008.

[86] L. Gasperini, F. Del Bianco, G. Stanghellini, and F. Priore, "Acquisition of geophysical data in shallow-water environments using autonomous vehicles: state of the art, perspectives and case histories," *GNGTS Repository*, 2014.

[87] F. Giordano, G. Mattei, C. Parente, F. Peluso, and R. Santamaria, "Integrating sensors into a marine drone for bathymetric 3d surveys in shallow waters," *Sensors*, vol. 16, no. 1, p. 41, 2016.

[88] ——, "Microvega (micro vessel for geodetics application): A marine drone for the acquisition of bathymetric data for gis applications," *The International Archives of Photogrammetry, Remote Sensing and Spatial Information Sciences*, vol. 40, no. 5, p. 123, 2015.

[89] R. Gawałkiewicz, D. Madusiok *et al.*, "The bagry reservoir–part 3. the application of hydro-drone smart-sonar-boat in bathymetric measurements of inaccessible water areas," *Geoinformatica Polonica*, vol. 2018, no. 2018), pp. 17–30, 2018.

[90] M. Kurowski, J. Thal, R. Damerius, H. Korte, and T. Jeinsch, "Automated survey in very shallow water using an unmanned surface vehicle," in *CAMS 2019*. IFAC, 2019, pp. –.

[91] S. G. Ackleson, J. P. Smith, L. M. Rodriguez, W. J. Moses, and B. J. Russell, "Autonomous coral reef survey in support of remote sensing," *Frontiers in Marine Science*, vol. 4, p. 325, 2017.

[92] A. Golini and S. Tersigni, "Pressione antropica sulle coste italiane," *FASCICOLO ABSTRACT*, p. 6, 2019.

[93] A. A. Mogstad, G. Johnsen, and M. Ludvigsen, "Shallow-water habitat mapping using underwater hyperspectral imaging from an unmanned surface vehicle: A pilot study," *Remote Sensing*, vol. 11, no. 6, p. 685, 2019.

[94] L. Naing, A. S. B. M. Ghani, M. I. Sahalan, M. B. A. Aziz, Z. Z. Abidin, and M. M. Rashid, "Development and fieldwork trial of autonomous surface vehicles for bathymetry mapping," in *2017 IEEE 7th International Conference on Underwater System Technology: Theory and Applications (USYS)*. IEEE, 2017, pp. 1–5.

[95] F. Marques, A. Lourenço, R. Mendonça, E. Pinto, P. Rodrigues, P. Santana, and J. Barata, "A critical survey on marsupial robotic teams for environmental monitoring of water bodies," in *OCEANS 2015 - Genova*, May 2015, pp. 1–6.

[96] J. Zhang, J. Xiong, G. Zhang, F. Gu, and Y. He, "Flooding disaster oriented usv & uav system development & demonstration," in *OCEANS 2016-Shanghai*. IEEE, 2016, pp. 1–4.

[97] M. Lindemuth, R. Murphy, E. Steimle, W. Armitage, K. Dreger, T. Elliot, M. Hall, D. Kalyadin, J. Kramer, M. Palankar *et al.*, "Sea robot-assisted inspection," *IEEE robotics & automation magazine*, vol. 18, no. 2, pp. 96–107, 2011.

[98] E. T. Steimle and M. L. Hall, "Unmanned surface vehicles as environmental monitoring and assessment tools," in *OCEANS 2006*. IEEE, 2006, pp. 1–5.

[99] D. V. for Scientific Survey, http://www.3dresearch.it/index.php/it/underwater-it/prodotti/devss, 2019.

[100] P. Duranti, "Catone, multitask unmanned surface vessel for hydro-geological and environment surveys," in *Engineering Geology for Society and Territory-Volume 3*. Springer, 2015, pp. 647–652.

[101] Z. Li and R. Bachmayer, "The development of a robust autonomous surface craft for deployment in harsh ocean environment," in *2013 OCEANS-San Diego*. IEEE, 2013, pp. 1–7.

[102] A. Odetti and M. Mastrangeli, "Multipurpose air cushion platform," *Proc. NAV 2015 Conference*, vol. 1, pp. 49–58, 2015.

[103] M. Caccia, M. Bibuli, R. Bono, G. Bruzzone, G. Bruzzone, and E. Spirandelli, "Aluminum hull usv for coastal water and seafloor monitoring," in *OCEANS 2009-EUROPE*. IEEE, 2009, pp. 1–5.

[104] M. Bibuli, G. Bruzzone, M. Caccia, E. Fumagalli, E. Saggini, E. Zereik, E. Buttaro, C. Caporale, and R. Ivaldi, "Unmanned surface vehicles for automatic bathymetry mapping and shores' maintenance," in *OCEANS 2014-TAIPEI*. IEEE, 2014, pp. 1–7.

[105] V. Piermattei, A. Madonia, S. Bonamano, R. Martellucci, G. Bruzzone, R. Ferretti, A. Odetti, M. Azzaro, G. Zappalà, and M. Marcelli, "Application of a low cost instrumentation in arctic extreme conditions," in *4th International Electronic Conference on Sensors and Applications*. Multidisciplinary Digital Publishing Institute, 2017.

[106] A. Odetti, M. Bibuli, G. Bruzzone, M. Caccia, E. Spirandelli, and G. Bruzzone, "e-urope: a reconfigurable auv/rov for man-robot underwater cooperation," *IFAC-PapersOnLine*, vol. 50, no. 1, pp. 11 203–11 208, 2017.

[107] R. Ferretti, M. Bibuli, M. Caccia, D. Chiarella, A. Odetti, A. Ranieri, E. Zereik, and G. Bruzzone, "Towards posidonia meadows detection, mapping and automatic recognition using unmanned marine vehicles," *IFAC-PapersOnLine*, vol. 50, no. 1, pp. 12 386–12 391, 2017.

[108] A. Baracco, M. Coggiola, G. Discalzi, F. Perrelli, C. Romano *et al.*, "Valutazione del rischio da movimentazione manuale dei carichi: la scelta dei valori di riferimento alla luce del d. lgs. 81/2008," *G Ital Med Lav Erg*, vol. 31, no. 2, pp. 172–176, 2009.

[109] K. Kebkal, I. Glushko, T. Tietz, R. Bannasch, O. Kebkal, M. Komar, and S. Yakovlev, "Sonobot - an autonomous unmanned surface vehicle for hydrographic surveys with hydroacoustic communication and positioning for underwater acoustic surveillance and monitoring," *proc. of 2^{n}d International Conference and Exhibition on Underwater Acoustics*, 2014.

[110] M. Altosole, G. Benvenuto, M. Figari, and U. Campora, "Dimensionless numerical approaches for the performance prediction of marine waterjet propulsion units," *International Journal of Rotating Machinery*, vol. Volume 2012, 2012.

[111] D. Harte, N. Bose, R. Clifford, T. Roberts, and G. Davidson, "An application of paddlewheel propulsion to a high speed craft," in *Second International Symposium on Marine Propulsors (SMP'11), Hamburg, Germany*, 2011.

[112] D. Smith, L. Cross, J. Rivet, and S. Hall, "Design of a semi-autonomous boat for measurements of coastal sedimentation and erosion," *Proceedings of the International Association of Hydrological Sciences*, vol. 367, p. 447, 2015.

[113] I. Ehrlich, D. Sloss, B. Hanamoto, and C. Nuttall, "The wheel pump propulsion system for floating vehicles," *Journal of Terramechanics*, vol. 8, no. 4, pp. 43–52, 1972.

[114] D. Osiński, K. Szykiedans, R. Szewczyk, C. Zieliński, and M. Kaliczyńska, *Small Remotely Operated Screw-Propelled Vehicle*. Springer International Publishing, 2015, pp. 191–200. [Online]. Available: http://dx.doi.org/10.1007/978-3-319-15847-1_19

[115] M. Caccia, R. Bono, G. Bruzzone, G. Bruzzone, E. Spirandelli, G. Veruggio, A. Stortini, and G. Capodaglio, "Sampling sea surfaces with sesamo: an autonomous craft for the study of sea-air interactions," *IEEE robotics & automation magazine*, vol. 12, no. 3, pp. 95–105, 2005.

[116] W.-V. A. M. Robotics, http://www.wam-v.com/wam-v-technology/, 2019.

[117] http://www.businessdictionary.com/definition/innovation.html, 2019.

[118] K. J. Rawson and E. C. Tupper, *Basic ship theory*. Butterworth-Heinemann, 2001, vol. 1.

[119] A. Odetti and M. Mastrangeli, "A shockproof hull made of foam: a useful project for operations on uneven ice," in *The 26th International Ocean and Polar Engineering Conference*. International Society of Offshore and Polar Engineers, 2016.

[120] J. Vasilj, I. Stančić, T. Grujić, and J. Musić, "Design, development and testing of the modular unmanned surface vehicle platform for marine waste detection," *Journal of multimedia information system*, vol. 4, no. 4, pp. 195–204, 2017.

[121] B. Metcalfe, B. Thomas, A. Treloar, Z. Rymansaib, A. Hunter, and P. Wilson, "A compact, low-cost unmanned surface vehicle for shallow inshore applications," in *2017 Intelligent Systems Conference (IntelliSys)*. IEEE, 2017, pp. 961–968.

[122] Surfbee, https://www.surfbee.io/surfbee-shop/22-queen, 2019.

[123] L. J. Gibson and M. F. Ashby, *Cellular solids: structure and properties*. Cambridge university press, 1999.

[124] L. Gibson and M. Ashby, *Cellular solids : structure and properties*, 2nd ed., ser. Cambridge solid state science series. Cambridge University Press, 1997.

[125] D. De Vries, "Characterization of polymeric foams," *Eindhoven University of Technology*, 2009.

[126] A. Blaise, S. André, P. Delobelle, Y. Meshaka, and C. Cunat, "Identification of the true elastic modulus of high density polyethylene from tensile tests using an appropriate reduced model of the elastoviscoplastic behavior," *arXiv preprint arXiv:1206.4268*, 2012.

[127] Fibrlolux, https://fibrolux.com/it/, 2019.

[128] J. Waterhouse, "50 years of double-ended ferry design," *ELLIOTT BAY DESIGN GROUP*, 2016.

[129] A. Minchev, C. Simonsen, and R. Zilcken, "Double-ended ferries: propulsive performance challenges and model testing verification," in *Proceedings of the second International Symposium on Marine Propulsor, Hamburg*, 2011.

[130] W. Wigley, "A comparison of experiment and calculated wave-profiles and wave-resistances for a form having parabolic waterlines," *Proceedings of the Royal Society of London. Series A, Containing Papers of a Mathematical and Physical Character*, vol. 144, no. 851, pp. 144–159, 1934.

[131] H. Moraes, J. Vasconcellos, and R. Latorre, "Wave resistance for high-speed catamarans," *Ocean Engineering*, vol. 31, no. 17-18, pp. 2253–2282, 2004.

[132] M. Insel and A. Molland, "An investigation into the resistance components of high speed displacement catamarans," University of Southampton, Tech. Rep., 1992.

[133] A. Molland, J. Wellicome, and P. Couser, "Theoretical prediction of the wave resistance of slender hull forms in catamaran configurations," University of Southampton, Tech. Rep., 1994.

[134] P. Sahoo and L. Doctors, "A study on wave resistance of high-speed displacement hull forms in restricted depth," in *Proceedings of the 7th International Conference of Fast Sea Transportation (FAST 2003), Ischia, Italy*, 2003.

[135] M. Vantorre, "Review of practical methods for assessing shallow and restricted water effects," in *International Conference on Marine Simulation and Ship Maneuverability. Kanazawa, Japan: International Marine Simulator Forum*, 2003.

[136] M. J. Briggs, "Ship squat predictions for ship/tow simulator," ENGINEER RESEARCH AND DEVELOPMENT CENTER VICKSBURG MS COASTAL AND HYDRAULICS LAB, Tech. Rep., 2006.

[137] V. Bertram, *Practical ship hydrodynamics*. Elsevier, 2011.

[138] T. Whittaker, "A physical study of fast ferry wash characteristics in shallow water," *MCA Research Project*, vol. 457, 2002.

[139] S. Brizzolara and D. Bruzzone, "Near and distant waves of fast ships in unlimited and limited depths," in *Proceedings, FAST*, 2003, p. H1.

[140] M. Senthil Prakash and B. Chandra, "Numerical estimation of shallow water resistance of a river-sea ship using cfd," *International journal of computer applications*, vol. 71, no. 5, pp. 33–40, 2013.

[141] K. A. P. Utama, A. Jamaluddin, and W. Aryawan, "Experimental investigation into the drag interference of symmetrical and asymmetrical staggered and unstaggered catamarans." *Journal of Ocean Technology*, vol. 7, no. 1, 2012.

[142] H. Y. Yeh *et al.*, "Series 64 resistance experiments on high-speed displacement forms," *Marine Technology and SNAME News*, vol. 2, no. 03, pp. 248–272, 1965.

[143] P. K. Sahoo, M. Salas, and A. Schwetz, "Practical evaluation of resistance of high-speed catamaran hull forms—part i," *Ships and offshore structures*, vol. 2, no. 4, pp. 307–324, 2007.

[144] P. K. Sahoo, S. Mason, and A. Tuite, "Practical evaluation of resistance of high-speed catamaran hull forms—part ii," *Ships and Offshore Structures*, vol. 3, no. 3, pp. 239–245, 2008.

[145] R. Eliasson, L. Larsson, and M. Orych, *Principles of yacht design.* A&C Black, 2014.

[146] D. (NETHERLANDS), "Double ended catamaran," www.stirlingdesign.fr, www.alumarine-shipyard.com, 2012.

[147] A. Molland, J. Wellicome, and P. Couser, "Resistance experiments on a systematic series of high speed displacement catamaran forms: variation of length-displacement ratio and breadth-draught ratio," University of Southampton, Tech. Rep., 1994.

[148] J. Van Manen and T. van Terwisga, "A new way of simulating whale tail propulsion," in *Twenty-first symposium on Naval Hydrodynamics*, 1997.

[149] K. Eloot, G. Delefortrie, M. Vantorre, and F. Quadvlieg, "Validation of ship manoeuvring in shallow water through free-running tests," in *34th ASME International Conference on Ocean, Offshore and Arctic Engineering (OMAE2015).* ASME, 2015, pp. 1–11.

[150] I. Dand, T. Dinham-Peren, and L. King, "Hydrodynamic aspects of a fast catamaran operating in shallow water," *Hydrodynamics of High Speed Craft. The Royal Institution of Naval Architects, London*, vol. 117, 1999.

[151] A. Molland, P. Wilson, and D. Taunton, "Resistance experiments on a systematic series of high speed displacement monohull and catamaran forms in shallow water," University of Southampton, Tech. Rep., 2003.

[152] ——, "A systematic series of experimental wash wave measurements for high speed displacement monohull and catamaran forms in shallow water," University of Southampton, Tech. Rep., 2001.

[153] A. Ali, A. Maimun, Y. M. Ahmed *et al.*, "Resistance analysis of a semi-swath design concept in shallow water," *Journal of Marine Science and Application*, vol. 16, no. 2, pp. 182–189, 2017.

[154] L. Barbieri, F. Cucinotta, A. Gallo, F. Bruno, M. Muzzupappa, N. Penna, and R. Gaudio, "Design and simulation of the hull of a small-sized autonomous surface vehicle for seabed mapping," in *International Conference on Design, Simulation, Manufacturing: The Innovation Exchange.* Springer, 2019, pp. 422–431.

[155] B. Muller-Graf, D. Radojcic, and A. Simic, "Resistance and propulsion characteristics of the vws hard chine catamaran hull series' 89," *SNAME Transactions*, vol. 110, pp. 1–29, 2002.

[156] W. Chengyi, "Resistance charicteristic of high-speed catamaran and its application. shipbuilding of china," 1994.

[157] D. Jürgens and R. Grabert, "New hydrodynamic aspects of double ended ferries with voith-schneider propeller," in *2nd International conference on Double Ended Ferries, Norway, Alesund*, 2003.

[158] E. Ageno, L. Bonfiglio, D. Bruzzone, G. Vernengo, and D. Villa, "A study on the added resistance performance of catamarans in waves," in *ASME 2018 37th International Conference on Ocean, Offshore and Arctic Engineering.* American Society of Mechanical Engineers, 2018, pp. V11AT12A019–V11AT12A019.

[159] D. Villa, M. Viviani, and E. Ferri, "Application of cfd calculations for the improvement of planing crafts manoeuvrability mathematical models," in *12th International Conference on Hydrodynamics, ICHD 2016*, 2016, p. 10.

[160] S. Brizzolara and D. Villa, "Cfd simulation of planing hulls," in *Proceedings of the 7th International conference on High-Performance Marine Vehicles, Melbourne, Florida, USA*, 2010.

[161] A. Jamaluddin, I. Utama, and A. Molland, "Experimental investigation into the drag characteristics of symmetrical and asymmetrical staggered and unstaggered catamarans," in *International Conference on Ship & Offshore Technology (ICSOT)-Indonesia*, 2010, pp. 11–12.

[162] A. Odetti, M. Altosole, G. Bruzzone, M. Caccia, and M. Viviani, "Design and construction of a modular pump-jet thruster for autonomous surface vehicle operations in extremely shallow water," *Journal of Marine Science and Engineering*, vol. 7, no. 7, p. 222, 2019.

[163] M. Caccia, M. Bibuli, G. Bruzzone, V. Djapic, S. Fioravanti, and A. Grati, "Modular usv and payload design for advanced capabilities in marine security applications," in *2011 19th Mediterranean Conference on Control & Automation (MED).* IEEE, 2011, pp. 430–435.

[164] B. Allotta, S. Baines, F. Bartolini, F. Bellavia, C. Colombo, R. Conti, R. Costanzi, C. Dede, M. Fanfani, J. Gelli, H. T. Gündogdu, N. Monni, D. Moroni, M. Natalini, M. A. Pascali, F. Pazzaglia, L. Pugi, A. Ridolfi, M. Reggiannini, D. Roig, O. Salvetti, and E. I. Tekdemir, "Design of a modular autonomous underwater vehicle for archaeological investigations," in *OCEANS 2015 - Genova*, May 2015, pp. 1–5.

[165] J. Pandey and K. Hasegawa, "Study on manoeuverability and control of an autonomous wave adaptive modular vessel (wam-v) for ocean observation," in *2015 International Association of Institutes of Navigation World Congress (IAIN)*, Oct 2015, pp. 1–7.

[166] Z. Peng, D. Wang, and J. Wang, "Cooperative dynamic positioning of multiple marine offshore vessels: A modular design," *IEEE/ASME Transactions On Mechatronics*, vol. 21, no. 3, pp. 1210–1221, 2015.

[167] M. C. Nielsen, "Modular underwater robots-modeling and docking control," Ph.D. dissertation, Technical University of Denmark, Department of Electrical Engineering, 2018.

[168] M. C. Nielsen, O. A. Eidsvik, M. Blanke, and I. Schjølberg, "Constrained multi-body dynamics for modular underwater robots—theory and experiments," *Ocean Engineering*, vol. 149, pp. 358–372, 2018.

[169] L. Furno, M. Blanke, R. Galeazzi, and D. J. Christensen, "Self-reconfiguration of modular underwater robots using an energy heuristic," in *2017 IEEE/RSJ International Conference on Intelligent Robots and Systems (IROS)*. IEEE, 2017, pp. 6277–6284.

[170] M. J. Doyle, X. Xu, Y. Gu, F. Perez-Diaz, C. Parrott, and R. Groß, "Modular hydraulic propulsion: A robot that moves by routing fluid through itself," in *2016 IEEE International Conference on Robotics and Automation (ICRA)*. IEEE, 2016, pp. 5189–5196.

[171] J. Paulos, N. Eckenstein, T. Tosun, J. Seo, J. Davey, J. Greco, V. Kumar, and M. Yim, "Automated self-assembly of large maritime structures by a team of robotic boats," *IEEE Transactions on Automation Science and Engineering*, vol. 12, no. 3, pp. 958–968, 2015.

[172] I. Ehrlich, I. Kamm, and G. Worden, "Water performance of amphibious vehicles part ii—propulsion and maneuverability," *Journal of Terramechanics*, vol. 7, no. 3, pp. 69–99, 1970.

[173] http://www.argovehicles.com/, 2019.

[174] A. Kurkin, D. Y. Tyugin, V. Kuzin, A. Chernov, V. Makarov, P. Beresnev, V. Filatov, and D. Zeziulin, "Autonomous mobile robotic system for environment monitoring in a coastal zone," *Procedia computer science*, vol. 103, pp. 459–465, 2017.

[175] F. Fish, "Advantages of natural propulsive systems," *Marine Technology Society Journal*, vol. 47, no. 5, pp. 37–44, 2013.

[176] B. Peter, R. Ratnaweera, W. Fischer, C. Pradalier, and R. Siegwart, "Design and evaluation of a fin-based underwater propulsion system," in *Robotics and Automation (ICRA), 2010 IEEE International Conference on*. IEEE, 2010, pp. 3751–3756.

[177] J. Hauge, "Oscillating foil propulsion," Master's thesis, NTNU, Department of Marine Technology, Norwegian University of Science and Technology, 2013.

[178] D. Beal, "Propulsion through wake synchronization using a flapping foil," Ph.D. dissertation, Massachusetts Institute of Technology, 2003.

[179] M. Babu, P. Krishnankutty, and J. Mallikarjuna, "Experimental study of flapping foil propulsion system for ships and underwater vehicles and piv study of caudal fin propulsors," in *2014 IEEE/OES Autonomous Underwater Vehicles (AUV)*, Oct 2014, pp. 1–7.

[180] http://www.doen.nl/web/projects/Green/Project Green/OFoil-1.htm, 2011.

[181] D. Radojcic, "Possible propulsors for inland waterway," Naval Architecture department at the University of Belgrade, Tech. Rep., 01 2006.

[182] "Schottel gmbh - spj - def applications," www.schottel.de/fileadmin/data/pdf/eng/eng_SPJ.pdf, 2019.

[183] D. Mu, G. Wang, Y. Fan, and Y. Zhao, "Modeling and identification of podded propulsion unmanned surface vehicle and its course control research," *Mathematical Problems in Engineering*, vol. 2017, 2017.

[184] http://www.maritimerobotics.com/mariner-usv/marinerlite usv/, 2016.

[185] D. Frank, A. Gray, and E. Schwartz, "Propagator 2: A planing autonomous surface vehicle with azimuth rimdriven thrusters," in *Proceedings of the 14th Annual Early Career Technical Conference*, 2014, pp. 1–6.

[186] E. Zakeri, S. Farahat, S. A. Moezi, and A. Zare, "Robust sliding mode control of a mini unmanned underwater vehicle equipped with a new arrangement of water jet propulsions: Simulation and experimental study," *Applied Ocean Research*, vol. 59, pp. 521–542, 2016.

[187] Y. Peng, Y. Yang, J. Cui, X. Li, H. Pu, J. Gu, S. Xie, and J. Luo, "Development of the usv 'jinghai-i'and sea trials in the southern yellow sea," *Ocean Engineering*, vol. 131, pp. 186–196, 2017.

[188] D. Machado, A. Martins, J. M. Almeida, H. Ferreira, G. Amaral, B. Ferreira, A. Matos, and E. Silva, "Water jet based autonomous surface vehicle for coastal waters operations," in *2014 Oceans - St. John's*, Sep. 2014, pp. 1–8.

[189] M. Li, S. Guo, H. Hirata, and H. Ishihara, "Design and performance evaluation of an amphibious spherical robot," *Robotics and Autonomous Systems*, vol. 64, pp. 21 – 34, 2015. [Online]. Available: http://www.sciencedirect.com/science/article/pii/S0921889014002498

[190] B. Allotta, R. Costanzi, A. Ridolfi, C. Colombo, F. Bellavia, M. Fanfani, F. Pazzaglia, O. Salvetti, D. Moroni, M. A. Pascali *et al.*, "The arrows project: adapting and developing robotics technologies for underwater archaeology," *IFAC-PapersOnLine*, vol. 48, no. 2, pp. 194–199, 2015.

[191] T. Salumäe, R. Raag, J. Rebane, A. Ernits, G. Toming, M. Ratas, and M. Kruusmaa, "Design principle of a biomimetic underwater robot u-cat," in *2014 Oceans-St. John's*. IEEE, 2014, pp. 1–5.

[192] R. A. Eldred, "Autonomous underwater vehicle architecture synthesis for shipwreck interior exploration," NAVAL POSTGRADUATE SCHOOL MONTEREY CA, Tech. Rep., 2015.

[193] S. Puente, F. Candelas, F. Torres, and D. Basalai, "Autonomous surface vessel based on a low cost catamaran design," in *Proceedings of the 13th International Conference on Informatics in Control, Automation and Robotics*. SCITEPRESS-Science and Technology Publications, Lda, 2016, pp. 452–457.

[194] E. Olenew, "Entwicklung von manövrier-und steuereinrichtungen für ein druckneutrales unterwasserfahrzeug," Ph.D. dissertation, Technische Universität Berlin, Fakultät V - Verkehrs- und Maschinensysteme, 2013.

[195] J. H. W. Gill, "Improvements in or relating to the propulsion and manoeuvring of vessels," 11 1919, patent: GB-140985-A. [Online]. Available: https://patents.google.com/patent/GB140985A/en

[196] www.vethpropulsion.com/products/bow thrusters/, "Veth propulsion b.v." 2019.

[197] www.schottel.de/marine-propulsion/spj-pump jet/, "Schottel gmbh - spj," 2019.

[198] www.jastram.net/products/azimuth-grid thrusters.html, "Jastram gmbh & co. kg," 2019.

[199] www.teesgillthrusters.com/products/vertical-shaft units, "Tees white gill," 2019.

[200] http://marinepropulsionsolutions.com/azimuthing pumpjet/, "Pt. marine propulsion solutions," 2019.

[201] J. Manaois, "Pumpjets in de binnenvaart," Master's thesis, TU Delft, Civil Engineering and Geosciences, 2011.

[202] W. Wikeckiewicz, "Hull impact on the performance of the thruster with bottom-mounted outlet nozzle," *14 Scientific Journals of the Maritime University of Szczecin*, vol. 1, no. 14, pp. 48–52, 2008.

[203] S. Kaul and S. Huth, "Hydrojet," May 28 1996, uS Patent 5,520,557.

[204] S. S. technical data, "Schottel gmbh - spj," 2019.

[205] A. Stepanoff, *Centrifugal and axial flow pumps: theory, design, and application*. Wiley New York, 1957.

[206] S. Srivastava, A. K. Roy, and K. Kumar, "Design of a mixed flow pump impeller blade and its validation using stress analysis," *Procedia materials science*, vol. 6, pp. 417–424, 2014.

[207] ——, "Design of a mixed flow pump impeller and its validation using fem analysis," *Procedia Technology*, vol. 14, pp. 181–187, 2014.

[208] F. Wiesner, "A review of slip factors for centrifugal impellers," *Journal of Engineering for Power*, vol. 89, no. 4, pp. 558–566, 1967.

[209] D. Zindani, A. K. Roy, and K. Kumar, "Design of mixed flow pump impeller blade using mean stream line theory and its analysis," *Scientia Iranica*, pp. –, 2018. [Online]. Available: http://scientiairanica.sharif.edu/article_20829.html

[210] ——, "Design of blade of mixed flow pump impeller using mean stream line method," *Procedia Technology*, vol. 23, pp. 464–471, 2016.

[211] G. Bibuli, M. Bruzzone, M. Caccia, G. Camporeale, D. Chiarella, M. Ferretti, R. Giacopelli, A. Odetti, A. Ranieri, E. Spirandelli, and E. Zereik, "An advanced guidance & control system for an unmanned vessel with azimuthal thrusters," in *International Ship Control Systems Symposium*, Oct. 2018. [Online]. Available: https://doi.org/10.24868/issn.2631-8741.2018.004

[212] F. Scibilia and R. Skjetne, "Constrained control allocation for vessels with azimuth thrusters," *IFAC Proceedings Volumes*, vol. 45, no. 27, pp. 7–12, 2012.

[213] A. Veksler, T. A. Johansen, F. Borrelli, and B. Realfsen, "Cartesian thrust allocation algorithm with variable direction thrusters, turn rate limits and singularity avoidance," in *2014 IEEE Conference on Control Applications (CCA)*. IEEE, 2014, pp. 917–922.

[214] S. Kikuchi, T. Sakata, E. Takahashi, and H. Kanno, "Development of wireless power transfer system for robot arm with rotary and linear movement," in *2016 IEEE International Conference on Advanced Intelligent Mechatronics (AIM)*. IEEE, 2016, pp. 1616–1621.

[215] M. Bestmann, F. Wasserfall, N. Hendrich, and J. Zhang, "Replacing cables on robotic arms by using serial via bluetooth," in *2017 IEEE International Conference on Robotics and Biomimetics (ROBIO)*. IEEE, 2017, pp. 189–195.

[216] powertechsystems, "The lithium difference," https://www.powertechsystems.eu/home/tech-corner/lithium-ion-battery-advantages/, 2019.

[217] Y. Wang, C. Zhang, and Z. Chen, "A method for state-of-charge estimation of li-ion batteries based on multi-model switching strategy," *Applied energy*, vol. 137, pp. 427–434, 2015.

[218] S. Li and B. Ke, "Study of battery modeling using mathematical and circuit oriented approaches," in *2011 IEEE Power and Energy Society General Meeting*. IEEE, 2011, pp. 1–8.

[219] M. Caccia and G. Veruggio, "Guidance and control of a reconfigurable unmanned underwater vehicle," *Control Engineering Practice*, vol. 8, no. 1, pp. 21–37, 2000.

[220] M. Caccia, M. Bibuli, R. Bono, and G. Bruzzone, "Basic navigation, guidance and control of an unmanned surface vehicle," *Autonomous Robots*, vol. 25, no. 4, pp. 349–365, 2008.

[221] M. Bibuli, G. Bruzzone, M. Caccia, and L. Lapierre, "Path-following algorithms and experiments for an unmanned surface vehicle," *Journal of Field Robotics*, vol. 26, no. 8, pp. 669–688, 2008.

[222] M. Bibuli, M. Caccia, G. Bruzzone, and L. Lapierre, "Guidance of unmanned surface vehicles: Experiments in vehicle following," *IEEE Robotics and Automation Magazine*, vol. 19, no. 3, pp. 92–102, 2008.

[223] A. Turetta, G. Casalino, and A. Sorbara, "Distributed control architecture for self-reconfigurable manipulators," *The International Journal of Robotics Research*, vol. 27, no. 3-4, pp. 481–504, 2008.

[224] D. AS, *Assessment of station keeping capability of dynamic positioning vessels*, 2016.

[225] L. M. S. Systems, "3dm-gx3 - importing magnetic vectors for hard and soft iron calibration," http://files.microstrain.com/8401-0053-Importing-Magnetic-Vectors.pdf, 2019.

[226] M. Caccia, G. Bruzzone, and R. Bono, "A practical approach to modeling and identification of small autonomous surface craft," *IEEE Journal of Oceanic Engineering*, vol. 33, no. 2, pp. 133–145, 2008.

[227] M. Bibuli, M. Caccia, L. Lapierre, and G. Bruzzone, "Guidance of unmanned surface vehicles: Experiments in vehicle following," *IEEE Robotics & Automation Magazine*, vol. 19, no. 3, pp. 92–102, 2012.

[228] M. Caccia, M. Bibuli, R. Bono, and G. Bruzzone, "Basic navigation, guidance and control of an unmanned surface vehicle," *Autonomous Robots*, vol. 25, no. 4, pp. 349–365, November 2008.

[229] D. Macciò and C. Cervellera, "Local models for data-driven learning of control policies for complex systems," *Expert Systems with Applications*, vol. 39, no. 18, pp. 13 399–13 408, 2012.

[230] C. Cervellera, M. Gaggero, and D. Macciò, "Efficient kernel models for learning and approximate minimization problems," *Neurocomputing*, vol. 97, pp. 74–85, 2012.

[231] C. Cervellera and M. Muselli, "A deterministic learning approach based on discrepancy," in *Italian Workshop on Neural Nets*. Springer, 2003, pp. 53–60.

[232] G. Tanaka, T. Yamane, J. B. Héroux, R. Nakane, N. Kanazawa, S. Takeda, H. Numata, D. Nakano, and A. Hirose, "Recent advances in physical reservoir computing: A review," *Neural Networks*, 2019.

[233] M. Lukoševičius and H. Jaeger, "Reservoir computing approaches to recurrent neural network training," *Computer Science Review*, vol. 3, no. 3, pp. 127–149, 2009.

[234] H. Jaeger, "The "echo state" approach to analysing and training recurrent neural networks-with an erratum note," *Bonn, Germany: German National Research Center for Information Technology GMD Technical Report*, vol. 148, no. 34, p. 13, 2001.

[235] Y. Yoshimura, I. Nakao, and A. Ishibashi, "Unified mathematical model for ocean and harbour manoeuvring," in *MARSIM'09 Conference Proceedings*. International Conference on Marine Simulation and Ship Maneuverability, 2009.

[236] D. Villa, M. Viviani, S. Gaggero, M. Vantorre, K. Eloot, and G. Delefortrie, "Cfd-based analyses for a slow speed manoeuvrability model," *Journal of Marine Science and Technology*, pp. 1–13, 2019.

[237] K. Kose, H. Hinata, Y. Hashizume, and E. Futagawa, "On a mathematical model of maneuvering motions of ships in low speeds," *Journal of the Society of Naval Architects of Japan*, vol. 1984, no. 155, pp. 132–138, 1984.

[238] A. Yumuro, "Some experiments on manoeuvring hydrodynamic forces in low speed condition," *Kansai Soc. Nav. Arch. J.*, vol. 209, p. 91, 1988.

[239] K. Karasuno, "A new mathematical model of hydrodynamic forces and moment acting on a hull during manoeuvring motion that occurs under conditions of slow speed and large turns (2nd report)," *Transactions of the West-Japan Society of Naval Architects*, vol. 217, pp. 125–135, 1993.

[240] D. Kang and K. Hasegawa, "Prediction method of hydrodynamic forces acting on the hull of a blunt-body ship in the even keel condition," *Journal of Marine Science and Technology*, vol. 12, no. 1, pp. 1–14, Mar 2007. [Online]. Available: https://doi.org/10.1007/s00773-006-0232-7

[241] K. Kijima, "On the practical prediction method for ship manoeuvring characteristics," *Transactions of the West-Japan Society of Naval Architects*, pp. 21–31, 2002.

[242] J. P. Hooft, "The cross-flow drag on a manoeuvring ship," *Ocean engineering*, vol. 21, no. 3, pp. 329–342, 1994.

[243] K. Karasuno, S. Okano, J. Miyoshi, and K. Maekawa, "Predictions of ship's hull hydrodynamic forces and maneuvering motions at slow speed based on a component-type mathematical model," *Proc. MARSIM2003, Kanazawa, Japan*, pp. 25–28, 2003.

[244] P. Oltmann and S. D. Sharma, "Simulation of combined engine and rudder maneuvers using an improved model of hull-propeller-rudder interactions," *Fifteenth ONR Symposium on Naval Hydrodynamics Hamburg, 3 - 7 September 1984*, 1984.

[245] K.-G. Oh, K. Hasegawa, K. Karasuno, and S. K. Lee, "Ship manoeuvring hydrodynamic forces and moment in low speed," in *Proc. of Advanced Maritime Engineering Conference*, 2012, pp. 1–8.

[246] Y. Yoshimura and N. Ma, "Manoeuvring prediction of fishing vessels," in *MARSIM'03 Conference Proceedings*. The Society of Naval Architects of Japan, Japan Institute of Navigation and . . . , 2003, pp. pRC–29.

[247] T. Fossen, "Guidance and control of ocean vehicles. john willey & sons," *Inc., New York*, 1994.

[248] D. Clarke, P. Gedling, and G. Hine, "The application of manoeuvring criteria in hull design using linear theory," *Transactions of the Royal Institution of Naval Architects, RINA.*, 1982.

[249] J. Carreño, J. Mora, and F. Pérez, "Mathematical model for maneuverability of a riverine support patrol vessel with a pump-jet propulsion system," *Ocean Engineering*, vol. 63, pp. 96–104, 2013.

[250] M. Viviani, C. P. Bonvino, R. Depascale, F. Conti, and M. Soave, "Identification of hydrodynamic coefficient from standard manoeuvres for a serie of twin-screw ships," *Genova, Italy: Unknow, Unknow*, 2007.

[251] M. Viviani, G. Dubbioso, C. Notaro, C. Bonvino, R. Depascale, and M. Soave, "Application of system identification for the improvement of manoeuvrability prediction for twin-screw ships," in *Proceedings of MARSIM*, 2009.